



University
of Glasgow

McArthur, Lisa (2017) *Investigating interactions between rat adult cardiac myocytes and fibroblasts in the heart*. PhD thesis.

<https://theses.gla.ac.uk/8512/>

Copyright and moral rights for this work are retained by the author

A copy can be downloaded for personal non-commercial research or study, without prior permission or charge

This work cannot be reproduced or quoted extensively from without first obtaining permission in writing from the author

The content must not be changed in any way or sold commercially in any format or medium without the formal permission of the author

When referring to this work, full bibliographic details including the author, title, awarding institution and date of the thesis must be given

Enlighten: Theses

<https://theses.gla.ac.uk/>
research-enlighten@glasgow.ac.uk

Investigating interactions between rat adult cardiac myocytes and fibroblasts in the heart

Lisa McArthur

MSci (Hons), MRes

**Submitted in fulfilment of the requirements for the degree of
Doctor of Philosophy to the Institute of Cardiovascular and Medical
Sciences, University of Glasgow.**

**Research conducted at the British Heart Foundation Glasgow
Cardiovascular Research Centre, Institute of Cardiovascular and
Medical Sciences, College of Medical, Veterinary and Life
Sciences, University of Glasgow, U.K.**

2017

© L. McArthur

Author's declaration

I declare that this thesis was written entirely by myself and is a record of the work performed by me with some exceptions as detailed below. Characterisation of AdCx43 as well as the qRT-PCR studies examining the effect of IL-1Ra on IL-1 β -mediated upregulation of Cx43 and IL-1 β regulation of TGF β 1 signalling was performed in collaboration with Miss Alexandra Riddell. The optical mapping studies were performed in collaboration with Dr. Allen Kelly. The image of cytopathic effect in the methods section was provided by Miss Aisling McFall. This thesis has not been submitted previously for a higher degree. The work included in this thesis was completed at the University of Glasgow Cardiovascular Research Centre in the Institute of Cardiovascular and Medical Sciences under the supervision of Professor Stuart A. Nicklin and Professor Godfrey L. Smith.

Lisa McArthur

2017

Acknowledgements

Firstly, I would like to thank my supervisors Professor Stuart Nicklin and Professor Godfrey Smith for all their help and guidance throughout this PhD. Particularly to Stu who has always had an open door policy and been there when things weren't going too well in the lab. I would also like to thank the British Heart Foundation for funding this work.

Many thanks to everyone in lab, past and present, for all their help and guidance. Thanks to Dr. Laura Denby for all her cloning advice, Dr. Scott Johnstone for answering all my connexin related questions, Dr. Lisa Chilton for her help establishing the *in vitro* co-culture model and to Aileen Rankin and Michael Dunne for their help with cardiac myocyte isolations. Special thanks to Elisabeth Beattie and Allen Kelly for the laughs during surgery and optical mapping experiments; I really appreciate all the time you put aside for them.

Thanks to the "Science Besties": Emma, Margaret, Nina, Small, Tall, and Laura for all the memories inside and out of work. Special thanks has to go to Emma, we started off as colleagues but now we're friends, this write up period would have been so much more difficult without you and all our trips for tea, caramel frappes and snacks. Thank you to all my non-science friends for all the encouragement and taking me out for a drink, or two or three...

A huge thanks has to go the McFarlane's (my Glasgow family), for their continual support and encouragement. Thanks to my mum, dad and two amazing sisters for all the visits and always being a phone call away, motivating me to keep going. Lastly, thanks to Grant for all his love and support throughout the years; this achievement was made so much easier having you in my life.

Table of Contents

Author's declaration	ii
Acknowledgements.....	iii
Table of Contents	iv
List of Figures.....	ix
List of Tables.....	xiii
List of publications, presentations and awards	xiv
List of Abbreviations and Definitions	xv
Summary	xxii
Chapter 1 General introduction	1
1.1 The heart	2
1.2 Cellular composition of the heart	2
1.2.1 Cellular markers of fibroblasts in the heart	3
1.3 Electrical conduction and cardiac contraction.....	3
1.3.1 Cardiac action potential.....	6
1.3.2 Excitation-contraction coupling	7
1.4 The intercalated disc	10
1.4.1 Adherens junctions and desmosomes.....	10
1.4.2 Gap junctions and cardiac connexins.....	10
1.4.3 Importance of intercalated disc components	14
1.5 Connexin channel regulation.....	15
1.5.1 Voltage gating.....	16
1.5.2 Chemical gating.....	19
1.5.3 Regulation of connexin channels by phosphorylation	20
1.6 The diseased heart	20
1.6.1 Pathological cardiac remodelling	21
1.6.2 Electrical remodelling and cardiac arrhythmias	31
1.6.3 Impaired excitation-contraction coupling	34
1.7 Current treatment of arrhythmias	35
1.8 Cardiac myocyte: fibroblast interactions	37
1.8.1 Membrane fusion interactions	37
1.8.2 Paracrine interactions	37
1.8.3 Electrical interactions and the role of connexins.....	39
1.8.4 Electrophysiological consequences of cardiac myocyte: fibroblast coupling	40
1.8.5 Mechanical interactions	44
1.9 Hypothesis and aims	45

Chapter 2	Materials and methods.....	46
2.1	Materials	47
2.1.1	Solutions	47
2.2	Cell isolation and culture.....	48
2.2.1	Cell lines	48
2.2.2	Obtaining hearts for cell isolation	48
2.2.3	Rat adult cardiac fibroblast culture	49
2.2.4	Rat adult cardiac fibroblast isolation.....	49
2.2.5	Adult rat cardiac myocyte isolation	52
2.2.6	Cell passage and cryopreservation.....	53
2.3	Stimulation of RACFs.....	53
2.3.1	Stimulation of RACFs with proinflammatory mediators.....	53
2.3.2	IL-1 β pathway inhibitor experiments	54
2.4	Nucleic acid extraction	57
2.4.1	Ribonucleic acid (RNA) and micro RNA extraction.....	57
2.4.2	Deoxyribonucleic acid (DNA) extraction	58
2.4.3	Nucleic acid quantification.....	60
2.5	Reverse transcription	61
2.5.1	Gene expression	61
2.5.2	miRNA expression.....	61
2.6	Quantitative PCR	62
2.6.1	Gene and miRNA expression	62
2.7	Molecular cloning.....	65
2.7.1	Restriction endonuclease digestion.....	65
2.7.2	Agarose gel electrophoresis.....	65
2.7.3	DNA extraction from ethidium bromide gel	65
2.7.4	Phenol chloroform clean-up of DNA	66
2.7.5	DNA dephosphorylation and ligation	67
2.7.6	Transformation of DNA and bacterial culture	67
2.7.7	DNA sequencing	68
2.8	Transfection of DNA to cultured cells	69
2.9	Lentiviral vector production and purification.....	70
2.9.1	Lentiviral vector titration	71
2.10	Adenoviral vector production and purification	75
2.10.1	Electroporation and homologous recombination	75
2.10.2	Transfection of adenoviral genomes to HEK 293 cells.....	75
2.10.3	Generation of crude adenovirus stocks	76
2.10.4	Plaque purification.....	78

2.10.5	Large scale adenovirus production	79
2.10.6	Caesium chloride gradient ultracentrifugation	79
2.10.7	Adenoviral vector dialysis.....	82
2.10.8	Adenoviral vector titration	82
2.11	Viral vector addition to cells	84
2.12	Protein preparation for western immunoblotting	84
2.12.1	Protein quantification	84
2.13	Western immunoblotting.....	85
2.14	Immunocytochemistry (ICC)	88
2.15	Cardiac myocyte and fibroblast co-culture model	90
2.15.1	Calcein dye transfer co-culture experiments	90
2.15.2	Cardiac myocyte contraction measurement	91
2.15.3	Cardiac myocyte action potential measurement.....	93
2.16	<i>In vivo</i> intramyocardial injection	93
2.16.1	Fibroblast and eGFP adenoviral vector preparation	94
2.16.2	Surgical procedure of intramyocardial injection	94
2.17	<i>Ex vivo</i> heart optical mapping	95
2.17.1	Experimental set up	95
2.17.2	Removal of heart under terminal anaesthesia.....	98
2.17.3	Action potential measurements in the intact heart.....	98
2.18	Histology.....	99
2.18.1	Tissue processing.....	99
2.18.2	Immunohistochemistry	100
2.19	Statistical analysis	104
Chapter 3 Generation of viral vectors to modulate connexin 43 expression in cardiac fibroblasts for use <i>in vitro</i> and <i>in vivo</i>		105
3.1	Introduction	106
3.2	Aims	110
3.3	Results	111
3.3.1	Lentiviral and adenoviral transduction into RACFs	113
3.3.2	Cloning of α SMA_eGFPNLS into a lentiviral shuttle plasmid.....	116
3.3.3	Cloning of α SMA_eGFPNLS into an adenoviral shuttle plasmid	120
3.3.4	Production of an adenoviral vector overexpressing Cx43.....	123
3.4	Discussion	129
3.5	Summary	131
Chapter 4 Interleukin 1 β regulates connexin 43 expression in primary cardiac fibroblasts 132		
4.1	Introduction	133
4.1.1	The role of interleukin-1 in inflammatory signalling in the heart..	133

4.1.2	Regulation of Cx43 by IL-1 β	137
4.1.3	MicroRNA regulation of connexin 43	138
4.2	Aims	139
4.3	Results	140
4.3.1	Characterisation of isolated adult rat cardiac fibroblasts.....	140
4.3.2	Assessment of Cx43 regulation by proinflammatory mediators.....	142
4.3.3	Dissection of the mechanism by which IL-1 β stimulates Cx43 up-regulation	144
4.3.4	IL-1 β -mediated regulation of the TGF β 1 pathway.....	154
4.4	Discussion.....	156
4.5	Summary.....	162
Chapter 5	Co-culture investigation of cardiac myocyte: fibroblast interactions 163	
5.1	Introduction	164
5.1.1	Culture effect on adult cardiac myocytes	164
5.1.2	Adult cardiac myocyte: fibroblast co-culture models.....	165
5.2	Aims	167
5.3	Results	168
5.3.1	Effect of control or IL-1 β treated RACFs on the contraction of cultured CMs.....	170
5.3.2	Effect of control or IL-1 β treated RACFs on the action potential of cultured CMs.....	178
5.3.3	Examination of RACF presence in control cultures	182
5.4	Discussion.....	184
5.5	Summary.....	186
Chapter 6	Establishing a model to investigate cardiac myocyte: fibroblast interactions via optical mapping in the intact heart.....	187
6.1	Introduction	188
6.1.1	Intramyocardial cell injection models.....	188
6.1.2	Optical mapping	190
6.2	Aims	192
6.3	Results	193
6.3.1	eGFP detection in the myocardium.....	195
6.3.2	Dynamic pacing	198
6.3.3	S1S2 pacing.....	203
6.3.4	Preliminary detection of eGFP positive cells within the rat myocardium.....	210
6.4	Discussion.....	212
6.5	Summary.....	214

Chapter 7	General discussion.....	215
7.1	Overall summary.....	216
7.2	Future perspectives	218
7.3	Conclusions	222
Appendix.....		223
List of References		224

List of Figures

Figure 1-1 Electrical conduction through the cardiac cycle.....	5
Figure 1-2 Ventricular cardiac myocyte action potential, calcium influx and contraction.	9
Figure 1-3 Cardiac myocyte calcium handling.....	9
Figure 1-4 Major components of the intercalated disc.	12
Figure 1-5 Structure of connexin hemichannels and gap junction channels.	13
Figure 1-6 Typical relationship between gap junctional conduction and transjunctional voltage.	18
Figure 1-7 Eccentric and concentric hypertrophy.	30
Figure 1-8 Establishment of a re-entry circuit.	33
Figure 1-9 Schematic of potential electrical consequences of increased cardiac myocyte: (myo)fibroblast coupling.	43
Figure 2-1 Cytopathic effect in HEK 293 cells.....	77
Figure 2-2 Purification of the mature virus following double CsCl gradient ultracentrifugation.	81
Figure 2-3 Visual representation of contraction parameters measured.	92
Figure 2-4 Experimental set up for <i>ex vivo</i> heart optical mapping.	97
Figure 3-1 Components sought in an artificial α SMA promoter hybrid.....	112
Figure 3-2 Schematic of designed insert, α SMA_eGFPNLS, and pLenti-promoter plasmid.....	112
Figure 3-3 Representative images of RACFs transduced with LVeGFP.....	114
Figure 3-4 Representative images of RACFs transduced with different concentrations of AdeGFP.....	115
Figure 3-5 Diagnostic digests and transfection of the p α SMA_eGFPNLS into RACFs.	117
Figure 3-6 Purification of the α SMA_eGFPNLS insert and linearised pLenti-promoter.....	119
Figure 3-7 Purification of α SMA_eGFPNLS insert and linearised pLenti-III-promoterless.	119
Figure 3-8 Cloning of α SMA_eGFPNLS or eGFPNLS into pVQ_K-NpA or pVQ_CMV_K-NpA respectively.....	122

Figure 3-9 Clone screening of pShuttle_Cx43 and the recombinant Ad plasmid containing Cx43.	125
Figure 3-10 Representative western immunoblot of protein from HeLa cells transduced with AdCx43.	126
Figure 3-11 Representative western immunoblot of protein from RACFs transduced with an AdCx43.	127
Figure 3-12 Immunolocalisation of Cx43 in RACFs transduced with AdCx43.	128
Figure 4-1 IL-1 signalling pathway.	136
Figure 4-2 Immunolocalisation of α SMA, vimentin, DDR2, S100A4 and Cx43 in passage 2 RACFs.	141
Figure 4-3 Effect of proinflammatory mediators on Cx43 mRNA expression in RACFs.	143
Figure 4-4 Representative images of control and IL-1 β treated RACFs.	143
Figure 4-5 Effect of IL-1 β on Cx43 protein expression in RACFs.	145
Figure 4-6 Effect of NF- κ B inhibition on IL-1 β mediated upregulation of Cx43 mRNA expression in RACFs.	147
Figure 4-7 Effect of NF- κ B inhibition on IL-1 β mediated upregulation of Cx43 protein expression in RACFs.	147
Figure 4-8 Effect of p38 MAPK, JNK or MEK1 inhibition on IL-1 β mediated up-regulation of Cx43 mRNA expression in RACFs.	149
Figure 4-9 Effect of p38 MAPK, JNK or MEK1 inhibition on IL-1 β mediated up-regulation of Cx43 protein expression in RACFs.	149
Figure 4-10 Effect of IL-1 receptor inhibition on IL-1 β mediated up-regulation of Cx43 mRNA expression in RACFs.	150
Figure 4-11 Effect of IL-1 β on miR19b, 30c, 101 and 125b expression in RACFs.	152
Figure 4-12 Effect of IL-1 β on Cx43 mRNA and miR-19b, -30c, -101, -101b and -125b expression in RACFs over different time periods.	153
Figure 4-13 Effect of IL-1 β or TGF β 1 alone or in combination on the mRNA expression of CTGF, α SMA, serpine, snail and slug in RACs.	155
Figure 5-1 Representative images showing the localisation of calcein in CMs and RACFs immediately after the addition of loaded CMs to the RACF monolayer (0-1 h) and following 20 h in culture.	169

Figure 5-2 Contraction traces and contraction parameters that can be measured from cultured CMs.	171
Figure 5-3 Representative images and stimulation threshold values of CMs cultured alone or with a RACF monolayer.	172
Figure 5-4 Contraction measurements in CMs cultured alone or with a RACF monolayer.	173
Figure 5-5 Stimulation threshold values of CMs cultured alone, with an RACF monolayer or with an IL-1 β treated RACF monolayer.	175
Figure 5-6 Contraction measurements in CMs cultured alone, with an RACF monolayer or with an IL-1 β treated RACF monolayer.	176
Figure 5-7 Action potential measurements in freshly isolated CMs and CMs cultured for 24 h.	179
Figure 5-8 Action potential measurements in CMs cultured alone, with an RACF monolayer or with an IL-1 β treated RACF monolayer.	180
Figure 5-9 Vimentin immunofluorescence in cultures of CMs seeded on laminin coated plates (control) or on a monolayer of untreated or IL-1 β treated RACF.	183
Figure 6-1 Representative images of pre-transduced RACFs with LVeGFP on the day of injection into the rat myocardium and of optical mapping.	194
Figure 6-2 Voltage signal, eGFP signal and analysis selection areas of hearts injected with eGFP positive RACFs.	196
Figure 6-3 Voltage signal, eGFP signal and analysis selection areas of hearts injected with AdeGFP.	197
Figure 6-4 Relationship between the action potential rise time and duration at different in cycle lengths during dynamic pacing in both RACF and AdeGFP injected hearts.	200
Figure 6-5 Action potential rise time of hearts injected with RACF or AdeGFP when paced at a cycle length of 120 or 200 ms.	201
Figure 6-6 Action potential duration of hearts injected with RACF or AdeGFP when paced at a cycle length of 120 or 200 ms.	202
Figure 6-7 Effective refractory period of hearts injected with eGFP positive RACFs or AdeGFP.	204
Figure 6-8 Selection areas for eGFP positive RACF and AdeGFP injected hearts for S1S2 pacing protocol.	205

Figure 6-9 Comparison of S2 action potential rise time and duration between the original injection selection and the smaller injection selection.	206
Figure 6-10 Relationship between the S2 action potential rise time and duration at different in cycle lengths in RACF and AdeGFP injected hearts.	207
Figure 6-11 The S2 action potential rise time and duration in the injection site of RACF and AdeGFP injected hearts at different cycle lengths.....	209
Figure 6-12 Example AdeGFP and RACF injected hearts showing crowding of activation over the epicardial surface during an S2 impulse.....	209
Figure 6-13 Preliminary immunofluorescence to identify eGFP positive RACFs within the rat left ventricular myocardium.	211

List of Tables

Table 2.1 Enzymatic digestion protocol for RACF isolation.	51
Table 2.2 Proinflammatory mediators used to stimulate RACFs.....	55
Table 2.3 IL-1 β pathway inhibitors.	56
Table 2.4 List of Taqman gene expression assays	64
Table 2.5 List of Taqman miRNA expression assays	64
Table 2.6 Sequences of primers and probe used in lentiviral vector titration. ..	74
Table 2.7 Primary antibody details used in western immunoblotting	87
Table 2.8 Primary antibodies used in immunocytochemistry.	89
Table 2.9 Definition of contraction parameters measure.	92
Table 2.10 Solution sequence for tissue embedding in paraffin wax	102
Table 2.11 Solution sequence to deparaffinise and rehydrate tissue sections for immunohistochemistry.....	102
Table 2.12 Primary antibodies used in immunohistochemistry	103
Table 5.1 Contraction parameter values of CMs in control, RACF monolayer and IL-1 β RACF monolayer treatment groups.	177
Table 5.2 Action potential parameter values of fresh CMs and cultured CMs in control, RACF monolayer and IL-1 β RACF monolayer treatment groups.	181

List of publications, presentations and awards

Publications

McArthur, L., Chilton, L., Smith, G.L., & Nicklin, S.A. (2015). Electrical consequences of cardiac myocyte: fibroblast coupling. *Biochem.Soc.Trans.*, 43, (3) 513-518

Fattah, C., Nather, K., McCarroll, C.S., Hortigon-Vinagre, M.P., Zamora, V., Flores-Munoz, M., **McArthur, L.**, Zentilin, L., Giacca, M., Touyz, R.M., Smith, G.L., Loughrey, C.M., & Nicklin, S.A. (2016). Gene Therapy With Angiotensin-(1-9) Preserves Left Ventricular Systolic Function After Myocardial Infarction. *J.Am.Coll.Cardiol.*, 68, (24) 2652-2666

Presentations

McArthur, L., Kelly, A., Chilton, L., Smith, G.L., & Nicklin, S.A. (2016). Interleukin 1 β mediated modulation of cardiac myocyte: fibroblast interactions. 40th EWGCCE meeting, Glasgow, UK. [poster communication]

McArthur, L., Chilton, L., Smith, G.L., & Nicklin, S.A. (2016). Interleukin 1 β regulation of connexin 43 in cardiac fibroblasts and the effects of adult cardiac myocyte: fibroblast co-culture on myocyte contraction. *Frontiers in cardiovascular biology*, Florence, Italy. [poster communication]

McArthur, L., Smith, G.L., & Nicklin, S.A. (2015). Investigating connexin gap junctions between adult rat cardiac myocytes and cardiac fibroblasts. BHF 4-year PhD annual conference. University of Cambridge, UK. [poster communication]

McArthur, L., Smith, G.L., & Nicklin, S.A. (2014). Investigating connexin gap junctions between adult rat cardiomyocytes and cardiac fibroblasts. 7th UK Gap Junction meeting, Glasgow Caledonian University, UK. [oral communication]

Awards

Oral communication prize winner, 7th UK Gap Junction meeting, December 2014.

List of Abbreviations and Definitions

α SMA	α -smooth muscle actin
Ad	Adenoviral
ADF	Autologous dermal fibroblast
AF	Atrial fibrillation
AJ	Adherens junction
ANEP	Aminonaphthylethylenylpyridinium
Ang II	Angiotensin II
ANOVA	Analysis of variance
AP	Action potential
AP-1	Activator protein-1
APD	Action potential duration
APD ₂₀	Action potential duration at 20 % repolarisation
APD ₅₀	Action potential duration at 50 % repolarisation
APD ₈₀	Action potential duration at 80 % repolarisation
APD ₉₀	Action potential duration at 90 % repolarisation
ATP	Adenosine triphosphate
AV	Atrioventricular
AVN	Atrioventricular node
AZ	AZD6244
BCA	Bicinchoninic acid
BDM	2,3-butanedione monoxime
bp	base pair
BSA	Bovine serum albumin
Ca ²⁺	Calcium ion
CAD	Coronary heart disease
CaM	Calmodulin
CCD	Charge-coupled device
CCM	CM conditioned media
CD	Contraction duration
CD10	Time from 10 % contraction to 90 % relaxation
CD25	Time from 25 % contraction to 75 % relaxation
CD50	Time from 50 % contraction to 50 % relaxation

CD75	Time from 75 % contraction to 25 % relaxation
CD90	Time from 90 % contraction to 10 % relaxation
CF	Cardiac fibroblast
CF-MI	Cardiac fibroblast from a myocardial infarction heart
CHF	Congestive heart failure
CKO	Conditional knockout
CM	Cardiac myocyte
CMOS	Complementary metal-oxide-semiconductor
CO ₂	Carbon dioxide
CPE	Cytopathic effect
CsCl	Caesium chloride
CT	Carboxyl-terminal
C _t	Threshold cycle
CTGF	Connective tissue growth factor
cTnl	Cardiac troponin I
CV	Conduction velocity
CVD	Cardiovascular disease
Cx	Connexin
DAD	Delayed afterdepolarisation
DAMPs	Damage-associated molecular patterns
DAPI	4',6-diamidino-2-phenylindole
DCM	Dilated cardiomyopathy
DDR2	Discoid domain receptor 2
DHA	Docosahexaenoic acid
DMSO	Dimethyl sulfoxide
DNA	Deoxyribonucleic acid
DTT	Dithiothreitol
dV/dt _{max}	Rate of depolarisation
EAD	Early after depolarisation
E-C	Excitation - contraction
ECC	Excitation contraction coupling
ECG	Electrocardiogram
ECM	Extracellular matrix
EDTA	Ethylenediaminetetraacetic

eGFP	Enhanced green fluorescent protein
EndMT	Endothelial-to-mesenchymal transition
ERK	Extracellular signal-regulated kinase
ERP	Effective refractory period
ET-1	Endothelin-1
FBS	Foetal bovine serum
FCM	Fibroblast conditioned media
fps	Frames per second
FRET	Fluorescence resonance energy transfer
FSP1	Fibroblast specific protein
GFP	Green fluorescent protein
g_j	Gap junctional conductance
GJ	Gap junction
GJIC	Gap junction intercellular communication
gp	Glycoprotein
h	Hour
HCN1	hyperpolarization activated cyclic nucleotide gated potassium channel 1
HDAd	Helper-dependent adenoviral
HEK	Human embryonic kidney
HF	Heart failure
HIV-1	Human immunodeficiency virus 1
HMGB1	High-mobility group box 1
h/R	Ratio of left ventricular wall thickness to radius
I_{CaL}	Inward Ca^{2+} current through the L-type Ca^{2+} channel
ICC	Immunocytochemistry
ICD	Implantable cardioverter-defibrillator
IHC	Immunohistochemistry
I κ B	Inhibitor of nuclear factor B
I_{k1}	Inward rectifier K^+ current
IKK	Inhibitor of nuclear factor B kinase
I_{Kr}	Rapid delayed rectifier potassium current
I_{Ks}	Slow delayed rectifier potassium current
I_{Kur}	Ultra-rapid delayed rectifier potassium current

IL	Interleukin
IL-1R	IL-1 receptor
IL-1Ra	IL-1 receptor antagonist
IL-1RacP	IL-1 receptor accessory protein
iNOS	Inducible nitric oxide synthase
I_{NCX}	Na^+/Ca^{2+} exchanger current
I/R	Ischaemia/reperfusion
IRAK	Interleukin-1 receptor-activated protein kinase
IRES	Internal ribosome entry site
I_{to}	Transient-outward potassium current
I.U	International units
JNK	c-Jun N-terminal kinase
K^+	Potassium ion
KB	Kraft Bruhn
KO	Knockout
L	Litre
LB	Luria broth
LED	Light-emitting diode
LTCC	L-type Ca^{2+} channel
LTR	Long terminal repeat
LV	Lentiviral
LVEF	Left ventricular ejection fraction
M	Molar
MAPK	Mitogen-activated protein kinase
MDP	Maximal diastolic potential
MEK1/2	Mitogen-activated protein/ extracellular signal-regulated kinase kinase 1/2
MEM	Minimal essential media
MF	Myofibroblast
MI	Myocardial infarction
mIL-6R	Membrane bound interleukin-6 receptor
min	Minute
miR	Micro ribonucleic acid
mL	Milliliter

mM	Millimolar
MMP	Matrix metalloproteinase
MOI	Multiplicity of infection
mRNA	Messenger ribonucleic acid
MSC	Mechanosensitive channel
MYD88	Myeloid differentiation primary response gene 88
N2A	Neuro2A neuroblastoma
Na ⁺	Sodium ion
NCX	Sarcolemmal Na ⁺ /Ca ²⁺ exchanger
NF-κB	Nuclear factor-κB
NLS	Nuclear localisation signal
NO	Nitric oxide
nS	Nanosiemens
OM	Optical mapping
p38 MAPK	p38 mitogen-activated protein kinase
PAGE	Polyacrylamide gel electrophoresis
PAI-1	Plasminogen activator inhibitor-1
PBS	Phosphate-buffered saline
PBS-T	Phosphate-buffered saline containing Tween 20
PCR	Polymerase chain reaction
PEI	Polyethylenimine
PFA	Paraformaldehyde
pfu	Particle forming unit
PIU	Particle infectious unit
PKA	Protein kinase A
PKC	Protein kinase C
PLN	Phospholamban
PMSF	Phenylmethylsulfonyl fluoride
PP	Protein phosphatases
qRT-PCR	Quantitative real-time polymerase chain reaction
RACF	Rat adult cardiac fibroblast
Rev	Regulator of expression of virion proteins
RMP	Resting membrane potential
RNA	Ribonucleic acid

ROS	Reactive oxygen species
rpm	Revolutions per minute
RQ	Relative quantification
RRE	Rev response element
RT	Reverse transcriptase
RyR	Ryanodine receptor
s	Seconds
SAN	Sinoatrial node
SB	SB203580
SC	SC-514
Ser	Serine residue
SERCA	Sarcoendoplasmic reticulum calcium transport ATPase
SFFV	Spleen focus-forming virus
sIL-6R	Soluble interleukin-6 receptor
SIN	Self-inactivating
SM	Skeletal myoblast
SMC	Smooth muscle cell
SOC	Super Optimal broth with Catabolite repression
SP	SP600125
SR	Sarcoplasmic reticulum
TAC	Transverse aortic constriction
TAR	Trans-activation response
Tat	Transactivator of transcription
TBE	Tris/Boric acid/EDTA
TBS	Tris-buffered saline
TBS-T	Tris-buffered saline containing Tween 20
TD	Tris density
TdP	Torsade de pointes
TE	Tris-EDTA
TGF β	Transforming growth factor β
TGF β R1	Transforming growth factor β receptor 1
TIMP	Tissue inhibitors of matrix metalloproteinase
TNF α	Tumor necrosis factor α
TRAF	Tumour necrosis factor-associated factor

T-tubule	Transverse tubule
TV	Transfer vector
UBC	Ubiquitin C
VEGF	Vascular endothelial growth factor
VSD	Voltage-sensitive dye
VT	Ventricular tachycardia
VF	Ventricular fibrillation
V_j	Transjunctional voltage
vp	Viral particle
VSMC	Vascular smooth muscle cell
VSV-G	Glycoprotein of vesicular stomatitis virus
v/v	Volume/volume
WT	Wild type
w/v	Weight/volume

Summary

Heart disease, as a consequence of cardiac injury, is a major cause of morbidity and mortality in the UK. Following cardiac insult, cardiac fibroblasts (CFs) proliferate in mass and undergo a phenotypic switch to become myofibroblasts (MFs). These cells have a contractile phenotype, by developing the expression of α -smooth muscle actin (α SMA), and secrete excessive volumes of extracellular matrix components, resulting in typical fibrosis seen after injury. This contributes to cardiac dysfunction and dramatically increases the proarrhythmic potential of the heart, by creating an anatomical structure for re-entry to occur. In the healthy heart, gap junctions (GJs), composed of connexin (Cx) proteins, are mainly present at the intercalated discs between neighbouring cardiac myocytes (CMs) and assist in rapid electrical conduction through the myocardium. Reduced and/or disorganised Cx43 (the main cardiac connexin) expression in CMs has been demonstrated in many cardiomyopathies. In contrast, in experimental models of myocardial infarction (MI), CFs have been demonstrated to have augmented Cx43 levels in comparison to control CFs. As there is growing evidence that GJs can be formed between CMs and CFs, greater levels of Cx43 in CFs in disease could increase heterocellular coupling therefore augment the effect of CFs on CMs. Co-culture studies, mainly using cells from a neonatal origin, have suggested CFs can enhance the risk for arrhythmias involving paracrine mediators and direct cell-to-cell interactions. However, more research is required determine the effect of adult CFs on adult CMs. Therefore, the primary aim of this thesis was to investigate the effect of rat adult CFs (RACFs) on the function of adult CMs in an *in vitro* co-culture model and in an *in situ* model following direct injection of CFs into the left ventricle.

Initially, the development of a lentiviral (LV) vector which would allow overexpression of Cx43 in RACFs and was suitable for *in vitro* investigation as well as *in situ* imaging was investigated. The initial cloning strategy to develop a LV plasmid which would permit the expression of Cx43 and nuclear localised enhanced green fluorescent protein (eGFP) reporter under the control of an artificial hybrid α SMA reporter was unsuccessful. However, a functional adenoviral (Ad) vector overexpressing Cx43 was successfully produced and characterised.

Next, mediators that are known to be upregulated in disease and could consequently enhance Cx43 levels in CFs including angiotensin II (Ang II), transforming growth factor β 1 (TGF β 1), tumor necrosis factor α (TNF α), interleukin (IL)-1 β , IL-1 α and IL-6 alone or in combination with the soluble IL-6 receptor (sIL-6R) were investigated for the effect on Cx43 mRNA expression in RACFs. Among these: TGF β 1, IL-6 in combination with the sIL-6R, IL-1 β and IL-1 α significantly upregulated Cx43 mRNA expression. Both IL-1 β and IL-1 α induced a similar large increase in Cx43 mRNA, however due to indistinguishable actions, only IL-1 β was investigated further. IL-1 β was found to induce a morphological change and augment Cx43 protein levels where clear punctate Cx43 expression could be detected at cell contact points. This IL-1 β -induced Cx43 upregulation was shown to involve activation of IL-1 receptor (IL-1R), nuclear factor- κ B (NF- κ B), p38 mitogen-activated protein kinase (MAPK) and MAPK/extracellular signal-regulated kinase (ERK) kinase (MEK) 1/2 as inhibition of these proteins with the recombinant human IL-1 receptor antagonist, SC-514, SB203580 and AZD6244 respectively, partially prevented IL-1 β -induced Cx43 upregulation. Furthermore, inhibition of c-Jun N-terminal kinase (JNK) with SP600125 was demonstrated to potentiate the IL-1 β -mediated increase in Cx43, suggesting activation of JNK acts to suppress Cx43 upregulation.

IL-1 β has also been reported to inhibit TGF β 1-mediated CF activation to the MF phenotype. Therefore the effect of IL-1 β and TGF β 1 alone or in combination on the mRNA levels of TGF β 1-regulated genes including connective tissue growth factor (CTGF), α SMA, plasminogen activator inhibitor-1 (PAI-1) and the transcriptional repressors, Snail and Slug were investigated. IL-1 β was found to significantly reduce the mRNA expression of the MF makers CTGF and α SMA as well as partially inhibit TGF β 1-mediated significant or partial upregulation of these proteins.

Next, an adult CM: CF co-culture model was established by seeding freshly isolated rat adult CM on a RACF monolayer and cultured overnight. Evidence for functional GJs between the cell types was demonstrated by the transfer of the fluorescent dye, calcein, from CMs to CFs over 20 h. Furthermore RACFs were found to shorten the contraction duration (CD) but not significantly alter the action potential

duration at 80 % repolarisation (APD_{80}) of CMs in comparison to CMs cultured alone. Interestingly the effect on CD was dampened when the RACF monolayer was treated with IL-1 β prior to CMs addition.

Finally, a technically challenging model aimed at studying CM: CF interactions *in situ* was established. This involved the injection of RACFs which had been pre-transduced with a LV vector overexpressing eGFP (LVeGFP) into the left ventricular wall of the rat heart. Hearts directly injected with AdeGFP were used as a control so that eGFP could be detected in an optical mapping preparation 7 days following injection. Indeed, eGFP signals were observed in both groups (RACF and AdeGFP injected hearts) and action potentials (APs) recorded over the epicardial surface of the heart during both dynamic and extrastimulus (S1S2) pacing protocols. Although this study contained small *n*-numbers, there was a potential prolongation of APD_{80} following the S2 impulse in the injection site in comparison to a similar myocardial area. Additionally, altered activation pattern around the injection site following of the S2 impulse at the shortest S1-S2 intervals was identified in one heart from each group. As these observations were present in both groups this may suggest damage to the myocardium during the injection procedure, however this requires further investigation.

Overall, these studies provide further evidence that CFs are able to alter CM function in an *in vitro* adult co-culture model. Additionally, for the first time the altered phenotype of IL-1 β -treated RACFs was shown to weaken the effect of RACFs on the CD of CMs. Finally, a model to investigate the effects of RACFs on CM electrical activity *in situ* has been established and will be valuable for future studies.

Chapter 1 General introduction

1.1 The heart

The ultimate function of the heart is to pump oxygenated blood around the body. In order to complete this function the anatomy of the heart is expertly designed so that deoxygenated and oxygenated blood remain separated in the right and left side of the heart respectively. Each side consists of an atrium and ventricle which are separated by valves preventing premature blood flow from the atrium to the ventricle or back flow into the atrium during ventricular contraction. The left and right atria contract simultaneously followed by ventricular contraction. The right atrium receives deoxygenated blood from the body through the superior and inferior vena cava which, following atrial contraction, is pushed into the right ventricle. Blood then travels to the lungs following ventricular contraction through the pulmonary artery. Once oxygenated, blood returns to heart into the left atrium through the pulmonary veins, then on to the left ventricle which, following ventricular contraction, enters the aorta and vasculature to the rest of the body.

1.2 Cellular composition of the heart

The heart is a multicellular organ consisting of cardiac myocytes (CMs) and non-myocytes including; cardiac fibroblasts (CFs), vascular smooth muscle cells (VSMCs) and endothelial cells (ECs) (Banerjee et al. 2007). CMs are rod shaped muscle cells which constitute approximately 65-75 % of the cardiac volume (Ongstad and Kohl 2016). Fibroblasts are interspersed within the layers of CMs and are vital for maintenance of the cardiac structural network, mediating the synthesis and degradation of extracellular matrix (ECM) components (Ongstad and Kohl 2016). Finally, both VSMCs and ECs make up the vascular network of the heart, allowing blood supply to the myocardium. Discrepancy exists between studies exploring the contribution of cellular populations to the makeup of the myocardium. For instance, one study reported the murine heart to contain approximately 56 % CMs, 27 % CFs, 10 % VSMCs and 7 % ECs (Banerjee et al. 2007). In contrast, more recently Pinto *et al.* (2016) demonstrated that in the murine heart, ECs were the most abundant cell type constituting around 55 %, whereas CMs, CFs and VSMCs made up approximately 33 %, 13 % and 6 %, respectively (Pinto et al. 2016). These variations are likely to reflect differences in cell isolation techniques, use of cellular markers and detection methods. Despite this,

heterocellular crosstalk plays a vital role in cardiac function and following injury (Howard and Baudino 2014).

1.2.1 Cellular markers of fibroblasts in the heart

Fibroblasts are a difficult cell type to study due to their lack of specific cell markers. Fibroblast-specific protein 1 (FSP1), vimentin and discoidin domain receptor 2 (DDR2) have been used to identify CFs (Camelliti et al. 2005a; Santiago et al. 2010; Swaney et al. 2007); however their expression is not exclusive to fibroblasts. Untrue to its name, detection of FSP1, a cytoplasmic calcium (Ca^{2+}) binding protein, has been reported in other cell types in the heart including VSMCs, ECs and hematopoietic cells (Kong et al. 2013). Vimentin is a type III intermediate filament protein present in fibroblasts, endothelial cells and mesenchymal cells (Fan et al. 2012). DDR2, considered to be a more specific fibroblast marker, is a receptor tyrosine kinase activated by fibrillar collagens, including collagen types I and III (Goldsmith et al. 2004; Xu et al. 2011a). It has been shown to play roles in fibroblast proliferation and migration through the ECM (Olaso et al. 2002). The expression of DDR2 was reported to be present in CFs but not in the other major cardiac cells including; CMs, VSMCs and ECs (Goldsmith et al. 2004). Conversely, others have detected DDR2 expression in VSMCs (Shyu et al. 2008). Despite this, studies using vimentin or DDR2 antibodies to stain heart tissue have elegantly illustrated the presence of fibroblasts in the interstitial space between CMs (Camelliti et al. 2005a; Camelliti et al. 2005b; Goldsmith et al. 2004).

1.3 Electrical conduction and cardiac contraction

Coordinated cardiac contraction is required for the normal functioning of the heart. Electrical signals are generated by the hearts pacemaker cells in the sinoatrial node (SAN), which is located in the right atrium, and are transmitted through the atria causing atrial contraction. When signals reach the atrioventricular node (AVN), positioned in the right atrium at the intersection of the atria and ventricles, there is a slowing of conduction. This slowing is essential to allow time for the blood to pass from the atria to ventricles. The signals are then transmitted through the Bundle of His, bundle branches and Purkinje fibres, mediating uniform ventricular contraction (Figure 1-1).

Clinically, the electrical activity of the heart can be assessed by an electrocardiogram (ECG) (Figure 1-1). A healthy ECG will typically show three main aspects; the P wave, QRS complex and the T wave, each of which represents a different electrical event in the cardiac cycle. The T wave indicates atrial depolarisation, the QRS complex shows ventricular depolarisation and the P wave signals ventricular repolarisation (Becker 2006).

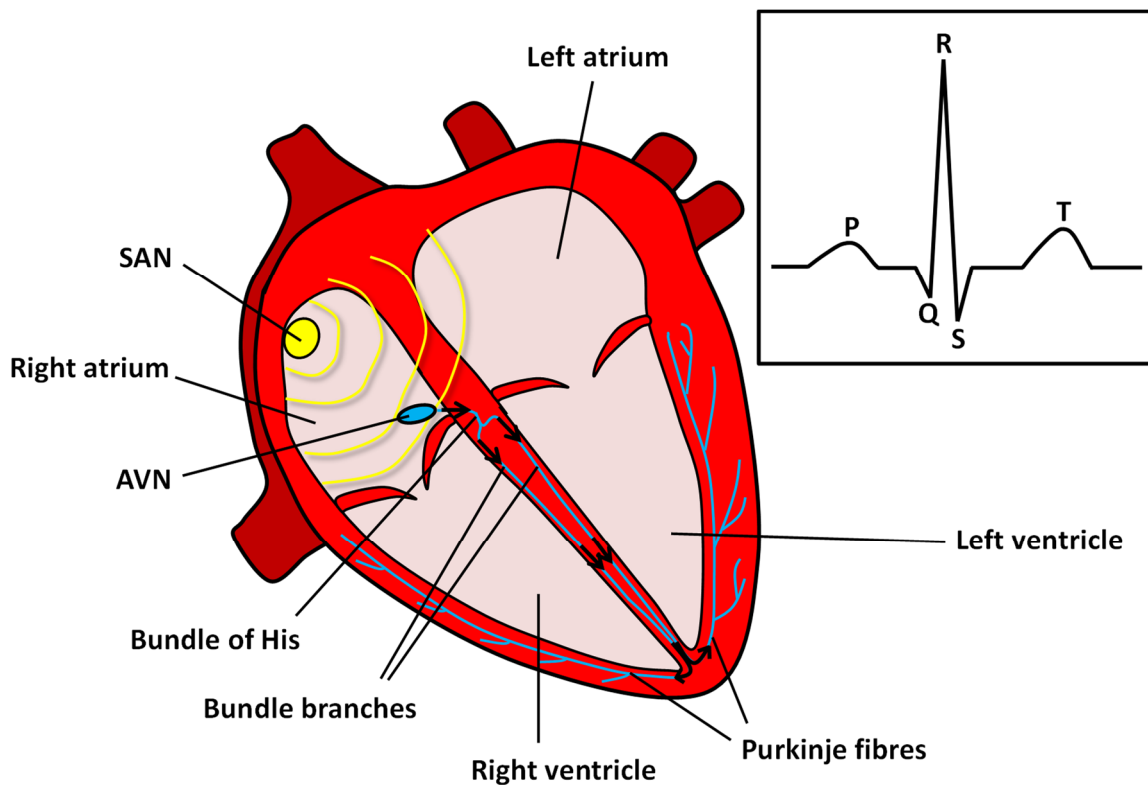


Figure 1-1 Electrical conduction through the cardiac cycle

Electrical impulses originate in the sinoatrial node (SAN), and pass through both atria causing them to contract. When the electrical impulse reaches the atrioventricular node (AVN), the signal travels through the bundle of His, the bundle branches and down to the purkinje fibres where the ventricles then contract. A typical electrocardiogram (ECG) trace with P, QRS and T waves depicted is shown. (This figure, with modifications, was originally published in McArthur et al. 2015)

1.3.1 Cardiac action potential

Although the shape of the ventricular action potential (AP) differs between species and within different areas of the heart, 5 phases (0-4) can be observed, each of which represents voltage changes in the membrane potential when a cell is activated by a cardiac impulse (Figure 1-2). This is created by a change in the permeability of different ion channels on the sarcolemma of the CM (Grant 2009). In the resting state (phase 4) the cell has very low permeability to sodium (Na^+) and Ca^{2+} relative to potassium (K^+), the three major ions involved in AP formation. This along with the action of ion pumps, establishes an electrochemical gradient whereby the extracellular concentration of Na^+ and Ca^{2+} is greater than the intracellular concentration. Conversely, ion pumps maintain a high K^+ concentration within the cells (Nattel and Carlsson 2006). During the AP upstroke (phase 0) the cell is rapidly depolarised from the resting membrane potential (RMP) which is approximately -90 mV to above 0 mV (Grant 2009). This rapid depolarisation, in response to stimulus, is a consequence of voltage-gated Na^+ channels opening and creating a Na^+ inward current (I_{Na}) in the cell which is then quickly inactivated. Depolarisation induces the opening of the L-type Ca^{2+} channels (LTCCs) to allow an inward Ca^{2+} current (I_{CaL}) resulting in Ca^{2+} induced Ca^{2+} release (CICR) from the sarcoplasmic reticulum (SR) (section 1.3.2) (Kleber and Rudy 2004). The cell is then slightly repolarised by the fast activated outward K^+ currents; transient-outward (I_{to}) and the ultra-rapid (I_{Kur}) inducing phase 1 of the AP. The plateau of the AP (phase 2) is caused by the balance of the inward Ca^{2+} and outward K^+ currents (Nattel and Carlsson 2006). The rising rapid and slow outward delayed K^+ currents (I_{Kr} and I_{Ks} respectively) during the plateau phase and following inactivation of the LTCCs induces the repolarisation of the cell back to the RMP (phase 3) (Kleber and Rudy 2004). The relationship between the AP, Ca^{2+} transient and contraction is shown in Figure 1-2.

Immediately after AP firing, CMs are unexcitable until a midpoint in repolarisation, known as the effective refractory period (ERP). The ERP is a consequence of Na^+ channel inactivation, and only when enough channels have recovered can another AP fire (King et al. 2013). This inactivity can prevent a premature stimulus eliciting an electrical impulse. The ERP is just short of the AP duration (APD), described as the time from the onset of phase 0 to full repolarisation back to the RMP (Burton

and Cobbe 2001). Experimentally, a percentage of the repolarisation is often used, for instance the APD at 90 % repolarisation (APD₉₀), due to difficulties in accurate detection of 100 % repolarisation. Within the intact heart some degree of dispersion, difference between the longest and shortest repolarisation time, exists (Burton and Cobbe 2001). For instance APD was shorter at the apex and progressively longer towards the base in guinea pig hearts (Choi and Salama 2000). A mean left ventricular apex to base dispersion of 42 ms in healthy human hearts under physiological conditions has been also reported (Ramanathan et al. 2006). Dispersion is also seen through the myocardial wall, known as transmural dispersion. The presence of electrically distinct M cells in the midmyocardium, which have a more prolonged APD than sub-epicardial and sub-endocardial cells, are thought to be a major contributor to this (Antzelevitch 2010). Additionally, the activation pattern influences the APD or activation-recovery intervals (ARI), as demonstrated by generally greater APD/ARI closer to the activation site which gets progressively shorter further from the activation site (Franz et al. 1987; Hanson et al. 2009; Myles et al. 2010; Yuan et al. 2001).

1.3.2 Excitation-contraction coupling

Excitation-contraction coupling (ECC) is the process whereby electrical signals lead to the contraction of CMs and ultimately the heart as a whole. Ca²⁺ is integral for contraction. When the CM is depolarised, voltage sensitive LTCCs open in response to the change in voltage and Ca²⁺ enters the cell (Figure 1-3) (Bers 2002). LTCCs are preliminary located on transverse tubules (T-tubules) as demonstrated by their close proximity with the ryanodine receptor (RyR) throughout the cell, not only at the cell surface (Scriven et al. 2000). An increase in intracellular Ca²⁺ concentration ([Ca²⁺]_i) induces the opening of the RyRs which are located on the SR, a major intracellular Ca²⁺ store. This promotes CICR from the SR, resulting in a further increase in [Ca²⁺]_i (Banerjee et al. 2007). High [Ca²⁺]_i acts in a negative feedback loop to close LTCCs and the RyRs (Bers 2002).

CM contraction requires the movement of the thin filament (actin) along the thick filament (myosin), which are arranged into many contractile units termed sarcomeres. Each sarcomere also contain regulatory proteins (troponin and tropomyosin [Tm]) and cytoskeletal proteins (titin and myosin binding protein C)

(Yin et al. 2015). Contraction is initiated when Ca^{2+} binds to the Ca^{2+} -binding subunit of the troponin complex, cardiac troponin C (cTnC), inducing a conformational reorganisation of the other troponin subunits including the inhibitory cardiac troponin I (cTnI) and the Tm-binding cardiac troponin T (cTnT). This leads to the movement of Tm, revealing a myosin-binding site on actin. Consequently, a cross bridge between the myosin head and actin is established. Energy from ATP is then utilised by the myosin head to complete a power stroke, moving actin along the myosin filament (Yin et al. 2015). The myosin head then detaches from actin and the process is repeated, known as cross bridge cycling, producing further cell shortening. For relaxation to occur, Ca^{2+} must leave the cytosol leading to dissociation from cTnC. This is mediated through four main Ca^{2+} handling proteins including the sarcolemmal $\text{Na}^+/\text{Ca}^{2+}$ exchanger (NCX), sarcolemmal Ca^{2+} -ATPase, mitochondrial Ca^{2+} uniport and the SR Ca^{2+} -ATPase (SERCA) (Bers 2002). Both the mitochondrial Ca^{2+} uniport and SERCA mediate uptake of cytosolic Ca^{2+} into the mitochondria and the SR respectively for storage until the next stimulus (Bers 2002). SERCA is inactive when the inhibitory protein, phospholamban (PLN), is bound its dephosphorylated form. However upon phosphorylation of PLN, by mainly protein kinase A (PKA) or Ca^{2+} /calmodulin (CaM)-dependent protein kinase II (CaMKII), PLN dissociates from SERCA allowing activation, hence Ca^{2+} uptake into the SR (Lou et al. 2012). Conversely, the NCX and the sarcolemmal Ca^{2+} -ATPase are involved in the transfer of Ca^{2+} out of the cell by exchanging one Ca^{2+} ion inside the cell for three extracellular Na^+ ions and using adenosine triphosphate (ATP) to actively extrude intracellular Ca^{2+} , respectively (Bers 2002).

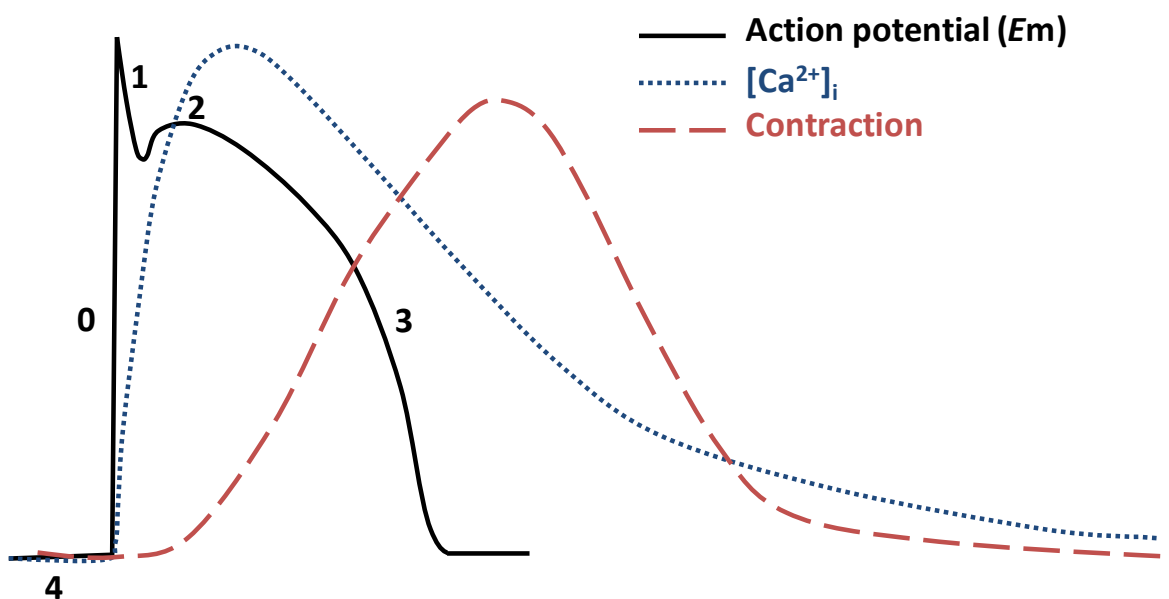


Figure 1-2 Ventricular cardiac myocyte action potential, calcium influx and contraction. The phases of the action potential and its relationship with intracellular calcium concentration and contraction in a rabbit cardiac myocyte are shown. E_m ; membrane potential.

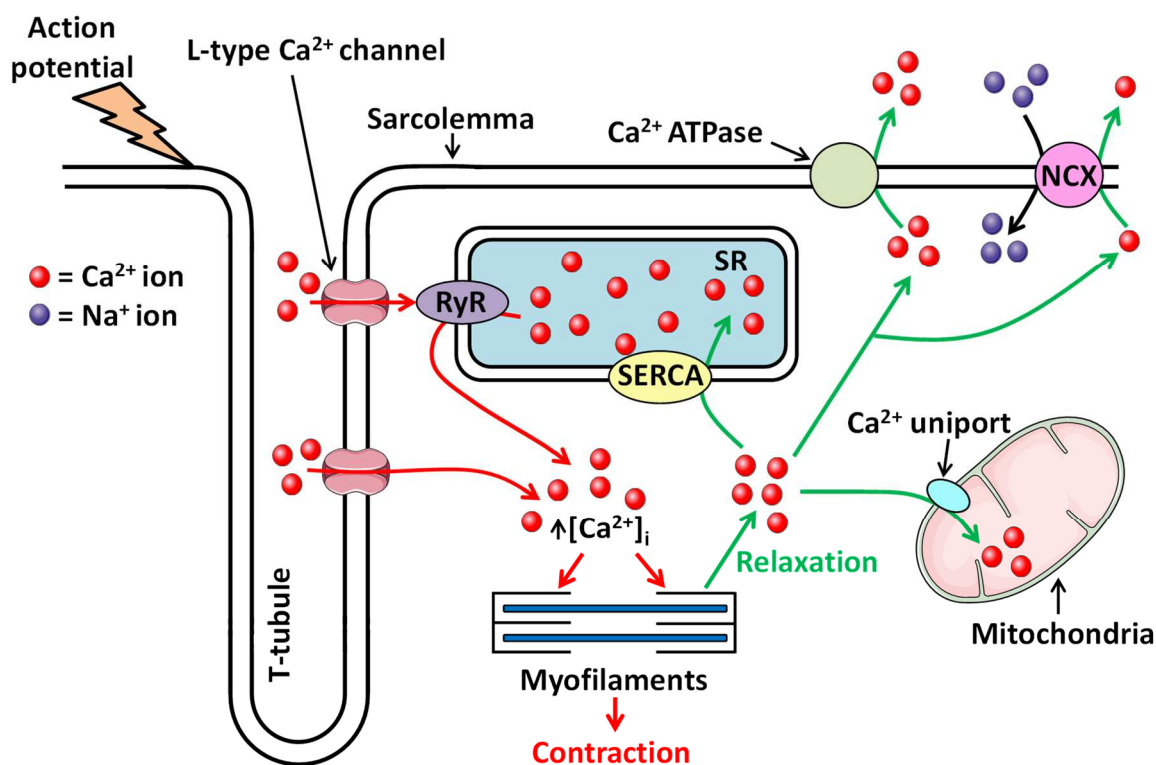


Figure 1-3 Cardiac myocyte calcium handling.

Red and green arrows represent Ca^{2+} influx and efflux respectively. Ca^{2+} ; calcium, Na⁺; sodium, RyR; ryanodine receptor, SR; sarcoplasmic reticulum, SERCA; sarcoplasmic reticulum Ca^{2+} -ATPase, NCX; sodium- calcium exchanger.

1.4 The intercalated disc

Coordinated contraction of the heart relies on both mechanical and electrical coupling, in which the so called 'intercalated discs' (IDs) play an essential role. IDs are located at the long ends of CMs and are made up of three main junctions: adherens junctions (AJs), desmosomes and gap junctions (GJs) (Figure 1-4). Both AJs and desmosomes mediate mechanical coupling, whereas GJs allow electrical coupling (Noorman et al. 2009).

1.4.1 Adherens junctions and desmosomes

Mechanical junctions are essential for the maintenance of the structural integrity of the heart. AJs consist of the transmembrane protein cadherin, N-cadherin being the main form at IDs, and cytosolic catenins; including α , β , γ (plakoglobin) and p120 isoforms which allow interaction with actin filaments (Noorman et al. 2009). AJs are important in maintaining CM connections during contraction and assist in the transfer of contractile force between cells due to the indirect coupling of the intercellular actin cytoskeleton (Noorman et al. 2009).

Conversely, desmosomes assist in structural support due to the interaction of cytosolic components with intermediate filaments. Desmosomes are made up of the two transmembrane desmosomal cadherins; desmocollin and desmoglein as well as the cytosolic proteins; plakoglobin, plakophilin and desmoplakin. Desmoplakin is responsible for intermediate filament association (Noorman et al. 2009).

1.4.2 Gap junctions and cardiac connexins

Electrical signals are transferred through the conduction system and on to CMs through GJs. GJs consist of numerous channels between cells allowing the passage of ions, second messengers and molecules up to 1 kDa (Zhou and Jiang 2014). This permits rapid signalling and co-ordinated cardiac contraction. GJs are predominately expressed at IDs however are also present at the lateral sides of CMs (Gutstein et al. 2001). Conduction is faster in the longitudinal in comparison to transverse direction (Valderrabano 2007), known as anisotropy which was first described in 1959 (SANO et al. 1959).

1.4.2.1 The structure of connexin channels

GJ channels consist of two hemi-channels, one from each of the contiguous cells. The basic component of hemi-channels are connexin (Cx) proteins which exist as four membrane spanning domains, two extracellular loops, an intracellular loop and cytosolic amino- and carboxyl-terminal (CT) tails (Figure 1-5) (Sohl et al. 2005). Six connexin proteins constitute a hemi-channel, which then docks onto another hemi-channel from a participating cell to form a GJ channel (Sohl et al. 2005) (Figure 1-5). In the heart, there are three main connexins; Cx40, Cx43 and Cx45 which are encoded by GJA5, GJA1 and GJA7 genes, respectively (Sohl and Willecke 2004). Hemi-channels can be composed of one connexin subtype or can be an arrangement of different connexins where they are then referred to as homomeric or heteromeric, respectively. The docking of two identical or dissimilar hemichannels are called homotypic or heterotypic GJ channels, respectively (Moreno 2004) (Figure 1-5).

A GJ consists of a few to thousands of GJ channels clustered together to form junctional plaques (Sosinsky and Nicholson 2005). These plaques were first visualised in the 1960s using the heavy metal, lanthanum, which fills the extracellular spaces allowing regions of cell contact points that are interconnected to remain free from lanthanum (Revel and Karnovsky 1967). Structures evidently distinct from so called tight junctions, that lanthanum cannot penetrate, were identified as GJs (Sosinsky and Nicholson 2005).

1.4.2.2 Distribution of connexin subtypes

Although the distribution of connexin subtypes varies between species (van Kempen et al. 1995), Cx43 is the most widely expressed connexin throughout both the atria and ventricles (Vozzi et al. 1999). Cx40 is highly expressed in healthy atrial tissue and throughout the conduction system (Dupont et al. 2001; van Rijen et al. 2001; Vozzi et al. 1999), while Cx45 is most abundant in the AVN and also expressed in healthy myocardium (Frank et al. 2012; Kreuzberg et al. 2009; Vozzi et al. 1999).

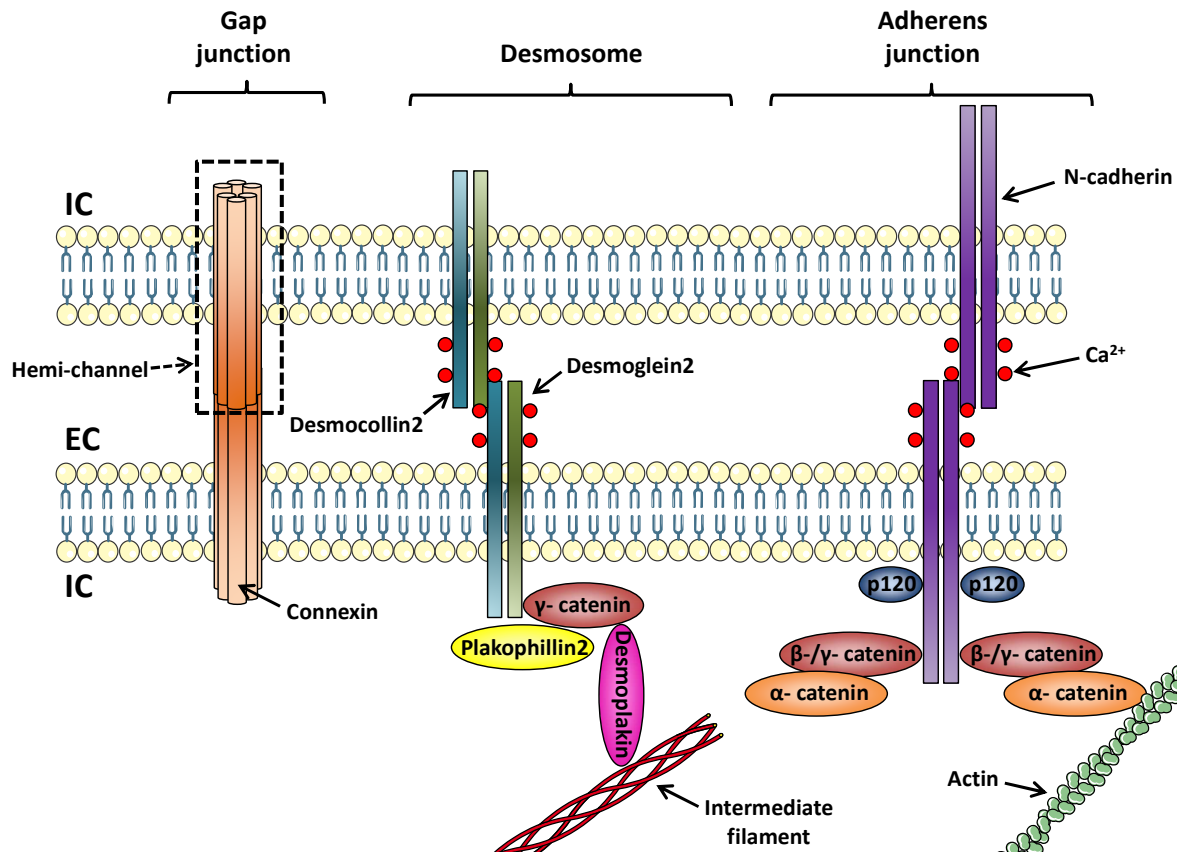


Figure 1-4 Major components of the intercalated disc.

The intercalated disc consists of three major junctions; gap junctions, desmosomes and adherens junctions. IC; intracellular, EC; extracellular, Ca^{2+} ; calcium.

1.4.3 Importance of intercalated disc components

Embryonic or neonatal lethality is common in homozygous knockout (KO) mouse models of ID proteins including; γ -catenin (Ruiz et al. 1996), desmoplakin (Garcia-Gras et al. 2006) and Cx43 (Reaume et al. 1995). Additionally, a loss of function mutation in N-cadherin in mouse embryos results in death by day 10 of gestation (Radice et al. 1997). Interestingly, the disruption of the ID has been reported in an N-cadherin conditional knockout (CKO) mouse model (Kostetskii et al. 2005). Here, cardiac specific tamoxifen-induced deletion of N-cadherin resulted in additional loss of the AJ and desmosomal components; α , β , γ and p120 catenins and desmoplakin (Kostetskii et al. 2005). Furthermore, Cx40 and Cx43 levels were reduced in the atrial and ventricular tissue, respectively (Li et al. 2005). Not surprisingly, sudden cardiac death (SCD) as a result of ventricular arrhythmias was observed between 1-2 months of tamoxifen treatment (Li et al. 2005). Additionally, Cx43 was shown to be reduced following adenoviral (Ad) mediated silencing of plakophilin 2 in neonatal rat CMs (Oxford et al. 2007) and in the human genetic conditions Naxos disease (Kaplan et al. 2004b) and Carvajal syndrome (Kaplan et al. 2004a) caused by mutations in plakoglobin and desmoplakin, respectively. Together this work suggests mechanical junctions assist in the formation of GJs. This is in agreement with the report that mechanical junctions are formed prior to GJ formation in a dedifferentiation adult rat CM culture model (Kostin et al. 1999) as well as in the postnatal development of the rat heart (Angst et al. 1997). Conversely, in human heart maturation GJ and AJ formation appears to occur simultaneously (Peters et al. 1994). However, due to the nature of limited stages in postnatal samples in this human study, AJ formation prior to GJ formation cannot be ruled out.

Despite regulation of connexins by mechanical junction proteins, the cardiac-specific CKO of Cx43 in mice does not alter the expression or cellular localisation of AJ or desmosomal components (Gutstein et al. 2003); suggesting GJs are not involved in the formation of these mechanical junctions. Cx45 homozygous KO mice die during embryogenesis from heart failure, suggesting a major role in heart development (Kumai et al. 2000). Although Cx40^{-/-} mice are viable, 50 % die in embryonic development and a further 16 % die shortly after birth (Kirchhoff et al. 2000). Viable Cx40^{-/-} mice show abnormalities in conduction

with prolongation in ECG PR interval, QRS complex and the QT interval, potentially reflecting issues in the conduction system where Cx40 is known to be abundant (Simon et al. 1998).

While a Cx43^{-/-} genotype is lethal, studies using Cx43^{+/-} mice have reported contradictory effects on cardiac electrical activity. For instance no alteration in ventricular conduction velocity (CV), as determined by optical mapping (OM), or ECG parameters in comparison to wild type (WT) controls were observed (Morley et al. 1999). Additionally, only small differences in ECG parameters were detected in these mice by others (Kirchhoff et al. 2000). Conversely, in other studies Cx43^{+/-} mice had a slowed CV (Guerrero et al. 1997) as well as the development of lethal arrhythmias in a cardiac specific Cx43 CKO model (Gutstein et al. 2001). Despite this controversy, disorganised Cx43 expression is associated with disease and enhances the susceptibility for ventricular arrhythmias (Kostin et al. 2003; Poelzing and Rosenbaum 2004; Smith et al. 1991) (section 1.6.2.1), suggesting a fundamental role of Cx43 in normal cardiac conduction.

1.5 Connexin channel regulation

Connexins are well established to have a rapid turnover rate, which is around 1-3 h for Cx43 (Beardslee et al. 1998; Hunter et al. 2005; Laird et al. 1991; Saffitz et al. 2000). This is mediated by a balance of synthesis and degradation, where both the proteasome and lysosome are implicated in the degradation of Cx43 (Laing et al. 1997). As well as the levels of connexin at the cell surface, the composition of GJ channels can affect the channel properties including conductance, permeability and selectivity. Many factors are also known to contribute to the regulation of channels including voltage, pH, calcium and phosphorylation (Hood et al. 2017; Peracchia 2004). Channels are known to exist in an open state where maximal conductance can be achieved, a residual or sub-conductance state where approximately 5-35 % conductance occurs depending on the connexins constituting the channel (Moreno et al. 2002) and a closed state where conductance is zero. The exact mechanism for channel inactivation and closure still remains to be fully elucidated however two main mechanisms may provide an explanation. The transition from open to residual state, also referred to as fast gating, may be explained by the ball-and-chain hypothesis where a region of the intracellular

domains, most likely the CT tail interacts with the channel pore ultimately reducing conductance (Moreno et al. 2002). Slow gating, also referred to as loop gating, of connexin channels is where the channel transitions from an open state to a fully closed state, has been suggested to be a result of conformational change involving the extracellular loops of connexin subunits (Bukauskas and Verselis 2004).

1.5.1 Voltage gating

The gap junctional conductance (g_j) influences the CV between cells, with a greater g_j producing a faster CV (Shaw and Rudy 1997), and is therefore important to consider in the electrical conduction between cells. G_j is regulated by transjunctional voltage (V_j), which is defined as the difference in voltage between two cells participating in a GJ (Bukauskas et al. 2002). This can be examined experimentally by voltage clamping two contiguous cells with separate patch clamps. The voltage of each cell can then be modulated and g_j monitored at varying V_j . Typically Cx40, Cx43 and Cx45 homomeric, homotypic channels have been reported to have maximal conductance when V_j is equal to zero. As the V_j deviates from zero in a positive or negative direction the conductance reduces in a sigmoidal fashion (Figure 1-6) (Barrio et al. 1997;Bukauskas et al. 2002;Desplantez et al. 2011;Lin et al. 2003). Interestingly, conductance with varying V_j does not reach an absolute zero with maximal V_j ; instead a residual state exists (Figure 1-6) (Moreno 2004). The voltage sensor for the residual state has been proposed to be located on the amino-terminal tail of connexin proteins (Verselis et al. 1994), and the CT tail has been suggested to be the effector (Moreno et al. 2002). Replacement of the charged amino acids at residues 12 and 13 on the amino terminal tail of Cx40 and Cx43 to glycine and serine (uncharged amino acids) respectively has been shown to reduce voltage gating in response to changes in V_j . This effect is more pronounced in Cx43 mutant channels, whereby very little voltage gating occurs with changes in V_j (Gemel et al. 2006). Truncation of the CT tail of Cx43 has been shown to prevent the induction of the residual state, which is recovered when the Cx43 CT tail is co-expressed (Moreno et al. 2002). Furthermore, the rate of transition between open and closed states in cells expressing this truncated form of the Cx43 CT tail is prolonged (Moreno et al. 2002).

The inactivation kinetics of V_j in connexin GJs is thought to be too slow to influence AP propagation. The effect of an AP on the conductance and current through Cx43 GJs has been investigated in neuro2A neuroblastoma (N2A) cells transfected with Cx43 (Lin et al. 2003). Two adjoining cells were voltage patch clamped, a ventricular AP mimicked in one of the cells while the other was maintained at the diastolic resting potential and the properties of the connexin GJ channels examined. The junctional current was shown to follow a similar trend to the AP, in terms of upstroke, plateau and recovery. Conversely conductance was shown to have a rapid increase from 0 to 4.1 nS during the AP upstroke, followed by an initial rapid downstroke which slowed to a plateau of 1.6 nS. Conductance was shown to recover in phase 3 of the AP as the V_j proceeded towards zero (Lin et al. 2003).

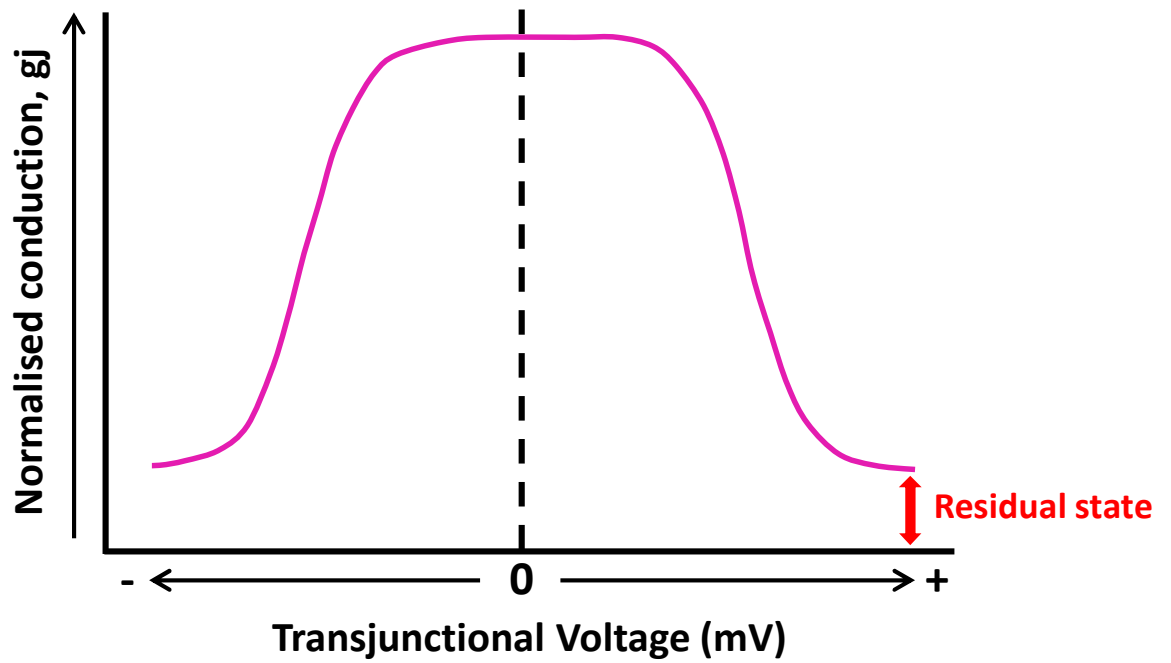


Figure 1-6 Typical relationship between gap junctional conduction and transjunctional voltage.

Maximal gap junctional conductance (g_j) is typically observed when there is no difference in voltage between two of the participating cells; that is the transjunctional voltage is equal to zero. As the voltage is increased or decreased in one of the cells, transjunctional voltage becomes more positive or negative respectively, and the g_j decreases symmetrically in both directions until the residual state of the channel is reached.

1.5.2 Chemical gating

High $[Ca^{2+}]_i$ and low intracellular pH (pH_i) are known to regulate negatively regulate g_j (Peracchia 2004). As both these conditions are known to occur following ischaemia, this may be a protective mechanism in disease to prevent the movement of damaging mediators to adjacent cells (Kalogeris et al. 2012). Gating by Ca^{2+} has been demonstrated in N2A cells in physiological Ca^{2+} solution following the addition of ionomycin, a reagent which acts to enhance $[Ca^{2+}]_i$, produced a 95 % reduction in Cx43 g_j (Xu et al. 2012). In contrast, Cx40 g_j was only reduced by <20 %, signifying Cx40 is less sensitive to $[Ca^{2+}]_i$. Interestingly, g_j in mouse neonatal atrial and ventricular CMs declined by 73 % and 93 % respectively, suggesting less contribution of Cx43 in GJs in atrial cells in comparison to ventricular CMs (Xu et al. 2012). These effects of $[Ca^{2+}]_i$ on g_j has been reported to be mediated through the Ca^{2+} binding protein, CaM, where inhibitors of CaM have resulted in inhibition of Ca^{2+} -dependent uncoupling (Lurtz and Louis 2007; Xu et al. 2012). Additionally, a CaM binding site has been identified on the intracellular loop of Cx43, supporting this interaction (Zhou et al. 2007).

Similarly, as the pH_i is reduced from physiological pH 7.4, uncoupling of connexin channels has been identified (Morley et al. 1996; Stergiopoulos et al. 1999). The CT tail of some connexin subtypes, such as Cx40 and Cx43, has been identified as an important mediator of this pH_i -induced uncoupling (Stergiopoulos et al. 1999). For instance, in *Xenopus* oocytes overexpressing a truncated form of the Cx40 or Cx43 CT tail, there is little to no change in g_j when the pH_i is reduced (Stergiopoulos et al. 1999). Comparatively, when the CT tail is re-introduced into these cells the effect of pH_i is restored, suggesting the CT tail acts in a ball-and-chain mechanism or as an intermediate molecule to decrease channel activity (Morley et al. 1996; Stergiopoulos et al. 1999). This however is not the case for Cx45, where g_j displays the same relationship with pH_i in both WT and truncated forms (Stergiopoulos et al. 1999).

1.5.3 Regulation of connexin channels by phosphorylation

Phosphorylation and dephosphorylation of the CT tail of connexin proteins play an essential role in the properties of the GJ channels, which can become dysregulated in disease (Hood et al. 2017). Cx43 primarily exists in a phosphorylated form in healthy hearts (Beardslee et al. 2000), where at least 19 different phosphorylation sites have been identified (Solan and Lampe 2014). Many protein kinases including PKA, protein kinase C (PKC) and casein kinase 1 have been reported to phosphorylate Cx43 (Hood et al. 2017) which may differentially regulate GJ intercellular communication (GJIC). For instance an increase in PKA activity has been shown to enhance GJIC (Matsumura et al. 2006), while PKC has been demonstrated to reduce GJIC by phosphorylating the serine residue (Ser) 368 (Lampe et al. 2000). Interestingly, phosphorylation of Ser368 has been reported to be enhanced in mouse hearts following ischaemia (Ek-Vitorin et al. 2006; Hund et al. 2007). Conversely, in an isolated rat heart model of ischaemia, complete dephosphorylation of this site within 30 min was shown, highlighting discrepancies between species and/or ischaemic models (Axelsen et al. 2006). Furthermore, dephosphorylation of numerous other sites including Ser306, Ser297 and Ser365 have been associated with ischaemia, electrical uncoupling and slowed CV (Hood et al. 2017). Protein phosphatases (PP) including type 2A (PP2A) and type 1 (PP1) mediate this dephosphorylation resulting in reduced GJIC and enhanced vulnerability to arrhythmias (Ai and Pogwizd 2005; Beardslee et al. 2000; Boulaksil et al. 2016; Remo et al. 2011).

1.6 The diseased heart

Cardiovascular disease (CVD) is the leading cause of morbidity worldwide according to the World Health Organisation (WHO). In 2015, approximately 17.7 million deaths occurred from CVD; around 7.4 million of these were attributed to coronary heart disease (CAD), a disease of the coronary arteries (WHO 2017). Narrowing or blockage of a blood vessel in the heart can lead to ischemia in a region of heart muscle ultimately causing a myocardial infarction (MI), defined as the death of CMs as a result of extended ischemia (Thygesen et al. 2012). The major cause of MI is atherosclerosis, where an accumulation of lipids, ECM and a variety of inflammatory cells within the inner lining of the

vascular wall form an atherosclerotic plaque (Hansson 2005). As the plaque develops, blood flow can be severely disrupted by remodelling of the plaque into the lumen, limiting downstream perfusion. Additionally, plaque rupture is common when the fibrosis cap is thinned or damaged which ultimately results in exposure of pro-thrombotic factors into the circulation leading to a coronary thrombosis and occlusion of the vessel (Hansson 2005). Following ischaemia, re-establishment of blood flow via thrombolytic therapy or primary percutaneous coronary intervention is mandatory in order to limit the size of myocardial infarct (Yellon and Hausenloy 2007). Paradoxically, complex events associated with reperfusion can aggravate tissue damage, produce ventricular arrhythmias and consequently lead to cardiac dysfunction, commonly described as ischaemia/reperfusion (I/R) injury (Ferdinandy et al. 2007).

CAD is not a prerequisite for MI; an imbalance between oxygen supply and demand due to an underlying condition such as coronary spasm, cardiac arrhythmia or high blood pressure (hypertension) can also result in a MI (Thygesen et al. 2012). The increased strain on the heart as a consequence of other areas of the cardiac muscle compensating for the impaired function of an ischemic region and or other contributing factors such as hypertension can result in progression towards heart failure (HF) (Burchfield et al. 2013). HF is defined as heart malfunction resulting in breathlessness, premature fatigue and/or oedema (Heineke and Molkentin 2006). Not surprisingly, infarct size has been shown to predict mortality (Burns et al. 2002; Miller et al. 1995). One study reported a 7 % mortality rate when the infarct size was ≥ 12 % of the left ventricle (median infarct size), conversely there were no patients deaths where the infarct size was < 12 % (Miller et al. 1995).

1.6.1 Pathological cardiac remodelling

It is well established that the heart remodels in response to pathological stimuli including MI, myocarditis and pressure or volume overload, for example hypertension and valvular regurgitation, respectively (Cohn et al. 2000). This process involves many molecular, cellular and ECM modifications (Cohn et al. 2000). Following ischaemia, the remodelling process acts to replace dead myocytes with scar tissue. However, this can become maladaptive if inflammation, fibroblast activation and ECM degradation and production persist.

Ultimately these events can lead to pathological cardiac fibrosis, hypertrophy and the development of HF (Burchfield et al. 2013).

1.6.1.1 Changes in ECM in cardiac remodelling

The cardiac ECM is essential for maintaining the structural integrity of the heart. It is composed of both fibrous proteins; such as collagen, laminin and elastins, and non-structural proteins; including glycoproteins, proteoglycans and glycosaminoglycans. Collagens are produced primarily by fibroblasts as procollagen, where they are then cleaved in the extracellular space to collagen. Collagen type I is the most abundant collagen within the heart, although other subtypes including type III and IV exist. The levels of collagen are known to be up-regulated in many animal models of cardiac disease including MI (Cleutjens et al. 1995b), dilated cardiomyopathy (DCM) (Fedak et al. 2003) and pressure overload (Jalil et al. 1989). In a rat model of MI, procollagen type I and III mRNA, precursors of collagen type I and III, were shown to be upregulated 4 and 2 days post-MI in the infarcted left ventricle, respectively. Interestingly, procollagen mRNA was also shown to be upregulated in the right ventricle and ventricular septum, albeit to a lesser extent (Cleutjens et al. 1995b), suggesting remodelling of the whole heart in response to MI. A combination of increased collagen levels, a greater collagen type I to type III ratio and an increase in collagen crosslinking may contribute to myocardial stiffness (Badenhorst et al. 2003; Nishikawa et al. 2001; Yamamoto et al. 2002; Zile et al. 2015). Myocardial stiffness can contribute to diastolic dysfunction (Chaturvedi et al. 2010) and is a good indicator of congestive heart failure patients (CHF) mortality (Watanabe et al. 2011), hence an important therapeutic target.

Wall thinning and left ventricular dilatation, risks for cardiac rupture (Schuster and Bulkley 1979), occur soon after the onset of a MI (Olivetti et al. 1990). This involves the degradation of the existing ECM mediated by a balance between zinc-containing matrix metalloproteinases (MMPs) and endogenous tissue inhibitors of MMPs (TIMPs). MMPs are a family of proteases which degrade the ECM components and can be subcategorised depending on the substrate specificity (Phatharajaree et al. 2007). These include collagenases (e.g MMP-1), gelatinases (MMP-2 and MMP-9) and stromelysins (MMP-3 and MMP-10), which typically degrade collagen,

gelatin and a range of ECM components respectively, although there are some exceptions (Phatharajaree et al. 2007). The activities of MMPs are known to be enhanced in animal models of numerous pathological cardiac conditions including DCM (Fedak et al. 2003) and MI (Cleutjens et al. 1995a). MMP1 activity has been reported to be significantly upregulated as early as 2 days post-MI (Cleutjens et al. 1995a), where a further increase to 6.5 fold above sham controls following 7 days from the onset of MI. A return to control levels was reported 14 days post MI. This trend was similar for both MMP2 and MMP9 (Cleutjens et al. 1995a). KO of MMP2 or MMP9 in mice has been shown to be protective against myocardial rupture following MI (Hayashidani et al. 2003; Heymans et al. 1999; Matsumura et al. 2005), indicating a role for these enzymes in detrimental remodelling.

The levels and/or activity of TIMPs are also known altered in cardiac remodelling. The protein levels of TIMP-1 and TIMP-3 have been reported to be significantly increased and decreased, respectively in DCM (Fedak et al. 2003). Interestingly, TIMP3^{-/-} mice developed CM hypertrophy, contractile dysfunction and left ventricular dilatation with aging (Fedak et al. 2004), a phenotype which is typical of DCM. Hampered expression of TIMP-3 has also been shown in end-stage HF patients (Fedak et al. 2003).

1.6.1.2 Cardiac fibrosis and fibroblast to myofibroblast differentiation

Cardiac fibrosis manifests as excessive deposition of ECM components, mainly collagen, within the myocardium (Wang et al. 2015). It can occur to replace dead CMs such as following ischaemia, so called replacement fibrosis or within the interstitial space in areas other than the infarct (Czubryt 2012; Nguyen et al. 2013). Interstitial fibrosis can also occur in cardiac injuries such as pressure or volume overload (de Meester de et al. 2015; Xia et al. 2009) and can develop into replacement fibrosis following necrosis of surrounding CMs (Travers et al. 2016). This can produce areas of patchy fibrosis, whereby surviving CM strands are located between dense scar tissue. Perivascular fibrosis seen in pressure overload animal models (Harada et al. 1998; Xia et al. 2009) is thought to reduce the supply of oxygen and nutrients to the myocardium.

A key cell in the development of fibrosis is the myofibroblast (MF). MFs are the activated form of the fibroblast, which express the contractile protein alpha smooth muscle actin (α SMA); the actin subtype present in smooth muscle cells (SMCs). However, although MFs express the actin subtype present in SMCs, the contraction in SMCs is rapid and short in duration whereas MF contraction is more prolonged and results in wound closure, suggesting different mechanisms between the cell types (Bochaton-Piallat et al. 2016). Indeed, in comparison to SMCs, increasing $[Ca^{2+}]_i$ to activate myosin light chain kinase (MLCK), the kinase important for myosin light chain phosphorylation and contraction, was not sufficient to induce MF contraction. Rho/Rho kinase activity was shown to be essential for MF contraction (Parizi et al. 2000). Additionally, α SMA expression in MFs has been shown to positively correlate with enhanced contraction (Hinz et al. 2001). MFs are absent in the healthy myocardium and only transdifferentiate from resident CFs or other cell types following cardiac insult (Kanisicak et al. 2016). The time course for the appearance of MFs in infarcted regions of the heart has been shown to differ between species. For instance in a *in vivo* mouse model of I/R, MF infiltration occurs rapidly within the first 72 h of reperfusion, where the numbers then progressively decline between 7 and 14 days (Dewald et al. 2004). In contrast MF infiltration in a canine I/R model is slower, where very little MFs were detected in the infarct at 72 h. However, substantial increases in MFs were reported after 7 days, which was negligible at 14 days reperfusion (Dewald et al. 2004). Additionally, CFs isolated from animal models of cardiac injury including a rat transverse aortic constriction (TAC) model (Cartledge et al. 2015) and a canine CHF model (Dawson et al. 2012) have been shown to express α SMA, supporting CF-to-MF conversion *in vivo* in response to injury.

Interestingly major contributors to cardiac fibrosis including angiotensin II (Ang II), endothelin-1 (ET-1) and transforming growth factor β (TGF β 1) (Li et al. 2007; Rosenkranz et al. 2002; Widyantoro et al. 2010) have been demonstrated to induce CF-to-MF conversion (Bai et al. 2013; Bronnum et al. 2013; Nishida et al. 2007). TGF β is known to be up-regulated in pathological cardiac conditions such as following an MI (Deten et al. 2001; Dewald et al. 2004). As well as promoting α SMA expression, TGF β 1 increases the contraction of collagen gels and promotes

the production of collagen I and fibronectin by CFs (Chen et al. 2000;Lijnen et al. 2003).

TGF β 1-mediated MF transdifferentiation has been reported to occur through Smad3 signalling, a protein classically activated by TGF β 1 (Dobaczewski et al. 2010;Hu et al. 2003). Although Smad3^{-/-} mice had an increased number of MFs in the infarct following MI, collagen deposition was significantly reduced in comparison to WT hearts (Dobaczewski et al. 2010). Furthermore, *in vitro* analysis of Smad3^{-/-} CFs showed impaired TGF β 1-induced α SMA expression, collagen gel contraction and mRNA increases in fibronectin, collagen I and III and the profibrotic protein, connective tissue growth factor (CTGF). Migration of these cells towards 1 % serum was also diminished (Dobaczewski et al. 2010). Together this study demonstrates that Smad3 is required to produce functional MFs, hence could be a therapeutic target.

Despite the known pro-fibrotic effects of TGF β 1 in cardiac injury, TGF β 1 is also known to promote cardioprotective effects in *in vitro* and *in vivo* models of I/R injury (Dandapat et al. 2008;Yang et al. 1999). This has been attributed to reduced CM apoptosis potentially due to reduced reactive oxidative species (ROS) production (Dandapat et al. 2008). This anti-apoptotic effect on CMs is also translated to CFs *in vitro*, where CF apoptosis induced by I/R was reduced following TGF β 1 treatment (Vivar et al. 2013). Inhibitors of both canonical and non-canonical TGF β 1 signalling pathways including; extracellular signal-regulated kinase (ERK)1/2, Akt and Smad3, were shown to prevent this anti-apoptotic effect on CFs (Vivar et al. 2013).

Cardiac fibrosis is also prominent in Ang II animal infusion models (Li et al. 2007;Sopel et al. 2011;Wang et al. 2015), which is again thought to be due to the actions on CFs. Losartan, the angiotensin receptor type 1 (AT₁) antagonist, has also been shown to reduce fibrosis in many animal models of cardiac injury (Lim et al. 2001;Yamamoto et al. 2005) and in patients with hypertensive heart disease (Diez et al. 2002). The transcription factor, Ets-1, has been recently been reported to promote Ang II-mediated increases in plasminogen activator inhibitor-1 (PAI-1) and CTGF expression in CFs (Hao et al. 2015). Both PAI-1 and CTGF have been linked to the production of fibrosis (Daniels et al. 2009;Takeshita et al. 2004),

although the role of PAI-1 is controversial (Takeshita et al. 2004; Xu et al. 2010). Additionally, *Ets-1*^{-/-} mice do not exhibit enlarged hearts in response to Ang II infusion, indicating a role for *Ets-1* in Ang II-induced hypertrophy (Zhan et al. 2005). Furthermore, rat adult CFs (RACFs) stimulated with Ang II resulted in production/mRNA expression of collagen I and III, which was diminished by the NADPH oxidase blocker, apocynin (Bai et al. 2013; Lijnen et al. 2006), suggesting Ang II-mediated ROS production in turn induces collagen production by RACFs. Apocynin was also shown to inhibit Ang II-mediated CF-to-MF transdifferentiation (Bai et al. 2013). Interestingly, Ang II increases the production of TGF β 1 by CFs (Campbell and Katwa 1997; Lee et al. 1995) which is prevented by Losartan (Campbell and Katwa 1997). Additionally, in human atrial myocardial samples, Ang II was demonstrated to significantly increase mRNA levels of TGF β 1 but have no effect on collagen I (Kupfahl et al. 2000). Conversely, TGF β 1 stimulation promoted an increase in mRNA levels of collagen I and III, but not fibronectin. Similar results were found in isolated human atrial CFs (Kupfahl et al. 2000) suggesting Ang II promotes fibrosis through increasing the release of TGF β 1.

ET-1 (Nishida et al. 2007) and platelet-derived growth factor-D (PDGF-D) (Zhao et al. 2013) have also been shown to induce CF activation. PDGF-D mediated MF transdifferentiation has been shown to be mediated through the production of TGF β 1 (Zhao et al. 2013). Recently, miRNAs have also been implicated in transition of CFs to MFs including miR-125b (Bie et al. 2016; Nagpal et al. 2016), miR-145 (Wang et al. 2014c) and miR-154 (Sun et al. 2016). Interestingly the miR-143/145 cluster has been suggested to be important in mediating the contractile phenotype of SMCs (Boettger et al. 2009).

The expression of α SMA in fibroblasts is well established to occur naturally in culture, as demonstrated by the progressive increase in expression from passage 0 to 2 (Santiago et al. 2010) or over 7 days in culture (Cartledge et al. 2015). Although α SMA expression is typically used to identify the MF phenotype, cultured CFs have been suggested to be dissimilar in phenotype from those resident *in vivo* (Cartledge et al. 2015; Dawson et al. 2012). Dawson *et al.* (2012) compared atrial CFs from CHF and control dogs and while there was marked differences at the time of isolation these variances were abolished after 48 h in culture.

Furthermore, the effect of mediators produced by cultured CFs were shown to reduce the amplitude of the CM Ca^{2+} transient, whereas it was enhanced by freshly isolated CFs (Cartledge et al. 2015). Together these studies suggest alterations in CF phenotype as a consequence of culture. Evidence for the similarity between cultured CFs and MFs from pressure overload hearts was shown in the same study by Cartledge *et al.* (2015) where MFs also produced a reduction in the CM Ca^{2+} transient. Ideally, experimental investigation of healthy CFs would be completed within 48 hrs from initial isolation. Unfortunately this is not practical in most investigations due to the length of studies and the quantity of cells required for a particular experiment.

1.6.1.3 Origin of myofibroblasts

The origin of cardiac MFs in disease has been a controversial topic. Some proposed origins include resident CFs (Kanisicak et al. 2016), ECs subsequent to endothelial-to-mesenchymal transition (EndMT) (Zeisberg et al. 2007) and bone marrow-derived cells (van Amerongen et al. 2008). Genetic lineage tracing has been indispensable in these studies. For instance to study EndMT, Zeisberg *et al.* (2007) crossed transgenic mice expressing Cre recombinase under the control of the endothelial promoter, *Tie1*, (*Tie1Cre* mice) with mice expressing the ubiquitous promoter, ROSA (R26R), driving the expression of *LacZ* only when Cre recombinase is present in the cell due to a stop codon floxed between two loxP sites upstream of *LacZ* (*R26RstoplacZ* mice) (Zeisberg et al. 2007). Hence in *Tie1Cre;R26RstoplacZ* double transgenic mice, only endothelial cells should express *LacZ* regardless of any phenotypic changes as a result of injury. Here it was shown that following aortic banding, *LacZ* was co-localised with FSP1 expression, suggesting EndMT had occurred in response to banding (Zeisberg et al. 2007). Conversely, Kanisicak *et al.* (2016) demonstrated little to no contribution of ECs to the MF population following MI and suggested resident CFs to be the major MF source (Kanisicak et al. 2016). However as with all these studies, lack of cell specific markers for CFs/MFs and/or issues with promoter specificity makes it difficult to confidently confirm MF origins.

Use of the periostin promoter has become an interesting tool for the investigation of MFs, which was able to identify virtually all MFs in the heart (Kanisicak et al.

2016). Periostin is a 90 kDa secreted extracellular matrix protein that can interact with other ECM components and has roles in cell adhesion (Snider et al. 2009). The expression of periostin is undetectable in the healthy heart however becomes substantial following injury (Kanisicak et al. 2016; Oka et al. 2007). Additionally, mice deficient in periostin have reduced fibrosis, impaired macrophage activation and enhanced mortality mainly due to cardiac rupture in MI and TAC injury models (Oka et al. 2007; Shimazaki et al. 2008), demonstrating the importance of periostin in essential cardiac repair.

1.6.1.4 Cardiac hypertrophy

In response to many cardiac injuries, and generally increased workload, the cellular size of CMs increases, termed hypertrophy (Heineke and Molkentin 2006). Two main forms of hypertrophy tend to occur following injury known as eccentric and concentric hypertrophy (Figure 1-7), which typically result from volume and pressure overload respectively (Grossman and Paulus 2013). In eccentric hypertrophy there is a normal ratio of left ventricular wall thickness to radius (h/R) with elongation of CMs due to the addition of sarcomeres to already existing myofibrils. Conversely, the h/R ratio is high in concentric hypertrophy, where CMs maintain a similar length but expand in width due to addition of new myofibrils. This initially acts to compensate for the increase in pressure by reducing systolic left ventricular wall stress as a result of increased left ventricular wall thickness and is therefore thought of as an adaptive mechanism (Grossman and Paulus 2013). However, with time this can develop into systolic dysfunction due to fibrosis and myocyte degeneration (Hein et al. 2003). Aortic stenosis patients with a severely reduced left ventricular ejection fraction (LVEF) of $<30\%$ had a 32 fold greater myocyte generation than control (Hein et al. 2003). Due to changes brought about by the development of eccentric and concentric hypertrophy, signals as a result of one type of hypertrophy can lead to the progression towards the other (Figure 1-7) (Grossman and Paulus 2013).

A range of factors have been shown to initiate cardiac hypertrophy including myocardial stretch, neurohormonal activation and other paracrine/autocrine mediators (Sutton and Sharpe 2000). Interestingly, the pro-hypertrophic stimuli, noradrenaline, ET-1 and Ang II, act through G-protein coupled receptors of the

$G_{\alpha q/\alpha 11}$ subtype (Heineke and Molkentin 2006). Mice overexpressing the $G_{\alpha q}$ protein have been shown to develop hypertrophy leading to HF (D'Angelo et al. 1997; Mende et al. 1998). Additionally, $G_{\alpha q/\alpha 11}$ activation results in enhanced IP_3 levels and activation of MAPK signalling pathways, both of which have been implicated in the development of hypertrophy (Bueno et al. 2000; Nakayama et al. 2010). Furthermore, Ang II and noradrenaline induced hypertrophy have been shown to involve other pro-hypertrophic stimuli including $TGF\beta 1$ and ET-1 respectively (Moser et al. 2002; Schultz et al. 2002), illustrating indirect actions of these mediators.

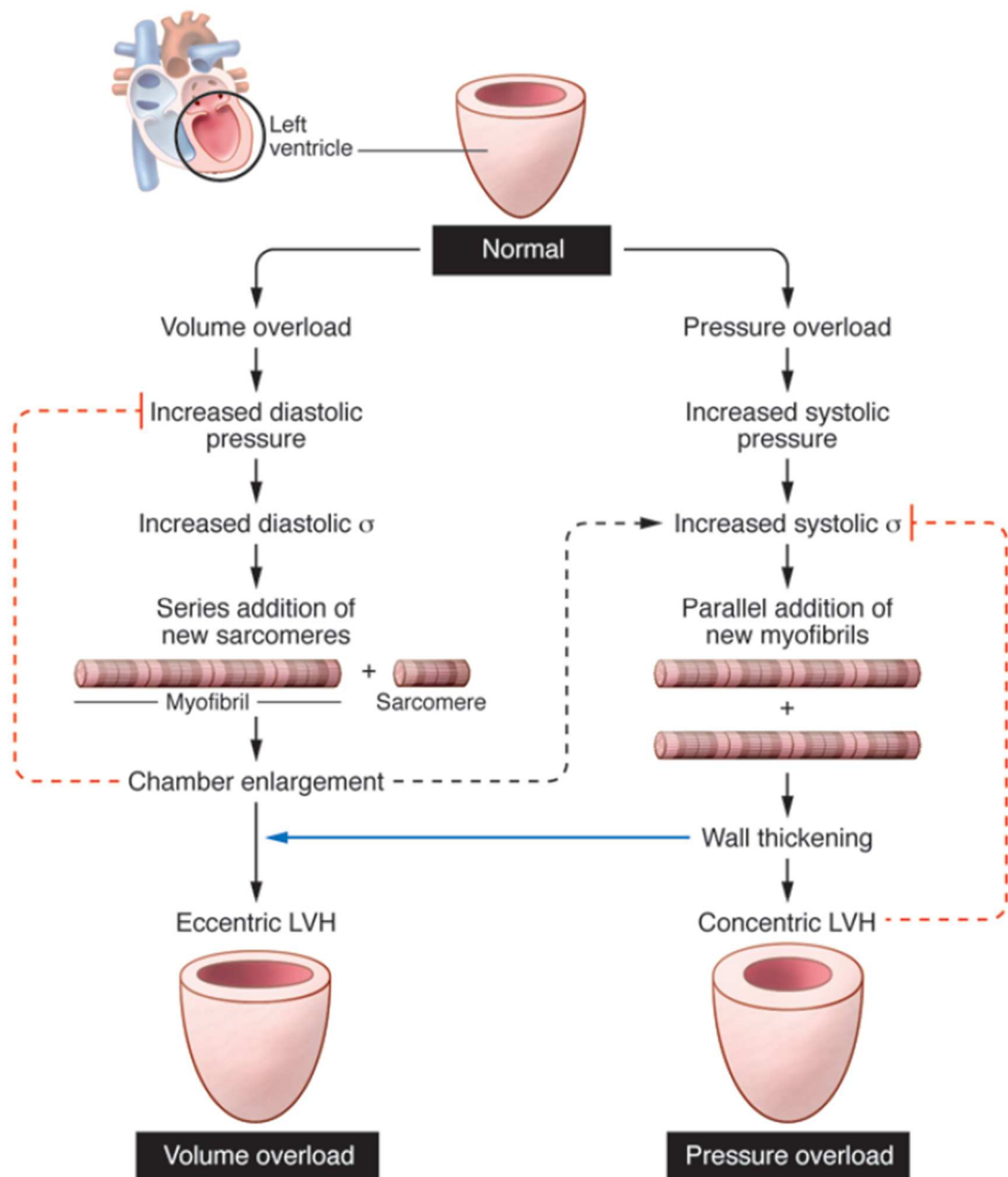


Figure 1-7 Eccentric and concentric hypertrophy.

Schematic demonstrating the process of eccentric and concentric hypertrophy by volume and pressure overload respectively. The increased diastolic wall stress as a result of enhanced diastolic pressure following volume overload can induce the addition of new sarcomeres to myofibrils and chamber enlargement. However this increases systolic wall stress which can prompt the parallel addition of new myofibrils (black dashed arrow) also observed in pressure overload in response to increased systolic pressure. Consequently, the left ventricular wall thickens not only leading to concentric hypertrophy but can also contribute to eccentric hypertrophy (blue arrow). Dashed red arrows represent negative feedback. LVH; left ventricular hypertrophy, σ ; wall stress (Reproduced with permission from Grossman and Paulus 2013)

1.6.2 Electrical remodelling and cardiac arrhythmias

Ventricular arrhythmias, defined as abnormal cardiac conduction, are a major cause of SCD (Roberts-Thomson et al. 2011). Due to the vast range of cardiac disease causes and severity, myocardial electrical consequences vary immensely. Cardiac fibrosis creates a vulnerable substrate which can create unidirectional conduction block and establish a re-entry loop of electrical activity (Nguyen et al. 2013) (Figure 1-8). Consequently, re-entry increases the rate of ventricular contraction, known as ventricular tachycardia (VT). Further wave breaks can lead to ventricular fibrillation (VF), where the ventricles quiver and the heart cannot efficiently pump blood around the body, which is often fatal (Jalife 2000).

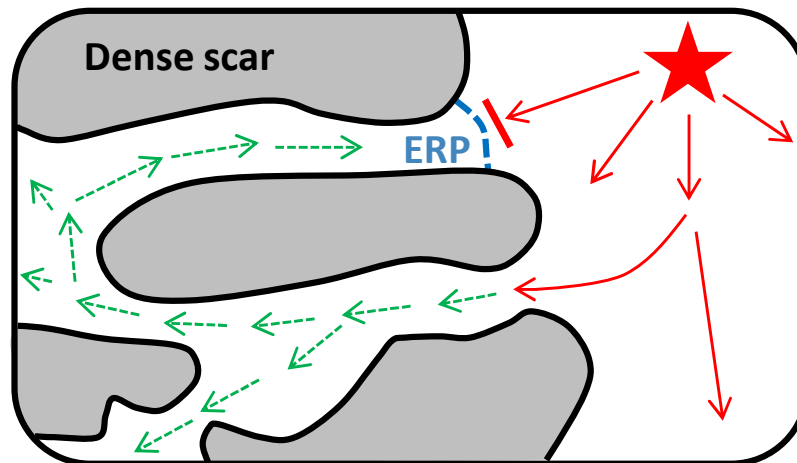
Interstitial fibrosis results in slowing of CV by promoting GJ uncoupling due to separation between CMs. Severe interstitial or patchy fibrosis has great arrhythmogenic potential, due to the live strands of CMs between areas of dense scar through which electrical signals cannot pass (Nguyen et al. 2013). Slowing of CV combined with the electrical signals travelling in a zig zag pattern through the CMs strands increases the risk of the slowed electrical signal looping back on itself and activating CMs which are not in the ERP, hence promoting re-entry (Figure 1-8) (Nguyen et al. 2013). Ectopic activity, such as following an early after depolarisation (EAD), defined as abnormal depolarisations during phases 2 or 3 of the AP, is required to trigger re-entry or worse, VF (Morita et al. 2011). EADs can occur when the repolarisation is impaired by a decrease in outward currents, an increase in inward currents or a combination of both. The I_{CaL} is the main current responsible for the upstroke of an EAD, although the NCX current (I_{NCX}), which also produces a net inward current by exchanging one Ca^{2+} ion for three Na^+ ions, may play a role following increased $[Ca^{2+}]_i$ induced by I_{CaL} (Weiss et al. 2010). Oxidative stress has been shown to induce EADs both in isolated CMs and in the intact heart (Morita et al. 2011; Song et al. 2006; Xie et al. 2009). EADs are associated with prolongation of the APD (Song et al. 2006) which is well established to occur in isolated CMs from failing human hearts (Beuckelmann et al. 1992; Piacentino et al. 2003) and from animal model hearts of HF (Kaab et al. 1996). A reduction in repolarisation currents, such as the I_{to} , inward rectifier K^+ current (I_{K1}) and I_{Ks} , have been detected in HF, suggesting a potential contributing factor to APD prolongation (Beuckelmann et al. 1993; Kaab et al. 1996; Li et al. 2004).

Spatial and temporal dispersion in APD has also been linked to the development of cardiac arrhythmias due to heterogeneity of the ERP in myocardial areas or between cardiac beats respectively (Frommeyer et al. 2017; Rosenbaum et al. 1994). Temporal dispersion in APD is described as APD alternans, where a long APD is followed by a short APD. Areas of the myocardium can either follow the same pattern; for instance long-short APD or vary spatially where areas of long-short APD are adjacent to areas following a short-long APD pattern, termed concordant or discordant alternans respectively (Burton and Cobbe 2001; Sato et al. 2006). The latter is somewhat more proarrhythmic by enhancing the risk of unidirectional block due to heterogeneity in ERPs (Sato et al. 2006). As the ECG T wave represents repolarisation, beat-to-beat variations in the T wave amplitude, shape or timing can be used to identify alternans (Narayan 2006). T wave alternans have been associated with the initiation of ventricular arrhythmias and mortality in man (Gold et al. 2000; Rosenbaum et al. 1994).

1.6.2.1 Connexin expression in the diseased heart

As well as fibrosis inducing CM uncoupling, Cx43 expression is known to be reduced in many cardiac pathologies including dilated, ischaemic and inflammatory cardiomyopathies (Kostin et al. 2003; Smith et al. 1991). In these conditions areas bordering the infarct displayed disorganised Cx43 expression, where movement of Cx43 from the IDs to the lateral surfaces of CMs was observed (Kostin et al. 2003; Smith et al. 1991). Similar lateralisation of Cx43 has also been demonstrated in rat and canine MI models (Matsushita et al. 1999; Peters et al. 1997). Consequently, reduced Cx43 expression at the ID would promote uncoupling and slow CV. Indeed, the uncoupling agent, carbenoxolone, slowed CV in the isolated rabbit heart (de Groot et al. 2003) and in the human heart *in vivo* (Kojodjojo et al. 2006). Additionally, mice with CM-specific Cx43 knockout had a slowed CV in both the longitudinal and transverse directions and developed ventricular arrhythmias leading to SCD within 2 months of birth (Gutstein et al. 2001). Together these studies provide evidence that organised GJ expression is essential for the normal electrical conduction of the myocardium.

1. Ectopic activity with unidirectional conduction block



2. First beat of re-entry

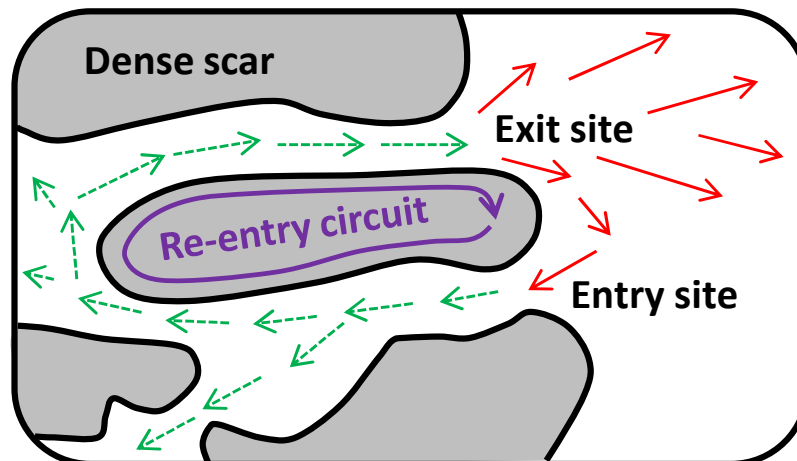


Figure 1-8 Establishment of a re-entry circuit.

Electrical activity outside the normal sinus rhythm (red star) acts as a trigger for re-entry. This impulse outside the scar conducts normally (red arrows) until it reaches the myocyte strands located between dense scar. Unidirectional block occurs at the interface between the normal tissue and upper myocyte strand due to this area being within the ERP. However the lower myocyte strand which has a shorter ERP conducts the impulse albeit at a slower rate (green dashed arrows). This slowed impulse travels around the dense scar to the upper myocyte strand where the impulse can exit and reactivate the normal cardiac tissue as well as the lower myocyte strand creating a re-entry circuit (purple arrow). ERP; effective refractory period.

1.6.3 Impaired excitation-contraction coupling

Alterations in Ca^{2+} transport into the cytoplasm and rate of removal can impact the initiation, intensity and duration of CM contraction (Lou et al. 2012). Abnormal Ca^{2+} handling is well established to occur in human HF, with an increase in the resting $[\text{Ca}^{2+}]_i$ and reductions in the Ca^{2+} transient amplitude, rate of Ca^{2+} removal, Ca^{2+} SR store and contractility (Beuckelmann et al. 1992; Kubo et al. 2001; Piacentino et al. 2003). In human HF the expression and/or the activity of numerous proteins involved in controlling $[\text{Ca}^{2+}]_i$ throughout contraction are known to be altered, which may explain these affects. For instance reduced protein expression and/or activity of SERCA2a, the main cardiac SERCA isoform, has been demonstrated in human HF (Hasenfuss et al. 1994; Piacentino et al. 2003). Although the protein expression of PLN is unchanged in failing hearts (Dash et al. 2001; Lou et al. 2011), a reduction in the phosphorylated form of PLN has been reported (Dash et al. 2001; Schwinger et al. 1999). This would therefore result in a reduction in SERCA activity and may explain the reduced Ca^{2+} SR store.

Ca^{2+} influx, mainly through the LTCCs, is generally unaltered in human HF (Mewes and Ravens 1994; Piacentino et al. 2003). However, disorganisation of T-tubules along with decreased co-localisation of LTCCs and RyRs in HF may contribute to impaired contraction (Crossman et al. 2011). Additionally, the RyR has been shown to have a damaged “leaky” phenotype in human HF, which is thought to be a result of hyperphosphorylation (Marx et al. 2000). This increased leak of Ca^{2+} from the SR can contribute to reduced Ca^{2+} SR store as well as an increase in cytosolic Ca^{2+} concentration, a risk factor for the development of delayed afterdepolarisations (DADs) (Antoons and Sipido 2008). A DAD is an abnormal depolarisation following completion of repolarisation. This can occur when cytosolic Ca^{2+} concentration is high due to activation of the I_{NCX} and the production of an inward current (Nagy et al. 2004). I_{Na} is activated if the inward current induces a substantial depolarisation (Tse 2016), consequently triggering an AP and the development of focal arrhythmias (Antoons and Sipido 2008).

1.7 Current treatment of arrhythmias

Current pharmacological treatments for the prevention of arrhythmias can typically be categorised by the ion channel which the drug targets. Class I, III and IV drugs block Na^+ , K^+ and Ca^{2+} channels respectively whereas class II act to inhibit β -adrenergic receptors (β -blockers) and class V have a wide range of actions (Karagueuzian et al. 2017). The use of these drugs has been limited by modest antiarrhythmic efficacy, toxicity and paradoxically, the promotion of arrhythmias (Williams and Viswanathan 2013).

Amiodarone and sotalol are the main pharmacological treatments for VT. Amiodarone was originally developed as an antianginal therapy due to its vasodilatory action but later shown to suppress arrhythmias (Vassallo and Trohman 2007). It has properties of class I, II, III and IV drugs and been demonstrated, in a meta-analysis of randomised trials, to reduce overall mortality by 10-19 % in patients at risk of SCD (Sim et al. 1997). Although, amiodarone causes prolongation of the QT interval, there was no development of torsade de pointes (TdP), a ventricular arrhythmia known to be induced by increased QT intervals, in MI survivors with a LVEF of ≤ 40 % (Julian et al. 1997). However, in the same study, nearly twice as many participants discontinued amiodarone treatment (38.5 %) in comparison to placebo group (21.4 %) due to a range of reasons, of which the most common was endocrine disorders (Julian et al. 1997). Other side effects of amiodarone include corneal microdeposits, pulmonary toxicity and hepatotoxicity (Vassallo and Trohman 2007). Additionally, as amiodarone is an iodine-containing drug it has been reported to cause thyroid dysfunction. Consequently a similar agent which is noniodinated has now been developed, known as dronedarone. This drug was reported to reduce hospitalisation as well as overall, cardiovascular-related and arrhythmic death of atrial fibrillation (AF) patients (Hohnloser et al. 2009), and is now approved for the treatment of AF. Dronedarone has not been investigated for VT/VF treatment but an increase in mortality of severe HF patients (Kober et al. 2008) as well as in patients with sustained AF which have a high risk of major vascular events such as MI, (Connolly et al. 2011) has raised safety concerns of this drug in these subset of patients.

Although used less often, sotalol is given to suppress ventricular arrhythmias (Dev et al. 2014). Sotalol is a racemic mixture of D-sotalol and L-sotalol which results in APD prolongation. Both stereoisomers have K^+ channel blocking properties, therefore a member of the class III anti-arrhythmics, however L-sotalol also acts as a β -blocker (Williams and Viswanathan 2013). Interestingly, in a small randomised trial, sotalol was shown to be more efficient at reducing mortality in patients with an ischemic compared to a nonischemic cardiomyopathy (Furushima et al. 2007). Like amiodarone, sotalol prolongs the QT interval, but is thought to pose a greater risk in the development of TdP (MacNeil 1997).

Currently, patients deemed at risk of lethal ventricular arrhythmias, including those presenting a LVEF of $\leq 35\%$ and/or sustained VT/VF are subjected to an implantable cardioverter-defibrillator (ICD) (Epstein et al. 2013). This device monitors the heart rate for dangerously high or low frequencies where on occurrence delivers a shock to re-start sinus rhythm. ICDs have been demonstrated to be more effective at preventing mortality in survivors of VF or patients with sustained VT than the front line antiarrhythmic drug, amiodarone (Connolly et al. 2000). However, one of the major limitations to ICD therapy is the discomfort caused by, sometimes inappropriate, shocks resulting in decreased quality of life (Irvine et al. 2002; Schron et al. 2002). Additionally, while an ICD terminates arrhythmias it does not prevent them, therefore they are normally used in combination with antiarrhythmic drugs (Dev et al. 2014). Indeed, oral sotalol was found to decrease the risk of death and ICD shock in comparison to placebo (Pacifco et al. 1999). Furthermore, combination therapy of with amiodarone and β -blockers was shown to decrease the incidence of shocks in comparison to β -blockers or sotalol alone (Connolly et al. 2006). Despite these successes no new antiarrhythmic therapies have been developed for the treatment of VT in over a decade, therefore greater understanding of basic mechanisms are required to develop new therapeutics.

1.8 Cardiac myocyte: fibroblast interactions

Due to the close proximity demonstrated between CMs and CFs (Camelliti et al. 2005a), strong heterocellular interactions are likely to exist. Membrane fusion, paracrine, electrical and mechanical interactions have been postulated.

1.8.1 Membrane fusion interactions

Membrane nanotubes were characterised as long, thin continuous membrane structures in cultured rat pheochromocytoma PC12 cells (Rustom et al. 2004). Similar structures have also been reported in many other cell types including normal rat kidney (NRK) cells, dendritic cells and rat CMs and have been proposed to be involved in the transport of electrical signals, Ca^{2+} and mitochondria (Plotnikov et al. 2008; Wang et al. 2010; Watkins and Salter 2005). However, the transfer of calcein through nanotubes in PC12 cells was prevented, suggesting impedance to passive transfer (Rustom et al. 2004). Interestingly, nanotube formation has also been demonstrated between neonatal CFs and CMs, with a mean length of $13.9 \pm 10.4 \mu\text{m}$ (He et al. 2011). The transport, in both directions, of small swelled vesicles was demonstrated within nanotubes connecting CFs and CMs. Additionally, mitochondria transfer and Ca^{2+} signal propagation *via* membrane nanotubes was demonstrated (He et al. 2011). Although regular punctate Cx43 expression was shown at one end of nanotubes connecting NRK cells (Wang et al. 2010), no Cx43 expression was detected in nanotubes between CFs and CMs (He et al. 2011). The presence of nanotube-like structures within the intact mouse heart has also been reported, suggesting a physiological role *in vivo* (He et al. 2011; Quinn et al. 2016). Membrane fusion between cultured adult CFs and CMs has also been reported (Driesen et al. 2005). Further elucidation of the role of membrane nanotubes in electrical communication is required.

1.8.2 Paracrine interactions

As CFs are known to be a major secretory cell, many studies have focussed on the effect of mediators released by CFs and their effect on the function of CMs. For instance, fibroblast conditioned media (FCM) is well established to promote the hypertrophy of CMs (Fredj et al. 2005a; Fredj et al. 2005b; LaFramboise et al. 2007) which has been attributed to many mediators including IL-6 and Ang II (Fredj et

al. 2005a;Fredj et al. 2005b). Additionally, the packaging of mediators within exosomes has become an interesting means of communication between CFs and CMs. The passenger strand, miR21*, was demonstrated to be in high abundance in exosomes released from CFs, which was reported to induce CM hypertrophy (Bang et al. 2014). Furthermore, miR21* antagomir treatment was shown to reduce Ang II-mediated hypertrophy (Bang et al. 2014).

Paracrine factors released from neonatal CFs were also shown to reduce the CV by 52 %, decrease the rate of AP upstroke by 80 %, increase the RMP by 21 % and finally induce a 217 % APD prolongation of neonatal CMs monolayers (Pedrotty et al. 2009). Additionally, in the same study gene expression of the channels responsible for I_{Na} , I_{K1} and I_{to} were downregulated by 3.8-, 6.6-fold and to undetectable levels respectively in CMs treated with FCM (Pedrotty et al. 2009), which may explain these electrophysiological changes. In agreement with this study, the peak of the I_{to} in rat adult CMs was reduced in cells treated with FCM (Kaur et al. 2013). However in contrast, the I_{Na} was enhanced in these cells (Kaur et al. 2013). Both effects on I_{to} and I_{Na} were attenuated by a TGF β 1 neutralising antibody and mimicked by TGF β 1 treatment. Furthermore, TGF β 1 was shown to prolong the APD of adult CMs, suggesting TGF β 1 released by CFs, which was increased by more than 3 fold in FCM, could be promoting electrical dysfunction in CMs (Kaur et al. 2013).

Furthermore, Cartledge *et al.* (2015) demonstrated that the phenotype of CFs can modify their effect on CM function. This study utilised a transwell co-culture method to determine the paracrine interactions between adult CMs and CFs. Freshly isolated CFs (α SMA negative) and MFs from pressure overloaded hearts (α SMA positive) not only reduced the viability of CMs but also shortened the Ca^{2+} transient and promoted hypertrophy. However, freshly isolated CFs were shown to increase the CM Ca^{2+} transient amplitude whereas MFs had the opposite effect. Through in-depth studies, all these effects were attributed to a TGF β 1-dependent interaction between the cells (Cartledge et al. 2015). This differential behaviour between healthy and diseased CFs was also shown in a study by Vasquez *et al.* (2010) using CFs isolated from rat MI (CF-MI) and healthy hearts. Here, conditioned media from CF-MI induced a significant reduction in the CV and APD of rat neonatal

cultures, whereas conditioned media from healthy CFs had no effect (Vasquez et al. 2010).

Additionally, CM conditioned media (CCM) can modulate CF activity. For example, Ang II was only able to increase collagen I and III mRNA levels in CFs when CCM was present, demonstrating mediators released from CMs potentiate the CF response to Ang II (Sarkar et al. 2004). Furthermore, CCM was shown to increase CF proliferation (Cartledge et al. 2015). In summary, the studies described in this section suggest that bidirectional paracrine interactions exist between CFs and CMs.

1.8.3 Electrical interactions and the role of connexins

CFs are regarded as an electrically inactive cell type (Ongstad and Kohl 2016). Despite this, CFs are known to express connexin proteins (Camelliti et al. 2004a; Camelliti et al. 2004b; Miragoli et al. 2006), and are thought to partially mimic APs of coupled CMs (Kohl et al. 1994). Although, GJs between CFs and CMs may be less abundant and distinct in comparison to GJs between CMs (Camelliti et al. 2004a), there is growing evidence for their presence. In fact, computer modelling has suggested that CFs could have an effect on CMs with as little as 10-30 connexin channels between them (Kohl et al. 1994), which may be difficult to detect.

1.8.3.1 Evidence for electrical coupling between cardiac myocytes and fibroblasts

Evidence to support the presence of GJs between CFs and CMs has come from dye transfer studies (Chilton et al. 2007; Driesen et al. 2005) where transfer of the fluorescent dye, calcein, has been shown to occur as early as 1 h from initiation of co-culture (Cho et al. 2007). Dye transfer between CFs and CMs has also been reported *in situ* in the rabbit SAN, an area very abundant in fibroblasts (Camelliti et al. 2004b). In this study, Cx45 was reported to be the most likely contributor, due to the greater presence at CM and CF contact points. Conversely, Cx43 was undetectable and Cx40 was shown at homocellular CF junctions (Camelliti et al. 2004b).

Although electrically unexcitable, CFs may assist in conduction between CM layers and through scar tissue. A study by Gaudesius *et al.* (2003) demonstrated that when CMs were separated by CFs in culture over distances of up to 300 μm , electrical signals were conducted between the bands of CMs (Gaudesius *et al.* 2003). Interestingly, greater conduction delays were correlated with increasing length of separation between the CMs (from 50 to 300 μm), typical of post cardiac injury (Gaudesius *et al.* 2003). Cx43 and Cx45 expression was identified at the heterocellular contact points, hence supporting a role for them in the electrical conduction (Gaudesius *et al.* 2003). Furthermore, electrical propagation through scar tissue resulting from MI in a rabbit and mouse model has been reported (Mahoney *et al.* 2016; Walker *et al.* 2007). Interestingly, in mice with a FSP1 driven KO of Cx43 (Cx43fsp1KO) no conduction through the scar was detected (Mahoney *et al.* 2016). Together these studies suggest that CFs have the ability to passively conduct electrical impulses both *in vitro* and in the intact heart *in situ*.

1.8.4 Electrophysiological consequences of cardiac myocyte: fibroblast coupling

The levels of Cx43 have been reported to be substantially increased in CFs derived from rat MI hearts in comparison to control hearts (Vasquez *et al.* 2010; Zhang *et al.* 2010). Additionally, a progressive increase in Cx45 and Cx43 expression within in infarct area was reported 1 to 6 days (Cx45) and 6 to 30 days (Cx43) post ischaemia respectively in sheep MI model (Camelliti *et al.* 2004a). These studies suggest that CF connexin expression is altered in a complex fashion following infarction. An enhanced Cx43 expression in CFs-MI, and therefore mostly likely of a myofibroblast phenotype, may augment CM: CF coupling resulting in a heightened electrical influence.

1.8.4.1 Effects on the cardiac myocyte resting membrane potential

The RMP of CFs has been shown to be relatively depolarised in comparison to CMs (-15 to -35 mV (Askar *et al.* 2012; Vasquez *et al.* 2010) vs. -65 to -80 mV (Askar *et al.* 2012; Nguyen *et al.* 2012); CFs vs. CMs). Therefore a modest depolarisation of CMs could be consequence of enhanced CM: CF coupling which may be arrhythmogenic by increasing the probability of ectopic beats due to nearing the threshold value. This depolarisation effect was demonstrated in a rat neonatal

CM: CF co-culture model, where increasing densities of α SMA positive CFs resulted in a progressive increase in the maximal diastolic potential (MDP; the most negative point of the AP) of CMs to values up to -55 mV (Miragoli et al. 2006). Both Cx43 and Cx45 were shown to be present at heterocellular contact points and therefore likely to be responsible. An increase in the CM MDP by CFs was also demonstrated by Askar *et al.* (2012), which was reduced by lentiviral (LV) vector-mediated silencing of Cx43 in CFs (Askar et al. 2012). Interestingly, this reduction induced by Cx43 silencing was reverse by inhibition of the repolarisation current, I_{K1} (Askar et al. 2012). Together these data support the role of Cx43 expression in CFs in the partial depolarisation of CMs. However, CF-MI were shown to have a more hyperpolarised reversal potential to that of healthy CFs (-51.0 ± 1.5 mV vs. -32.0 ± 3.5 mV, CFs-MI vs. healthy CFs) (Vasquez et al. 2010), which may alleviate the depolarising effects on coupled CMs. On the contrary, the elevated Cx43 levels in CFs-MI (Vasquez et al. 2010; Zhang et al. 2010) may enhance heterocellular coupling consequently increasing the RMP of CMs.

1.8.4.2 Effects on the conduction velocity between cardiac myocytes

Similar to within an infarct, CV is altered in CM: CF co-culture models. A biphasic effect on CV along cultured neonatal CM strands was reported when the density of CFs was increased (Miragoli et al. 2006). That is, a gradual increase in CV was seen at CM: CF ratios of up to 100:7, however at greater ratios a progressive slowing of CV was observed (Miragoli et al. 2006). This could be explained by weak cell coupling at low densities, resulting in CM depolarisation nearing the AP threshold. However, following increased coupling at greater CFs densities, the larger depolarising effect on the CM could lead to the inactivation of voltage-gated Na^+ channels, essential channels for phase 0 of the AP, hence slowing conduction (Miragoli et al. 2006). This phenomenon has been termed “supernormal conduction” whereby CV has the same biphasic relationship with increasing membrane potential of the CM. Supernormal conduction has been described by elevating external K^+ concentrations to depolarise the RMP (Rohr et al. 1998). Additionally, the rate of CM depolarisation (dV/dt_{max}) followed a similar trend to CV, thought to be due to the same depolarising effect (Miragoli et al. 2006). Furthermore, at a CM: CF ratio of 1:1, CV was reduced by approximately 2 fold compared to cultured CMs alone (Askar et al. 2012), providing additional

evidence of this effect. In the same study, LV vector-mediated Cx43 knockdown in CFs resulted in a significant increase in CV in comparison to CFs treated with a control LV (Askar et al. 2012). The negative correlation between CV of monolayers of the murine atrial CM cell line, HL-1 cells, and the percentage of neonatal rat CFs (NRCFs) was attenuated when NRCFs were substituted for the mouse embryonic fibroblast cell line which had no Cx43 expression (Fahrenbach et al. 2007). These studies provide evidence for heterocellular coupling between CMs and CFs and suggest that enhanced Cx43 expression in CFs may promote proarrhythmic effects.

1.8.4.3 Arrhythmic consequences of cardiac myocyte: fibroblast coupling

Co-culture studies have also been utilised to investigate the impact of CFs on the vulnerability of CMs to arrhythmias. In a hybrid biological-computational study, where adult rabbit CMs were patch-clamped to a computer generated virtual CF based on mathematical models of their electrical profile (Nguyen et al. 2012), early EADs were more common in comparison to CMs alone. Interestingly, when the RMP of the virtual CF was more depolarised (-25 vs. -50 mV) the probability of EAD generation was greater (Nguyen et al. 2012). Spontaneous depolarisations of CMs has also been shown when CF density is greater than 15 % in a co-culture model (Miragoli et al. 2007). Interestingly, the ability of CFs to trigger spontaneous AP generation in myocytes is dependent on α SMA expression in CFs, suggesting a specific effect of the MF phenotype (Rosker et al. 2011). Additionally, α SMA expression was shown to contribute to the relatively depolarised RMP of CFs (Rosker et al. 2011).

Ectopic activity and re-entrant arrhythmia incidence were shown to be enhanced in CM: CF co-culture versus CM monolayers (Askar et al. 2012). This effect was partially attributed to Cx43 expression in CFs (Askar et al. 2012). Zlochiver *et al.* (2008) also demonstrated an increase in the number of activation waves as the density of CFs increased, indicating a highly arrhythmic environment (Zlochiver et al. 2008). Antiproliferative treatment of CM: CF cultures over nine days was shown to suppress ectopic activity and re-entrant arrhythmias in comparison to untreated cultures (Askar et al. 2011), which may indicate a potential therapeutic avenue.

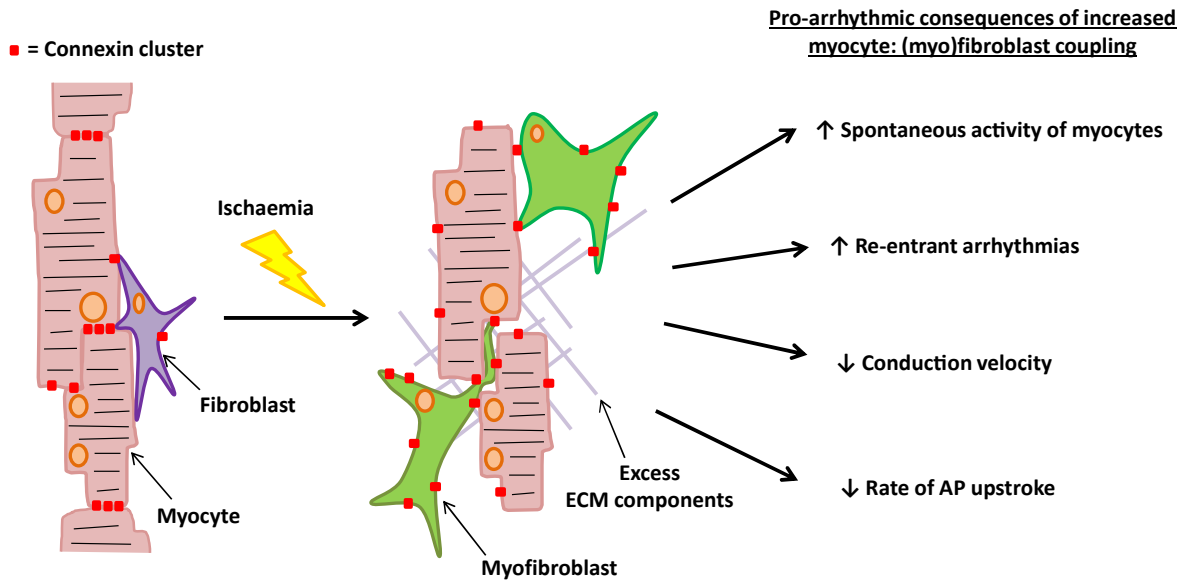


Figure 1-9 Schematic of potential electrical consequences of increased cardiac myocyte: (myo)fibroblast coupling.

In the healthy heart connexin expression is primarily localized to the intercalated discs between myocytes (pink cells). Fibroblasts (purple) are thought to form gap junctions with myocytes which may assist the electrical impulse to be transmitted through myocyte layers. However following ischaemia, the fibroblasts are activated and become myofibroblasts. Myofibroblasts (fibroblasts from infarcted hearts – green cells) have been reported to increase connexin expression and therefore potentially increase heterocellular coupling. Connexin expression in myocytes in disease is reduced and is relocated to the lateral surfaces of the myocyte. The resulting pro-arrhythmic effects are detailed at the right-hand side of the figure (This figure was originally published in McArthur et al. 2015).

1.8.5 Mechanical interactions

In both neonatal and adult CM: CF co-culture models, heterocellular mechanical interactions have been demonstrated. CFs are shown to pull on CMs in culture (Driesen et al. 2005;Thompson et al. 2014) and cadherin, a component of AJs, has been detected at CM: CF cell contact points (Thompson et al. 2011;Thompson et al. 2014).

Mechanosensitive channels (MSCs) are channels activated by stretching, for instance in diastole of the cardiac cycle. As MFs are known to express α SMA and have the ability to contract (Dobaczewski et al. 2010;Thompson et al. 2011), the role of MSCs in CF/MFs has been investigated. MSCs were demonstrated to be constitutively active in CFs and were shown to contribute to their less negative RMP (Grand et al. 2014). Interestingly, inhibition of MSCs with streptomycin or gadolinium in CM strands coated with CFs at a CM: CF ratio of 3:1 was shown to partially inhibit the slowing of CV and dV/dt_{max} induced by CFs, despite no effect in control CM strands. Additionally, physiological stretching by plating cells onto silicone membranes to which stretch force was applied led to MSC activation and resulted in depolarisation of both neonatal CMs and CFs. Furthermore, in CM: CF strands, conduction was significantly slowed in comparison to control CM strands when 5 % stretch was applied (Grand et al. 2014). The CV of neonatal rat ventricular cells (NRVCs) was also found to be slowed when treated with TGF β 1, with the aim of promoting the MF phenotype. However, in this cellular model effects of TGF β 1 directly on the CMs may occur and is therefore difficult to state an effect of the MF phenotype, nonetheless this was representative of a fibrotic culture. Additionally, the dV/dt_{max} and the APD were shown to be prolonged in fibrotic cultures in comparison to control. The effects on CV, dV/dt_{max} and the APD were reversed when treated with the EC upcoupler, blebbistatin, or the MSC blockers; streptomycin and gadolinium (Thompson et al. 2011). In a follow up study, the CV slowing of NRVCs was seen as soon as 30 min following the addition of MFs (TGF β 1-treated CFs) (Thompson et al. 2014). Interestingly, this was reversed when, the AJ component, N-cadherin, was silenced in MFs (Thompson et al. 2014). Together these studies demonstrate a role for MSCs in CFs and AJ between CMs and CFs in conduction slowing, which are likely to have implications in fibrotic hearts.

1.9 Hypothesis and aims

CFs are known to play an integral role in the pathogenesis of heart disease by secreting numerous factors contributing to cardiac fibrosis and arrhythmogenesis. Co-culture CM: CF studies, mainly from neonatal origin, have suggested that CFs can couple to and alter the function of CMs. Therefore it was hypothesised that the function of CMs would be altered in an *in vitro* adult CM: CF co-culture model in comparison to CMs in culture alone and that RACFs implanted into the left ventricle would alter the electrical activity in that region of the heart.

The primary aim of this thesis was to determine the effects of RACFs on the function of CMs both *in vitro* and *in situ*. This was addressed by the following experimental aims:

- Develop a viral vector to overexpress Cx43 which is suitable for *in vitro* investigation and *in situ* imaging.
- Identify potential mediators that could be responsible for enhanced Cx43 expression reported in CFs from MI hearts, and to further dissect mechanisms for this upregulation.
- Assess the effect of different phenotypes of RACFs on adult CM contraction and electrical activity in an *in vitro* CM: CF co-culture model.
- Establish a model to investigate CM: CF interactions *in situ*.

Chapter 2 Materials and methods

2.1 Materials

All tissue culture reagents, reverse transcription and quantitative real-time polymerase chain reaction (qRT-PCR) reagents were purchased from ThermoFisher Scientific (Loughborough, UK). Tissue culture plastics were purchased from Sigma-Aldrich (Poole, UK). All restriction endonucleases were obtained from New England BioLabs (NEB; Ipswich, UK). Sutures for surgery were attained from Herny Schein (Dumfries, UK).

2.1.1 Solutions

- ADS buffer (in mM): 116.4 NaCl, 199.7 HEPES, 1.0 NaH₂PO₄, 5.6 Glucose, 5.4 KCl, 0.8 MgSO₄.
- 1x Citric saline (in mM): 130.0 KCl, 17.0 sodium citrate dihydrate
- Kraft Bruhn buffer (KB) (in mM): 70.0 KOH, 40.0 KCl, 50.0 L-Glutamic Acid, 20.0 Taurine, 20.0 KH₂PO₄, 3.0 MgCl₂.6H₂O, 10.0 Glucose (Anhydrous), 10.0 4-(2-hydroxyethyl)-1-piperazineethanesulfonic acid (HEPES), 0.5 ethylene glycol-bis[β-aminoethyl ether]-N,N,N',N'-tetraacetic acid (EGTA). pH to 7.2 with KOH at 37 °C.
- Krebs-henseleit solution (in mM): 120.0 NaCl, 20.0 HEPES, 5.4 KCl, 0.5 NaH₂PO₄, 3.5 MgCl₂.6H₂O, 20.0 Taurine, 10.0 Creatine, 11.0 Glucose (Anhydrous). pH to 7.4 with NaOH at 37 °C
- 10x Phosphate-buffered saline (PBS) (in mM): 1369.0 NaCl, 27.0 KCl, 101.0 Na₂HPO₄, 17.0 KH₄PO₄. pH to 7.4 with HCl at room temperature.
- 1x Protein lysis buffer stock (in mM): 50.0 Tris-HCl, 50.0 NaF, 1.0 Na₄P₂O₇-10H₂O, 1.0 ethylenediaminetetraacetic acid (EDTA) and 1 EGTA
- 10mM Sodium citrate (in mM): 10.0 sodium citrate dihydrate. pH to 6.0 with HCl at room temperature.

- Transfer buffer: 192.0 mM Glycine, 25.0 mM Tris-Base, 20 % volume/volume (v/v) methanol
- 10x Tris-buffered saline (TBS) (in mM): 247.6 Tris-Base, 1368.9 NaCl, 26.8 KCl. pH to 7.4 with HCl at room temperature.
- 10x Tris density (TD) buffer (in mM): 750.0 NaCl, 50.0 KCl, 250.0 Tris-base, 10.0 Na₂HPO₄-12H₂O. pH to 7.4 with HCl at room temperature.
- 10x Tris-EDTA (TE) buffer (in mM): 10.0 Tris-HCl, 1.0 EDTA. pH to 8.0 at room temperature.
- Tyrodes (in mM): 116.0 NaCl, 20.0 NaHCO₃, 0.4 Na₂HPO₄, 1.0 MgSO₄-7H₂O, 5.0 KCl, 11.0 glucose, 1.8 CaCl₂

2.2 Cell isolation and culture

All cell culture was performed within a sterile class II biological vertical laminar flow cabinet to maintain sterility. Cells were cultured in 75 or 150 cm² tissue culture flasks in a humidified chamber at 37 °C and 5 % carbon dioxide (CO₂).

2.2.1 Cell lines

The immortalised human cervical epithelial carcinoma cell line, HeLa, and Human Embryonic Kidney (HEK) 293 cells and 293Ts were cultured in minimal essential media (MEM) supplemented with 10 % (v/v) foetal bovine serum (FBS), 2 mM L-glutamine, 100 international units (I.U)/mL penicillin and 100 µg/mL streptomycin. Cells were cultured in 150 cm² flasks and the media was changed every 2-3 days.

2.2.2 Obtaining hearts for cell isolation

Adult male Wistar rats were killed by Schedule 1 according to the UK Animals (Scientific Procedures) Act 1986. Hearts were removed from the thorax and lungs, placed in ice cold ADS buffer (for RACF isolation) or heparinised Krebs solution

(for CM isolation). Instruments for both RACF and CM isolation were soaked in 70 % ethanol to sterilize prior to use.

2.2.3 Rat adult cardiac fibroblast culture

Isolated RACFs were cultured in Dulbecco's Modified Eagle Medium: Nutrient Mixture F-12 (DMEM/F-12) reconstituted from powder in 1 L of double distilled H₂O (ddH₂O) with 14.3 mM sodium bicarbonate added and the pH adjusted to 7.2 at room temperature. The media was then filter sterilised and supplemented with 10 % or 0.5 % (v/v) FBS (culture media and reduced serum media respectively), 100 I.U/mL penicillin and 100 µg/mL streptomycin.

Plastics used to culture RACFs were treated with poly-L-lysine unless stated otherwise. To coat, poly-L-lysine (Sigma-Aldrich) was added and incubated for 5 min at room temperature. The poly-L-lysine was then removed and two washes with sterile PBS performed.

2.2.4 Rat adult cardiac fibroblast isolation

RACF cultures were obtained by an enzymatic digestion method of the ventricular heart muscle, modified from previous published papers (Louch et al. 2011;Shivakumar et al. 2003). Hearts were prepared for digestion in cold ADS buffer in a sterile class II biological vertical laminar flow cabinet. Atria were discarded and blood was removed by gently pressing on the walls of the ventricles. Hearts were then moved into fresh ADS buffer and minced using small scissors. Pieces of heart were transferred into a sterile 100 mL Duran bottle and ADS buffer removed by allowing the tissue to gravitate to the bottom when the bottle was slightly tilted on its side. Next, 10 mL of an enzyme solution (0.8 mg/mL collagenase type II [Worthington Chemicals, US] and 0.6 mg/mL pancreatin [Sigma-Aldrich] made up in ADS buffer and filter sterilised using a 0.2 µm syringe filter) was added to the tissue and incubated in a shaking water bath (180 strokes/min) at 37 °C for 10 min. The supernatant from this first digestion, containing digested ECM components, was discarded and 10 mL of enzyme solution added before being incubated again at 37 °C in the shaking water bath at 160 strokes/min. Following the 2nd digestion the supernatant was taken and added to

2 mL FBS prior to centrifugation at $310 \times g$ for 5 min. The supernatant was discarded; the pellet gently resuspended in 4 mL FBS and incubated in a humidified incubator at 37°C and 5 % CO_2 in a 50 mL Falcon tube with the lid loosened. This was repeated for digestion steps 3-10 (Table 2.1) with varying enzyme solution volumes, times and strokes/min. Following each digestion, cells were collated. On completion of digestion step 10 the cells were subjected to centrifugation at $310 \times g$ for 6 min. The supernatant was discarded, resuspended in 12 mL culture media and added to a poly-L-lysine coated 75 cm^2 vented flask. Cells were left to attach for 2-3 h in a humidified incubator at 37°C and 5 % CO_2 before being washed twice with sterile PBS and fresh media applied. The media was then changed the following day.

Table 2.1 Enzymatic digestion protocol for RACF isolation.

Digest	Volume of the enzyme solution (mL)	Time (min)	Speed (strokes/min) at 37 °C
1	10	10	180
2	10	10	160
3	8	10	150
4	8	10	150
5	6	10	160
6-9	6	10	150
10	6	30	150

2.2.5 Adult rat cardiac myocyte isolation

Adult rat CMs were isolated using a Langendorff perfusion set up. Prior to the isolation; 200 mL 70 % ethanol followed by 500 mL sterile dH₂O was used to clean the perfusion apparatus. All solutions used for the isolation were filtered sterilised in a sterile class II biological vertical laminar flow cabinet.

Hearts were washed in ice cold Krebs, aortas isolated by dissection and cannulated using a 2 mm diameter catheter and 4-0 silk braided suture (Pearsalls, Somerset, UK). Hearts were retrograde perfused with Krebs heated to 37 °C at a constant flow rate of 8 mL/min. Following clearance of blood, the heart was perfused with 0.25 U/mL collagenase type I constituted in a 0.1 % (weight/volume [w/v]) bovine serum albumin (BSA) Krebs solution. The enzyme was recirculated only once the initial enzyme level was low to prevent unnecessary dilution and deactivation of the enzyme. The enzyme was perfused until suitable digestion was completed, determined by a spongy texture of the heart. The time taken for each heart to complete digestion varied (approximately 12 min). The ventricles were then cut from the atria and transferred into the laminar flow cabinet for the remainder of the digestion. Kraft Bruhn (KB) buffer containing 1 % (w/v) BSA was added and the hearts were minced using sterile scissors. The solution was triturated for 1-2 min using a sterile Pasteur pipette, prior to filtering through a 250 µm polyamide mesh to separate the solution from undigested tissue. Next, 1 % (w/v) BSA in KB buffer was added to the remaining heart tissue and the process repeated. The solutions were subjected to centrifugation for 2 min at 300 × g and CMs examined under the microscope.

The cells were allowed to recover from the digestion in KB buffer for 30 min. The solution was then removed and cells slowly introduced to increasing concentrations of calcium by incubation in 100 µM followed by 1 mM CaCl containing sterile Krebs for 20 mins per solution. Cells were then added to reduced serum media (0.5 % (v/v) FBS) and live CMs (rods) counted using a haemocytometer.

2.2.6 Cell passage and cryopreservation

All cell types were passaged once the cells had reached 80-90 % confluency. This was achieved by washing twice with sterile PBS followed by the addition of 3 or 5 mL 0.05 % (v/v) trypsin- EDTA (for HeLas and RACFs) or 1x citric saline (HEK 293 and 293Ts), for 75 cm² or 150 cm² flasks respectively. Cells were incubated for approximately 5 min at 37 °C and 5 % CO₂ until the cells had detached and at least 2 volumes of media containing 10 % (v/v) FBS added to the flasks. Next, the cells were subjected to centrifugation at 460 × g for 5 min and the pellet resuspended in the appropriate volume of media prior to addition to the culture flask.

Cryopreservation was performed by harvesting the cells as described above and the pellet resuspended in media containing 10 % dimethyl sulfoxide (DMSO). Cells were then aliquoted into 1 mL aliquots in cryovials and stored in the vapour phase of liquid nitrogen (ranging from -135 to -195 °C).

To recover cells from a frozen stock, cells were rapidly thawed at 37 °C before being added to fresh media. Cells were then subjected to centrifugation at 460 × g for 5 min to remove DMSO and the pellet resuspended in the appropriate volume of media and added to a culture flask.

2.3 Stimulation of RACFs

RACFs were seeded at 2×10^5 cells per well in a 6 well plate or down scaled for smaller well formats. To induce quiescence the cells were washed once with PBS to remove the serum prior to the addition of reduced serum media. Cells were left for 24 h before stimulation detailed in sections 2.3.1 and 2.3.2.

2.3.1 Stimulation of RACFs with proinflammatory mediators

Subsequent to serum starvation, as detailed above, cells were cultured in reduced serum media, stimulated with a range of proinflammatory mediators in reduced serum media or reintroduced into normal culture media. Mediators examined were Ang II, TGFβ1, tumor necrosis factor α (TNFα), recombinant human IL-1β,

recombinant rat IL-1 α and the recombinant human IL-6 (with or without the recombinant human soluble IL-6 receptor α [sIL-6R α]). Preparation of the proinflammatory mediator stocks, final concentrations used and the supplier is detailed Table 2.2.

2.3.2 IL-1 β pathway inhibitor experiments

A range of IL-1 β pathway inhibitors were utilised to dissect the IL-1 β pathway. A nuclear factor (NF)- κ B inhibitor, SC-514, was diluted in reduced serum media to a final concentration of 100 μ M from a stock solution which was reconstituted in DMSO (see Table 2.3). Reduced serum media containing 0.1 % DMSO was also prepared. Cells were incubated with SC-514, 0.1 % DMSO or media alone for 30 min before the addition of 10 ng/mL IL-1 β . In a subset of experiments cells were pre-incubated with a p38 MAPK, a c-Jun N-terminal kinase (JNK) or a MAPK/ERK kinase (MEK1) inhibitor (SB203580, SP600125 and AZD6244 respectively), at the concentrations detailed in Table 2.3 for 1 hour prior to stimulation with 10 ng/mL IL-1 β .

Finally, 10 ng/mL IL-1 β and recombinant human IL-1 receptor antagonist (IL-1Ra) at 0.25, 0.5 or 1 μ g/mL were added simultaneously to the cells. All stimulations were performed for 24 h.

Table 2.2 Proinflammatory mediators used to stimulate RACFs.

Proinflammatory mediator	Dilution buffer	Stock concentration	Final concentration	Company
Ang II	Sterile dH ₂ O	10 μ M	500 nM	Sigma-Aldrich
Recombinant human TGF- β 1	Sterile 4mM HCl containing 1mg/mL BSA	20 μ g/mL	10 ng/mL	R & D systems
Recombinant human TNF- α	Sterile dH ₂ O containing 5 % (w/v) trehalose	50 μ g/mL	10 ng/mL	Peprotech
Recombinant human IL-1 β	Sterile PBS containing 0.1 % (v/v) BSA	10 μ g/mL	10 ng/mL	R & D systems
Recombinant rat IL-1 α	Sterile dH ₂ O containing 0.1 % (v/v) BSA	10 μ g/mL	10 ng/mL	Peprotech
Recombinant human IL-6	Sterile dH ₂ O containing 5 % (w/v) trehalose	20 μ g/mL	50 ng/mL	Peprotech
Recombinant human sIL-6R α	Sterile dH ₂ O containing 0.1 % (v/v) BSA	20 μ g/mL	50 ng/mL	Peprotech

Table 2.3 IL-1 β pathway inhibitors.

Inhibitor	Target	Dilution buffer	Stock concentration	Final concentration	Company
SC-514	NF- κ B	DMSO	100 mM	100 μ M	Cayman Chemical
SB203580	p38 MAPK	DMSO	25 mM	10 μ M	InvivoGen
SP600125	JNK	DMSO	50 mM	20 μ M	InvivoGen
AZD6244	MEK1	DMSO	10 mM	10 μ M	Selleckchem
Recombinant human IL-1Ra	IL-1R	Sterile dH ₂ O containing 0.1 % (v/v) BSA	100 μ g/mL	0.25, 0.5 and 1 μ g/mL	Peprotech

2.4 Nucleic acid extraction

2.4.1 Ribonucleic acid (RNA) and micro RNA extraction

Ribonucleic acid (RNA) and micro RNA (miRNA) were isolated using the miRNeasy mini kit (Qiagen, Manchester, UK) as per manufacturer's instructions, including the DNase digest step to remove contaminating deoxyribonucleic acid (DNA). RNase-free filter tips and plastics were used throughout the procedure and all steps were performed at room temperature unless stated otherwise.

Briefly, cells were washed in PBS before the addition of 700 μ L QIAzol lysis reagent to each well. Wells were scraped using the end of a 1000 μ L tip to remove any cells which were still attached and the lysates transferred to 1.5 mL Eppendorf tubes. Lysates were stored at -80°C or extraction performed immediately following lysis.

To extract the RNA, 140 μ L chloroform was added to each sample and shaken vigorously for 15 s. Samples were incubated for 2-3 min prior to centrifugation at $12,000 \times g$ for 15 min at 4°C . The upper clear phase, containing RNA, was transferred to a fresh Eppendorf tube and 525 μ L ethanol (1.5 volumes) was added to assist binding of RNA to the RNeasy[®] Mini column. Samples were mixed by pipetting and 700 μ L added to an RNeasy[®] Mini column in a 2 mL collection tube. Samples were subjected to centrifugation at $8,000 \times g$ for 15 s and the flow through discarded. This was repeated with the remaining sample before a wash using 350 μ L RWT buffer, a guanidine salt and ethanol containing buffer, to remove contaminants was performed. Columns were then subjected to centrifugation at $8,000 \times g$ for 15 min to remove the buffer. A stock solution of DNase was then prepared by dissolving DNase (1,500 Kunitz units) in 550 μ L RNAase free water. This was then diluted 1:7 in RDD buffer to make a working DNase solution and 80 μ L added to each column. The column was incubated for at least 15 min before a further wash with 350 μ L RWT buffer and subjected to centrifugation at $8,000 \times g$ for 15 s. Columns were then subjected to 2 x 500 μ L washes with RPE buffer to remove salts introduced by RWT washes. The columns were subjected to centrifugation at $8,000 \times g$ for 15 s following the first RPE wash, whereas for the second wash they were subjected to centrifugation at $8,000 \times g$

for 2 min. The columns were then placed in new collection tubes and subjected to centrifugation at 1 min at $16,000 \times g$ to dry the membrane. To elute the RNA, columns were added to 1.5 mL Eppendorf tubes, 30 μL RNase-free water added and incubated for 5 min prior to centrifugation at $8,000 \times g$ for 1 min. The elute was then passed back through the column to concentrate the RNA. RNA was quantified as detailed in section 2.4.3.

2.4.2 Deoxyribonucleic acid (DNA) extraction

2.4.2.1 Mini-Preparation

DNA extractions from 10 mL bacterial cultures were completed using the PureLink[®] Quick Plasmid Miniprep Kit (Invitrogen, Paisley, UK). Overnight bacterial cultures were prepared as described in section 2.7.6. All centrifugation steps were performed at room temperature unless stated otherwise.

Briefly, 3 mL of the overnight bacterial culture was subjected to centrifugation at $3,000 \times g$ and the pellet resuspended in 250 μL resuspension buffer (R3) containing 100 $\mu\text{g}/\text{mL}$ RNase A until the sample was homogeneous. To lyse cells, 250 μL lysis buffer (L7) was added to each sample and the sample mixed by inverting, again until homogeneous. This was incubated for 5 min, prior to the addition of 350 μL precipitation buffer (N4) and mixed by inverting. Lysates were subjected to centrifugation at $12,000 \times g$ for 10 min. Supernatants were transferred into a spin column in a collection tube prior to centrifugation at $12,000 \times g$ for 1 min. The flow through was discarded and 500 μL of an ethanol-based wash buffer (W10) added to each column. Columns were subjected to centrifugation at $12,000 \times g$ for 1 min and 700 μL of a second ethanol-based wash buffer (W9) added. Centrifugation was repeated and a further centrifugation at $12,000 \times g$ for 1 min performed to fully remove any remaining buffer. To elute the DNA, columns were transferred into 1.5 mL Eppendorf tubes and 30 μL nuclease free water added. Columns were incubated for 5 min prior to centrifugation at $12,000 \times g$ for 2 min. DNA concentration was then determined (section 2.4.3) and stored at -20°C .

2.4.2.2 Maxi-Preparation

To produce a large-scale DNA preparation, 500 mL bacterial cultures were prepared as described in section 2.7.6. DNA was extracted using the PureLink® HiPure Plasmid Filter Maxiprep Kit (Invitrogen) as per manufacturer's instructions. All centrifugation steps were performed at room temperature unless stated otherwise.

The bacterial pellet was obtained through centrifugation at $6,000 \times g$ for 15 min at 4 °C using and resuspended in 10 mL resuspension buffer (R3) containing 100 µg/mL RNase A. Cells were lysed by the addition of 10 mL lysis buffer (L7) and mixed by inverting. Following a 5 min incubation, 10 mL precipitation buffer (N3) was added and was mixed by inverting until the mixture was homogeneous. The lysate was then subjected to centrifugation at $20,000 \times g$ for 20 min. Meanwhile 30 mL equilibration buffer (EQ1) was added to an anion-exchange resin PureLink® HiPure filter column and allowed to pass by gravity flow to equilibrate the column. Following centrifugation and only once the EQ1 had drained; the clear DNA containing supernatant was added to the column and allowed to pass through. This column was then washed by the addition of 60 mL wash buffer (W8) which again was allowed to pass by gravity flow. DNA was then eluted by adding 15 mL elution buffer (E4) and was collected in a sterile centrifuge tube. To precipitate and desalt the DNA, 10.5 mL isopropanol was added prior to mixing by inversion and subjected to centrifugation at $15,000 \times g$ for 30 min at 4 °C. The supernatant was then discarded and the DNA pellet washed in 4 mL 70 % ethanol. The DNA was then subjected to centrifugation at $16,000 \times g$ for 5 min at 4 °C and the supernatant discarded. The pellet allowed to air dry prior to the addition of 200 µL nuclease free water. DNA concentration was determined by NanoDrop™ as described in section 2.4.3.

2.4.2.3 DNA extraction for lentiviral vector titre

DNA for LV vector titration (section 2.9.1) was extracted using the DNeasy blood and tissue kit (Qiagen) as per manufacturer's instructions. Briefly, 20 µL proteinase K (600 Anson unit [AU]/mL) was added to the 200 µL cell suspension in PBS (see section 2.9.1) to digest cellular proteins. To lyse the cells, 200 µL buffer

AL was added to each sample and vortexed prior to incubation at 56 °C for 10 min. Next, 100 % ethanol was added and the components mixed by vortexing. The mixture was then added to a DNeasy Mini spin column and subjected to centrifugation at 6000 × g for 1 min in order to isolate the DNA, which binds to the membrane of the spin column, from the solution. The flow through was then discarded and 500 µL of the ethanol containing wash buffer, buffer AW1, was added prior to centrifugation at 6000 × g for 1 min. This was followed by a second wash step involving the addition of 500 µL buffer AW2 (ethanol containing buffer). The columns were subjected to centrifugation at 20,000 × g for 3 min and the flow through discarded. Next the DNA was eluted by adding 50 µL nuclease free H₂O and incubated for 5 min prior to centrifugation at 6,000 × g for 1 min. This was repeated by adding the flow through back into the column to maximise DNA concentration. DNA concentration was determined by NanoDrop™ as described in section 2.4.3.

2.4.3 Nucleic acid quantification

The concentration and quality of both RNA and DNA was quantified using a NanoDrop™ 1000 Spectrophotometer (ThermoFisher Scientific). Initially, 1.4 µL of the sample was loaded onto a receiver fibre optic cable and the source fibre optic cable lowered onto the sample. Light was then passed through the sample using a xenon flash lamp and the absorbance at different wavelengths measured by a spectrometer. Nucleic acids absorb light at 260 nm and can therefore be used to determine the concentration of the sample using the Beer-Lambert equation as follows:

$$c = \left(\frac{A \times e}{b} \right)$$

Where: c is the concentration (ng/µL)

A is the absorbance (arbitrary units [AU])

e is the wavelength-dependent extinction coefficient (ng-cm/µL)

b is the path length (cm)

260/280 nm ratios of approximately 1.8 and 2 were considered pure for DNA and RNA respectively.

2.5 Reverse transcription

Complementary DNA (cDNA) was produced by reverse transcription of mRNA or miRNA to allow the levels to be detected and analysed.

2.5.1 Gene expression

mRNA templates were transcribed into cDNA using Taqman[®] Reverse Transcription Reagents. Reactions were prepared in a 96 well plate and contained 1x RT buffer, 5.5 mM MgCl₂, 2.0 mM dNTPs mix (0.5 mM each), 2.5 μM random hexamers, 0.4 U/μL RNase inhibitor, 1.25 U/μL multiscribe RT and 300 ng of the mRNA template. RNase free water was added to each reaction to adjust all reactions to the same volume. To allow the synthesis of cDNA, reactions were placed on a thermal cycler at 25 °C for 10 min to allow the random hexamers to anneal to the mRNA templates, followed by 48 °C for 30 min to permit reverse transcription and finally 95 °C to inactivate the multiscribe RT. cDNA was then stored at -20 °C for future use.

2.5.2 miRNA expression

MiRNA templates were reverse transcribed into cDNA using the Taqman[®] MicroRNA Reverse transcription Kit, with specific primers for each miRNA supplied in Taqman[®] miRNA assays. Each reaction was composed of 1 mM dNTP (with dTTP), 3.3 U/μL multiscribe RT, 1x RT buffer, 0.25 U/μL RNase inhibitor, 1x RT primer and 2.1 μL RNase free water. All RNA was diluted in RNase free water to 2 ng/μL prior to the addition of 2.5 μL to each reaction, to give 5 ng RNA in total. Reactions were then subjected to 16 °C for 30 min to allow primers to anneal to the miRNA templates, 42 °C for 30 min for reverse transcription to occur and 85 °C for 5 min to deactivate the multiscribe RT using a thermal cycler.

2.6 Quantitative PCR

Gene/miRNA expression was quantified by Taqman[®] qRT-PCR. Taqman[®] assays contain both a forward and reverse primer which is specific to the gene/miRNA of interest and a Taqman[®] probe. The probe has a fluorescent reporter dye attached to the 5' end and a quencher at the 3' end. When the probe is intact minimal fluorescence is emitted due to the close proximity of the fluorescent dye to the quencher, established by the principle of fluorescence resonance energy transfer (FRET) (Cardullo et al. 1988). The Taqman[®] probe binds to DNA downstream of the primers; therefore once the primer extension reaches the probe, Taq polymerase cleaves it. This releases the fluorescent reporter from the quencher resulting in an increase in fluorescence. The increase in fluorescence is exponential over time; therefore a plateau will eventually be reached, hence the end point is not a reliable measure of gene expression. The threshold cycle (Ct) is the PCR cycle at which fluorescence reaches an arbitrarily placed threshold on the exponential phase of amplification (Schmittgen and Livak 2008). The Ct value can be used to consistently measure expression (Higuchi et al. 1993). On all plates a housekeeper is measured to allow discrepancies in RNA concentrations to be accounted for. Data can then be normalised to the housekeeper levels and the fold change expressed as relative quantification (RQ) using the $2^{-\Delta\Delta C_t}$ method (Schmittgen and Livak 2008). All Taqman[®] assays used in this thesis utilised 6-carboxyfluorescein (FAM) as the fluorescent reporter dye and 6-carboxytetramethylrhodamine (TAMRA) as a quencher. The housekeeping gene used was Ubiquitin C (UBC).

2.6.1 Gene and miRNA expression

Taqman[®] was performed in a 384 well plate. For gene expression each reaction contained a final volume of 12.5 μ L including 5.25 μ L 2x Taqman[®] Universal Master Mix II - no UNG, 0.625 μ L 20x probe/primer mix (assay details are included in Table 2.4), 3.625 μ L RNase free water and 2 μ L cDNA. MiRNA expression was examined in a similar manner although a final reaction volume of 10 μ L was used. This consisted of 5 μ L 2x Taqman[®] Universal Master Mix II - no UNG, 0.5 μ L miRNA probe/primer mix (assay details are included in Table 2.5), 3.838 μ L RNase free water and 0.67 μ L cDNA. Plates was then sealed with an optical adhesive lid and

qRT-PCR performed on either the Applied Biosystems 7900HT Sequence Detection System or the QuantStudio 12K Flex Real-Time PCR System. The thermal cycling conditions were as follows; 95 °C for 10 min to activate the polymerase followed by 40 cycles of 95 °C for 15 sec to denature the DNA then 60 °C for 1 min for the primer/probe to anneal and extend.

Table 2.4 List of Taqman gene expression assays

Gene	Assay ID	RefSeq Gene ID
GJA1	Rn01433957_m1	NM_012567.2
GJA5	Rn00570632_m1	NM_019280.1
GJA7	Rn01750705_m1	NM_001085381.1
UBC	Rn01499642_m1	BC103477.1
ACTA2	Rn01759928_g1	NM_031004.2
CTGF	Rn01537279_g1	NM_022266.2
SERPINE	Rn01481341_m1	NM_012620.1
SNAI1	Rn00441533_g1	NM_053805.1
SNAI2	Rn01404476_m1	NM_013035.1

Table 2.5 List of Taqman miRNA expression assays

miRNA	Assay ID	MIRBASE ID
hsa-miR-19b	000396	Rno-miR-19b-3p
hsa-miR-30c	000419	Rno-miR-30c-5p
hsa-miR-101	002253	Rno-miR-101a-3p
mmu-miR-101b	002531	Rno-miR-101b-3p
U87	001712	AF272707 (NCBI accession)

2.7 Molecular cloning

2.7.1 Restriction endonuclease digestion

Restriction endonuclease digestions were performed to check DNA for the presence of restriction sites or to prepare DNA for ligation into a plasmid backbone. All digests were performed as per manufacturer's instructions in a total volume of either 20 μ L or 250 μ L for small or large quantities of DNA, respectively. Each reaction contained the appropriate DNA, reaction buffer and restriction endonuclease(s) and was incubated at 37 °C for 2 hours or overnight for small or large digests, respectively. The success of restriction endonuclease digestion was analysed by performing gel electrophoresis (section 2.7.2).

2.7.2 Agarose gel electrophoresis

The percentage of agarose gel prepared was determined by the size of DNA fragments expected. UltraPure™ Agarose (Thermo Fisher Scientific) was added to x1 UltraPure™ Tris/Boric acid/EDTA (TBE) buffer and dissolved by heating. The gel was allowed to cool for 5 min prior to the addition of 150 ng/mL ethidium bromide to enable DNA imaging. The gel was poured into mould and a comb used to create appropriate sized wells. Samples were prepared by adding the appropriate volume of 6x blue/orange loading dye (Promega, Southampton, UK). Samples and a suitable ladder (100 bp and/or 1 Kb; Promega) were loaded into the wells of the gel in an electrophoresis tank submerged in TBE buffer. Gels were subjected to 10 V/cm to allow DNA fragments to separate. DNA bands were visualised using a Bio-Rad ChemiDoc XRS ultra violet (UV) transilluminator.

2.7.3 DNA extraction from ethidium bromide gel

The Wizard® SV Gel and PCR Clean-up System (Promega) was used to extract DNA from agarose gel as per manufacturer's instructions. This kit is based on the ability of DNA to bind to a silica membrane in the presence of chaotropic salts (Boom et al. 1990).

Following agarose gel electrophoresis (section 2.7.2), DNA was visualised using a UV transilluminator and the segment of gel containing the DNA band excised from the excess gel. A guanidine isothiocyanate (chaotropic salt) containing solution (Membrane Binding Solution) was added to the agarose gel segment at a ratio of 10 μ L to 10 mg gel segment. This was incubated at 50-56 °C for approximately 10 min until the gel had fully dissolved. The solution was then transferred into a SV Minicolumn, incubated for 1 min and subjected to centrifugation at 16,000 \times g for 1 min. The flow through was discarded and 700 μ L of the ethanol containing Membrane Wash Solution was added to each column prior to centrifugation at 16,000 \times g for 1 min. This was repeated with a volume of 500 μ L preceding centrifugation at 16,000 \times g for 5 min. The columns were then subjected to centrifugation at 16,000 \times g for 1 min without the centrifuge lid to allow maximal ethanol evaporation. The columns were then transferred to a 1.5 mL Eppendorf tube and 40 μ L nuclease-free water was added directly to the membrane in preparation for DNA elution, followed by 5 min incubation and centrifugation at 16,000 \times g for 1 min. The eluted DNA was passed through the column one further time to increase the yield. DNA concentration was then quantified (section 2.4.3).

2.7.4 Phenol chloroform clean-up of DNA

To remove potential contaminants from DNA, a phenol chloroform extraction was performed. An equal volume of a phenol:chloroform:isoamyl alcohol (Sigma-Aldrich) was slowly added on top of the DNA solution. The mixture was then subjected to vortexing for 30 sec prior to centrifugation at 16,000 \times g for 2 min. The upper phase, containing DNA, was then transferred into a fresh Eppendorf tube and an equal volume of chloroform added to remove phenol. Next, the solution was subjected to vortexing for 30 sec, prior to centrifugation at 16,000 \times g for 2 min and the upper phase transferred to a clean Eppendorf tube. A tenth of the total volume of 3M sodium acetate (pH 5.2) was added along with 2 volumes of 100 % ethanol followed by incubation on dry ice for 15 min. The sample was then subjected to centrifugation at 16,000 \times g for 10 min to pellet the DNA. The DNA pellet was resuspended in 70 % ethanol to de-salt and subjected to centrifugation at 16,000 \times g for 2 min. Next, the solution was discarded and the pellet left to air dry prior to being resuspended in nuclease free water.

2.7.5 DNA dephosphorylation and ligation

In preparation for ligation of a DNA fragment into a vector, linearised vectors underwent dephosphorylation of 5' DNA ends in order to prevent the re-ligation of vector “sticky ends”. Reactions consisted of 1 µg DNA, 5 units Antarctic phosphatase, 1x Antarctic phosphatase buffer and nuclease free water which was incubated at 37 °C for 15 min followed by 70 °C for 5 min to heat inactivate the Antarctic phosphatase.

Ligation reactions were performed using a range of insert:vector molar ratios. The mass of vector backbone was maintained at 50 ng and the mass of insert calculated using the following equation:

$$\text{Mass of insert (ng)} = \frac{\text{mass of vector (ng)} \times \text{size of insert (Kb)}}{\text{size of vector (Kb)}} \times \text{molar ratio}$$

Ligation reactions were performed in a total volume of 10 µL and consisted of the appropriate insert/dephosphorylated vector masses, 1 µL T4 DNA Ligase (NEB), 1x T4 DNA Ligase Buffer (NEB) and nuclease free water. Reactions were incubated at 15 °C overnight then stored at 4 °C until transformation into bacteria (section 2.7.6) the same day.

2.7.6 Transformation of DNA and bacterial culture

To allow the amplification of intact vectors, they were transformed into bacteria via heat shock or electroporation (section 2.10.1). Both methods cause bacterial cell membranes to briefly become permeable to allow the vectors to pass into the cell. Vectors utilised contain an antibiotic resistance gene which was used to select colonies that contain the vector of interest. Ampicillin or kanamycin at 100 µg/mL or 50 µg/mL, respectively were used.

For heat shock, JM109 competent *Escherichia coli* (*E. coli*), produced in-house or purchased from Promega were used. Cells were stored at -80 °C and thawed on ice. For each ligation reaction (section 2.7.5), 5 µL of the reaction was added to 50 µL of cells. For vectors, 1 or 10 ng was added to 50 µL cells. Cells and DNA were

then mixed gently and incubated on ice for 30 min. Next, samples were heated at 42 °C for 30 sec and rapidly placed back on ice for 2 min. Next, 450 µL Super Optimal broth with Catabolite repression (SOC) medium was gently added to the sample and agitated at 37 °C for 1 hr prior to spreading on an agar plate containing the appropriate antibiotic. Agar plates were incubated at 37 °C overnight to allow the bacteria to form colonies.

The following day, single colonies were picked and added to 10 mL Luria Broth (LB) containing the appropriate antibiotic and incubated at 37 °C overnight shaking at 200 rpm. Mini preparations (section 2.4.2.1), diagnostic restriction endonuclease digests (section 2.7.1) and cryopreservation of the bacteria (section 2.7.6.1) were performed at this stage. The remainder of the bacterial culture was added to 500 mL LB containing the appropriate antibiotic to grow a large scale culture and a maxi preparation (section 2.4.2.2) performed. Diagnostic restriction endonuclease digests and cryopreservation were also completed on the extracted DNA.

2.7.6.1 Cryopreservation of bacterial stocks

To preserve bacterial cultures, 800 µL of the culture and 200 µL sterile glycerol were mixed together in a cryovial and stored at -80 °C. To re-establish bacterial growth from a frozen stock, it was thawed on ice and a small volume added to an agar plate containing the appropriate antibiotic to allow single colonies to grow.

2.7.7 DNA sequencing

DNA sequencing was performed to confirm the success of cloning and to identify any DNA mutations. BigDye™ Terminator v3.1 Cycle sequencing kit (ThermoFisher Scientific) utilises Sanger sequencing to allow sequencing in a single reaction and detection by fluorescence.

Sequencing was performed by first performing a PCR reaction consisting of 100 ng of DNA template (in a total volume of 1-2 µL), 1x BigDye™ Terminator v3.1 Sequencing Buffer, 1 µL BigDye™ Terminator v3.1 Ready Reaction Mix, 2 µL 2 µM primer and nuclease free water in a final volume of 20 µL. Samples were then subjected 25 cycles of the following temperatures on a thermal cycler; 96 °C for

45 sec to allow DNA denaturing, 50 °C for 25 sec for primers to anneal and 60 °C for 4 min for extension. The reaction was then cooled to 4 °C prior to DNA clean up.

The PCR product was then cleared of all reagents using Agencourt® CleanSeq® (Beckman Coulter, High Wycombe, UK) as per manufacturer's instructions. Briefly, 10 µL CleanSeq® reagent, which contains magnetic beads that DNA is able to bind to, was added to the 20 µL PCR reaction followed by 62 µL 85 % ethanol. The samples were then vortexed prior to incubation on a magnetic plate for 2 min. Next, the solution was discarded while still on the magnetic plate to avoid losing the DNA/magnetic beads. DNA was washed with 150 µL 85 % ethanol and vortexed to mix. Samples were incubated on the magnetic plate for a further 2 min, the solution removed and left to air dry for 10 min. To detach the DNA from the beads, 40 µL of nuclease free water was added to each sample and resuspended by pipetting. Finally, to remove the beads from the samples, they were placed on the magnetic plate and 20 µL of the water containing DNA was removed and added to a MicroAmp® Optical 96-well reaction plate (ThermoFisher Scientific). DNA sequencing was performed on the 3730 DNA Analyser (ThermoFisher Scientific) and electropherograms analysed using CLC Genomics Workbench 7.0 software.

2.8 Transfection of DNA to cultured cells

Xfect™ transfection reagent (Takara Bio, Saint-Germain-en-Laye, France) was used as per manufacturer's instructions to introduce DNA to cultured cells. A day prior to transfection, cells were seeded in the appropriate well format so that they were 50-70 % confluent at the time of transfection. All steps were completed under laminar flow to maintain sterility. A range of DNA masses (2.5-7.5 µg for 1 well of a 6 well plate) were combined with Xfect™ reaction buffer to achieve a final volume appropriate for that well format (100 µL for a 6 well plate). The samples were mixed by vortex for 5 sec prior to the addition of the Xfect™ polymer at a ratio of 0.3 µL polymer: 1 µg DNA. Samples were then vortexed for 10 sec and incubated for 10 min to allow nanoparticle complexes to form. Fresh complete media was then replaced on the cells (1 mL for a 6 well plate) and the entire volume of nanoparticle complex solution slowly added. Cells were incubated at

37 °C and 5 % CO₂ and the media replaced 4 h after the initial transfection. Typically, cells were cultured for 48 h before DNA expression was examined.

2.9 Lentiviral vector production and purification

A second generation, self-inactivating (SIN) LV vector expressing eGFP was produced in-house using published methods (Demaison et al. 2002). This system utilises 3 plasmids whereby the HIV genes are split across the 3 plasmids; a transfer vector, an envelope plasmid and a packaging plasmid (Merten et al. 2016; Sakuma et al. 2012). The transfer vector contains the gene to be expressed by the LV vector along with the promoter that will drive the expression. Two long terminal repeats (LTRs) are located either side of this segment of DNA allowing insertion into the genome (Sakuma et al. 2012). The envelope plasmid used (pMDG) expresses the glycoprotein (gp) of vesicular stomatitis virus (VSV-G). Finally, the packaging plasmid (pCMVΔ8.74) encodes Gag, Pol, Rev and Tat genes. pMDG and pCMVΔ8.74 were a gift from Didier Trono (Addgene plasmid #12259 and #22036 respectively).

One day prior to transfection, 80-90 % confluent 293T HEK cells in 150 cm² flasks were passaged at a ratio of 1:2 to make 13 flasks. The following day, 12 flasks were triple transfected with a transfer vector containing eGFP under the control of the spleen focus-forming virus (SFFV) promoter (pHR-SIN-SFFV-GFP), pMDG and pCMVΔ8.74. For each flask 50 µg pHR-SIN-SFFV-GFP, 17.5 µg pMDG and 32.5 µg pCMVΔ8.74 was added to 5 mL Optimem (ThermoFisher Scientific). Next, the transfection reagent, polyethylenimine (PEI) (Sigma-Aldrich), was added to a further 5 mL per flask to produce a final concentration of 6 µM. These solutions were mixed, filtered and left for 20 min at room temperature to allow DNA:PEI complexes to form. Meanwhile each flask was gently washed with 5 mL Optimem before the addition of 10 mL of the DNA:PEI complexes. Cells were incubated for 4 h at 37 °C and 5 % CO₂. The transfection media was then removed and 20 mL complete MEM added.

LV vectors were harvested 48 h later by filtering the media and storing at 4 °C. Next, 10 mL of fresh media was added and cells were incubated for a further 24 h. The media was then filtered and the two sets of media mixed prior to ultracentrifugation.

Beckman 17 mL thinwalled, ultra-clear ultracentrifuge tubes were sterilised using 70 % ethanol followed by sterile PBS. Tubes were then loaded with media and subjected to centrifugation at $90,000 \times g$ for 1 h at room temperature. The supernatant was then discarded and more media loaded into the tubes. This centrifugation step was repeated until all the media had been loaded. Subsequent to the final spin tubes were placed on ice and 100 μ L Optimem added to each tube. The tubes were then left on ice for 20 min and the virus resuspended. The virus was then aliquoted and stored at -80 °C.

2.9.1 Lentiviral vector titration

293T HEK cells were seeded at 5×10^4 cells per well in a 12 well plate. The following day the media was replaced with 1 mL complete MEM. Next, the LV preparation was initially diluted 1 in 100 in media and four serial 1 in 10 dilutions prepared thereafter. These dilutions were then added to the cells giving the final dilutions that ranged from 3×10^{-7} - 1×10^{-4} . The cells were left for 72 h before media was removed and 200 μ L PBS was added to each well. Cells in PBS were stored at -20 °C and thawed before DNA extraction performed as detailed (section 2.4.2.3). All samples were diluted to 250 ng/ μ L ready for titration.

The concentration of LV vector was determined by qRT-PCR (section 2.6). The primer/probe mix used consisted of a forward and reverse primer (both at 1.2 μ M) as well as a FAM labelled probe containing a TAMARA quencher at 0.4 μ M (primer and probe sequences are shown in Table 2.6). Serial dilutions of pHR-SIN-SFFV-GFP were performed in nuclease free H₂O ranging from 1×10^{13} to 1×10^4 copies of the plasmid to produce a standard curve. The top standard was prepared by performing the following calculations:

1. Calculate the weight of one plasmid copy

$$\frac{\text{Size of plasmid (bp)} \times \text{Weight of 1 bp (Da)}}{\text{Avogadro's constant}} = \text{g/plasmid copy}$$

Where: The weight of 1 bp = 660 Da

$$\text{Avogadro's constant} = 6.023 \times 10^{23} \text{ molecules/mole}$$

2. Determine the number of plasmid copies in 1 mL

$$\frac{\text{Concentration of plasmid stock (g/mL)}}{\text{g/plasmid copy}} = \text{no. of plasmid copies/mL}$$

3. Preparation of the top standard

$$\frac{\text{no. of plasmid copies/mL}}{1 \times 10^{13}} = \text{dilution factor for top standard}$$

$$\frac{1000}{\text{dilution factor for top standard}}$$

$$= \mu\text{L of plasmid stock required to make 1 mL } 1 \times 10^{13} \text{ standard}$$

Each reaction was comprised of 6.25 μL Taqman® Universal Master Mix II - no UNG, 3.125 μL primer/probe mix (described above), 2.125 μL nuclease free H_2O and 1 μL standard or sample. All samples were performed in triplicate and the plate run in the same manner as described (section 2.6.1).

To determine the final LV titer the C_t values from the standards were plotted against the plasmid copies and a logarithmic trendline applied. The equation of the line was then applied to the C_t values of the samples to determine the number of plasmid copies within the samples. This was then corrected for the volume and dilution of the virus added to the cells in the titer plate by performing the following calculations:

1. DNA concentration (ng/ μ L) \times volume of DNA eluted (30 μ L)
= total DNA extracted (ng)

2. Determine the percentage of DNA used in the qRT-PCR

$$\left(\frac{\text{DNA used in qRT-PCR (250ng)}}{\text{total DNA extracted (ng)}} \right) \times 100 = \% \text{ of total cell DNA used}$$

3. Determine the number of cells used for qRT-PCR

$$\left(\frac{\text{no. of cells (5} \times 10^4 \text{)}}{100} \right) \times \% \text{ of total cell DNA used} = \text{no. of cells used}$$

4. Determine the copies of plasmid in 1 cell

$$\frac{\text{no. of plasmid copies in samples}}{\text{no. of cells used}} = \text{plasmid copies/cell}$$

5. Calculate the titre of the LV vector in particle infectious units (PIU) per mL

$$\text{plasmid copies/cell} \times \left(\frac{\text{dilution of virus stock} \times 1000}{\mu\text{L of virus dilution added}} \right) = \text{PIU/mL}$$

Obvious outliers were excluded and an average of the PIU/mL values were taken to produce a final titre. Two batches of a LV vector overexpressing eGFP (LVEGFP) were produced giving similar titers of 1.2×10^9 and 1.1×10^9 PIU/mL.

Table 2.6 Sequences of primers and probe used in lentiviral vector titration.

Primer/probe	Sequence
Forward primer	5'-TGTGTGCCCGTCTGTTGTGT-3'
Reverse primer	5'-GAGTCCTGCGTCGAGAGAGC-3'
Probe	5'FAM-CAGTGGCGCCCGAACAGGGA-(TAMRA)-3'

2.10 Adenoviral vector production and purification

The commercially available AdEasy system (Agilent Technologies, Stockport, UK) was used to produce first generation Ad vectors. Ad production followed a published protocol (Alba et al. 2012). HEK 293 cells contains the left-hand portion of the adenovirus serotype 5 genes (Graham et al. 1977) for the production of recombinant Ad vectors and were therefore used in this study.

2.10.1 Electroporation and homologous recombination

Homologous recombination of a shuttle vector, containing the gene of interest, and the pAdEasy-1 vector, a gift from Bert Vogelstein (Addgene plasmid #16400) (He et al. 1998), which contains most of the Ad serotype 5 genes, was performed in electrocompetent BJ5183 cells (Agilent Technologies). The shuttle vector used was pShuttle-CMV. Prior to transformation, pShuttle-CMV was linearised using the restriction endonuclease, *PmeI*, overnight (section 2.7.1). The DNA was then dephosphorylated (section 2.7.5) and excess reagents removed by a phenol chloroform extraction (section 2.7.4).

BJ5183 cells that contain pAdEasy-1 were thawed on ice and 100 ng of the linearised pShuttle-CMV, made up in 6 μ L, was added to 50 μ L BJ5183 cells. The solution was gently mixed, transferred to a chilled 2 mm electroporation cuvette (Geneflow, Lichfield, UK) and incubated on ice for 3 min. The sample was then pulsed at 200 Ω , 2.5 kV and 25 μ F using a BioRad MicroPulser™. Next, 450 μ L SOC media was added and cells were shaken at 37 °C for 1 hr. Either, 25 or 100 μ L was spread over an agar plate containing 50 μ g/mL kanamycin and incubated at 37 °C overnight. The following day the smallest colonies were picked and processed as detailed in section 2.7.6.

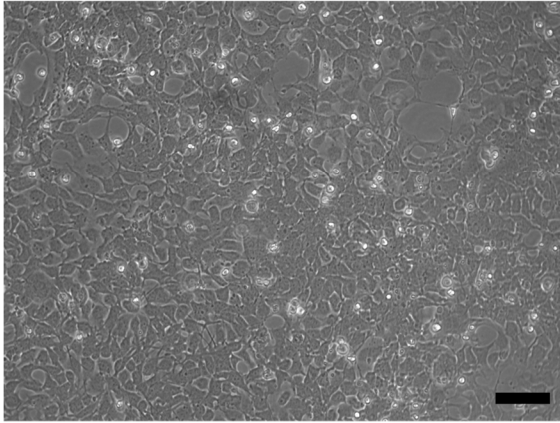
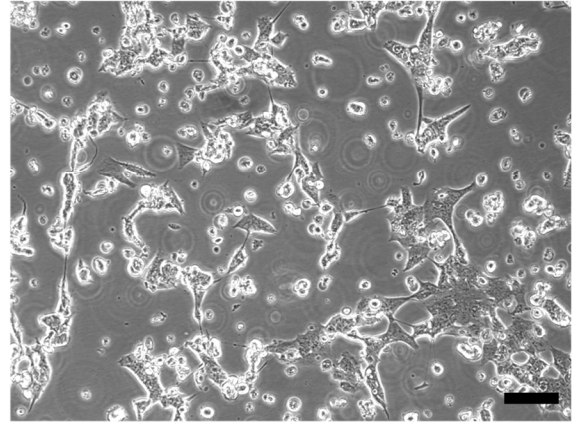
2.10.2 Transfection of adenoviral genomes to HEK 293 cells

Ad genomes are required to be linear prior to transfection into HEK 293 cells, to prevent the expression of the antibiotic resistance gene and the origin of replication. This was achieved by digesting 50 μ g DNA with *PacI* (section 2.7.1) and subsequently performing phenol: chloroform extraction of the DNA as detailed

in section 2.7.4. Next, 5 µg of linearised DNA was transfected into HEK 293 cells in 6 well format as described in section 2.8. Media was replaced every 2-3 days and the cells monitored for the presence of plaques which represent generation of Ad vector progeny.

2.10.3 Generation of crude adenovirus stocks

Successful transfections, showed the presence of plaques after 6-10 days. At this point the media was not changed, to allow the cytopathic effect (CPE) to move through the well (Figure 2-1). Once CPE was complete the media and cells were collected and subjected to centrifugation at 300 × g for 10 min. The pellet was resuspended in 1 mL sterile PBS and an equal volume of Arklone P (1,1,2-Trichlorotrifluoroethane [Sigma-Aldrich]) added to the sample. The sample was inverted for 10 sec followed by shaking for 5 sec. This mixing step was repeated and the sample subjected to centrifugation at 800 × g for 10 min. The upper, virus containing layer was then removed and stored at -80 °C in 50 µL aliquots. This crude preparation was plaque purified as detailed in section 2.10.4.

Control HEK 293 cells**HEK 293 cells showing CPE****Figure 2-1 Cytopathic effect in HEK 293 cells.**

Images of control HEK 293 cells and cells showing cytopathic effect (CPE), following adenoviral vector production. CPE is an indication of cell lysis. Scale bar represents 100 μm .

2.10.4 Plaque purification

To ensure the Ad vector purified has originated from a single generated virion, two rounds of plaque purification were performed. HEK 293 cells from a confluent T150 cm² flask were resuspended in 15 mL media and 3 mL of the cell suspension was added to 10 mL fresh media. Next, 100 µL of the diluted cell suspension was added to each of 80 wells of a 96 well plate which produced cells at a confluency of 50-60 % at the time of Ad vector addition. The following day, serial dilutions of the crude preparation (section 2.10.3) were performed to produce 1×10^{-4} and 1×10^{-6} - 1×10^{-11} dilutions. The media was then removed from the cells and 100 µL of the diluted Ad preparations or fresh media (for control cells) were added. The media was replaced the following day and every 2-3 days thereafter. The plate was monitored daily and the presence of plaques noted. Once plaques were apparent, the media was not replaced in that well. Seven days after the addition of the crude Ad vector dilutions, a second 96 well plate was prepared in the same manner as above for the second plaque purification. On the eighth day, the media/cells from wells at the greatest dilution that were CPE positive were collected. All samples were subjected to centrifugation at $300 \times g$ for 10 min and all except one of the pellets were stored at $-80 \text{ }^{\circ}\text{C}$. One pellet was resuspended in 200 µL PBS and the Ad vector extracted in the same manner as detailed (section 2.10.3). Next, 50 µL of Ad vector stock was used to prepare the same serial dilutions and added to the cells seeded the day before as described above. This second plaque purification plate was completed in the same manner and 100 µL of the plaque pure Ad vector stock added to an 80-90 % confluent flask of HEK 293 cells. Once CPE was completed the media/cells were collected and subjected to centrifugation at $300 \times g$ for 10 min. The pellet was resuspended in 1 mL PBS and the Ad vector extracted as previously described (section 2.10.3). This Ad vector seed stock was stored in 100 µL aliquots at $-80 \text{ }^{\circ}\text{C}$. A large scale Ad preparation was then performed as detailed (section 2.10.5).

2.10.5 Large scale adenovirus production

To amplify a pure recombinant Ad vector, 50 μL of the Ad seed stock was added to 500 mL complete media. Next, media on 20 T150 cm^2 flasks of 80-90 % confluent HEK 293 cells was removed and replaced with 20 mL of the Ad vector containing media. The media was replaced every 3 days until CPE was apparent, fresh media was then added (not replaced) until CPE complete. Next, the media and cells was collected and subjected to centrifugation at $300 \times g$ for 10 min. The pellet was resuspended in 6 mL sterile PBS and an equal volume of Arklone P added to the sample. The sample was inverted for the slightly longer time of 30 sec followed by shaking for 10 sec. This mixing step was repeated and the sample subjected to centrifugation at $800 \times g$ for 15 min. The upper virus containing layer was then removed and subjected to double caesium chloride gradient ultracentrifugation (section 2.10.6).

2.10.6 Caesium chloride gradient ultracentrifugation

Caesium chloride (CsCl) gradient ultracentrifugation was performed using two gradients to both purify and concentrate Ad vector preparations. CsCl solutions were prepared by dissolving the appropriate densities in 1x Tris density (TD) buffer to produce 1.25, 1.34 and 1.40 g/mL solutions. Beckman 14 mL thinwalled, ultra-clear ultracentrifuge tubes were sterilised using 70 % ethanol and rinsed with sterile PBS prior to the addition of 2.5 mL 1.25 g/mL density CsCl. This was followed by the gentle addition of 2.5 mL 1.40 g/mL density CsCl creating a gradient with the 1.25 g/mL density above the CsCl 1.40 g/mL density CsCl. The Ad vector solution was then gently added avoiding disruption to the CsCl gradient and PBS added to fill the tube. The samples were then subjected to centrifugation at $90,000 \times g$ for 90 min at 20°C . Following centrifugation, three distinct bands were observed; the top band contained cellular debris, the middle band consisted of empty viral capsids and the bottom white layer at the intercept of the two CsCl layers was the Ad vector (Figure 2-2). Next, a 21-gauge needle was used to pierce the tube just below the adenoviral vector layer and the virus collected into a syringe. This was then added to a second CsCl gradient which consisted of 5 mL 1.34 g/mL density CsCl in a fresh ultracentrifuge tube. The samples were then

subjected to centrifugation at $90,000 \times g$ overnight at $20\text{ }^{\circ}\text{C}$. The following day, one distinct band was present and removed in the same manner as above. Dialysis of the Ad vector was then performed as described (section 2.10.7).

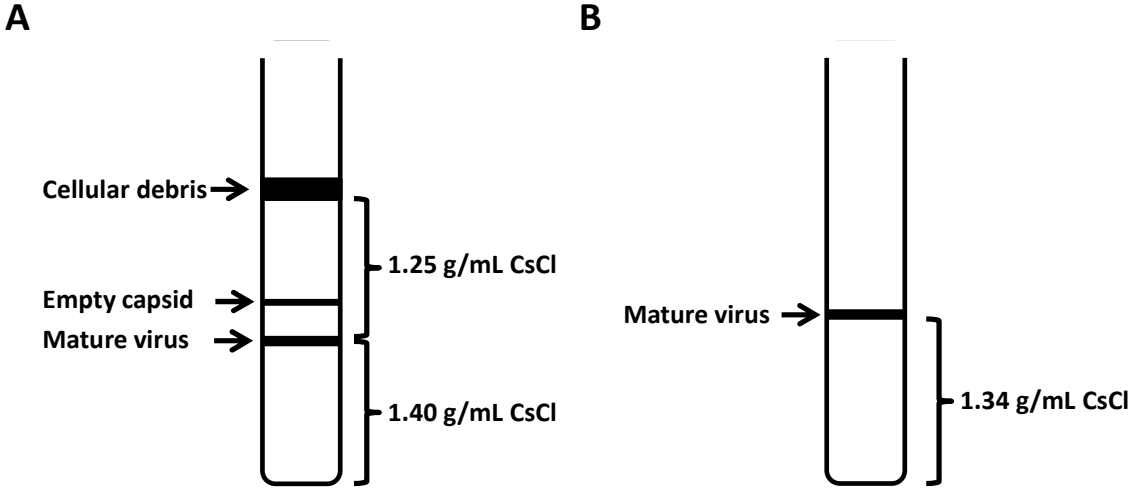


Figure 2-2 Purification of the mature virus following double CsCl gradient ultracentrifugation.

(A) Following the first ultracentrifugation, three clear bands can be observed; the top band contains cellular debris, the middle band consists of empty capsid and the bottom band at the intercept of the CsCl layers is the mature virus. (B) The mature virus is then extracted and subjected to a second CsCl gradient ultracentrifugation, where one distinct band of mature virus is detected.

2.10.7 Adenoviral vector dialysis

To remove CsCl from the Ad preparations, dialysis was performed. The Ad vector preparation was added to a Slide-A-Lyzer™ cassette with a molecular weight cut off of 10,000 kDa (ThermoFisher Scientific) and dialysed in a beaker containing 2 L of sterile 1x TE buffer for 90 min. The buffer was then replaced and the dialysis continued for 2 h. Finally, the buffer was changed to 5 L 1x TE buffer containing 10 % glycerol and dialysed for a further 3 h. The Ad vector was then removed from the cassette and stored in aliquots at -80 °C. The titer of the purified Ad vector was determined as detailed in section 2.10.8.

2.10.8 Adenoviral vector titration

The titer of the Ad vector was determined by two methods; end point dilution, to determine the ability of the vector to transduce cells, and micro-BCA, to examine the number of viral particles (vp).

2.10.8.1 Titration by end point dilution

HEK 293 cells were seeded into a 96-well plate and serial dilutions added as previously detailed (section 2.10.4). Following 8 days from addition of Ad vector to the cells, the plate was examined for the presence of plaques. The following calculations were then performed to obtain the titer of the purified Ad vector (Alba et al. 2012).

$$\text{Proportionate distance} = \frac{\% \text{ positive above } 50 \% - 50 \%}{\% \text{ positive above } 50 \% - \% \text{ positive below } 50 \%}$$

Log infectivity dose (ID)₅₀ = Log dilution above 50 % +
(Proportionate distance × -1)

$$\text{Tissue culture (TC) ID}_{50} \text{ (per mL)} = \frac{1}{\text{ID}_{50}} \times \text{Dilution factor (10)}$$

As one TCID₅₀ is equal to 0.7 particle forming units (pfu) the TCID₅₀ was multiplied by 0.7 to calculate the final titer in pfu/mL. An identical process was also completed in HeLa cells to ensure the Ad preparation was free from replication competent adenovirus. The Ad vectors overexpressing Cx43 and eGFP, AdCx43 and AdeGFP, used in the current study had a titer of 1.5×10^{10} and 1.1×10^{11} pfu/mL, respectively.

2.10.8.2 Viral particle titration by micro-BCA

A micro bicinchoninic acid (BCA)[™] Protein Assay Kit (ThermoFisher Scientific) was used to determine the number of viral particles in the purified Ad vector preparation as per manufacturer's instructions. This assay utilises the reduction of copper from its Cu²⁺ state to its Cu¹⁺ form by protein. Chelation of one Cu¹⁺ ion with two BCA molecules results in the formation of a purple-coloured product which can be quantified through its absorbance at 562 nm. The protein concentration has a linear relationship with absorbance and therefore a standard curve can be used to determine unknown concentrations of protein samples.

Briefly, BSA standards ranging from 0-200 µg/mL were prepared in PBS and 150 µL added in duplicate to individual wells of a 96-well plate. Next, 1, 3 and 5 µL of the Ad vector were added in duplicate to wells of the plate and the total volume made up to 150 µL with PBS. The micro-BCA working reagent was prepared by mixing the micro-BCA reagent A (MA), B (MB) and C (MC) at a ratio of 25:24:1. Next, 150 µL of the working reagent was added to each well and incubated at 37 °C for 2 h and the absorbance at 562 nm measured on the Perkin Elmer Victor x3 plate reader.

The protein concentrations were calculated by subtracting the average blank absorbance value and applying to the equation of the linear line of best fit created from the standards. The concentrations were then corrected for the volume of virus used. As 1 µg of protein is equal to 4×10^9 vp (Alba et al. 2012) the corrected protein concentration in µg/mL was multiplied by 4×10^9 to calculate the final titre in vp/mL. The AdCx43 used in the current study had a titer of 2.8×10^{11} vp/mL.

2.11 Viral vector addition to cells

LV and Ad vectors, produced by methods described in sections 2.9 and 2.10 respectively, were added to target cell types in complete media. Cells were seeded in the appropriate well format one day prior to viral vector addition. The viral vector required was added to the cells at a range of multiplicity of infection (MOI). The volume of viral vector required was calculated using the following equation:

$$\text{Volume of viral vector required (mL) per well} = \frac{\text{no. of cells} \times \text{MOI}}{\text{Viral titre (PIU/mL or pfu/mL)}}$$

The viral vector was diluted in complete media prior to the addition to the cells.

2.12 Protein preparation for western immunoblotting

On the day of cell lysate preparation, 1x complete protease inhibitor cocktail (Roche Diagnostics, West Sussex, UK), 1 % (v/v) Triton X-100, 250 mM mannitol, 1 mM dithiothreitol (DTT), 1 mM Na₃VO₄ and 0.1 mM phenylmethylsulfonyl fluoride (PMSF) was added to protein lysis buffer. To prepare cell lysates, cells were placed on ice and washed once with ice cold PBS. Next, 200 µL of complete protein lysis buffer was added to each well and scraped with the end of a 1 mL syringe plunger. Lysates were then added to a 1.5 mL Eppendorf tube and rotated at 4 °C for at least 30 min to allow sufficient lysis of the cells. This was followed by centrifugation at 16,000 × g at 4 °C and the protein containing supernatants stored at -20 °C.

2.12.1 Protein quantification

Protein concentrations were determined using a Pierce™ BCA Protein Assay Kit (ThermoFisher Scientific), as per manufacturer's instructions. This assay is based on the same principle as the micro-BCA (section 2.10.8.2). Briefly, standards were prepared by performing serial dilutions of the top BSA solution (2000 µg/mL) in protein lysis buffer. Final concentrations were as follows: 2000, 1500, 1000, 750, 500, 250, 125, 25 and 0 µg/mL. Samples were prepared as described (section

2.12), thawed on ice and a 1:5 dilution in lysis buffer performed prior to quantification. In a 96 well plate, 25 μ L of each standard or diluted sample were added to the plate in duplicate. The BCA working reagent was prepared by mixing reagent A and B in a ratio of 50:1 prior to the addition of 200 μ L to each well. The plate was then incubated for 30 min at 37 °C protected from light and the absorbance at 562 nm measured on a Perkin Elmer Victor x3 plate reader. The concentration of protein was determined by applying the standard curve to the absorbance values of the unknown concentration of the protein samples and corrected for dilution.

2.13 Western immunoblotting

Protein samples were separated by polyacrylamide gel electrophoresis (PAGE). This method allows proteins to be separated according to size and charge, whereby smaller proteins travel further through the gel (Mahmood and Yang 2012). TBS contained 0.1 % (v/v) Tween 20 (TBS-T).

Depending on protein concentration, as determined by BCA assay (section 2.12.1), 9-15 μ g of each sample was prepared for PAGE. All samples were corrected to the same volume using lysis buffer and the appropriate volume of NuPAGE® LDS sample buffer (ThermoFisher Scientific) added to produce a final concentration of 1x. Samples were mixed by vortex and denatured at 95 °C for 5 min using a thermal cycler. Meanwhile NuPAGE® MES SDS running buffer (x20) (ThermoFisher Scientific) was prepared by adding 50 mL to 950 mL dH₂O and added to the gel tank. Following denaturing, samples were placed on ice to cool before loading into wells of 4-12 % Bis-Tris precast polyacrylamide gel (ThermoFisher Scientific). A full range rainbow ladder (GE Healthcare Life Sciences, Buckinghamshire, UK) was also added to a well to allow the size of proteins to be identified. A current of 150-200V was then passed through the gel for approximately one hour to separate the proteins.

Prior to transfer of protein to a 0.2 μ m nitrocellulose membrane (GE Healthcare Life Sciences, UK), the membrane was soaked in dH₂O for 5 min to permeabilise the membrane. The membrane and four sheets of filter paper were then soaked in transfer buffer 10 min prior to transfer. The gel was removed from its cassette

and placed in transfer buffer to prevent drying out. A sponge was placed on the black (negative) side of the transfer tank cassette, followed by two filter sheets of paper, the gel then the membrane. Another two filter papers were placed on top and pressure applied to the stack rolled to remove any air bubbles. Finally a sponge was positioned on top, the cassette closed and moved into the transfer tank. Transfer was performed at 100 V for 1 hr 30 min at 4 °C.

Following transfer, the membrane was washed once in PBS for 5 min then blocked in blocking buffer (TBS-T:SEA BLOCK Blocking buffer [ThermoFisher Scientific]) at a ratio of 1:1) to prevent non-specific binding of antibodies. The primary antibody was then made up in blocking buffer at the dilution indicated in Table 2.7. Antibodies for GAPDH or β -tubulin were used as a loading control. Two antibodies, could be incubated simultaneously providing the antibodies were raised in different species. The antibody mixtures were applied to the membrane and incubated at 4 °C overnight on a shaker.

The following day, the primary antibody was removed and four 15 min washes in TBS-T performed. To detect antibody binding, membranes were then incubated for 1 hr at room temperature on a shaker with a 1:15,000 dilution of the IRDye® 680RD Goat anti-Mouse IgG (H + L) secondary antibody (LI-COR Biosciences, Cambridge, UK) and Alexa Fluro® 790 Goat anti-Rabbit IgG secondary antibody (ThermoFisher Scientific) in blocking buffer. This step and all preceding steps were protected from light. The membrane was then washed three times in TBS-T for 10 min per wash followed by a 10 min wash in PBS. The membrane was then imaged on the Odyssey® CLx Imaging System (LI-COR Biosciences) using the appropriate channel and quantified using Image Studio Lite v5 Software.

Table 2.7 Primary antibody details used in western immunoblotting

Protein	Host Species	Antibody Clonality	Concentration	Molecular Weight (kDa)	Dilution	Company (clone number)
Connexin 43	Rabbit	Polyclonal	0.8 mg/mL	43	1: 5,000	Sigma-Aldrich
GAPDH	Rabbit	Monoclonal	-	37	1: 2,000	Cell Signalling Technology (14C10)
β -tubulin	Mouse	Monoclonal	2.4 mg/mL	-50	1: 5,000	Sigma-Aldrich (clone AA2)

2.14 Immunocytochemistry (ICC)

To fix cells the media was removed and 3 washes in PBS performed. Cells were then incubated with 4 % (v/v) paraformaldehyde (PFA) for 15 min at room temperature. This was followed by 3 washes in PBS to remove PFA and cells were stored submerged in PBS at 4 °C until ICC performed.

On the day of staining, cells underwent 3 x 5 min washes in PBS containing 0.1 % Tween 20 (PBS-T). Cells were then permeabilised by adding 0.1 % Triton X-100 in PBS and incubated for 10 min. This was followed by 3 x 5 min washes in PBS-T to remove the residual Triton X-100 prior to blocking in 10 or 20 % goat serum made up in PBS-T (see Table 2.8) for 1 h. The blocking buffer was then removed and primary antibodies diluted as appropriate (Table 2.8) in blocking buffer added to the cells. To control for non-specific antibody binding, some cells were incubated with rabbit IgG or mouse IgG (both from Vector Laboratories, Peterborough, UK) the same final concentration as the primary antibodies. Primary antibodies and IgGs were incubated overnight at 4 °C. The following day cells were washed in the same manner as above and incubated with an 1:500 dilution (in blocking buffer) of a Alexa Fluoro® 488 Goat anti-Rabbit IgG or a Alexa Fluoro® 555 Goat anti-Mouse IgG secondary antibody (both from ThermoFisher Scientific) for primary antibodies raised in rabbit and mouse, respectively. Secondary antibodies were incubated for 1 hr protected from light. All steps from this point onwards were performed in the dark. Cells were then washed as described above prior to mounting on glass slides with ProLong® Gold Antifade Mountant with 4',6-diamidino-2-phenylindole (DAPI) (ThermoFisher Scientific) which counterstains nuclei. Slides were left to dry prior to imaging on the LSM 510 Meta laser scanning confocal microscope and the LSM510 software (Zeiss, Cambridge, UK). The Argon/2 (488), HeNe543 or Diode 405-30 lasers were used to detect green, red and blue fluorescence respectively.

Table 2.8 Primary antibodies used in immunocytochemistry.

Protein	Host Species	Antibody Clonality	Concentration (mg/mL)	% goat serum in blocking buffer	Dilution	Company (clone number)
Connexin 43	Rabbit	Polyclonal	0.80	20	1:1000	Sigma-Aldrich
α SMA	Mouse	Monoclonal	0.04	10	1:200	Sigma-Aldrich (IA4)
DDR2	Rabbit	Polyclonal	1.00	10	1:200	ThermoFisher Scientific
FSP1	Rabbit	Polyclonal	0.72	10	1:100	Abcam
Vimentin	Mouse	Monoclonal	0.70	10	1:400	Sigma-Aldrich (LN-6)

2.15 Cardiac myocyte and fibroblast co-culture model

RACFs were seeded at 5×10^4 cells/35 mm glass bottomed petri dish and cultured for 48 h to allow the cells to reach a confluent monolayer. Cells were then serum starved for 24 h prior to the addition of 1×10^4 CM rods. In experiments that involved the stimulation of RACFs with 10 ng/mL IL-1 β , RACFs were serum starved for 24 h before stimulation. Cells were then washed once with sterile PBS prior to the addition of 1×10^4 CM rods. CMs were seeded at the same density on laminin coated plates. To coat plates, laminin from Engelbreth-Holm-Swarm murine sarcoma basement membrane (Sigma-Aldrich) was diluted in sterile PBS to 4 μ g/mL and 2 mL added to each plate. Plates were incubated at 37 °C for at least 1 h and washed once with sterile PBS before the addition of CMs to the plate. CMs for calcein dye transfer (section 2.15.1) and CM contraction experiments (section 2.15.2) were added to RACF monolayers in phenol red, reduced serum DMEM/F-12 whereas cells for CM AP measurements (section 2.15.3) were maintained in phenol red-free, reduced serum DMEM/F-12.

2.15.1 Calcein dye transfer co-culture experiments

In order to determine if GJ channels between CMs and RACFs were functional calcein dye transfer studies were performed. Calcein acetoxymethyl ester (AM) is a cell-permeant dye, which once inside cells is converted to green fluorescent calcein following hydrolysis by cytosolic esterases (Neri et al. 2001). The green fluorescent calcein is cell impermeable due to its lipid insolubility, therefore retained within live cells and can be transferred through functional GJs (Neri et al. 2001).

Calcein AM (ThermoFisher scientific) was reconstituted in DMSO at 1 mg/mL and stored in aliquots at -20 °C. Freshly isolated CMs (section 2.2.5) were loaded with 5 μ M calcein made up in media and incubated for 30 mins at 37 °C. CMs were then washed 3 times in PBS before the addition of 1×10^4 CM rods to each dish. Images were taken on the on the LSM 510 Meta laser scanning confocal microscope using the Argon/2 (488) laser, immediately and 20 h following CM addition, both focusing on the CM and RACF layer to detect the calcein location. The laser intensity was increased at the 20 h time point due to the calcein fluorescence

fading over time and to detect the transfer of calcein to the underlying RACF layer.

2.15.2 Cardiac myocyte contraction measurement

CM contraction measurements were recorded following 24 h of culture while cells were maintained at 5 % CO₂, 37 °C and in phenol red, reduced serum media for the duration of the recordings. A myopacer field stimulator (IonOptix, Dublin, Ireland) was used to pace the cells at 1 Hz and at 2 ms duration V pulses. The threshold voltage of each cell was determined by increasing the voltage by 1 V increments until the cell started to contract. The threshold value was noted and the CM paced at 30 % above the threshold for 1 min before images were taken at 100 frames per second (fps) for 10 s using HClmage Live software. Typically, the contraction of 13 cells per condition was recorded. The individual images were then stacked to construct a video of CM contraction and analysed on Image J using a macro (kind gift from Dr. Francis Burton). This macro measures optical differences from a reference frame (typically frame 1) to determine the contraction duration (CD) at numerous points as described in Table 2.9 and Figure 2-3. This indirect measure of contraction is plotted as the sum of absolute difference (SAD) against time.

Table 2.9 Definition of contraction parameters measure.

Contraction parameter	Description
Up90	Time from 10 % contraction to 90 % contraction
Dn90	Time from 10 % relaxation to 90 % relaxation
CD10	Time from 10 % contraction to 90 % relaxation
CD25	Time from 25 % contraction to 75 % relaxation
CD50	Time from 50 % contraction to 50 % relaxation
CD75	Time from 75 % contraction to 25 % relaxation
CD90	Time from 90 % contraction to 10 % relaxation

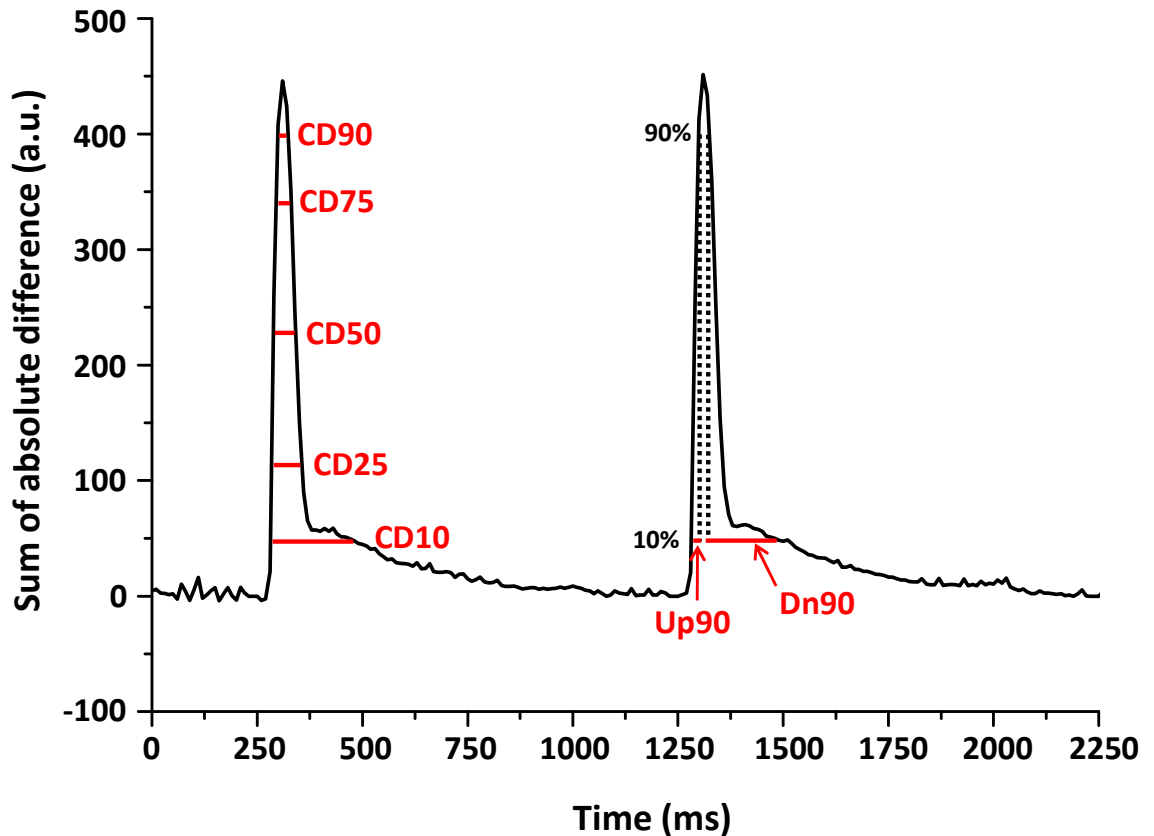


Figure 2-3 Visual representation of contraction parameters measured.

Contraction transients measured using an image J macro based on optical differences from a reference image of the cell, where a greater sum of absolute difference depicts increased shortening. Parameters are indicated by red lines.

2.15.3 Cardiac myocyte action potential measurement

AP recordings were taken from CMs that had been freshly isolated and from CMs that had been cultured for 24 h. Phenol red can produce fluorescence (Ettinger and Wittmann 2014) potentially generating artefacts in the AP traces so all recordings were performed in reduced serum media absent of phenol red. FluoVolt™ membrane potential kit (ThermoFisher Scientific) was used to detect changes in the CM membrane potential. To load cells, media was replaced with a 1:6000 dilution of FluoVolt™ in media. Cells were then incubated for 25 min at 5 % CO₂ and 37 °C prior to the replacement of fresh media. Loading of the cells in each plate was staggered so that the recordings were taken soon after loading was complete. AP measurements were performed at 37 °C within a darkened room. Similar to contraction experiments, cells were paced at 1 Hz and at 2 ms duration 40 V pulses using the IonOptix field stimulator. Cells were allowed to acclimatise for 5 min prior to the first recording. Next, cells were chosen at random and a shutter positioned around an individual cell using HCLImage Live software to restrict the area of recording and reduce noise in the trace. The white light was then switched off and 470 nm light used to excite the FluoVolt™ within the CMs. Changes in membrane potential detected by CelloPTIQ software (Clyde Biosciences, Lanarkshire, UK) over a 10 s period amplified by two photomultipliers set at 550.

APs were analysed using the CelloPTIQ software, where APs were averaged and the average TRise (time taken from 10-90 % depolarisation), APD₂₀, APD₅₀ and APD₈₀ values recorded for each cell.

2.16 *In vivo* intramyocardial injection

All animal procedures were performed in accordance with the Animals Scientific Procedures Act (1986). Male Wistar rats (Envigo, Alconbury, UK) were housed in a controlled environment including a 12 h light/dark cycle, ambient temperature and a standard chow diet. Animals were allowed to acclimatise for at least 1 week prior to surgery.

2.16.1 Fibroblast and eGFP adenoviral vector preparation

In preparation for RACF injection into the heart, cells were plated at 6×10^5 cells/100 mm dish. The following day cells were transduced with a LVeGFP at an MOI of 25. The media was replaced the following day to allow cells to recover. The following day, RACFs were then removed from the dish by incubation with trypsin-EDTA at 37 °C for 5 min, counted and resuspended in the appropriate volume so that 1×10^6 cells were present in 60 μ L PBS. For control animals, 60 μ L PBS containing 5×10^8 pfu of AdeGFP was prepared. Both cells and AdeGFP were placed on ice until injection was performed (section 2.16.2).

2.16.2 Surgical procedure of intramyocardial injection

All surgery was performed under an aseptic technique. Animals (280-390 g) were placed in an induction box filled with 5 % (v/v) isoflurane and 2 L/min oxygen to anaesthetise. Once anaesthetised, animals were shaven on the left side of the chest and the area sterilised using betadine. Animals were then intubated and artificially ventilated at a tidal volume of 1.5 mL and a respiratory rate of 60 strokes/min with 3 % (v/v) isoflurane and 0.2 L/min oxygen. Animals were placed on their right side on a sterile drape which was positioned on top of a heated mat. The left front leg was then taped over the head to expose the left side of the chest. To ensure all unshaven hair was separated from the surgical area a small drape with an area cut out was placed over the animal followed by an 10 cm x 12 cm 3M™ Tegaderm™ transparent film dressing (Nu-Care products Ltd, Bedfordshire, UK). An incision from the xiphisternum across the left side of the chest perpendicular to the sternum was made and a left thoracotomy performed in the fourth intercostal space. The ribs were retracted to allow access to the chest cavity and the left lung collapsed by the insertion of a small non-woven swab. The heart was then removed from the pericardium and two 30 μ L injections of either the cell or AdeGFP solution (prepared as detailed in section 2.16.1) performed above and below the left anterior descending artery using a BD Micro-Fine™ 0.5 mL insulin syringe with 29 gauge needle (Nu-Care products Ltd). The lung was then re-inflated and the chest rapidly closed using a 3-0 Ethicon Monocryl® suture ensuring all air was expelled from the chest cavity. The muscle layers were then sutured using 3-0 Ethicon Ethibond Excel® suture, followed by a

continuous internal stitching with a 2-0 Polysorb™ suture. Finally, three external stitches were applied with the same suture used for the continuous stitching.

Following chest closure the isofluorane was progressively decreased throughout the remaining surgery to speed up the recovery on completion of surgery. Animals were given post-operative analgesia of 60 µg buprenorphine and 1.5 mg carprofen by intraperitoneal injections and monitored throughout recovery (Home Office licence number: 60/4286).

2.17 *Ex vivo* heart optical mapping

2.17.1 Experimental set up

The isolated retrograde-perfused Langendorff heart in a horizontal orientation was used for this study. Tyrodes was heated to 37 °C and bubbled with Carbogen (5 % CO₂ and 95 % O₂) for at least 20 min before the addition of 1.8 mM CaCl. The myosin II inhibitor, blebistatin (Enzo, Exeter, UK) reconstituted in DMSO was then added to a stock of Tyrodes solution to produce a final concentration of 10 µM. Blebistatin was used to inhibit excitation contraction coupling, hence preventing movement artefacts in the AP trace recordings. A glass coverslip was typically placed over the surface of the heart as an extra preventative movement measure. ECG electrodes were positioned at both sides of the apex to provide a marker of electrical activity and a pacing electrode was positioned on the epicardial surface the heart to allow pacing protocols to be conducted. All experiments were performed in a darkened room and excess Tyrodes solution was aspirated by a vacuum positioned next to the heart mould.

Hearts were loaded with the voltage sensitive dye, RH-237 (Biotium, Fremont, US), for AP recordings. To excite eGFP and RH-237 simultaneously, two light-emitting diodes (LEDs) were fitted with a 470/20 nm filter and focussed on the surface of the left ventricle. Since the emission spectrums of eGFP and RH-237, have little overlap, with eGFP typically having an emission peak around 510 nm (Spiess et al. 2005) and RH-237 emitting light in the red part of the spectrum, wavelengths can be separated using a dichroic mirror. Following excitation, fluorescence was collected by a camera lens and directed at a long

pass dichroic mirror at 593 nm, enabling the longer wavelengths to travel through and the shorter wavelengths to be reflected. The longer wavelengths were then passed through an >715 nm emission filter to a MiCAM complementary metal-oxide-semiconductor (CMOS) camera (SciMedia Ltd., California, USA) and the shorter wavelengths passed through a 520/28 nm emission filter to another identical CMOS camera (Figure 2-4). CMOS cameras were set up to image an array of 100×100 pixels.

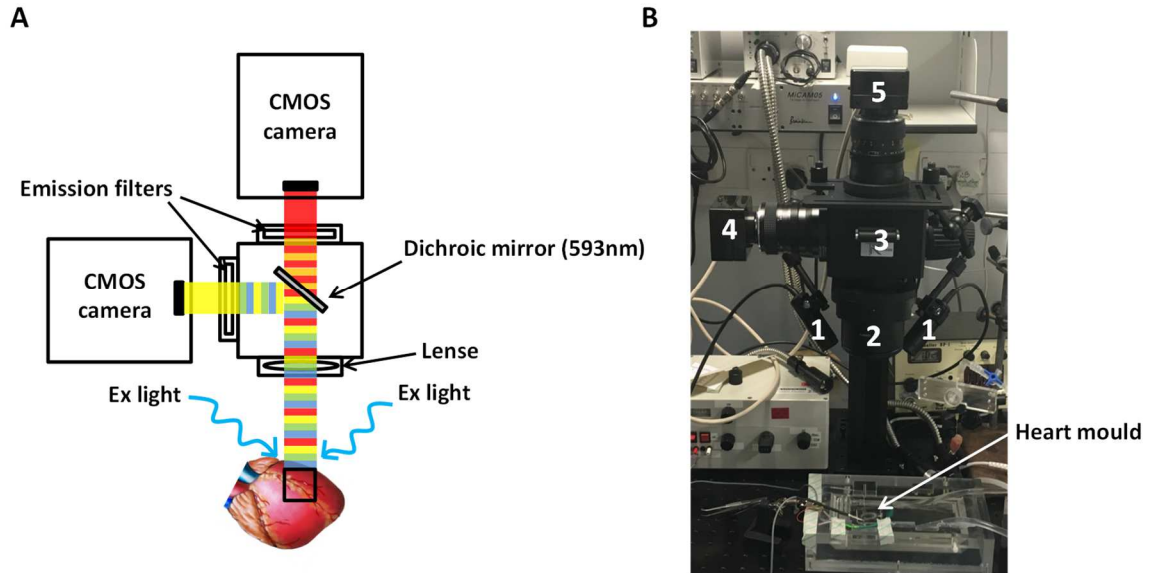


Figure 2-4 Experimental set up for *ex vivo* heart optical mapping.

(A) An illustration and (B) image of experimental set up showing the main components, labelled 1-5 in B. 1 = LEDs emitting 470/20 nm light, 2 = lense, 3 = box holding the dichroic mirror, 4 = CMOS camera detecting the eGFP signal and 5 = CMOS camera detecting voltage signals.

2.17.2 Removal of heart under terminal anaesthesia

One week following surgery (section 2.16.2), animals were anaesthetised in an induction box filled with 5 % (v/v) isoflurane and 2 L/min oxygen. The animal was then moved to a facemask supplying the same gas mixture and front legs taped to the mask to allow access to the chest. The hair from the leg was removed and the skin pulled to one side so an incision could be made without damaging the underlying femoral vein. The femoral vein was visualised under a light microscope and pressure applied to the upper part of the vein to stop flow for a few seconds before the insertion of a slightly bent 29 gauge needle, with bevel side facing up. Next, the pressure was removed and 350 μ L of 1000 I.U./mL heparin sodium (Wockhardt, Wrexham, UK) was injected. The needle was then removed and pressure placed on the site of injection. The heparin was allowed to reach the heart by waiting approximately 30 s and the heart rapidly excised from the thorax and placed in ice cold heparinised Tyrodes solution. The heart was then quickly transferred to the experimental room where it was rapidly retrograde perfused with Tyrodes solution (section 2.17.3).

2.17.3 Action potential measurements in the intact heart

Aortas were isolated by dissection and cannulated using a 2 mm diameter catheter and 4-0 silk braided suture (Pearsalls). This allowed for retrograde perfusion with Tyrodes solution at an initial flow rate of 10 mL/min. Following cannulation, hearts were placed horizontally in a mould suitable for a rat heart. The flow rate was altered to maintain a pressure of 80-120 mmHg as measured by a pressure monitor. If the pressure became too high an outlet was created by inserting small piece of tubing through an incision in the left atrium to the left ventricle. The heart was orientated so the eGFP signal could be observed. Tyrodes solution containing blebistatin was then supplied to the heart to stop movement. Next, 50 μ L RH-237 (Biotium, California, US), reconstituted in DMSO at 1 mg/mL, was administered very slowly through a port proximal to the catheter. The pressure was closely monitored during administration. An AP recording was taken at sinus rhythm before pacing.

The pacing threshold for each heart was determined by slowly increasing the voltage until the heart could be paced at a cycle length (CL) of 200 ms (5 Hz). Double the threshold value was chosen for pacing, unless it above 1 V, where only an additional 1 V was applied. A dynamic pacing and an extra stimulus (S1S2) pacing protocol was performed in each preparation. In dynamic pacing the heart rate was progressively increased by decreasing the CL. Initially, the CL was 200 ms for 300 stimuli which was then decreased by 20 ms every 300 stimuli until 100 ms was reached. Next, the CL was reduced by 10 ms every 300 stimuli until the heart could no longer be paced. The S1S2 protocol consisted of pacing at a constant CL of 200 ms (S1) for 200 stimuli followed by a single premature stimulus (S2), consequently decreasing the S1-S2 interval. The extra stimulus was progressively reduced below 200 ms until the ERP of each heart was noted.

A ten second AP recording was captured at each CL in the dynamic pacing protocol and at every S1S2 combination using the OPTIQ software (developed by Dr Francis Burton at the University of Glasgow, Glasgow UK). OPTIQ software was also used to perform data analysis whereby areas of the heart were selected and an average AP trace created for each area. To prepare the data for analysis, a Gaussian spatial filter and temporal filters were applied. In dynamic pacing, typically six consecutive APs were analysed for each CL. One S1 AP and the S2 AP were analysed from the traces obtained from the S1S2 pacing. The 10-90 % rise time and APD_{80} were examined in both protocols.

2.18 Histology

2.18.1 Tissue processing

Hearts were harvested one week following surgery or after the OM experiments were complete and washed once in PBS. The section(s) containing the injection site was noted at this time and cut transversely into 4 pieces using a scalpel. Heart sections were fixed in 4 % PFA (v/v) for 48 h at 4 °C, washed twice in PBS and stored in 70 % ethanol until processing.

Heart sections were processed on a Shandon Excelsior tissue processor (ThermoFisher Scientific) which slowly dehydrates the tissues prior to the addition

of paraffin wax using the solution sequence detailed (Table 2.10). The Shandon Histocenter 3 was used to embed heart tissue in paraffin wax in transverse orientation. Heart sections were then cut at 5 μm using a microtome and baked on to glass slides by overnight incubation at 60 °C. The paraffin block containing the injection site was continually cut with minimal sections discarded to maximise the likelihood of detecting the eGFP signal.

2.18.2 Immunohistochemistry

Prior to staining, tissue sections were deparaffinised and rehydrated by adding them to a sequence of solutions, for 5 min each (Table 2.11). To perform antigen retrieval, 10 mM sodium citrate was heated until boiling and the slides added. The slides were then further heated, covered with cling film at medium to low heat for 15 min. Slides were then left to cool at room temperature for 30 min to allow the antigens to fold correctly. The slides were then put under running tap water for 5 min to fully cool. Slides were then transferred to TBS for 3 x 5 min washes. To prevent non-specific binding of primary antibodies, sections were incubated with 15 % (v/v) goat serum in TBS-T (0.05 % [v/v] Tween 20 - used throughout protocol) and incubated for 30 min in a humidified chamber. Primary antibodies were made up in 10 % goat serum in TBS-T at the dilution indicated (Table 2.12). Normal rabbit and mouse IgG were used at the same final concentration as the primary antibodies to provide an antibody control. Primary antibodies and IgG controls were incubated overnight at 4 °C in a humidified chamber. The following day, slides were washed 3 x 5 min in TBS before addition of secondary antibodies. Alexa Fluor® 488 Goat anti-Rabbit and Alexa Fluor® 555 Goat anti-Mouse were diluted 1:250 in TBS-T and incubated with heart sections for 3 h at room temperature protected from light. All subsequent steps were performed at minimal light exposure to prevent photo-bleaching of fluorophores. Following a further 3 x 5 min washes in TBS, 0.1 % (v/v) Sudan Black B prepared in 70 % ethanol was added to the sections to remove lipofuscin-mediated autofluorescence. Sudan Black B was incubated for 10 min in a humidified chamber prior to 3 x 5 min washes in TBS. Nuclei were then stained using 100 $\mu\text{g}/\text{mL}$ DAPI (Sigma-Aldrich) in TBS for 10 min. Finally, slides were mounted on glass coverslips using ProLong® Gold Antifade Mountant DAPI before being imaged on the LSM 510 Meta laser scanning

confocal microscope using the Argon/2 (488), HeNe543 or Diode 405-30 lasers to detect green, red and blue fluorescence respectively.

Table 2.10 Solution sequence for tissue embedding in paraffin wax

Solution	Incubation time (min)
70 % Ethanol	30
95 % Ethanol	30
100 % Ethanol	30
100 % Ethanol	30
100 % Ethanol	45
100 % Ethanol	45
100 % Ethanol	60
Xylene	30
Xylene	30
Xylene	30
Paraffin wax	30
Paraffin wax	45
Paraffin wax	45

Table 2.11 Solution sequence to deparaffinise and rehydrate tissue sections for immunohistochemistry

Solution
Histoclear
Histoclear
100 % Ethanol
100 % Ethanol
90 % Ethanol
70 % Ethanol
50 % Ethanol
Running tap water

Table 2.12 Primary antibodies used in immunohistochemistry

Protein	Host Species	Antibody Clonality	Concentration	Dilution	Company (clone number)
eGFP	Rabbit	Polyclonal	0.5 mg/mL	1:1,250	Abcam
Cardiac troponin I	Mouse	Monoclonal	2.0 mg/mL	1:4,000	Abcam (4C2)

2.19 Statistical analysis

Data from qRT-PCR experiments is represented as $RQ \pm rq_{\max}$, where rq_{\max} is indicative of the standard error of the mean (SEM) and is calculated from the ΔC_t value from each experiment. All other data is represented as mean \pm SEM. In experiments where two conditions are present, an unpaired, two-tailed Student's t-test was performed. A repeated measures one-way analysis of variance (ANOVA) with a Dunnett's or Tukey's multiple comparisons test was performed on qRT-PCR data where there were three or more conditions. For single CM data, statistical analysis was performed on the mean values for each heart and a one-way ANOVA with Tukey's multiple comparisons test used in experiments containing three or more conditions. No statistical analysis was completed on whole heart experiments due to small n -numbers. All statistical analysis was performed using Graphpad Prism 4 software (GraphPad Software Inc., California, USA) and a P value <0.05 was considered statistically significant.

Chapter 3 Generation of viral vectors to modulate connexin 43 expression in cardiac fibroblasts for use *in vitro* and *in vivo*

3.1 Introduction

Viral vectors have been extensively used to modulate genes both *in vitro* and *in vivo*. Due to the pathogenic nature of many WT viruses, parts of the viral genome have been deleted, consequently rendering them replication-defective and of low toxicity (Bouard et al. 2009). The main viral vectors used in research studies include LV, Ad and adeno-associated viral (AAV) vectors, each of which have particular features which are suited to different research questions. Both LV and Ad vectors have been used to overexpress Cx43 (Fernandes et al. 2009;Kizana et al. 2005;Reinecke et al. 2004;Zlochiver et al. 2008).

LV vectors are a subtype of retroviral vectors, modified from the human immunodeficiency virus 1 (HIV-1). LV vectors have many desirable characteristics as a gene transfer vector (TV) including the ability to transduce both dividing and non-dividing cells as well as the capability to integrate into the target cell genome resulting in the permanent modification and presence of the introduced DNA in descendant cells (Sakuma et al. 2012). Additionally, transduction into target cells does not result in viral protein expression and allows for complex DNA sequences, for instance polycistronic sequences, to be expressed (Sakuma et al. 2012).

Retroviral vectors are characterised by their use of RT and integrase to convert viral single stranded RNA into double stranded DNA once inside the host cell and prior to integration into host DNA. HIV-1 has nine viral genes amounting to approximately 9 Kb (Sakuma et al. 2012). These genes include: *gag*, *pol*, *env*, *tat*, *rev* and genes which encode the accessory proteins; *Vif*, *Vpr*, *Vpu* and *Nef*. *Gag* and *pol* encode both the core viral proteins and enzymes necessary for viral replication (RT, integrase and protease) respectively (Ramezani and Hawley 2002). The *env* gene encodes gp160 which is subsequently cleaved into the proteins gp120 and gp41 prior to expression on the outer viral membrane. Gp120 and gp41 bind to the CD4 receptor, mainly present on immune cells, initiating the fusion of the viral membrane with the cell membrane, allowing entry of the viral genome into the cell cytoplasm (Sakuma et al. 2012). Next, viral RT mediates the synthesis of double stranded DNA, which is transported to the nucleus and integrated into the host DNA by integrase (Nisole and Saib 2004;Sakuma et al. 2012). LTRs are positioned at either end of the viral genome and are important

for integration and transcription (Ramezani and Hawley 2002; Sakuma et al. 2012). The regulatory genes, *tat* and *rev*, encode the proteins transactivator of transcription (Tat) and regulator of expression of virion proteins (Rev) respectively. Tat binds to the trans-activation response (TAR) element to regulate viral gene transcription (Feng and Holland 1988), whereas Rev associates with the Rev response element (RRE) to allow transportation of viral transcripts to the cytoplasm (Malim et al. 1989).

As an alternative to the gp120 and gp41 expression on the outer membrane of HIV-1, most current LV vectors display the VSV-G increasing tropism for a broad range of cell types (Sakuma et al. 2012). The exact receptor for VSV-G remains elusive; however there is evidence to suggest that the ubiquitous membrane lipid, phosphatidylserine, assists in membrane fusion (Carneiro et al. 2002; Schlegel et al. 1983). Conversely, other studies have disputed the role of phosphatidylserine, by demonstrating a lack of correlation between the levels of phosphatidylserine within the plasma membrane and VSV (which expresses VSV-G as its envelope protein) infection and binding (Coil and Miller 2004).

Replication-defective and non-pathogenic LV vectors are produced by dividing the LV genome over three (1st and 2nd generation) or four (3rd generation) plasmids. First generation LV vectors consist of a packaging plasmid; which includes the *gag*, *pol* and accessory protein genes, an *env* encoding plasmid; which commonly contains the VSV-G gene, and a TV. Within the TV, the transgene and *cis*-active sequences necessary for packaging, reverse transcription and integration (the packaging signal, 5' and 3'LTRs and RRE) are present (Sakuma et al. 2012). Second generation LV vectors are very similar to first generation, however the accessory proteins are deleted, increasing the safety by only including four of the nine original HIV genes. Safety is then further enhanced in third generation LV vectors whereby the *tat* gene is removed and the *rev* gene is positioned on a separate plasmid; hence 4 plasmids are required (Sakuma et al. 2012).

Dissimilar to lentiviruses, the Ad genome exist as a stable extra chromosomal episome within the host nucleus (Thomas et al. 2003). Due to the lack of integration into host DNA, transient expression occurs which may be advantageous in some cases, such as in the treatment of the saphenous vein prior to coronary

artery bypass grafting (George et al. 2011). The Ad genome consists of linear double stranded DNA, which is packaged into a viral capsid consisting of three main proteins: the fiber, penton base and hexon (Reddy and Nemerow 2014). First generation Ad vectors, derived from serotype 5 (Ad5) are the most common gene transfer vector (Wold and Toth 2013). Entry of Ad5 into cells is initiated by binding of the fiber protein to the coxsackievirus and adenovirus receptor (Meier and Greber 2004). Consequently, the virion is endocytosed by the cell and transported within endosomal compartments (Meier and Greber 2004). The adenovirus however quickly escapes from the endosome and travels into the nucleus where gene transcription and replication can occur (Rauschhuber et al. 2012).

Replication-defective vectors are produced by deleting the E1 gene of the Ad genome, consequently allowing a relatively small cloning capacity of around 5 Kb (Graham et al. 1977). In order to enhance transgene capacity, to approximately 8 Kb, Ad vectors with additional deletions in the E3 gene were developed (Danthinne and Imperiale 2000). Further deletions in the E2 and/or E4 genes have resulted in second generation Ad vectors (Danthinne and Imperiale 2000). Additionally, third generation vectors, also known as helper-dependent Ad (HDA) vectors, have been developed whereby all of the viral coding sequences have been deleted except the inverted terminal repeats and the viral packaging signal (Rosewell et al. 2011). These vectors rely on co-transfection with a helper virus in the packaging cell line to promote replication and packaging of the HDA genome which makes purification technically challenging (Rosewell et al. 2011). In comparison to first and second generation Ad vectors, HDA vectors have been demonstrated to reduce the inflammatory response *in vivo*, increase the longevity of transgene expression (Maione et al. 2001) and create a larger cloning capacity; up to 36 Kb (Rauschhuber et al. 2012). First-generation E1/E3-deleted E4+ Ad vectors (AdE4+) have been reported to increase Cx40 and decrease Cx43 expression in endothelial cells promoting their survival (Zhang et al. 2005). Hence some caution may be required when using Ad vectors to modulate connexin proteins.

In this chapter a second generation LV vector utilising an artificial α SMA promoter to drive expression of the gene of interest was sought. The artificial α SMA promoter hybrid selected, was developed by Hirschfeld *et al.* (2009), who reported it drove eGFP expression specifically in α SMA expressing cells (Hirschfeld *et al.* 2009). This promoter consisted of three components; a 720 bp regulatory sequence of the rat SMA gene, a 754 bp intron 1 enhancer sequence of the chicken β actin gene and a 93 bp intron/exon junction of the rabbit β globin gene (Figure 3-1). The 720 bp regulatory sequence was found to provide additional flanking sequences to drive expression specifically in α SMA expressing cells in comparison to shorter regulatory fragments that contained components which permitted expression in a non-SMC specific fashion. Additionally, as the first intron of the SMA gene, containing a conserved CArG box, has been shown to be important in expression of α SMA in SMCs and MFs (Mack and Owens 1999; Tomasek *et al.* 2005), an enhancer sequence containing this CArG box was included. Finally, an intron/exon junction was incorporated to ensure intron termination (Hirschfeld *et al.* 2009). RACFs utilised in the current study have been shown to express high levels of α SMA (section 4.3.1) and therefore the artificial promoter would be suitable in these cells.

3.2 Aims

- Design and produce viral gene transfer vectors which can overexpress Cx43 in RACFs and are suitable for *in vitro* investigation and *in situ* imaging.

3.3 Results

A vector which allowed the expression of Cx43 as well as a reporter which was nuclear localised, both under the control of the artificial α SMA promoter hybrid, was designed with the aim of facilitating optimal *in situ* imaging of transduced RACFs. An internal ribosome entry site (IRES) allowing the attachment of ribosomes to begin transcription of a reporter protein separately from the connexin (Martinez-Salas 1999) was incorporated into the vector. Nuclear localisation of the reporter may provide a discrete structure for identification of RACFs in the myocardium using whole heart imaging, hence enhancing the resolution. The insert, α SMA_eGFPNLS (Figure 3-2A), was designed to offer flexibility in cloning prior to the synthesis by Invitrogen GeneArt Gene Synthesis (ThermoFisher Scientific). Unique restriction endonuclease sites (Figure 3-2B), were positioned throughout the insert to allow the α SMA promoter to be exchanged for the cytomegalovirus (CMV) promoter, connexins to be cloned into the MCS and the nuclear localised high energy, readily detectable emitter, eGFP, to be exchanged for a far-red fluorescent protein, such as mCherry, which is more suited to deep tissue imaging (Deliolani et al. 2008).

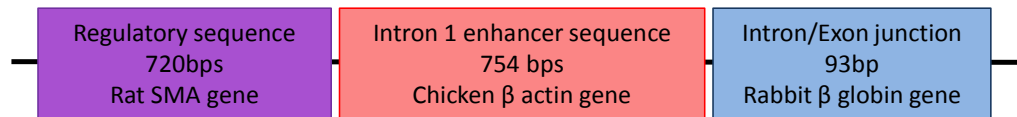


Figure 3-1 Components sought in an artificial α SMA promoter hybrid.

An artificial promoter hybrid consisting of the regulatory sequence of the rat α SMA gene, the intron 1 enhancer sequence of the chicken β actin gene and the intron/exon junction of the rabbit β globin gene, designed by Hirschfeld *et al.* (2009).

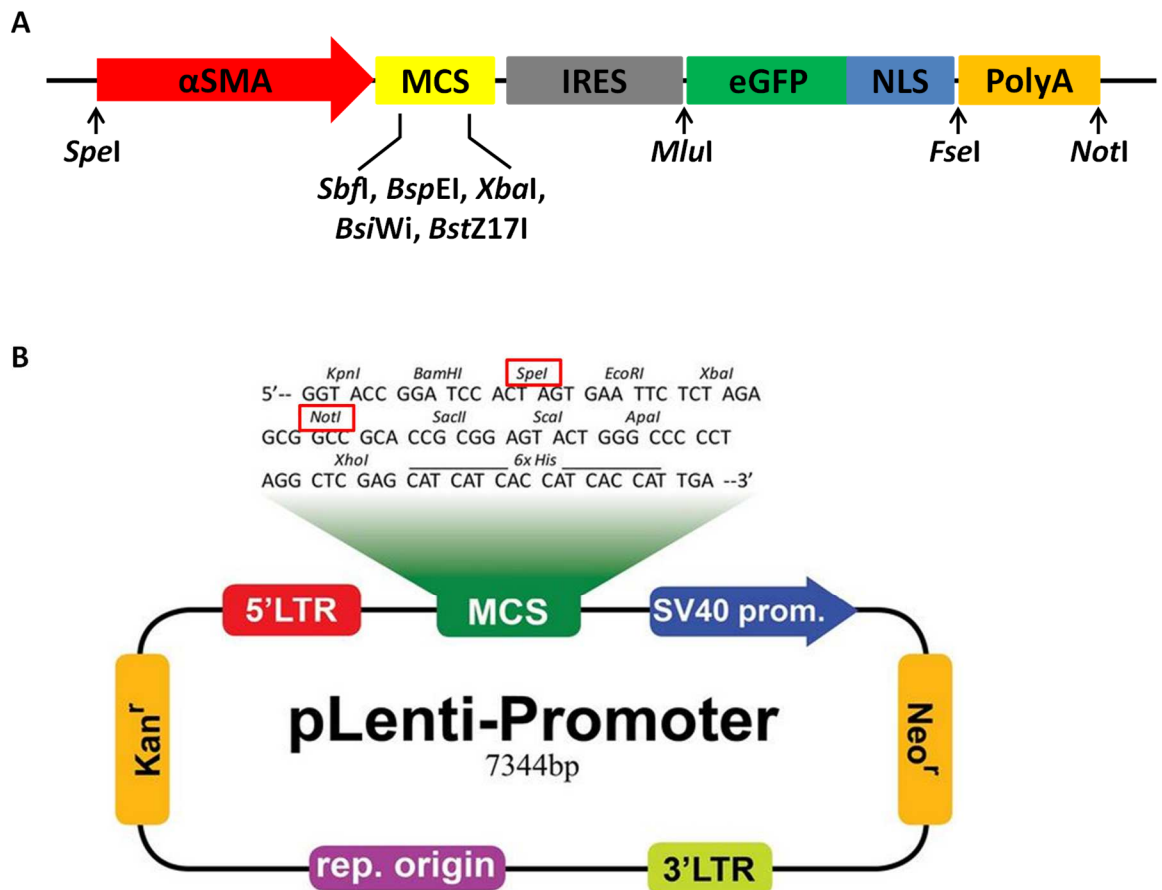


Figure 3-2 Schematic of designed insert, α SMA_eGFPNLS, and pLenti-promoter plasmid.

(A) α SMA_eGFPNLS (3081 bp) was designed with flexible enzyme restriction sites to allow the promoter to be altered, the gene of interest to be subcloned into the multiple cloning site (MCS) and the nuclear localised eGFP to be changed to a far-red emitter. (B) Plasmid map of pLenti-promoter. The *SpeI* and *NotI* restriction sites (red boxes) can be used to clone the α SMA_eGFPNLS insert into the commercial pLenti-promoter plasmid. IRES; internal ribosome entry site, NLS; nuclear localisation signal, PolyA; polyadenylation signal.

3.3.1 Lentiviral and adenoviral transduction into RACFs

Initially, the ability of LV and Ad vectors to transduce RACFs was assessed. RACFs were transduced with LV or Ad vectors overexpressing eGFP (LVeGFP and AdeGFP respectively) at varying MOI and imaged following 72 or 48 h transduction, respectively. A dose dependent increase in eGFP expression with little toxicity was observed when cells were transduced with LVeGFP at a MOI of 3, 6 or 12 (Figure 3-3). The majority of cells had detectable eGFP expression at a MOI of 12, suggesting an optimal concentration for use in further LV studies. High expression of eGFP was observed when cells were transduced with AdeGFP at MOIs of 100 or 250, however toxicity was observed in cultures transduced with an MOI of greater than 500 (Figure 3-4).

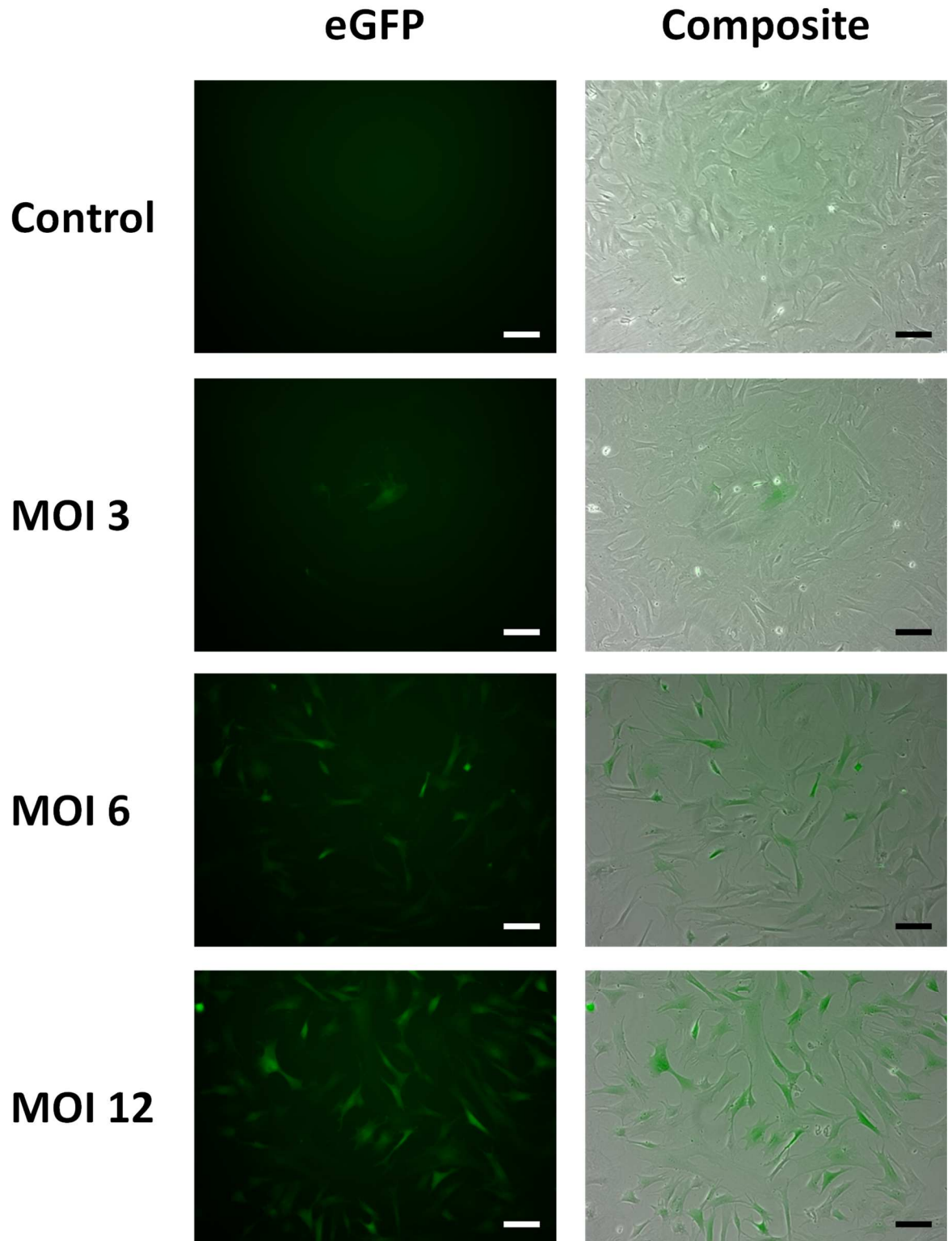


Figure 3-3 Representative images of RACFs transduced with LVeGFP.

LVeGFP was added to RACF cultures at a multiplicity of infection (MOI) of 3, 6 or 12 and cells imaged 72 h thereafter (n=1). Cells maintained in culture media were used as a control. The eGFP signal and an overlay on to the bright field image are shown. Scale bar represents 100 μ m.

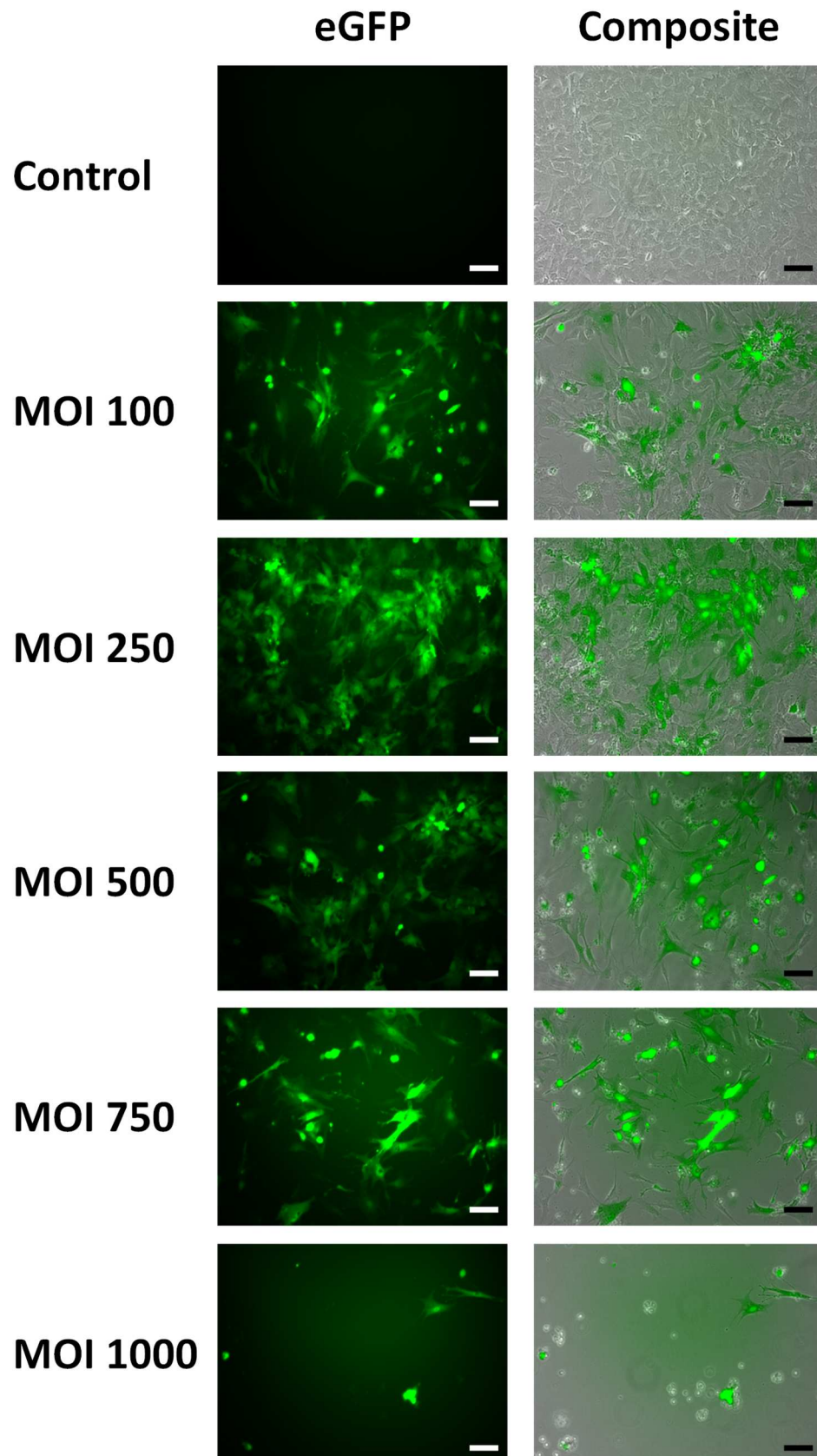


Figure 3-4 Representative images of RACFs transduced with different concentrations of AdeGFP.

AdeGFP was added to RACFs cultures at a multiplicity of infection (MOI) of 100, 200, 500, 750 and 1000. Cells were imaged 96 h thereafter (n=1). Cells maintained in culture media were used as a control. The eGFP signal and an overlay on to the bright field image are shown. Scale bar represents 100 μm .

3.3.2 Cloning of α SMA_eGFPNLS into a lentiviral shuttle plasmid

Prior to ligation of the α SMA_eGFPNLS insert (Figure 3-2A) into pLenti-promoter, the intact insert, was subjected to endonuclease restriction digestion analysis in its parental shuttle vector to ensure the presence of functional restriction sites. All unique sites including; *SpeI*, *SbfI*, *BspEI*, *XbaI*, *BsiWI*, *BstZ17I*, *MluI*, *FseI* (Figure 3-5A) and *NotI* (Figure 3-5B), were confirmed by the presence of a DNA fragment upon agarose gel electrophoresis which migrated with an apparent molecular mass of 5,500 bp. *SbfI* and *FseI* only partially digested the plasmid, demonstrated by two further bands which resembled uncut (UC) plasmid. The α SMA_eGFPNLS (3081 bp) fragment was excised from the shuttle vector via dual *SpeI* and *NotI* restriction endonuclease digestion (DC) as shown by the presence of a DNA fragment migrating with an apparent molecular mass of approximately 3000 bp (Figure 3-5B).

The functionality of α SMA_eGFPNLS was assessed by transfection of the shuttle vector (p α SMA_eGFPNLS) into RACFs using the transfection reagent, Xfect. Cells were also transfected with a LV plasmid which overexpressed eGFP under the control of the SFFV promoter as a positive control. Toxicity was apparent in cells treated with the Xfect reagent alone in comparison to untransfected cells (Figure 3-5C). The transfection efficacy was also very low however, eGFP positive nuclei in cells transfected with p α SMA_eGFPNLS were evident in comparison to cytoplasmic eGFP expression in pSFFV_eGFP transfected cells (Figure 3-5C).

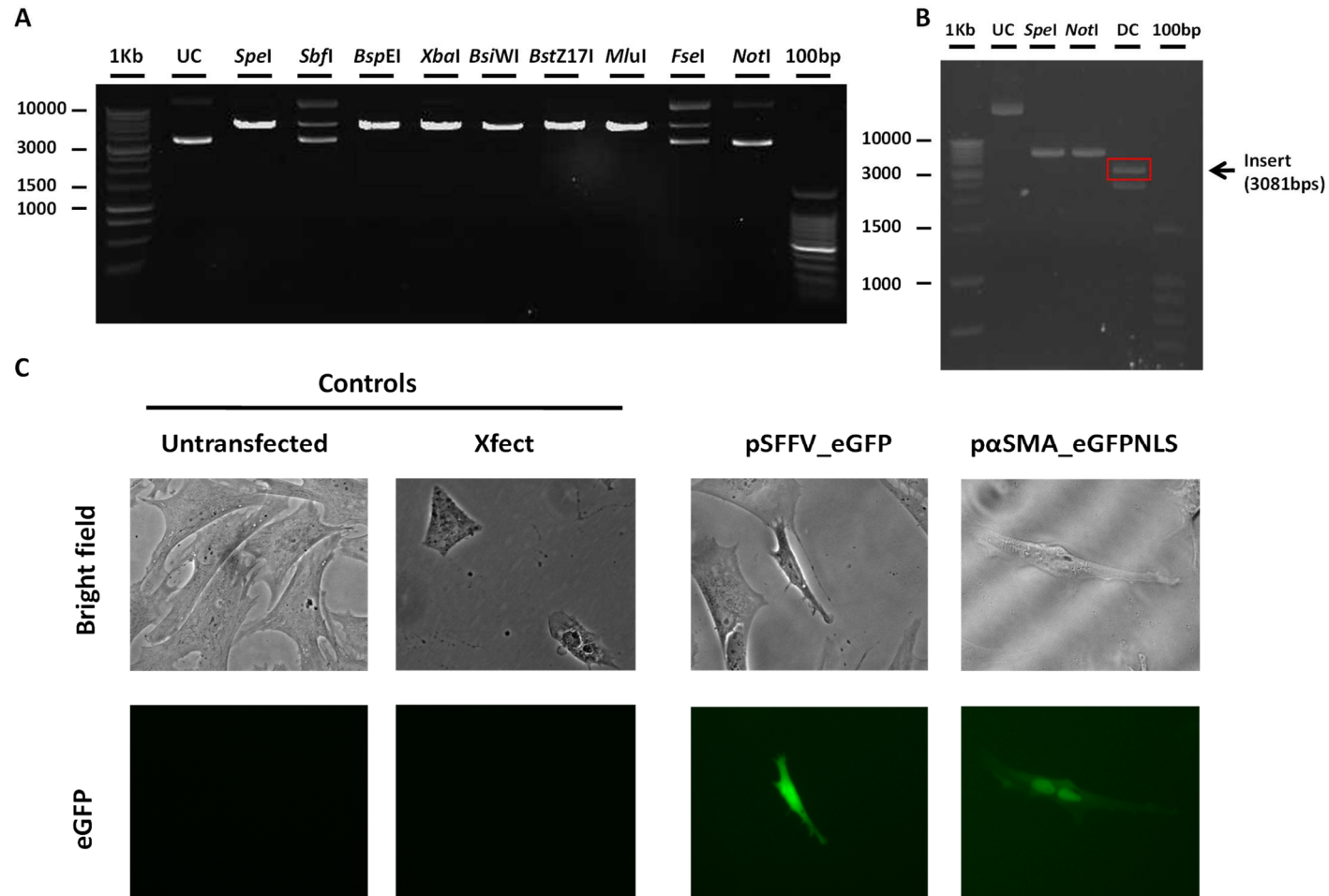


Figure 3-5 Diagnostic digests and transfection of the pαSMA_eGFPNLS into RACFs.

(A) Ethidium bromide agarose gel showing the presence of a DNA band around 5,500 bp following endonuclease restriction digests of the plasmid containing the αSMA_eGFPNLS insert with *SpeI*, *SbfI*, *BspEI*, *XbaI*, *BsiWI*, *BstZ171*, *MluI*, *FseI* and (B) *NotI*. Separation of the αSMA_eGFPNLS insert (3081 bp – red box) from the plasmid was observed following a double *SpeI* and *NotI* restriction digest. (C) RACFs were transfected with 2μg pSFFV_eGFP or pαSMA_eGFPNLS using the transfected reagent, Xfect (n=2). Cells which were untransfected or received Xfect alone were used as controls. Images were taken 48 hr subsequent to transfection. Specific cells have been expanded for illustrative purposes. 1Kb; 1 Kb ladder, UC; uncut, DC; double cut with *SpeI* and *NotI*.

Next, the α SMA_eGFPNLS insert was excised from the shuttle vector and the pLenti-promoter plasmid linearised by dual *SpeI* and *NotI* restriction endonuclease digestion. Following gel extraction of the DNA, separation by agarose gel electrophoresis was performed to confirm the expected DNA fragment sizes of 3,081 and 7344 bp (α SMA_eGFPNLS and pLenti-promoter respectively; Figure 3-6). However, on assessment of the purified α SMA_eGFPNLS insert via agarose gel electrophoresis, two faint extra DNA bands were also apparent, suggesting contaminating DNA was present. Unfortunately, numerous attempts to eliminate this contaminating DNA and to clone the α SMA_eGFPNLS insert into the pLenti-promoter plasmid were unsuccessful.

An alternative strategy to generate a vector suitable for LV production was attempted via cloning of the α SMA_eGFPNLS insert into an alternative LV shuttle vector, pLenti-III-promoterless (Figure 3-7A), using the same restriction endonuclease sites (*SpeI* and *NotI*) was investigated. However, contaminating DNA was again observed in the extracted DNA fragments (Figure 3-7B) and no colonies were formed following ligation. Blunt cloning of the insert into pLenti-III-promoterless following Klenow treatment was also attempted without success.

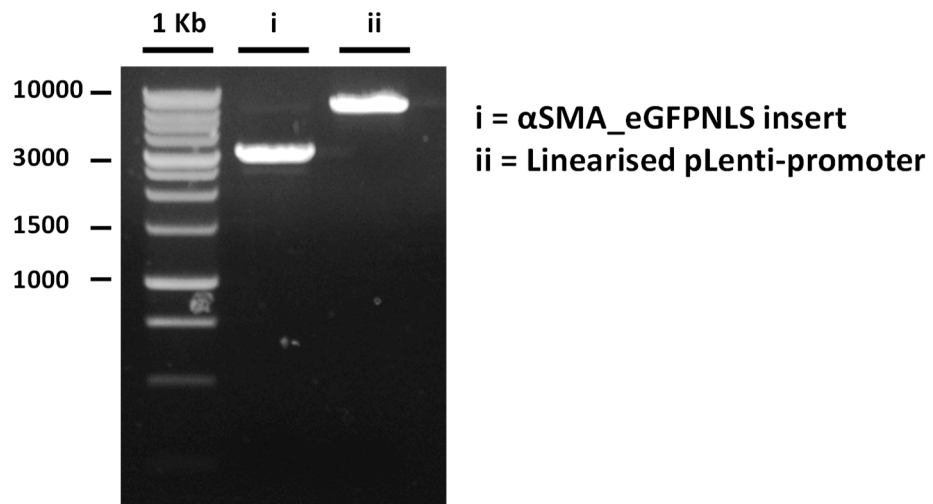
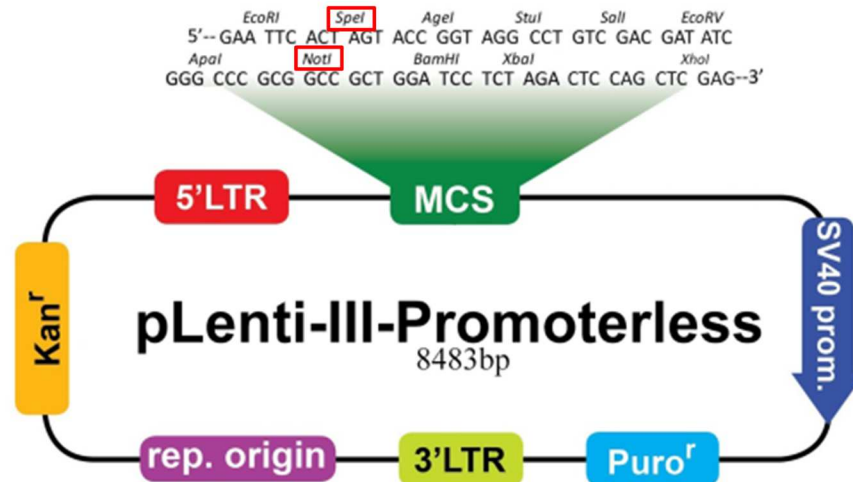


Figure 3-6 Purification of the α SMA_eGFPNLS insert and linearised pLenti-promoter. Ethidium bromide agarose gel showing the DNA fragments following gel extraction of the α SMA_eGFPNLS insert (i) and the linearised pLenti-promoter (ii) after double *SpeI* and *NotI* digests.

A



B

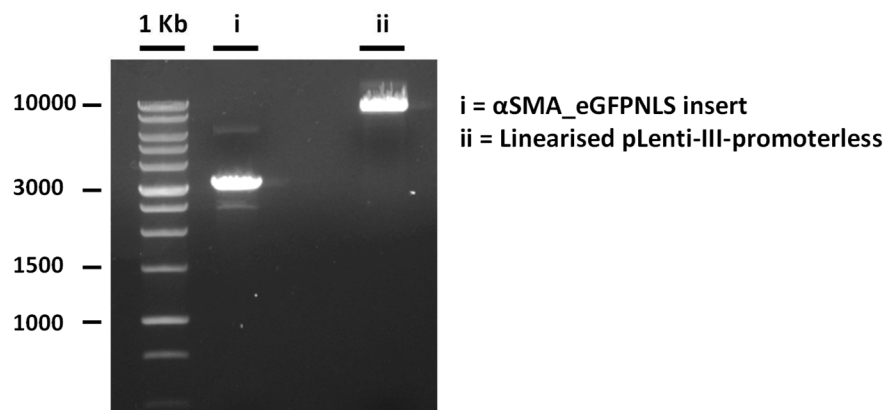


Figure 3-7 Purification of α SMA_eGFPNLS insert and linearised pLenti-III-promoterless. (A) Plasmid map of pLenti-III-promoterless containing *SpeI* and *NotI* restriction sites in the multiple cloning site (MCS) which are compatible with the α SMA_eGFPNLS insert. (B) Ethidium bromide agarose gel showing separation of DNA fragments following gel extraction of the α SMA_eGFPNLS insert (i) and the linearised pLenti-III-promoterless (ii) after double *SpeI* and *NotI* digests. 1Kb; 1 Kb ladder.

3.3.3 Cloning of α SMA_eGFPNLS into an adenoviral shuttle plasmid

Due to the unsuccessful attempts to clone α SMA_eGFPNLS into a compatible LV plasmid, a cloning strategy was formulated to produce two Ad plasmids; one which would enable the expression of eGFPNLS under the control of the hybrid α SMA promoter and the other under the control of the CMV-immediate early (CMV-IE) promoter. For this the RAPAd[®] system shuttle vectors (Anderson et al. 2000), pVQ_K-NpA or pVQ_CMV_K-NpA (Figure 3-8Ai and ii respectively) were utilised. *SpeI* and *NotI* restriction endonuclease sites present in both vectors facilitated the insertion of full length α SMA_eGFPNLS sequence into the promoterless, pVQ_K-NpA vector. Conversely, *XbaI* and *NotI* sites facilitated the DNA fragment downstream of the α SMA promoter (eGFPNLS) to be inserted into CMV-IE promoter driven, pVQ_CMV_K-NpA vector.

Following double *SpeI* and *NotI* or *XbaI* and *NotI* restriction endonuclease digestion of the respective inserts and vectors and gel extraction of the fragments, agarose gel electrophoresis was performed to confirm the purity of the DNA prior to ligation (Figure 3-8B). Only one DNA band was observed in the eGFPNLS insert (Bii) and in the linearised pVQ_K-NpA (Biii) and pVQ_CMV_K-NpA (Biv) lanes. Conversely, there was an additional faint band with an apparent molecular mass of approximately 7,000 bp in the α SMA_eGFPNLS (Bi) lane.

Next, ligation of α SMA_eGFPNLS: pVQ_K-NpA and eGFPNLS: pVQ_CMV_K-NpA (insert: vector) and transformation into *E.coli* was performed. Unfortunately, no colonies were detected from the α SMA_eGFPNLS: pVQ_K-NpA culture. However, screening of colonies produced in the eGFPNLS: pVQ_CMV_K-NpA culture demonstrated two positive colonies, as confirmed by a DNA fragment of approximately 1,500 bp following a double *XbaI* and *NotI* restriction endonuclease digestion (Figure 3-8C).

In order to produce an adenoviral vector from this plasmid, first *PacI* was used to linearise both the pVQ_CMV_K-NpA containing the eGFPNLS insert and the RAPAd[®] Ad backbone vector. Next, cotransfection of these linearised vectors into HEK 293

cells was performed. However following 15 days of observation no CPE, which would indicate production of a recombinant Ad vector, had occurred.

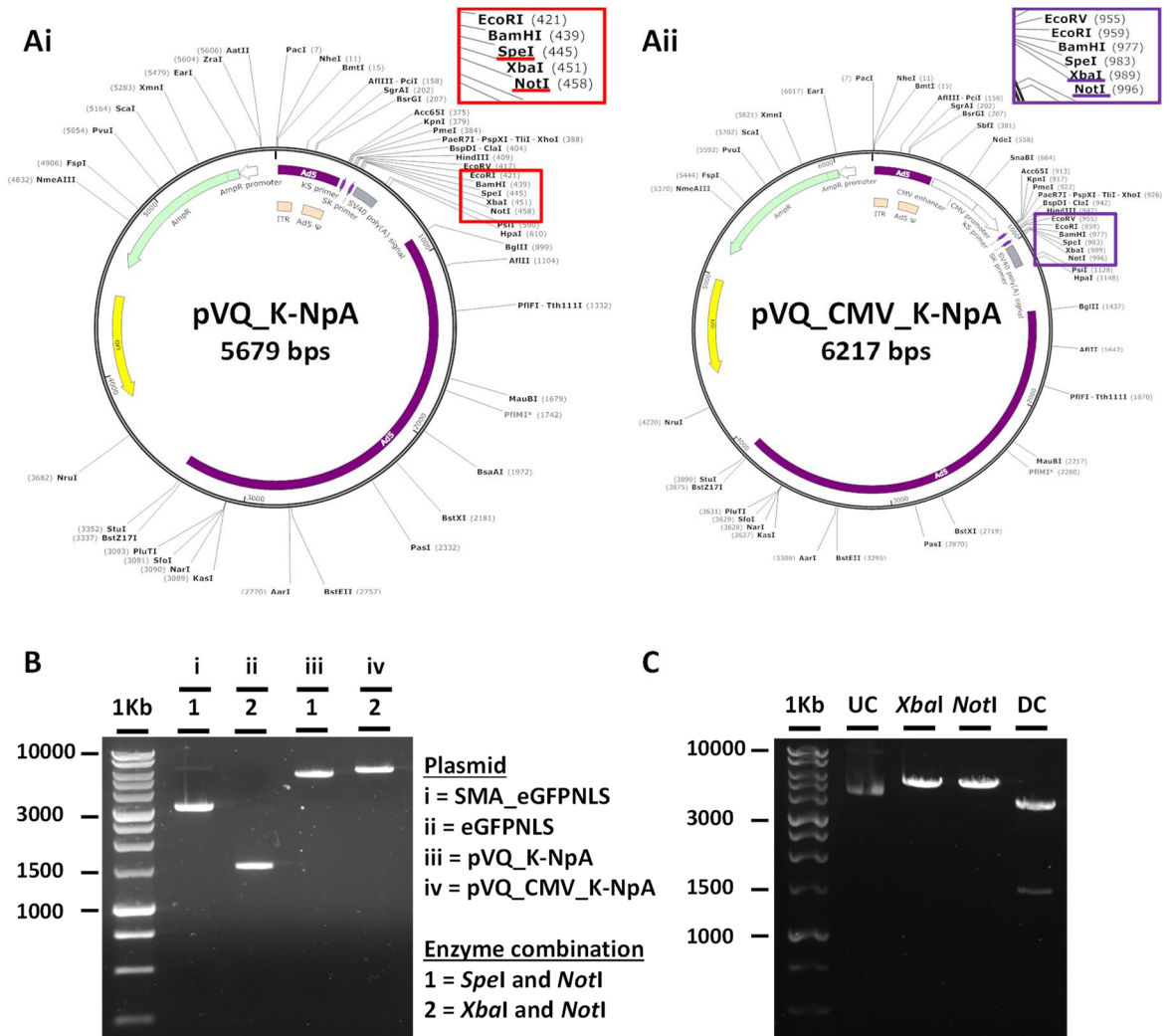


Figure 3-8 Cloning of α SMA_eGFPNLS or eGFPNLS into pVQ_K-NpA or pVQ_CMV_K-NpA respectively.

(A) Plasmid maps of pVQ_K-NpA and pVQ_CMV_K-NpA showing the endonuclease restriction sites compatible (underlined) to clone in the full α SMA_eGFPNLS insert or eGFPNLS without the α SMA promoter respectively. (B) Ethidium bromide agarose gel showing separation of the α SMA_eGFPNLS insert (i), eGFPNLS insert (ii) and the linearised pVQ_K-NpA (iii) and pVQ_CMV_K-NpA (iv) vectors following gel extraction and prior to ligation. (C) Gel showing separation of DNA fragments from a positive eGFPNLS: pVQ_CMV_K-NpA clone digested with *XbaI* or *NotI* alone or in combination. 1Kb; 1 Kb ladder, UC; uncut, DC; double cut with *XbaI* and *NotI*.

3.3.4 Production of an adenoviral vector overexpressing Cx43

Following many issues with the development of a LV and Ad vectors expressing the α SMA_eGFPNLS insert, a simple Ad vector overexpressing Cx43 was produced. This involved the excision of the rat Cx43 sequence (1149 bp) which was already cloned into pcDNA3.1 using *KpnI* and *NotI* and subsequent ligation into pShuttleCMV. All colonies screened by double *KpnI* and *NotI* restriction endonuclease digestion were confirmed positive as shown by visualisation of a DNA fragment of approximately 1,200 bp following agarose gel electrophoresis (Figure 3-9A). Next, pShuttleCx43 was linearised via *PmeI* restriction endonuclease digestion and electroporated into BJ5183-AD-1 bacteria which are ready transformed with the Ad genome plasmid, pAdEasy-1. Colonies were screened by *PacI* endonuclease restriction digestion and successful recombination of the pShuttleCx43 and pAdEasy-1 confirmed by the presence of two DNA bands; one of approximately 30,000 bp and another at either 3,000 or 4,500 bp depending on where recombination has occurred (between the left arms or at the origin of replications, respectively). Mini-culture preparations were performed and 5 individual colonies were detected as positive clones indicating recombination of the two vectors had occurred (Figure 3-9B). Sequencing analysis of the putative Cx43 positive recombinant plasmid showed a point mutation (G to A) at position 27, however this mutation was silent and therefore the clone was utilised to produce an Ad vector. The plasmid was amplified in a maxi-preparation, purified and linearised using *PacI* restriction endonuclease digestion and transfected into HEK 293 cells to produce an AdCx43.

To confirm the functionality of AdCx43, HeLa cells or RACFs were transduced at a MOI of 50, 100 or 150 (RACFs only) and Cx43 protein expression assessed by western immunoblotting (Figure 3-10 and Figure 3-11) and ICC (Figure 3-12). Representative western blot analysis showed no change in the expression of Cx43 in HeLa cells which were transduced with the control virus AdeGFP (0.9 fold change vs. control; Figure 3-10). Conversely, a dose-dependent increase in Cx43 protein was demonstrated in HeLa cells transduced with AdCx43 (4.3 and 13.2 fold increase from control; MOI 50 and 100 respectively; Figure 3-10). To confirm AdCx43 was functional in the target cells the experiment was repeated in RACFs (Figure 3-11). AdeGFP transduction did not alter endogenous Cx43 expression in RACFs (0.7 fold change from control; Figure 3-11). While an 8.1, 27.1 and 67.1

fold increase in Cx43 levels following AdCx43 transduction at an MOI of 50, 100 and 150, respectively, was observed (Figure 3-11). The increase in Cx43 was also confirmed by ICC (Figure 3-12), whereby punctate expression was observed throughout the cell and at the cell membrane. Very little Cx43 expression was seen in control cells, similar to western blot analysis. Furthermore, although green immunofluorescence was detected throughout AdeGFP transduced cells, this was likely to be residual eGFP fluorescence not removed by fixation. Despite this some basal Cx43 expression was detected as shown by the punctate areas.

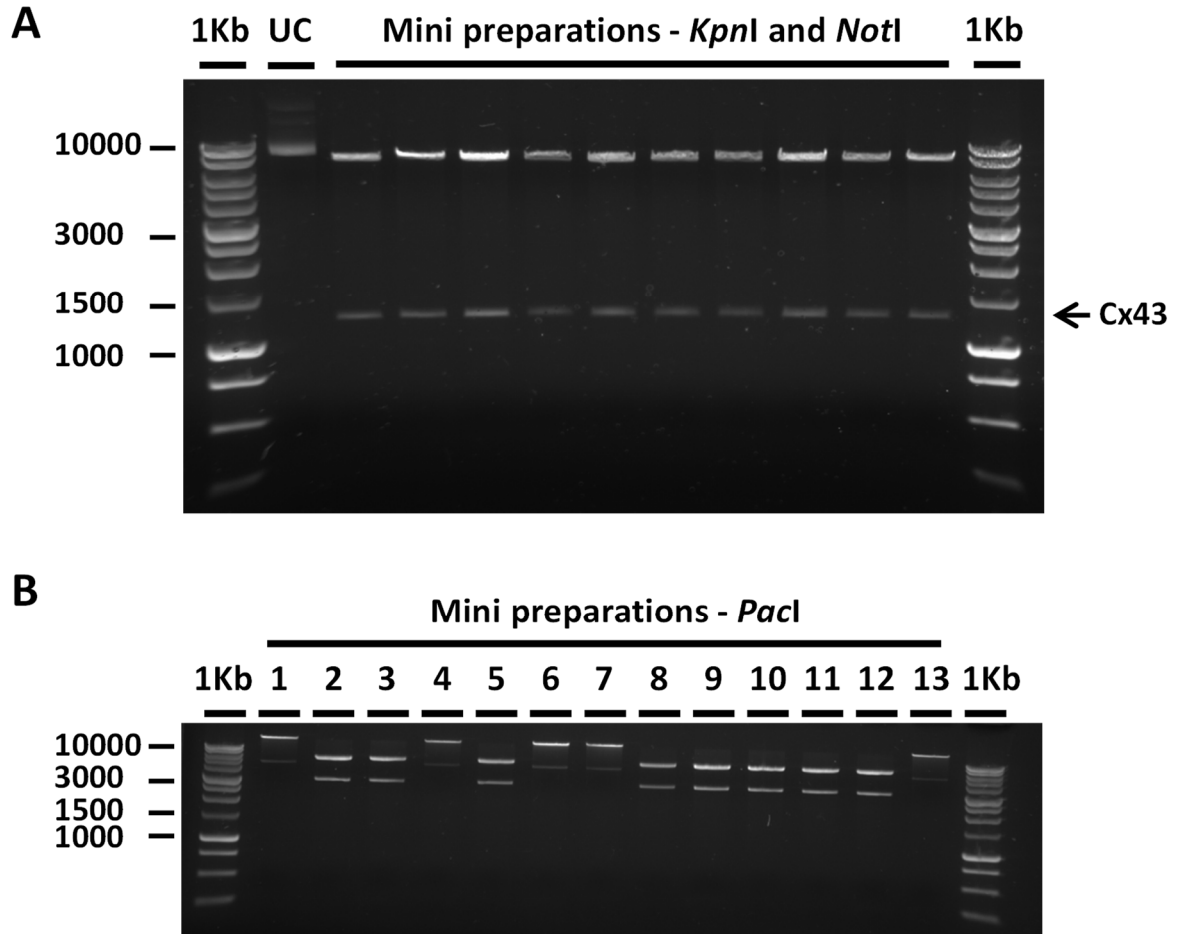


Figure 3-9 Clone screening of pShuttle_Cx43 and the recombinant Ad plasmid containing Cx43.

Ethidium bromide agarose gels showing (A) the separation of Cx43 from pShuttle following a double *KpnI* and *NotI* restriction digest and (B) successful recombination of pShuttle_Cx43 and pAdEasy-1 vector in mini preparations 1, 4, 6, 7 and 13 cut with *PacI*. 1Kb; 1 Kb ladder, UC; uncut.

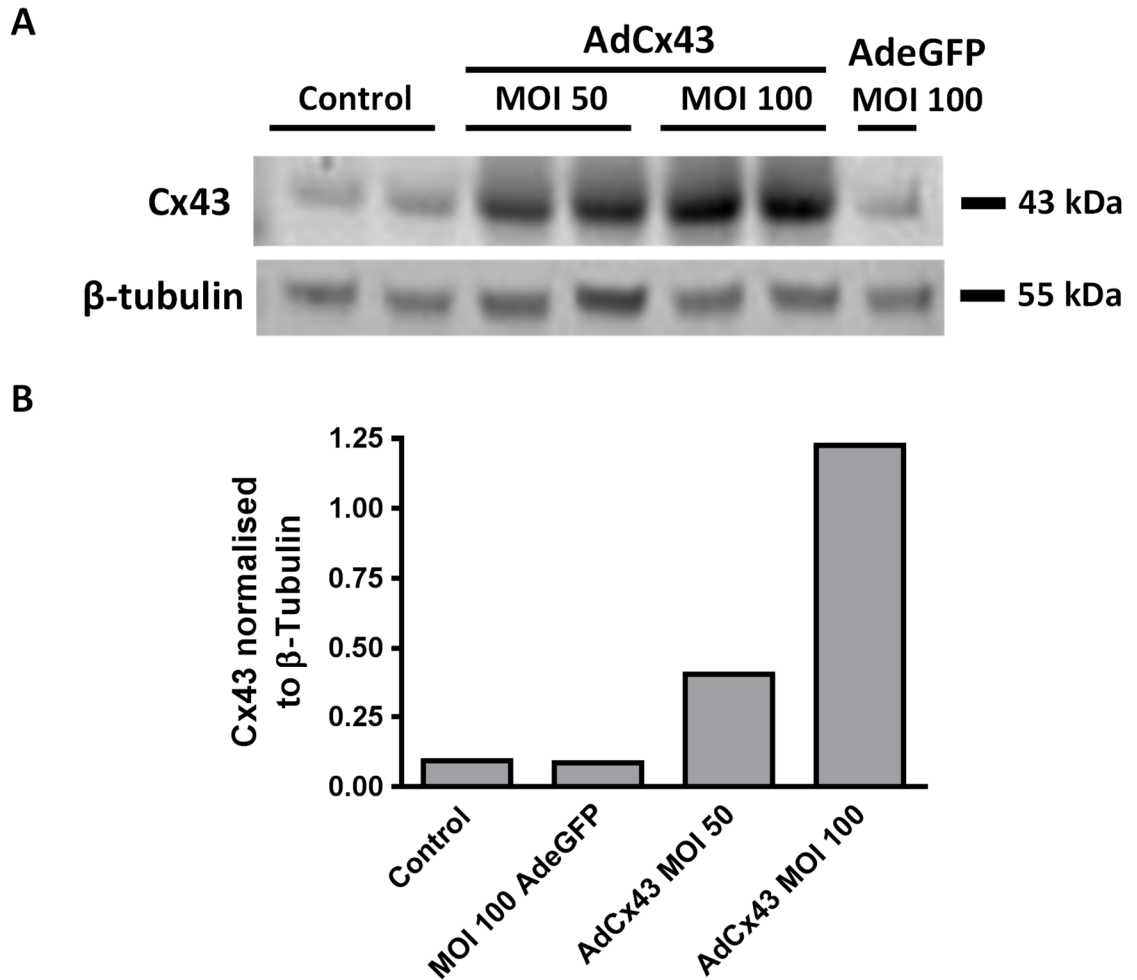


Figure 3-10 Representative western immunoblot of protein from HeLa cells transduced with AdCx43.

(A) Cx43 and β -tubulin protein expression from replicate wells of HeLa cells that were not transduced (control), transduced with AdeGFP at a multiplicity of infection (MOI) of 100 or AdCx43 at an MOI of 50 or 100. Protein was collected following at 48 h transduction. (B) Representative densitometry analysis of an experiment performed on two independent occasions showing Cx43 expression normalised to β -tubulin.

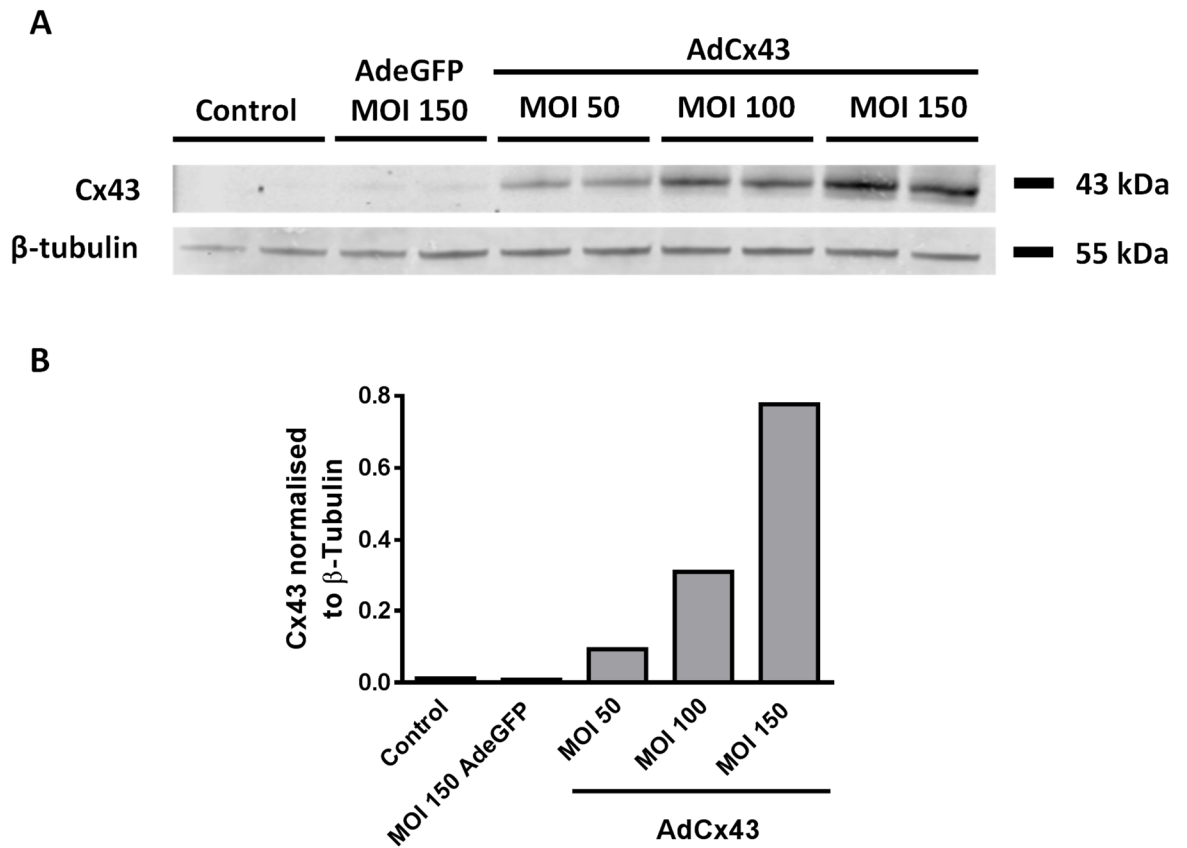


Figure 3-11 Representative western immunoblot of protein from RACFs transduced with an AdCx43.

(A) Cx43 and β -tubulin protein expression from replicate wells of RACFs that were not transduced (control), transduced with AdeGFP at a multiplicity of infection (MOI) of 150 or AdCx43 at an MOI of 50, 100 or 150. Protein was collected 48 h following transduction. (B) Representative densitometry analysis of an experiment performed on two independent occasions showing Cx43 expression normalised to β -tubulin.

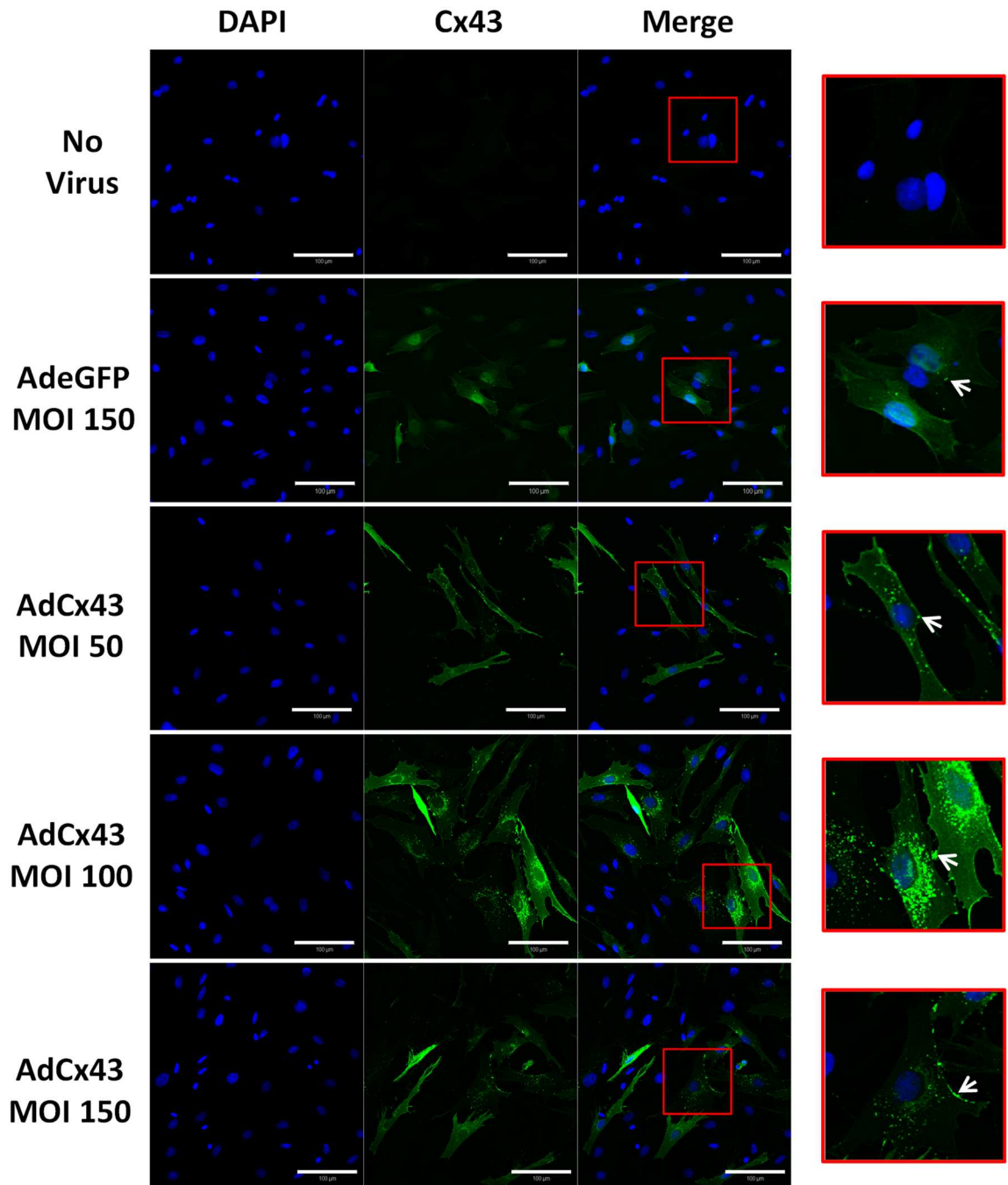


Figure 3-12 Immunolocalisation of Cx43 in RACFs transduced with AdCx43.

AdCx43 was added to RACF cultures at a multiplicity of infection (MOI) of 50, 100 or 150. Cells with no viral vector and cells transduced with AdeGFP, at a MOI of 150, were used as a control. Cells were fixed 48 h following transduction and immunocytochemistry for Cx43 (green) performed. Nuclei were counterstained with DAPI (blue). Images are representative of ICC performed on two independent occasions. Areas surrounded by the red boxes are expanded on the right. Punctate expression of Cx43 is depicted by white arrows. Scale bar represents 100 μ m.

3.4 Discussion

In this study, LV and Ad vectors were shown to efficiently transduce RACFs. Unfortunately, due to numerous issues with cloning, a LV vector overexpressing Cx43 and a nuclear localised eGFP under the control of the hybrid α SMA promoter was not produced. However, functional AdCx43 was successfully generated, as demonstrated by a dose dependent increase in Cx43 protein levels in HeLa cells and RACFs.

Transgene expression is generally apparent 72 h following LV vector transduction (Kizana et al. 2005) and was therefore the time point selected to examine eGFP expression. The transfection reagent, polybrene, is often used to enhance retroviral transduction (Davis et al. 2002), and has been used in many studies to transduce fibroblasts with LV vectors. Despite this, high MOIs of 50-200 (Duan et al. 2012; Kane et al. 2010; Kizana et al. 2005) are still often used without toxicity, suggesting that fibroblasts are a difficult cell type to transduce and relatively resistant to LV vector toxicity. In the present study, an MOI of 12 produced eGFP expression in most cells. Therefore, in comparison to other studies, the LVeGFP vector produced appears to be efficient for transduction of CFs.

Since the LVeGFP was shown to efficiently transduce RACFs, initial steps to produce a LV vector which would allow the expression of eGFPNLS under the control of the hybrid α SMA promoter (Hirschfeld et al. 2009) were taken. First, the functionality of the α SMA_eGFPNLS insert was examined by transfection. Green nuclei, although at very low levels, were demonstrated in RACFs transfected with p α SMA_eGFPNLS. RACFs transfected with the control plasmid, pSFFV_eGFP, were also shown to have low eGFP expression. It is well established that non-viral gene transfer is inefficient in comparison to viral-mediated delivery, therefore greater expression is likely to be observed via using an LV vector (Thomas et al. 2003). Indeed the SFFV promoter has been shown to be a potent driver of eGFP expression when packaged into a LV vector in the current study and by others (Laurie et al. 2007). However, as the Xfect reagent was shown to be toxic to the cells this could also be a contributing factor to the low expression levels observed.

In theory, the cloning of α SMA_eGFPNLS into plenti-promoter or plenti-III-promoterless should have been straightforward. Interestingly, any cloning attempted involving the hybrid α SMA promoter was unsuccessful, suggesting an issue with the promoter. However, no issues were reported by Hirschfeld *et al.* (2009) and due to no other use of this hybrid promoter in the literature, it is difficult to predict the reason for the lack of success. Some explanations may include toxicity of the insert to *E coli*. or inefficient ligation potentially due to the presence of the contaminating bands of DNA that were seen following gel extraction. Although the size of the α SMA_eGFPNLS insert was within the cloning capacity of both LV and Ad vectors, and therefore should not have been an issue, the reduction in size following removal of the promoter (eGFPNLS) may explain successfully cloning into the Ad plasmid, pVQ_CMV_K-NpA.

Ad vector expression has been examined at 48 h following transduction (Lovelock *et al.* 2005) and was therefore the time point examined in the Ad vector studies presented here. Indeed, high expression of eGFP was observed following AdeGFP transduction at a MOI of 100 and 150. However, toxicity was apparent when the MOI was increased to 500 and above. AdeGFP was used as the control vector in studies testing the functionality of AdCx43. Fixation has been shown to reduce eGFP fluorescence but not completely ablate it (Schnell *et al.* 2012), therefore to distinguish the detection of Cx43 expression in AdGFP transduced control cells via ICC, an empty control virus or a red emitting, such as Alexa Fluoro[®] 555, secondary antibody should have been utilised. Regardless, little punctate expression was detected (similar to non-transduced cells) which also agrees with the western immunoblot analysis. Interestingly, Ad vectors which contain the AdE4 gene, similar to that used in the current study, have been reported to downregulate Cx43 expression in endothelial cells (Zhang *et al.* 2015). This effect was not apparent in the current study in RACFs. This may reflect differential cellular responses to Ad vectors in different cell types.

A dose dependent increase in Cx43 protein expression was also observed over an MOI of 50-150, without toxicity. This is significantly greater than an MOI of 5 that was used in rat neonatal fibroblasts to overexpress Cx43 (Zlochiver *et al.* 2008). Furthermore, 500 vp/cell of an AdCx43 was reported to transduce skeletal myoblasts (SMs) (Reinecke *et al.* 2004) which is also substantially lower than the

700, 1400 and 2800 vp/cell (for an MOI of 50, 100 and 150 pfu/cell respectively) used in the present studies. Together this suggests low transduction efficiency for the Ad vector produced in the current study, however this may reflect different titering methods and therefore is difficult to make a direct comparison. Despite this, Cx43 expression pattern in neonatal rat fibroblasts was similar to that of the present study, whereby transduced cells showed expression throughout the cell with punctate expression at the cell membrane and surrounding the nucleus (Zlochiver et al. 2008). Interestingly, two nuclear localisation signals (NLSs) have been detected at the C-terminal of the Cx43 protein (Gago-Fuentes et al. 2015). This along with the rapid turnover of Cx43 (Beardslee et al. 1998; Hunter et al. 2005; Laird et al. 1991) and therefore trafficking through the cytoplasm may explain the unconfined Cx43 localisation to the cell membrane.

3.5 Summary

Although a LV vector overexpressing Cx43 and nuclear localised eGFP under the control of a α SMA hybrid promoter was not produced, LVeGFP, AdeGFP and AdCx43 were shown to be functional in RACFs. Therefore, in order to enable detection of injected RACFs *in situ* with the current viral vectors available, dual transduction of RACFs with LVeGFP or AdeGFP along with AdCx43 could be performed prior to injection.

Chapter 4 Interleukin 1 β regulates connexin 43 expression in primary cardiac fibroblasts

4.1 Introduction

4.1.1 The role of interleukin-1 in inflammatory signalling in the heart

It is well established that inflammation following a cardiac insult is both essential and detrimental to the healing heart. Initially, the death of CMs in response to ischaemia results in the release of damage-associated molecular patterns (DAMPs) including ATP, high-mobility group box 1 (HMGB1) and more recently IL-1 α (Epelman et al. 2015;Forrester and Williams 1977;Xu et al. 2011b). DAMPs activate resident macrophages and attract neutrophils to the ischemic area (Epelman et al. 2015). A large neutrophil infiltration within 24 h following I/R injury has been reported in both canine and mouse experimental models (Dewald et al. 2004). This is followed by an influx of macrophages, a key cell in the removal of cellular debris (Frangogiannis 2015), 24 to 72 h post reperfusion in mouse and canine experimental models (Bujak et al. 2008;Dewald et al. 2004). Furthermore, mRNA levels of the inflammatory cytokines; IL-1 β , TNF α , IL-6 and TGF β have been reported to be increased as soon as 15 min following the initiation of reperfusion in a rat I/R injury model (Herskowitz et al. 1995). Although inflammation is essential for the infarct to be cleared of cellular debris and the scar forming process to begin, excessive production of ROS and inflammatory cytokines can potentiate CM death (Epelman et al. 2015).

As well as inflammatory cells, fibroblasts are also known to be a major contributor to inflammatory cytokine production. CFs have been reported to be particularly resistant to cell death induced by oxidative stress in comparison to CMs as seen by their little or no DNA fragmentation in response to hydrogen peroxide (Zhang et al. 2001). This characteristic would allow CFs to respond to ischaemia instead of undergoing cell death. *In vitro*, hypoxia has been reported to induce MF transdifferentiation (Clancy et al. 2007), increase collagen synthesis (Tamamori et al. 1997) and promote TNF α production by CFs (Shivakumar et al. 2008). Furthermore, the inflammasome, a multi-protein complex which initiates the inflammatory process, has been shown to be activated in CFs but not CMs in response to lipopolysaccharide (Kawaguchi et al. 2011). Inflammasome activation results in the activation of caspase 1 which cleaves the inactive forms of pro-

inflammatory cytokines to the active form, mainly pro-IL-1 β to IL-1 β (Toldo et al. 2015). IL-1 β is increased in numerous pathological conditions including congestive heart failure and acute MI (Di et al. 2003). Interestingly, hypoxia/reoxygenation was demonstrated to significantly augment IL-1 β production by CFs suggesting inflammasome activation (Kawaguchi et al. 2011). Additionally, IL-1 α released by necrotic CMs was identified to induce an inflammatory response in CFs, including activation of MAPKs and NF- κ B along with secondary production of proinflammatory cytokines (Lugrin et al. 2015). These data together suggest an important role for CFs in the detection of cardiac injury and initiation of the inflammatory response.

To mediate their effects, both IL-1 α and IL-1 β bind to IL-1 receptor type 1 (IL-1R1) to activate downstream signalling (Weber et al. 2010) (Figure 4-1). Mice lacking IL-1R1 have been shown to have a dampened inflammatory response to I/R injury, including a reduced number of neutrophils and macrophages as well as reduced mRNA levels of a variety of chemokines and cytokines 24 h after initiation of reperfusion (Bujak et al. 2008). Furthermore, MF infiltration, collagen deposition and MMP levels were all reduced in IL-1R1^{-/-} mice vs. WT, despite there being no difference in infarct size (Bujak et al. 2008).

Initial binding of IL-1 to the IL-1R1 mediates a conformational change in IL-1R1, consequently recruiting the IL-1R accessory protein (IL-1RacP), a co-receptor essential for IL-1 signalling (Weber et al. 2010). Intracellular proteins including myeloid differentiation primary response gene 88 (MYD88) and interleukin-1 receptor-activated protein kinase (IRAK) 1, 2 and 4 are then recruited to the cell membrane (Weber et al. 2010). IRAKs interact with the TNF-associated factor (TRAF) 6 ultimately resulting in the activation of inhibitor of nuclear factor B (I κ B) kinase (IKK), p38 MAPK, JNK and MEK1/2 (Weber et al. 2010). In the resting state, I κ B is bound to the p50 and p65 subunits of NF- κ B in the cytosol of the cell holding NF κ B in an inactive state. Activated IKK phosphorylates I κ B which leads to its polyubiquitination and consequent degradation (Chen 2005). Subsequently, the transcription factor, NF- κ B, is activated and the p50 and p65 subunits translocate into the nucleus to mediate gene transcription (Chen 2005). IL-1 β can also initiate gene transcription by activating p38 MAPK, JNK and ERK1/2, resulting in subunits

of the transcription factor, activator protein-1 (AP-1), becoming activated and translocating to the nucleus (Weber et al. 2010).

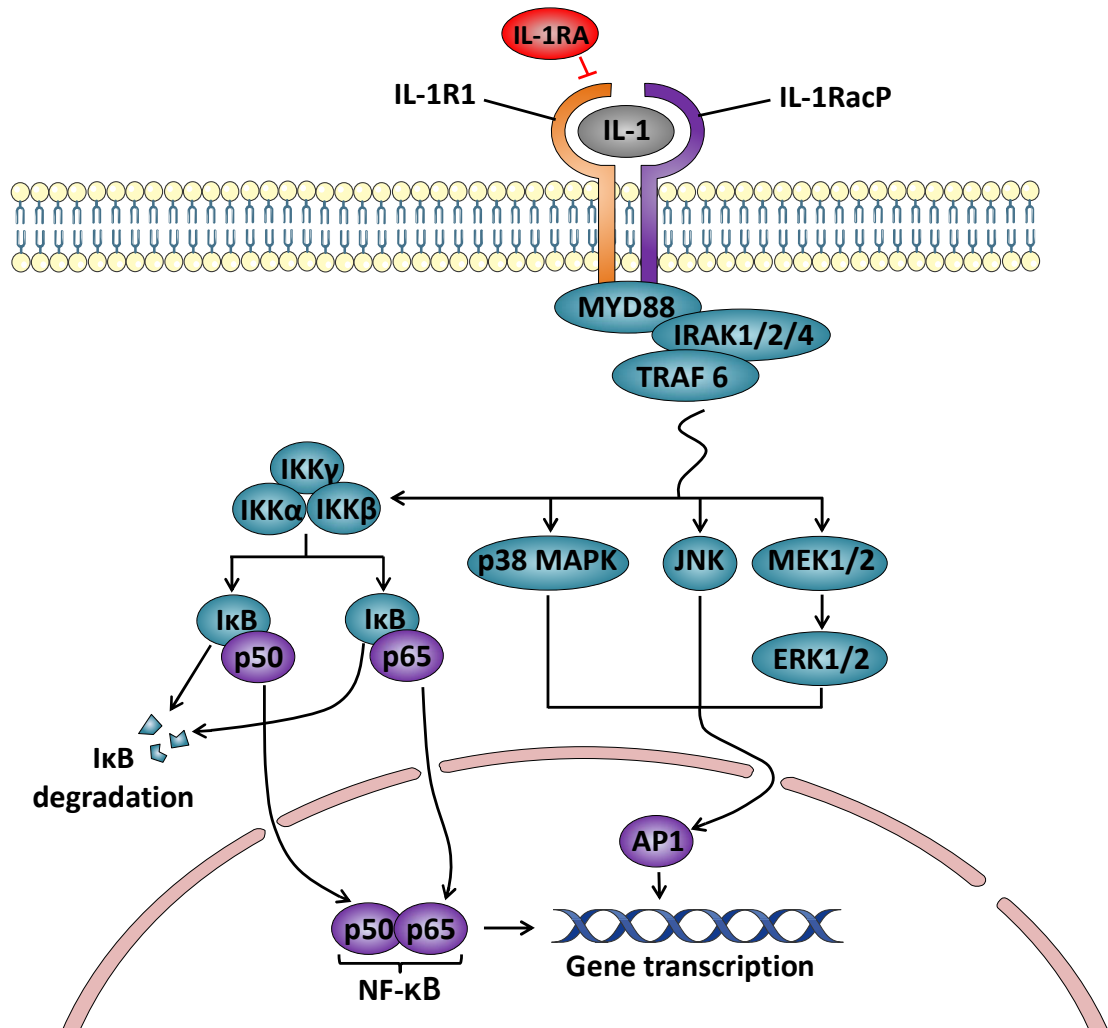


Figure 4-1 IL-1 signalling pathway.

IL-1 α and IL-1 β bind to the IL-1 receptor (IL-1R1) resulting in a conformational change and subsequent recruitment of the co-receptor, IL-1 receptor accessory protein (IL-1RacP). The endogenous IL-1 receptor antagonist (IL-1RA) blocks IL-1 signalling. Following receptor activation myeloid differentiation primary response gene 88 (MYD88) and IL-1 receptor-activated protein kinase (IRAK) 1, 2 and 4 are recruited to the cell membrane. IRAKs interact with tumour necrosis factor-associated factor (TRAF) 6 resulting in the transmission of downstream signals. Consequently, the inhibitor of nuclear factor B (I κ B) kinase (IKK), p38 mitogen-activated protein kinase (MAPK), c-Jun N-terminal kinase (JNK) and MAPK/extracellular signal-regulated kinase (ERK) kinase (MEK)1/2 (which subsequently activates ERK1/2) are activated. IKK phosphorylates I κ B to signal its degradation freeing the p50 and p65 subunits of NF- κ B, which are then able to translocate into the nucleus and initiate gene transcription. p38 MAPK, JNK and ERK1/2 activate activator protein-1 (AP-1) subunits, which then move into the nucleus to mediate gene transcription.

4.1.2 Regulation of Cx43 by IL-1 β

The effect of IL-1 β on Cx43 expression has been shown to vary between cell types. IL-1 β was initially reported to downregulate Cx43 in both foetal human astrocytes (Duffy et al. 2000; John et al. 1999) and neonatal CMs (Baum et al. 2012a; Coppen et al. 2008). This finding led to speculation that enhanced IL-1 β levels following cardiac injury could be a contributing factor to the reduced Cx43 levels seen in many cardiac pathologies (Baum et al. 2012b). Conversely, in other cell types including rabbit articular chondrocytes (Tonon and D'Andrea 2000) and a rabbit synovial fibroblast cell line (Niger et al. 2010) Cx43 expression has been shown to be upregulated by IL-1 β . The mechanisms for up-regulation were attributed to an increase in cytosolic calcium and ERK signalling, respectively (Niger et al. 2010; Tonon and D'Andrea 2000). Interestingly, one AP-1 binding site has been found within the human and mouse Cx43 promoter (Chen et al. 1995b; De Leon et al. 1994) and two sites have been identified in the rat Cx43 promoter (Teunissen et al. 2003; Yu et al. 1994). An NF- κ B binding site has also been detected in the Cx43 promoter in rat SMCs (Alonso et al. 2010). However, NF- κ B mediated regulation of Cx43 is complex, with studies reporting an increase and decrease in expression with different cell types and stimuli (Alonso et al. 2010; Zhao et al. 2006). The effect of IL-1 β on Cx43 expression in fibroblasts from cardiac origin is yet to be investigated.

Cx43 regulation in fibroblasts by proinflammatory mediators is interesting due to studies reporting enhanced Cx43 expression in CFs from infarcted hearts in experimental models of MI (Vasquez et al. 2010; Zhang et al. 2010). Furthermore, TGF β 1-mediated CF-to-MF transition has been shown to involve Cx43 in rat neonatal CFs (Asazuma-Nakamura et al. 2009), although TGF β 1 did not alter Cx43 expression (Asazuma-Nakamura et al. 2009).

Interestingly, IL-1 β inhibits TGF β 1-mediated MF transdifferentiation in cardiac, dermal and lung fibroblasts (Bronnum et al. 2013; Mia et al. 2014; Saxena et al. 2013). This could be a consequence of IL-1 β -mediated downregulation of the TGF β 1 receptor 1 (TGF β R1), the signal propagating receptor involved in TGF β signalling, or downregulation of the TGF β co-receptor, endoglin (Bronnum et al.

2013;Saxena et al. 2013). Although TGF β 1 is increased in the early stages of infarct healing following MI, MF accumulation is delayed, peaking at around 5-7 days post reperfusion in a canine model of I/R injury (Frangogiannis et al. 2000). As IL-1 β is important in early inflammation it may act to inhibit premature fibroblast activation allowing the inflammatory phase to clear cellular debris before scar forming processes are underway.

4.1.3 MicroRNA regulation of connexin 43

MiRNAs are defined as short non-coding RNAs, consisting of approximately 22 nucleotides, which negatively regulate protein expression. Binding of miRNAs to target mRNA strands can either inhibit gene translation or signal untranslated mRNA for degradation (van and Olson 2012). Many miRNAs have been shown to be dysregulated in cardiac pathologies. For example, miR-21 was found to be upregulated in the failing human myocardium as well as the infarct of a murine model of I/R injury (Roy et al. 2009;Thum et al. 2008). Additionally, inhibition of miR-21 promoted many beneficial effects, including reduced fibrosis by targeting the negative regulator of ERK, sprout homologue 1, in both a murine model of I/R injury and a rat MI model (Cardin et al. 2012;Thum et al. 2008). Another miRNA reported to promote anti-fibrotic effects is miR-101a/b, which targets c-Fos consequently reducing TGF β 1 expression (Pan et al. 2012). Furthermore, miR-101a/b are both downregulated in the peri-infarct area in a rat MI model (Leicht et al. 2000).

MiRNAs have also been implicated in the regulation of Cx43. MiR-19a/b, which is part of the miR-17-92 cluster, was reported to directly target Cx43, consequently reducing cardiac Cx43 protein levels in transgenic mice overexpressing the miR-17-92 cluster (Danielson et al. 2013). MiR-125b, a vital miRNA for CF-to-MF transition and cardiac fibrosis (Nagpal et al. 2016), has also been shown to directly target Cx43 in HEK 293 cells (Jin et al. 2013). IL-1 β is also able to regulate miRNAs including miR-101 and -146 (Perry et al. 2008;Wang et al. 2014b), however a link between IL-1 β -mediated miRNA regulation and Cx43 expression has not yet been established.

4.2 Aims

- To assess the effect of different proinflammatory cytokines on Cx43 expression in RACFs.
- Dissect the IL-1 β signalling pathway for mechanisms of IL-1 β mediated regulation of Cx43 in RACFs.

4.3 Results

4.3.1 Characterisation of isolated adult rat cardiac fibroblasts

Unfortunately, fibroblasts lack a specific cell marker (Souders et al. 2009) and should generally be stained with more than one marker to identify them. CFs isolated from adult male Wistar rats were cultured until passage 2 and stained with antibodies against a range of fibroblast/MF markers including; α SMA, vimentin, DDR2 and S100A4 (FSP1). A Cx43 antibody was also used to identify Cx43 expression in normal cultured fibroblasts. All images were corrected to an IgG control for each antibody to remove false positive staining.

High expression of the myofibroblast marker, α SMA, was detected in stress fibers of RACFs (Figure 4-2), suggesting fibroblast-to-myofibroblast differentiation had occurred in culture by passage 2. Fibroblasts were also shown to express vimentin, DDR2 and S100A4 (FSP1) throughout the cell (Figure 4-2). DDR2 expression was punctate and appeared to be concentrated around the nucleus in some cells (white arrows; Figure 4-2). Punctate expression of Cx43 at the cell membrane was also detected (white arrows; Figure 4-2), which may suggest the ability of these cells to form GJs when in close contact to other cells.

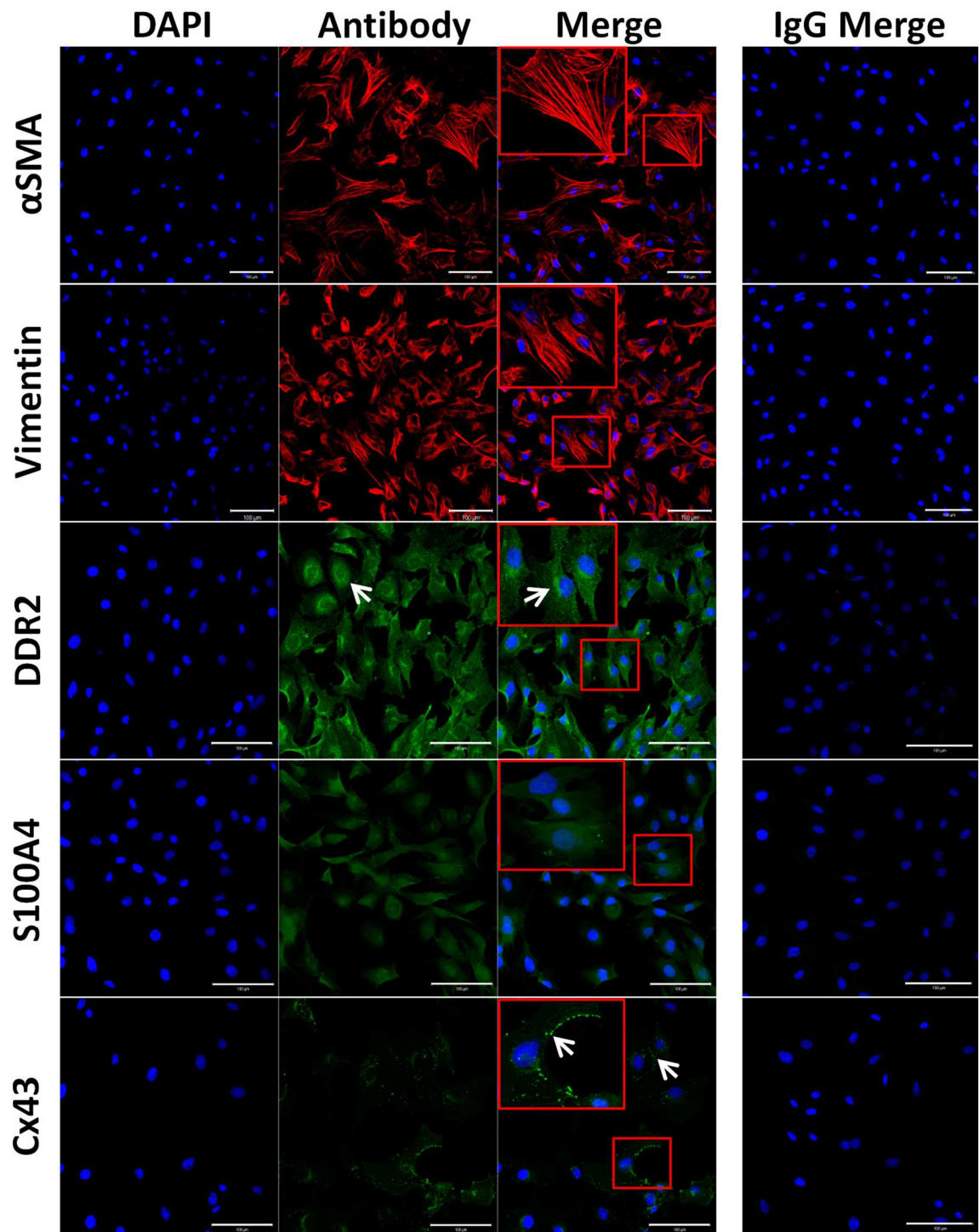


Figure 4-2 Immunolocalisation of α SMA, vimentin, DDR2, S100A4 and Cx43 in passage 2 RACFs.

Cells were seeded at 1.8×10^4 per chamber of a 4 well chamber slide and fixed 48 h thereafter. Staining was completed and normalised to individual IgG shown down the right hand side. White arrows show areas where DDR2 is in high abundance surrounding the nucleus or the punctate expression of Cx43. $n=3,3,1,2,3$ for α SMA, vimentin, DDR2, S100A4 and Cx43 respectively. Images were taken at $\times 25$ magnification. Scale bar represents 100 μm .

4.3.2 Assessment of Cx43 regulation by proinflammatory mediators

Cx43 expression has been reported to be increased in CFs from infarcted hearts (Vasquez et al. 2010; Zhang et al. 2010). As proinflammatory mediators are also augmented in cardiac disease, the effect of a range of molecules able to mediate inflammatory responses, including Ang II, TGF β 1, IL-1 β , IL-1 α , TNF α , IL-6 and IL-6 in combination with the sIL-6R on Cx43 mRNA expression was examined in RACFs. All RACFs were quiesced in reduced serum media (0.5 % FBS) for 24 h and subsequent stimulations performed in this media.

Cx43 mRNA expression in RACFs reintroduced into culture media (10 % FBS) was shown to be significantly greater than in control cells (RQ: 3.3 ± 2.1 ; $P < 0.001$; Figure 4-3). Stimulation of RACFs with TGF β 1, IL-1 β , IL-1 α or IL-6 in combination with the sIL-6R induced significant up-regulation of Cx43 mRNA expression (RQ: 1.7 ± 1.1 [$P < 0.05$], 10.2 ± 3.1 [$P < 0.001$], 10.0 ± 4.9 [$P < 0.001$] and 2.0 ± 1.3 [$P < 0.01$] respectively; Figure 4-3). Conversely, there were no significant changes in Cx43 mRNA following stimulation with Ang II, TNF α or IL-6 alone (RQ: 0.7 ± 0.4 , 1.3 ± 0.8 , 1.2 ± 0.8 respectively; Figure 4-3).

Interestingly, a morphological change was observed in RACFs stimulated with IL-1 β (Figure 4-4). Cells adopted a phenotype with an increased number of projections, the extent of which varied amongst individual cells. A representative cell which has a particularly high level of projections is shown as a magnified inset within the image of IL-1 β -treated cells (Figure 4-4B). Interestingly these cellular projections were observed to extend towards surrounding cells, suggesting they were potentially involved in enhancing cell-to-cell contact.

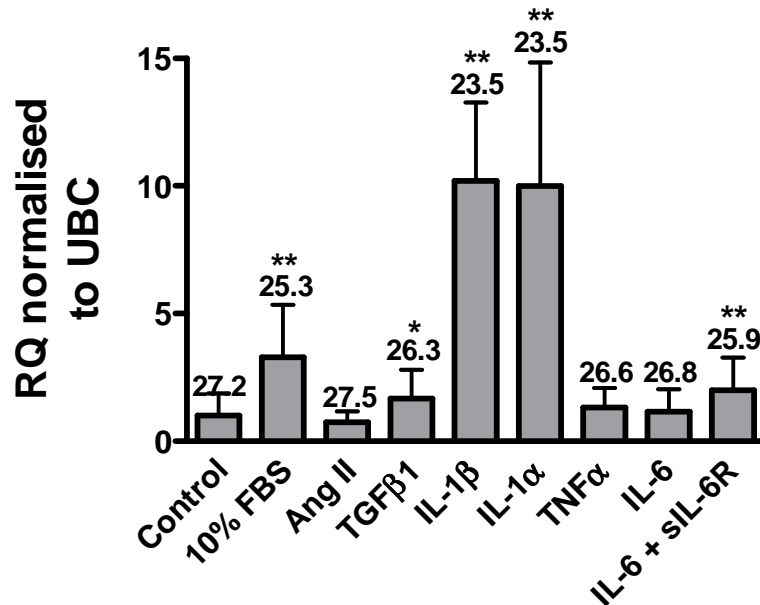


Figure 4-3 Effect of proinflammatory mediators on Cx43 mRNA expression in RACFs.

Quiesced cells were stimulated with 10 % FBS, Ang II (500nM), TGFβ1, IL-1β, IL-1α, TNFα (all 10ng/mL) or IL-6 in the presence or absence of the sIL-6R (both 50 ng/mL) for 24 h. Cells maintained in 0.5 % FBS media were used as a control. Data represented as relative quantification (RQ) \pm $r_{q_{max}}$ normalised to UBC (n=3). * P <0.05, ** P <0.01, *** P <0.001 vs. control (one-way repeated measures ANOVA with Dunnett's multiple comparison test). Average threshold cycle (C_t) values are shown above each bar.

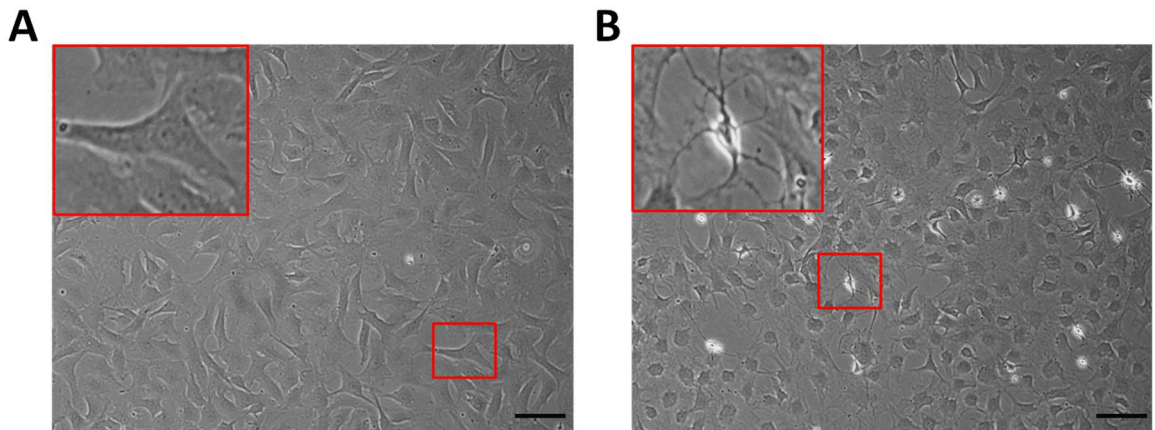


Figure 4-4 Representative images of control and IL-1β treated RACFs.

Quiesced cells were (A) maintained in 0.5 % or (B) stimulated with 10 ng/mL IL-1β and images captured 24 h thereafter. The area surrounded by a red box is expanded within the image to highlight the morphology of specific cells (n=4). Images were taken at x10 magnification. Scale bar represents 100 μm.

4.3.3 Dissection of the mechanism by which IL-1 β stimulates Cx43 up-regulation

As IL-1 β was demonstrated to increase Cx43 mRNA levels, this was examined at the protein level. Cx43 protein was examined in normal cultured, quiesced and IL-1 β stimulated RACFs by western immunoblotting (Figure 4-5A). RACFs maintained in reduced serum media for 48 h (quiesced cells) were shown to mediate a 1.9 fold reduction in Cx43 protein in comparison to cells in normal culture media (10 % FBS) (0.034 vs. 0.018 Cx43/GAPDH, 10 % FBS vs. 0.5 % FBS; Figure 4-5B). Cx43 protein was 8-fold greater when stimulated with IL-1 β when compared to unstimulated cells (0.5 % FBS cells) (0.145 vs. 0.018 Cx43/GAPDH, IL-1 β vs. 0.5 % FBS; Figure 4-5B).

ICC was also performed to visualise the localisation of Cx43 in control (cells maintained in reduced serum media) and IL-1 β stimulated cells. Although Cx43 was present in control cells, staining was more pronounced in cells stimulated with IL-1 β (Figure 4-5C). Interestingly, IL-1 β enhanced the presence of Cx43 at the cell membrane, highlighted by white arrows in the area expanded within the red box in the lower right panel. All images were corrected to the IgG control (Figure 4-5C - upper right panel).

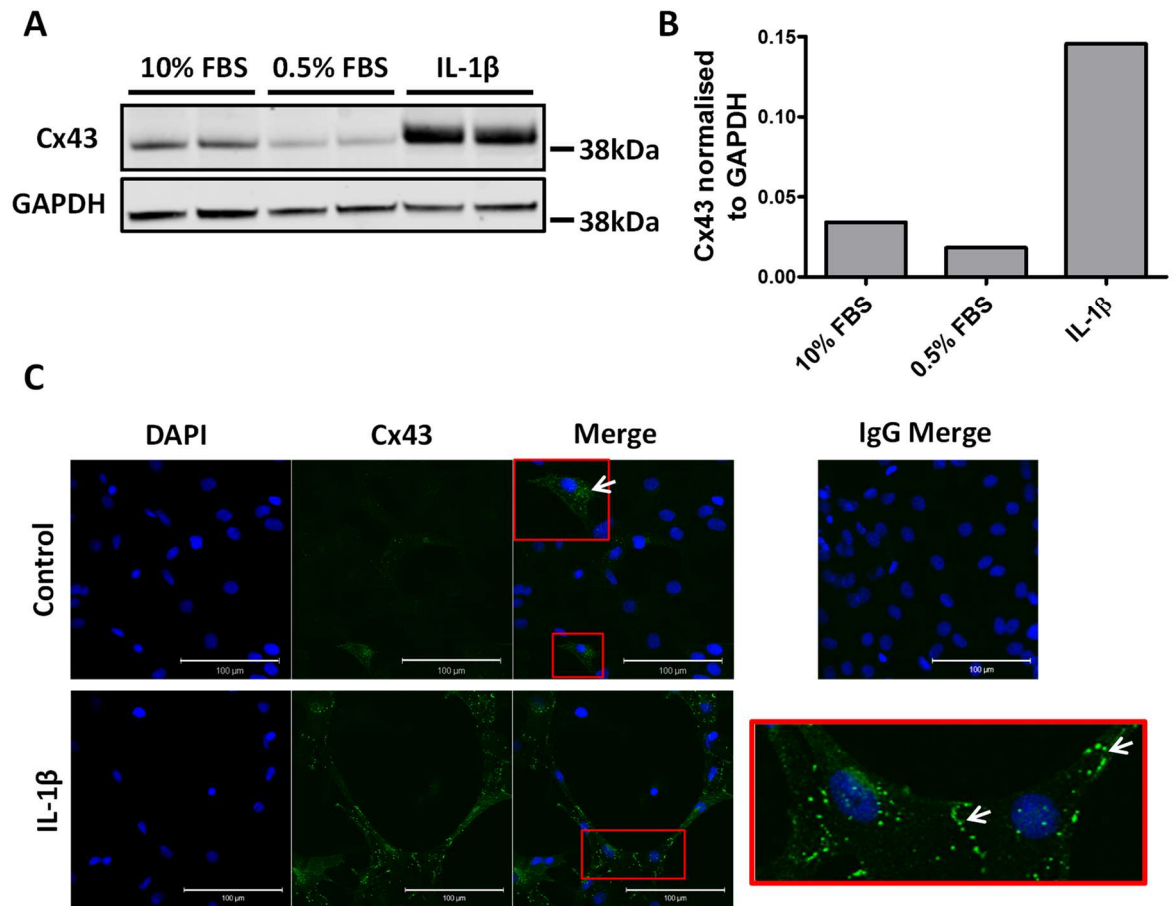


Figure 4-5 Effect of IL-1 β on Cx43 protein expression in RACFs.

Quiesced cells were stimulated with 10ng/mL IL-1 β for 24 h. Cells maintained in 0.5 % FBS media were used as a control. (A) Western blot of Cx43 protein and GAPDH from replicate wells of cells maintained in normal culture media (10 % FBS), 0.5 % FBS media or cells stimulated with 10 ng/mL IL-1 β ($n=1$). (B) Densitometry analysis of Cx43 expression normalised to GAPDH ($n=1$). (C) Representative images of control RACFs (maintained in 0.5 % FBS media) or cells treated with 10 ng/mL IL-1 β ($n=3$). Images were normalised to an IgG control shown in the upper right panel. The areas surrounded by a red box are expanded within the merged image or in the lower right panel for control and IL-1 β stimulated cells respectively. White arrows indicate punctate Cx43 expression. Images were taken at x25 magnification. Scale bars represent 100 μ m.

4.3.3.1 Effect of inhibitors of the IL-1 β pathway on Cx43 expression

IL-1 β pathway inhibitors were utilised to investigate the mechanism of IL-1 β -mediated upregulation of Cx43 in RACFs. For experiments in which inhibitors were reconstituted in DMSO, DMSO was added to a subset of cells to determine its effect on Cx43 expression.

NF- κ B is known to be an important regulator of IL-1 β actions on CFs (Xie et al. 2004), and was therefore investigated using the specific inhibitor, SC-514 (SC) (Gomez et al. 2005; Riis et al. 2011). Quiesced cells were incubated with SC for 30 min prior to stimulation with IL-1 β . DMSO at a final concentration of 0.1 % (vehicle control) did not significantly affect the expression of Cx43 mRNA (RQ: 1.5 ± 0.2 , Figure 4-6A), indicating that any changes with SC can be attributed to the action of SC and not the vehicle. IL-1 β induced a significant upregulation of Cx43 mRNA, which was significantly inhibited by SC (RQ: 11.2 ± 1.3 vs. 4.3 ± 1.9 , IL-1 β vs. IL-1 β + SC; $P < 0.05$; Figure 4-6B). This pattern was also observed at the protein level as determined by western immunoblotting, however these changes were not considered significant due to large variation in extent of this response to IL-1 β (Figure 4-7; Appendix figure 1 shows all immunoblots used in densitometry). There was no change in Cx43 protein expression when cells were stimulated with DMSO (0.066 ± 0.039 vs. 0.064 ± 0.036 Cx43/ β -tubulin, control vs. DMSO; Figure 4-7B). IL-1 β stimulation increased Cx43 protein expression by 31.6 fold in comparison to cells treated with DMSO alone (2.001 ± 1.106 vs. 0.064 ± 0.036 Cx43/ β -tubulin, IL-1 β vs. DMSO; Figure 4-7B). This effect was reduced to a 5.3 fold increase when cells were stimulated with IL-1 β in the presence of SC (0.336 ± 0.199 vs. 2.001 ± 1.106 Cx43/ β -tubulin, IL-1 β + SC vs. IL-1 β + DMSO; Figure 4-7B).

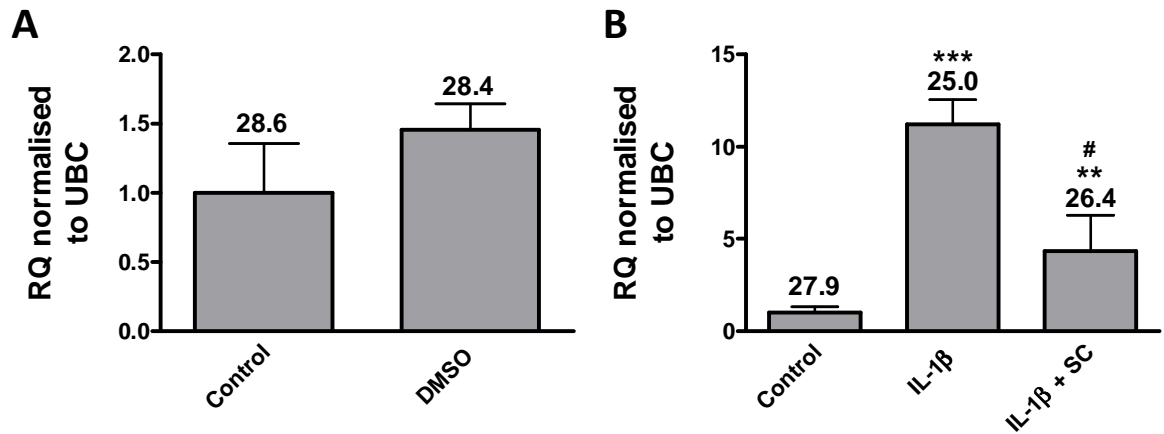


Figure 4-6 Effect of NF- κ B inhibition on IL-1 β mediated upregulation of Cx43 mRNA expression in RACFs.

Quiesced cells were stimulated with (A) 0.1 % DMSO (vehicle), ($n=2$) or (B) 10 ng/mL IL-1 β in the presence or absence of 100 μ M SC-514 (SC), an NF- κ B inhibitor ($n=3$). Cells were pre-incubated with SC for 30 min prior to IL-1 β stimulation and all stimulations were performed for 24 h. Cells maintained in 0.5 % FBS were used as a control. Data represented as relative quantification (RQ) \pm RQ_{max} normalised to UBC. No significant changes were detected between control and 0.1 % DMSO using an unpaired, two-tailed t-test. ** $P < 0.01$, *** $P < 0.001$ vs. control, # $P < 0.05$ vs. IL-1 β (one-way repeated measures ANOVA with Tukey's multiple comparison test). Average threshold cycle (C_t) values are shown above each bar.

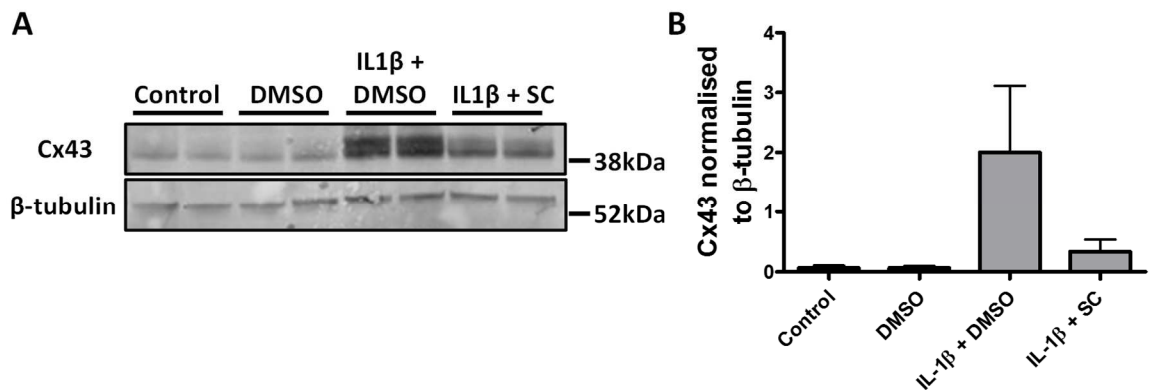


Figure 4-7 Effect of NF- κ B inhibition on IL-1 β mediated upregulation of Cx43 protein expression in RACFs.

Quiesced cells were stimulated with 0.1 % DMSO (vehicle), 10 ng/mL IL-1 β in combination with 0.1 % DMSO or 100 μ M SC-514 (SC), an NF- κ B inhibitor. Cells were pre-incubated with SC for 30 min prior to IL-1 β stimulation and all stimulations were performed for 24 h. Cells maintained in 0.5 % FBS media were used as a control. (A) Representative Western immunoblot of Cx43 and β -tubulin (loading control) from replicate wells ($n=3$). (B) Densitometry analysis of Cx43 expression normalised to β -tubulin from three independent experiments. No significant changes were detected using a repeat measures ANOVA with Tukey's multiple comparison test.

Next, the role of p38 MAPK, JNK and MEK1 in IL-1 β -mediated up-regulation of Cx43 was examined using pharmacological inhibitors for these proteins. At the mRNA level, inhibition of p38 MAPK with SB203580 (SB) did not significantly reduce IL-1 β -mediated upregulation of Cx43, although there was a partial reduction (RQ: 4.4 ± 0.8 vs. 7.4 ± 1.1 , IL-1 β + SB vs. IL-1 β + DMSO; Figure 4-8). AZD6244 (AZ), an inhibitor of MEK1, induced significant inhibition of IL-1 β -induced increases in Cx43 expression (2.4 ± 0.3 vs. 7.4 ± 1.1 , IL-1 β + AZ vs. IL-1 β + DMSO; $P < 0.05$; Figure 4-8). Conversely, inhibition of JNK with SP600125 (SP) had no significant effect on IL-1 β -mediated augmentation of Cx43 (12.6 ± 3.1 vs. 7.4 ± 1.1 , IL-1 β + SP vs. IL-1 β + DMSO; Figure 4-8). At the protein level, IL-1 β alone or in the presence of DMSO induced an 11.7 or 9.6 fold increase in Cx43 protein in comparison to control cells (0.347 ± 0.073 or 0.286 ± 0.002 vs. 0.023 ± 0.166 Cx43/ β -tubulin, IL-1 β or IL-1 β + DMSO vs. control; Figure 4-9B; Appendix figure 2 shows all immunoblots used in densitometry). This was reduced to a 4.6 or 5.3 fold increase from control in the presence of SB or AZ, respectively (0.136 ± 0.096 or 0.157 ± 0.057 vs. 0.023 ± 0.166 Cx43/ β -tubulin, SB + IL-1 β or AZ + IL-1 β vs. control; Figure 4-9B). Inhibition of JNK potentiated IL-1 β -induced increases in Cx43 protein expression by 2.8 fold (26.9 fold increase from control) (0.801 ± 0.081 vs. 0.286 ± 0.002 Cx43/ β -tubulin, IL-1 β + SP vs. IL-1 β + DMSO; Figure 4-9B). Although this change in Cx43 was not significant from IL-1 β + DMSO it was shown to be significant from control cells ($P < 0.01$).

As IL-1 β exerts its actions through the IL-1R, the endogenous IL-1Ra was utilised at range of concentrations. Indeed, IL-1Ra dose-dependently inhibited increases in Cx43 induced by IL-1 β (Figure 4-10), confirming a role for the IL-1R in IL-1 β -mediated Cx43 up-regulation. The RQ \pm r q_{\max} of Cx43 expression was significantly reduced from 10.1 ± 0.7 in IL-1 β stimulated cells to 6.9 ± 0.8 , 6.0 ± 1.0 or 4.4 ± 0.5 in cells stimulated with IL-1 β in the presence of 0.25, 0.5 or 1 μ g/mL IL-1Ra respectively ($P < 0.05$, 0.01 and 0.001).

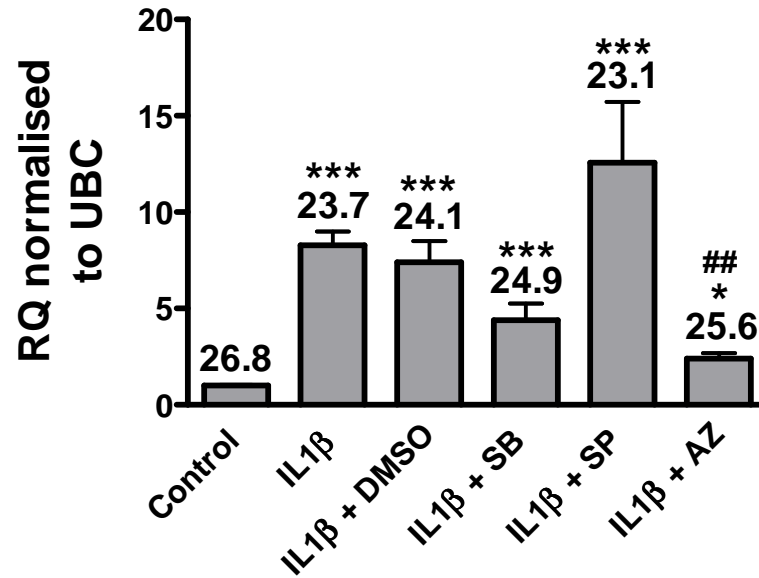


Figure 4-8 Effect of p38 MAPK, JNK or MEK1 inhibition on IL-1 β mediated up-regulation of Cx43 mRNA expression in RACFs.

Cells were quiesced in 0.5 % FBS for 24 h prior to the addition of 0.1 % DMSO, 10 μ M SB203580 (SB), 20 μ M SP600125 (SP) or 10 μ M AZD6244 (AZ) for vehicle control or inhibition of p38 MAPK, JNK or MEK1 respectively. Cells were incubated for 1 h with inhibitors prior to the addition of 10 ng/mL IL-1 β and stimulations were performed for 24 h. Cells maintained in 0.5 % FBS were used as a control. Data represented as relative quantification (RQ) \pm $r_{q_{max}}$ normalised to UBC ($n=3$). * $P<0.05$, *** $P<0.001$ vs. control; ## $P<0.01$ vs. IL-1 β + DMSO (one-way repeated measures ANOVA with Tukey's multiple comparison test). Average threshold cycle (C_t) values are shown above each bar.

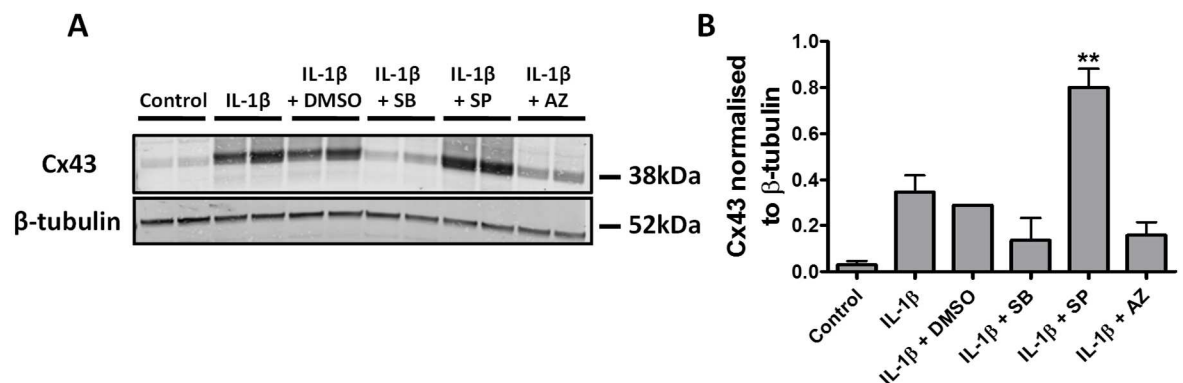


Figure 4-9 Effect of p38 MAPK, JNK or MEK1 inhibition on IL-1 β mediated up-regulation of Cx43 protein expression in RACFs.

Quiesced cells were stimulated with 0.1 % DMSO, 10 μ M SB203580 (SB), 20 μ M SP600125 (SP) or 10 μ M AZD6244 (AZ) for vehicle control or inhibition of p38 MAPK, JNK or MEK1 respectively. Cells were incubated for 1 h with inhibitors prior to the addition of 10 ng/mL IL-1 β and stimulations performed for 24 h. Cells maintained in 0.5 % FBS media were used as a control. (A) Representative Western blot from replicate wells. (B) Densitometry analysis of Cx43 expression normalised to β -tubulin ($n=2$). ** $P<0.01$ vs. control (one-way repeated measures ANOVA with Tukey's multiple comparison test).

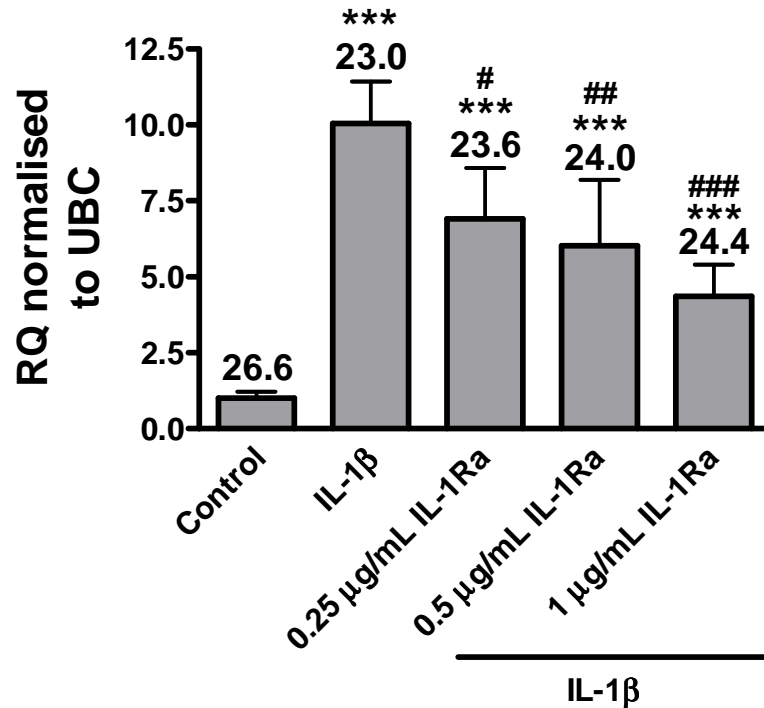


Figure 4-10 Effect of IL-1 receptor inhibition on IL-1 β mediated up-regulation of Cx43 mRNA expression in RACFs.

Quiesced cells were stimulated with 10 ng/mL IL-1 β alone or in the presence of 0.25, 0.5 or 1 μ g/mL human recombinant IL-1 β receptor antagonist (IL-1Ra). Stimulations were performed for 24 h and cells maintained in 0.5 % FBS media were used as a control. Data represented as relative quantification (RQ) \pm r q_{\max} normalised to UBC ($n=3$). *** P <0.001 vs. control; # P <0.05, ## P <0.01, ### P <0.001 vs. IL-1 β (one-way repeated measures ANOVA with Tukey's multiple comparison test). Average threshold cycle (C_t) values are shown above each bar.

4.3.3.2 Role of miRNAs in IL-1 β regulation of Cx43

MiRNAs have been implicated in the regulation of Cx43 (Danielson et al. 2013; Jin et al. 2013), hence the candidate miRNAs (miR-19b, -30 [predicted by target scan] and -125b) along with miRNAs, miR-1, -101 and -133a reported to be regulated by pro-inflammatory cytokines (Georgantas et al. 2014; Wang et al. 2014b) were examined in control and IL-1 β stimulated RACFs.

MiR-1 and -133a have been demonstrated to be downregulated and inversely correlated with proinflammatory cytokine levels in inflammatory myopathies (Georgantas et al. 2014). MiR-1 has also reported to target Cx43 and its overexpression *in vivo* leads to the downregulation of Cx43 (Curcio et al. 2013). Interestingly, miR-101 has been reported to be repressed by IL-1 β in non-small cell lung cancer cells (Wang et al. 2014b) and is therefore a promising miRNA to investigate in CFs. Quiesced cells were stimulated with 10 ng/mL IL-1 β or maintained in 0.5 % FBS (control) for 24 hr prior to cell collection. The expression of miR-1, -19b, -30c, -101a/b, -125b and -133a were examined by qRT-PCR. However, neither miR-1 nor -133a were detectable in control and IL-1 β stimulated RACFs. MiR-19b and -125b have both been reported to target Cx43 (Danielson et al. 2013; Jin et al. 2013), however IL-1 β did not alter the levels of these miRNAs (Figure 4-11 A and D). Next, the expression of miR-30 and -101 were assessed as these have been predicted to bind to Cx43 by Target Scan (version 6.2); a database which predicts genes containing the miRNA target seed sequence (Lewis et al. 2005). However, again no significant changes were found between conditions (Figure 4-11B-C).

As there was no change in these miRNAs following a 24 h IL-1 β stimulation, the expression of Cx43, miR-19b, -30c, -101, -101b or -125b was examined following a 1, 3 or 6 h stimulation. IL-1 β significantly up-regulated Cx43 mRNA expression within 1 h (RQ: 1.4 ± 0.1 , $P < 0.05$; Figure 4-12A), suggesting a rapid upregulation of Cx43. Cx43 mRNA expression was further increased after 3 h (RQ: 5.7 ± 0.2 , $P < 0.001$; Figure 4-12A) to levels that were maintained at 6 h IL-1 β stimulation (RQ: 5.6 ± 0.3 , $P < 0.001$; Figure 4-12A). No significant changes in miR19b, 30c, 101, 101b or 125b expression was observed over the 1-6 h time course (Figure 4-12B-F).

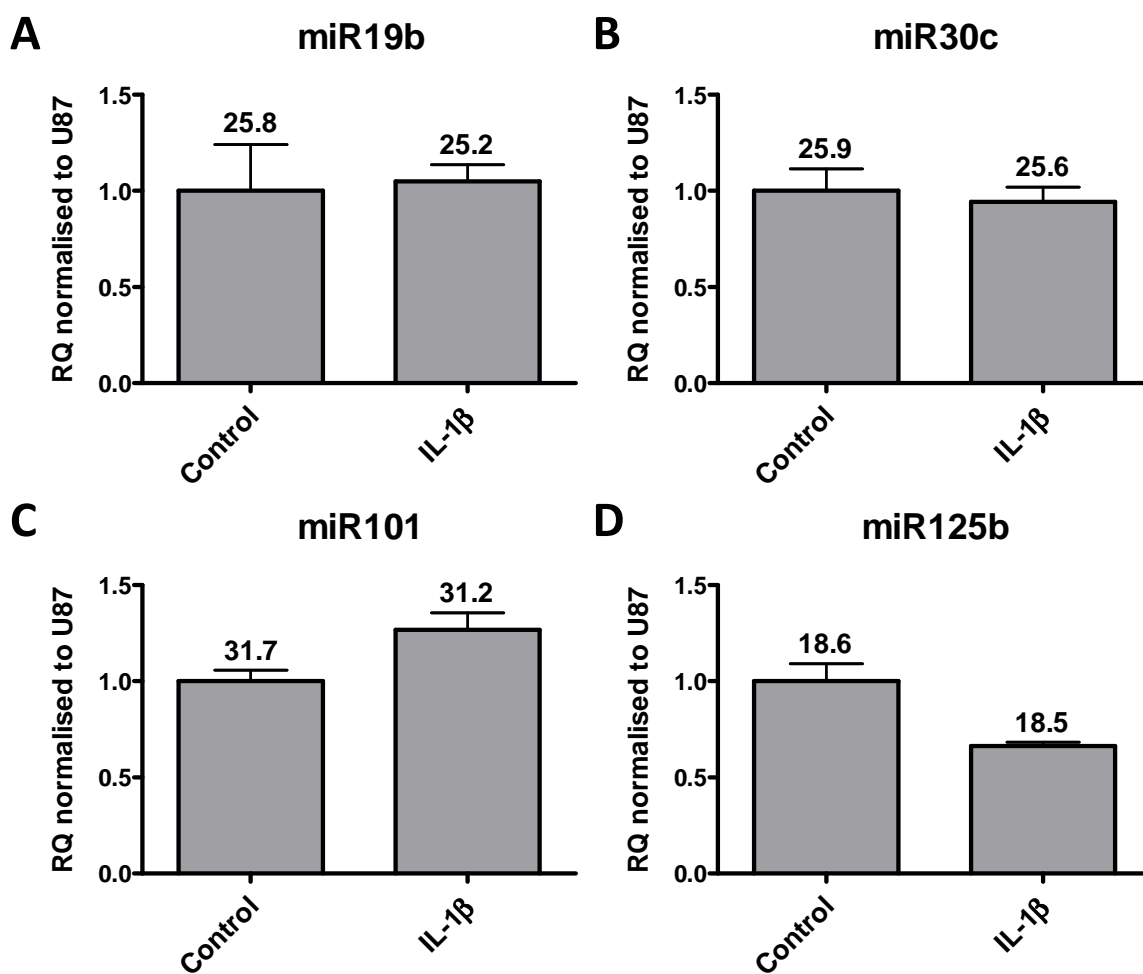


Figure 4-11 Effect of IL-1 β on miR19b, 30c, 101 and 125b expression in RACFs.

Quiesced cells were stimulated with 10ng/mL IL-1 β for 24 h. Cells maintained in 0.5 % FBS were used as a control. The expression of (A-D) miR19b, miR30c, miR101 and miR125 was examined. Data represented as relative quantification (RQ) \pm RQ_{max} normalised to U87 ($n=1$). Threshold cycle (C_t) values are shown above each bar. Error bars show the variation between the technical replicates. Unpaired, two-tailed t-tests performed on technical replicates showed no significant differences.

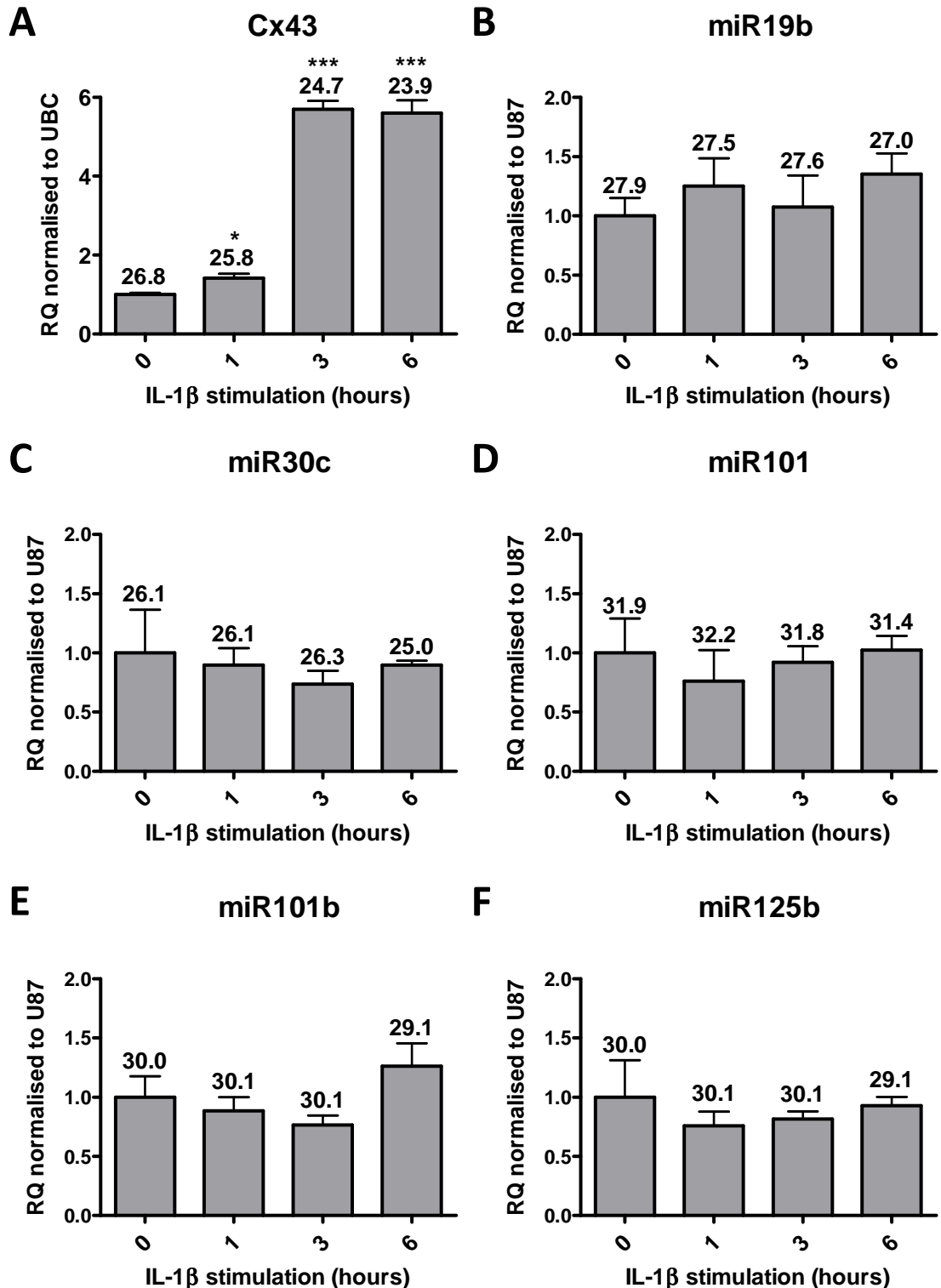


Figure 4-12 Effect of IL-1 β on Cx43 mRNA and miR-19b, -30c, -101, -101b and -125b expression in RACFs over different time periods.

Quiesced cells were stimulated with 10 ng/mL IL-1 β for 1, 3 and 6 h. Cells maintained in 0.5 % FBS media were used as a control (0 h). The expression of (A) Cx43 mRNA and (B-F) miR-19b, -30c, -101, -101b and -125b was examined. Data represented as relative quantification (RQ) \pm $r_{q_{max}}$ normalised to UBC (Cx43) or U87 (miRNAs) ($n=1$). Error bars show the variation between the technical replicates. Statistics were performed on technical replicates; * $P < 0.05$, *** $P < 0.001$ vs. 0 h (one-way ANOVA with Tukey's multiple comparison test). Threshold cycle (C_t) values are shown above each bar.

4.3.4 IL-1 β -mediated regulation of the TGF β 1 pathway

IL-1 β has been reported to inhibit TGF β 1-mediated fibroblast-to-MF transition (Bronnum et al. 2013; Mia et al. 2014; Saxena et al. 2013). To assess whether IL-1 β prevented TGF β 1-induced gene expression, quiescent RACFs were stimulated with IL-1 β , TGF β 1 or with a combination of both for 24 h. The expression of reported TGF β -regulated genes including CTGF, α SMA, PAI-1 and the transcriptional repressors, Snail and Slug (Biswas and Longmore 2016; Chen et al. 2000; Cooley et al. 2014; Kawano et al. 2000; Li et al. 2008), were examined by qRT-PCR.

IL-1 β stimulation was found to have predominantly opposing actions on gene expression to TGF β 1. For instance, IL-1 β promoted an 8 and 59 fold reduction in CTGF (RQ: 0.1 ± 0.03 , $P < 0.001$; Figure 4-13A) and α SMA (RQ: 0.02 ± 0.01 , $P < 0.001$; Figure 4-13B), respectively. Conversely, TGF β 1 induced a significant up-regulation of CTGF (RQ: 2.5 ± 0.2 , $P < 0.05$; Figure 4-13A) but no significant change in α SMA expression (RQ: 2.1 ± 0.1 ; Figure 4-13B). α SMA expression in IL-1 β and TGF β 1 co-stimulated cells was significantly reduced in comparison to cells treated with TGF β 1 alone (RQ: 0.3 ± 0.1 vs. 2.1 ± 0.1 , IL-1 β + TGF β 1 vs. TGF β 1 alone, $P < 0.05$; Figure 4-13B).

There were no significant changes in PAI-1 or snail expression by IL-1 β (RQ: 1.3 ± 0.2 ; Figure 4-13C and RQ: 0.6 ± 0.1 ; Figure 4-13D, respectively) or TGF β 1 stimulation (RQ: 4.0 ± 1.2 ; Figure 4-13C and RQ: 1.3 ± 0.1 ; Figure 4-13D, respectively). A 6.5 fold decrease in Slug was also induced by IL-1 β (RQ: 0.2 ± 0.01 , $P < 0.001$; Figure 4-13E), however no change was detected following TGF β 1 stimulation (RQ: 1.0 ± 0.1 ; Figure 4-13E).

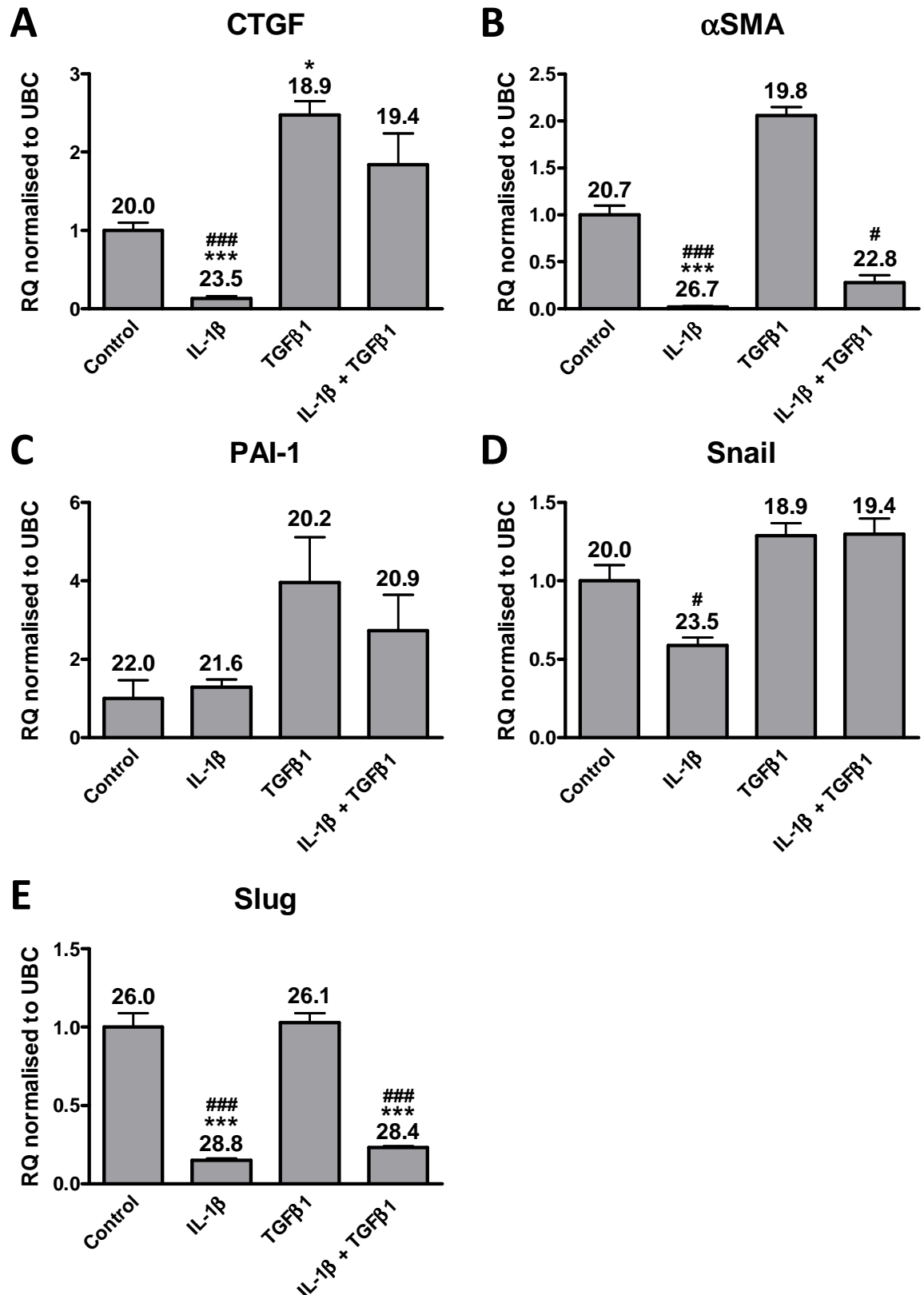


Figure 4-13 Effect of IL-1 β or TGF β 1 alone or in combination on the mRNA expression of CTGF, α SMA, serpine, snail and slug in RACs.

Quiesced cells were stimulated with IL-1 β , TGF β 1 or IL-1 β plus TGF β 1 (all at 10 ng/mL) for 24 h. Cells maintained in 0.5 % FBS media were used as a control. Data represented as relative quantification (RQ) \pm $r_{q_{max}}$ normalised to UBC ($n=3$). * P <0.05 *** P <0.001 vs. control; # P <0.05, ### P <0.001 vs. TGF β 1 (one-way repeated measures ANOVA with Tukey's multiple comparison test). Threshold cycle (C_t) values are shown above each bar.

4.4 Discussion

As Cx43 expression in CFs is enhanced following MI (Vasquez et al. 2010; Zhang et al. 2010), this study has investigated potential factors that may be responsible for this. Of the mediators investigated TGF β 1, IL-1 α , IL-1 β and IL-6 in combination with the sIL-6R significantly upregulated Cx43 mRNA in cells expressing numerous fibroblasts markers including α SMA, vimentin, DDR2 and S100A4. This upregulation was translated to the protein level with IL-1 β stimulation, where enhanced Cx43 expression was observed at the cell membrane and at cell-to-cell contact points. NF- κ B, MEK1 and the IL-1R were shown to be involved in IL-1 β -mediated upregulation of Cx43, by the use of specific pharmacological inhibitors. Conversely, the miRNAs; 19b, 30c, 101a/b or 125b did not appear to be regulated by IL-1 β over a 1-24 h period, suggesting little or no participation in IL-1 β -induced Cx43 up-regulation in primary RACFs.

The ability of IL-1 β to modulate TGF β 1 signalling in RACFs was also examined. TGF β 1 significantly upregulated CTGF mRNA but had no significant effects on α SMA, PAI-1 and snail mRNA, although trends for increases in these latter genes were observed. Stimulation of RACFs with IL-1 β alone generally produced no effect or had the opposite effect on these genes to TGF β 1. IL-1 β was found to significantly inhibit the trend for a TGF β 1-mediated increase in α SMA mRNA levels which is consistent with previous reports (Bronnum et al. 2013; Mia et al. 2014; Saxena et al. 2013).

Cx43 mRNA was significantly upregulated in RACFs stimulated with IL-6 in combination with the sIL-6R. IL-6 signalling can occur through the membrane bound IL-6R (mIL-6R) or the sIL-6R (Mihara et al. 2012). The sIL-6R lacks the intracellular fraction of the mIL-6R and can form an IL-6-sIL-6R complex prior to binding to gp130 to initiate IL-6 signalling (Mihara et al. 2012). Gp130 is expressed ubiquitously throughout tissues; therefore the IL-6-sIL-6R complex could hypothetically initiate IL-6 signalling in most cell types (Mihara et al. 2012). The results in the present study suggest that sIL-6R is required for IL-6 mediated upregulation of Cx43 mRNA in RACFs, suggesting little expression of the mIL-6R. Indeed, the sIL-6R was previously reported to be essential for IL-6-induced

CF-to-MF transition and collagen synthesis by CFs (Melendez et al. 2010). Cx43 mRNA levels were also unchanged in human sub-urothelial MFs following the longer stimulation of 48 h with IL-6 alone (Heinrich et al. 2011). Despite this, the number of coupled cells and levels of Cx43 protein were augmented in the same study, suggesting post-translational regulation of Cx43 by IL-6 in the absence of the sIL-6R (Heinrich et al. 2011).

A modest, but significant increase in Cx43 mRNA was detected in TGF β 1-treated RACFs. Conversely, no change in Cx43 protein levels was detected in neonatal CFs treated with TGF β 1 (Asazuma-Nakamura et al. 2009). This may suggest that the slight increase in mRNA is not substantial enough to induce an increase at the protein level, however this requires further investigation. Enhanced Cx43 reported in diseased CFs (Vasquez et al. 2010; Zhang et al. 2010) could be attributed to the action of another factor; one potential candidate is IL-1 β .

IL-1 β is one of the earliest cytokines to be detected in the plasma of MI patients (Guillen et al. 1995), therefore its effects on CF function are particularly interesting. In the present study, IL-1 β was shown to induce a morphological change in RACFs. An early report also described a similar morphological alteration by IL-1 β in human synovial fibroblasts, where the cells were described as being a “stellate” fibroblasts (Heino 1986). A similar phenotype was also observed in RACFs treated with IL-1 β ; however this was attributed to the expression of inducible nitric oxide (NO) synthase (iNOS) leading to NO production and cellular apoptosis (Tian et al. 2002). Apoptosis was not investigated in the current study, highlighting an avenue for further investigation. The role of Cx43 in cell death has been controversial with studies reporting either an enhancement or reduction in Cx43 expression, as well as increased or decreased GJIC in different cell types and models of cell death (Decrock et al. 2009). Therefore, the suggestion that Cx43 upregulation is a secondary result of IL-1 β -induced apoptosis cannot be concluded from current literature. These morphological changes however have not been reported in other studies using rat and mouse CFs despite similar IL-1 β concentrations being used (Bronnum et al. 2013; Saxena et al. 2013).

Although the effect of IL-1 β on Cx43 expression in CMs has been investigated, inducing downregulation of Cx43 and inhibiting GJIC (Baum et al. 2012a; Coppen et al. 2008), the effect on CFs has generally been overlooked. In this study, both IL-1 α and IL-1 β were found to increase Cx43 mRNA levels to similar extents, suggesting the opposite result than that reported in CMs. This was further investigated at the protein level following IL-1 β stimulation, which demonstrated a marked increase in Cx43. Interestingly, in a rabbit synovial fibroblast cell line (HIG-82 cells), Cx43 expression was only increased at the protein, not gene level following a 24 h IL-1 β stimulation (Niger et al. 2010), suggesting post-transcriptional regulation. These results differ to that reported in the current study where both Cx43 mRNA and protein were augmented, which may be a result of fibroblasts from a different species or tissue subtype. Interestingly, IL-1 β -mediated Cx43 protein increase in HIG-82 cells was associated with enhanced GJIC (Niger et al. 2010). In the present study, Cx43 immunofluorescence following treatment with IL-1 β demonstrated punctate expression at cell contact points, typical of GJ plaques, suggesting increased communication between fibroblasts. However, requires further investigation. Niger *et al.* (2010) also showed no additional increase in Cx43 protein when the stimulation was extended to 48 h supporting the time point examined in the current study (Niger et al. 2010).

Dual stimulation with IL-1 β and TNF α of bladder SMCs has also been demonstrated to increase Cx43 expression (Li et al. 2011), which was mediated by NF- κ B and PKA. NF- κ B binding sites have been detected in Cx43 promoter and been shown to be important in Cx43 regulation (Alonso et al. 2010). In the present study, IL-1 β -mediated Cx43 increase in RACFs was also dependent on NF- κ B. Additionally, NF- κ B activation was reported in neonatal CMs stimulated with IL-1 β inducing reduced Cx43 levels (Baum et al. 2012a). NF- κ B activation and Cx43 upregulation were inhibited with docosahexaenoic acid (DHA, an Omega-3 fatty acid), suggesting NF- κ B could be responsible for downregulating Cx43 (Baum et al. 2012a). These conflicting regulatory actions of NF- κ B on Cx43 highlight complex interactions.

IL-1 β was also found to induce the phosphorylation, and therefore activation, of p38 MAPK, JNK and ERK1/2 in HIG-82 cells within 10 min (Niger et al. 2010). The

IL-1 pathway was further dissected in this current study, using inhibitors of p38 MAPK, JNK and MEK1, which to our knowledge has not been previously investigated in IL-1 β mediated upregulation of Cx43 in CFs. Our data demonstrates that inhibition of MEK1 significantly blunts Cx43 upregulation by IL-1 β . In addition, inhibition of p38 MAPK reduced IL-1 β mediated Cx43 upregulation, however this did not reach significance. Consistent with these results, p38 MAPK and ERK1/2 activation have been shown to promote Cx43 upregulation in various cell types (Jia et al. 2008; Polontchouk et al. 2002). Additionally, p38 MAPK and ERK1/2 activation can not only mediate Cx43 expression but have also been shown to regulate phosphorylation of Cx43, and hence alter GJIC (Polontchouk et al. 2002). However, phosphorylation of Cx43 can either enhance or reduce GJIC depending on the site of phosphorylation (Solan and Lampe 2014). Interestingly, phosphorylation of ERK1/2 was associated with Ser279/Ser282 Cx43 phosphorylation, resulting in a reduction in GJIC in an isolated rabbit heart preparation (Naitoh et al. 2006). On the contrary, IL-1 β induced a dose dependent amplification of GJIC in HIG-82 cells, which was inhibited by MEK1/2 inhibitors (Niger et al. 2010). Furthermore, MEK1/2 inhibition has also been shown to reduce cyclic mechanical stretch-induced Cx43 upregulation in rat neonatal CMs (Salameh et al. 2010). An increase in Cx43 by the anti-depressant drug, amitriptyline, has also been reported in rat primary cultured cortical astrocytes, which interestingly was prevented by p38 MAPK inhibition (Morioka et al. 2014). Together these studies support the role of p38 MAPK and MEK1/2 in Cx43 upregulation.

A trend for potentiation of IL1 β -mediated upregulation of Cx43 expression by JNK inhibition was shown in the current study. This is consistent with the reported downregulation of Cx43 in rat neonatal CMs following Ad overexpression of JNK (Petrich et al. 2002). Additionally, TNF α -induced downregulation of Cx43 in WT fibroblasts did not occur in JNK^{-/-} fibroblasts, suggesting JNK acts to suppress Cx43 expression (Tacheau et al. 2008). Experiments using the IL-1Ra demonstrated a dose dependent reduction in IL-1 β -mediated Cx43 expression, confirming the well-established signalling of IL-1 β through the IL-1R (Weber et al. 2010).

Cx43 mRNA was shown to be upregulated as early as 1 h following IL-1 β stimulation, suggesting a rapid induction of Cx43 gene transcription. However, no

change in miR-19b, -30c, -101a/b or -125b was detected between control and IL-1 β treated RACFs, suggesting a lack of involvement in IL-1 β -induced Cx43 upregulation. However, this was only investigated in one experiment therefore further replication is required to make solid conclusions from this data.

The additional cytokines/mediators investigated in the present study including Ang II and TNF α were not shown to significantly alter Cx43 mRNA expression. Ang II was found to promote an increase in Cx43 protein levels as early as 2 h stimulation of mouse aortas, which was maintained following 48 h of stimulation (Alonso et al. 2010). Additionally, neonatal CMs exhibited an augmentation in Cx43 protein and increased GJIC subsequent to Ang II stimulation at the same concentration and time point used in the current study (Polontchouk et al. 2002). Furthermore, Cx43 protein in rat neonatal CFs was rapidly increased following 3 h stimulation with Ang II (Adam et al. 2010). Unfortunately Cx43 mRNA levels were not examined in any of these studies, which makes it difficult to make a direct comparison to the current results.

TGF β 1 is an important mediator in the development of fibrosis, inducing MF transdifferentiation and the expression of many profibrotic proteins (Dobaczewski et al. 2011; Yan et al. 2011). TGF β 1 is known to promote the expression of a vast range of genes/proteins including CTGF (Chen et al. 2000; van Nieuwenhoven et al. 2013), α SMA and PAI-1 (Kawano et al. 2000; Li et al. 2008) in CFs. CTGF has been shown to be upregulated in human cardiac disease (Chen et al. 2000; Koitabashi et al. 2007; Wu et al. 2014) and has been implicated in the promotion of cardiac fibrosis (reviewed in Daniels et al. 2009). In the present study, TGF β 1 was shown to upregulate CTGF, which was slightly reduced by combination treatment with IL-1 β . A slight reduction in TGF β 1-mediated increase in CTGF protein was also observed in airway SMCs following IL-1 β treatment (Xie et al. 2005). Conversely, in human CFs, TGF β 1 did not induce a significant increase in CTGF mRNA following 24 h stimulation (van Nieuwenhoven et al. 2013). In the same study, IL-1 α significantly reduced CTGF mRNA expression, which was inhibited by combination treatment with TGF β 1 (van Nieuwenhoven et al. 2013), similar to the results found in the present study with IL-1 β . This illustrates very similar effects of IL-1 α and IL-1 β on CTGF expression.

RACFs used in this study were already shown to have a high expression of α SMA, suggesting conversion to MFs in culture. The levels of α SMA mRNA levels were significantly reduced by IL-1 β treatment, which is in line with data from other studies completed in CFs (Bronnum et al. 2013; Saxena et al. 2013). TGF β 1 is well established to enhance α SMA expression in CFs (Bronnum et al. 2013; Yan et al. 2011), however in the present study only a trend for upregulation of α SMA was found. This may be a consequence of already high α SMA levels in the RACFs utilised, which could also be the case for other TGF β 1 controlled genes examined in this study. Similarly, Saxena *et al.* (2013) reported no change in α SMA following 24 h stimulation with TGF β 1 of CFs that had high basal levels of α SMA mRNA. In this study the increase in α SMA was only beginning to reach significance following 72 h stimulation with TGF β 1, suggesting longer stimulations may be required to see a significant increase. Conversely, in lung and dermal fibroblasts an increase in α SMA was seen following 24 h stimulation with TGF β 1 (Mia et al. 2014). In agreement with other reports, co-stimulation of fibroblasts with IL-1 β and TGF β 1 resulted in a significant reduction in α SMA mRNA (Mia et al. 2014; Saxena et al. 2013). Additionally, IL-1 β inhibits TGF β 1-induced contraction of collagen pads by CFs (Saxena et al. 2013), supporting the ability of IL-1 β to prevent fibroblast activation.

The levels of PAI-1 mRNA were also examined in the present study, which has been previously been shown to be upregulated by TGF β 1 treatment in CFs (Li et al. 2008). In the present study, there were no significant changes in PAI-1 mRNA over all conditions examined, although a trend for upregulation was seen in RACFs stimulated with TGF β 1.

The transcriptional repressors snail and slug have been predominately investigated in the setting of epithelial-mesenchymal transition, the process of epithelial cells transdifferentiating to a cell with a mesenchymal phenotype (Lamouille et al. 2014). TGF β 1-mediated increases in CTGF and collagen 1 α 1 mRNA were prevented in CFs that had snail knocked out (Biswas and Longmore 2016). These snail-depleted CFs also had reduced α SMA levels in comparison to control CFs, demonstrating the importance of snail in CF activation. Snail has previously been reported to be increased after TGF β 1 stimulation of CFs (Biswas and Longmore

2016), however in the present study only a small increase in snail was detected. A tendency for a reduction in snail expression was seen in cells stimulated with IL-1 β . Conversely, others have found IL-1 β to increase snail expression in squamous cell carcinoma cell lines (Lee et al. 2015;St John et al. 2009). The reasons for these differences are unknown, however if snail is important in fibroblast activation it may reflect the reported inhibitory effect of IL-1 β on fibroblast activation (Bronnum et al. 2013;Mia et al. 2014;Saxena et al. 2013). IL-1 β also induced a decrease in slug mRNA expression. It is important to note that these experiments only examined the effect of IL-1 β and TGF β 1 on gene expression therefore further work is required to demonstrate the effects at the protein level.

4.5 Summary

IL-1 β upregulates Cx43 at the gene and protein level in RACFs. The data suggest IL-1 β acts at the IL-1R activating NF- κ B, p38 MAPK and MEK1 as well as inhibiting JNK to promote increases in Cx43. Furthermore, IL-1 β inhibits expression of the profibrotic marker, CTGF and the MF marker, α SMA, as well as reducing the expression of snail in RACFs. This suggests IL-1 β may have anti-fibrotic actions on RACFs. Conversely, TGF β 1 significantly enhanced CTGF expression but had no significant effect on α SMA, PAI-1, snail and slug expression. Interestingly, TGF β 1 inhibited IL-1 β -induced downregulation of CTGF and snail and slightly reduced the reduction in α SMA expression. There was no effect of TGF β 1 on IL-1 β -mediated decrease in slug expression. Together these data suggest opposing actions of IL-1 β and TGF β 1 on CF activation.

Chapter 5 Co-culture investigation of cardiac myocyte: fibroblast interactions

5.1 Introduction

As described in section 1.8 co-culture studies have illustrated many paracrine, mechanical and electrical interactions between CMs and CFs. Although neonatal CMs are useful to study the interactions between CMs and CFs, their clinical significance is limited due to many differences between neonatal and adult CMs. For instance, neonatal CMs have no to very little development of T-tubules (Chen et al. 1995a;Haddock et al. 1999), altered Ca^{2+} handling (Haddock et al. 1999;Poindexter et al. 2001) and display spontaneous contractions (Qu et al. 2001). These dissimilarities illustrate the importance of studying the effects of CFs on adult CMs. However, issues with adult CM culture makes this difficult.

5.1.1 Culture effect on adult cardiac myocytes

Adult CMs are a terminally differentiated cell type, however in culture they are well established to dedifferentiate (Fredj et al. 2005a;Fredj et al. 2005b). This results in a morphological change from rod shaped to neonatal-like (Poindexter et al. 2001). Some studies have utilised dedifferentiated CMs instead of CMs from a neonatal origin in anticipation that they would mimic a more mature phenotype. Indeed, in terms of Ca^{2+} handling, dedifferentiated CMs appeared to have an intermediate phenotype. For instance, like freshly isolated CMs, dedifferentiated adult CMs have Ca^{2+} transients which rely on the RyR, but also have an IP_3 mediated component, which is typical of neonatal CMs (Poindexter et al. 2001). Additionally, Ca^{2+} and electrical activity in functional monolayers produced from long term culture (over 21 days) of guinea pig adult CMs were similar to that of the adult phenotype (Joshi-Mukherjee et al. 2013). Interestingly, in HF reactivation of foetal genes has been observed (Thum et al. 2007), which may suggest the initiation of CM dedifferentiation in disease. Additionally, in co-culture, CFs were reported to promote CM dedifferentiation, which may have an impact in the setting of disease (Dispersyn et al. 2001).

In short term culture adult CMs develop rounded edges (Leach et al. 2005;Louch et al. 2004;Stimers and Dobretsov 1998), show decreased T-tubule density (Leach et al. 2005;Louch et al. 2004) and disorganised expression of Ca^{2+} handling proteins including the RyR and the pore forming subunit of the LTCC (Leach et al. 2005).

Although the rod shape of adult CMs is maintained for up to 72 h culture (Ellingsen et al. 1993; Louch et al. 2004), contractile and electrophysiological alterations have been reported. For instance rat adult CMs show a 30-50 % reduction in contractility over 6-24 h in culture, which was maintained from 24 to 72 h (Ellingsen et al. 1993). Additionally, the APD₅₀ was markedly reduced by 60-70 % following 24 h (Ellingsen et al. 1993). Similarly, in swine adult CMs the APD₅₀ was progressively reduced over 72 h in culture (Louch et al. 2004). In contrast APD₉₀ was gradually prolonged in culture indicating an AP shape change (Louch et al. 2004). This may reflect reductions in the I_{CaL} and I_{K1} therefore shortening the AP plateau and prolonging late repolarisation respectively. Indeed, I_{K1} was shown to be reduced at potentials between -20 and -60 mV in these cells (Louch et al. 2004).

Modifications of T-tubules, LTCCs and RyRs are likely to alter Ca²⁺ handling within the cell. Indeed, delayed SR release in swine adult CMs was demonstrated to become more evident after 24 and 72 h culture compared to freshly isolated cells (Louch et al. 2004). Additionally, the rise of the Ca²⁺ transient was significantly delayed at 24 and 72 h of culture and there was a trend for reduced Ca²⁺ transient amplitude (Louch et al. 2004). The reduction in the density of T-tubules in culture has been shown to differ between species. Mouse adult CMs showed no reduction in T-tubules over 72 h, conversely in rat adult CMs there was a progressive reduction over 72 h, which could not be prevented by chronic pacing (Pavlovic et al. 2010). Despite this, mouse adult CM did not respond to acute pacing 24 h following isolation while 85 % of rat adult CM still produced contraction following 72 h (Pavlovic et al. 2010). This suggests rat CMs are more resistant to some effects of culture than murine cells.

5.1.2 Adult cardiac myocyte: fibroblast co-culture models

To date, there has been a limited number of studies investigating the functional effects of direct CM: CF interactions in adult cells. Typically co-culture models have involved the seeding of freshly isolated CMs on to preplated cultured fibroblasts (Chilton et al. 2007; Dispersyn et al. 2001). As well as calcein dye transfer between adult CMs and CFs (Chilton et al. 2007; Driesen et al. 2005), stimulation of adult rabbit CMs in co-culture resulted in a progressive increase in

$[Ca^{2+}]_i$ of surrounding CFs, which was inhibited by the GJ uncoupler, heptanol, providing further evidence of heterocellular coupling (Chilton et al. 2007). Despite this no impact on APD_{90} was detected. A similar co-culture model has been utilised in the current study to provide information on the effects of co-culture on contraction and APs of rat adult CMs.

5.2 Aims

- To assess the effects of untreated control and IL-1 β treated RACFs on rat adult CM contraction and electrical activity.

5.3 Results

This study utilised a cell culture model where freshly isolated CMs were seeded on to laminin coated dishes (control) or RACF monolayers and cultured overnight. Initially, the ability of calcein to transfer from pre-loaded CMs to the underlying RACFs was assessed. Following addition of CMs to the RACF monolayer, cells were imaged using confocal microscopy, typically between 0 and 1 h from CM addition, to locate the presence of calcein. Cells were then cultured overnight and imaged following approximately 20 h from initial CM addition. At 0-1 h, calcein was only detected in the overlaying CMs (top panel -Figure 5-1), however the following day, calcein could be detected in RACFs located below (middle and bottom panels - Figure 5-1), suggesting functional heterocellular GJ formation. As well as transfer of calcein, RACFs were shown to pull on the CMs suggesting mechanical interactions between the cells (red arrows - Figure 5-1).

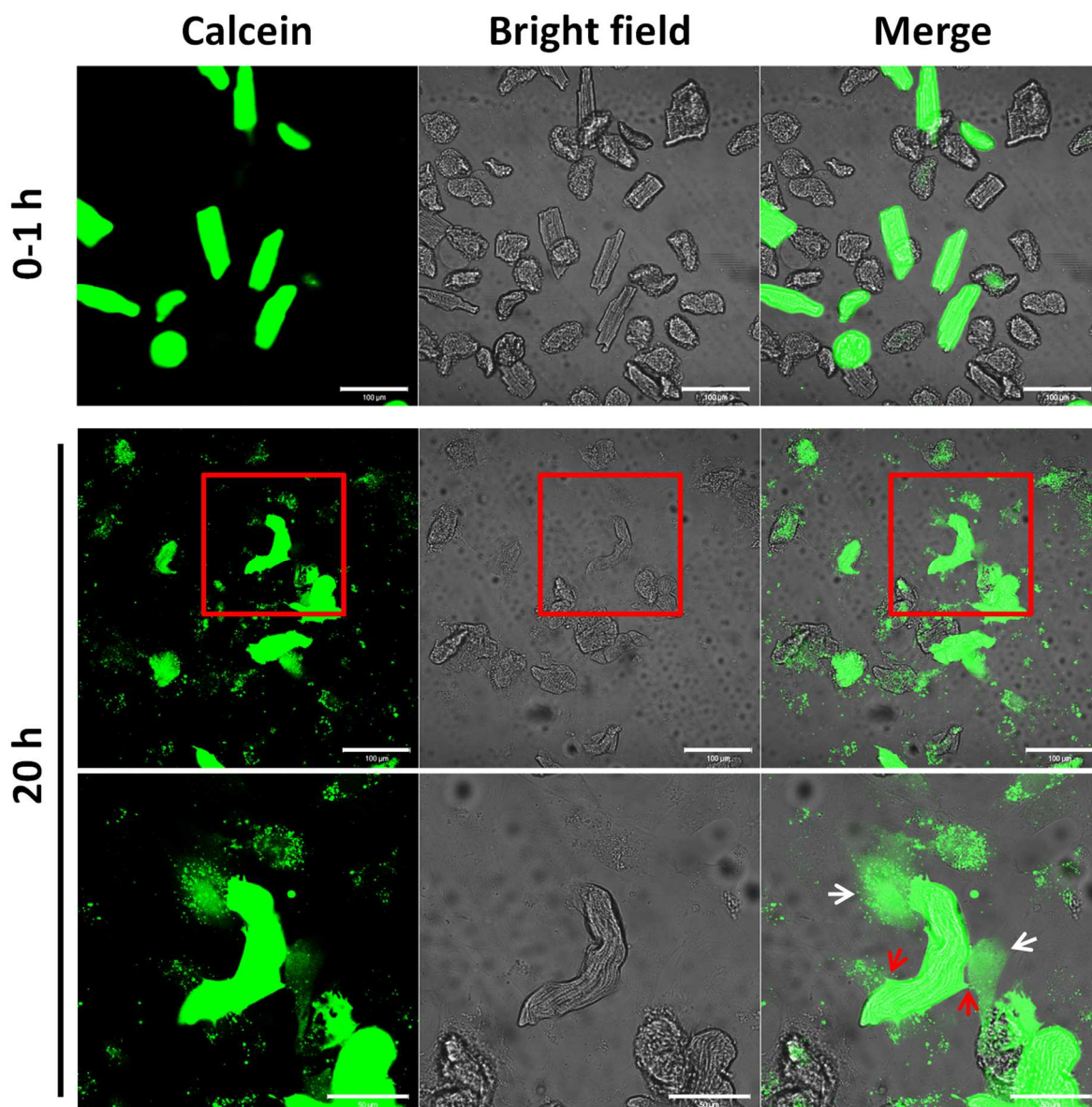


Figure 5-1 Representative images showing the localisation of calcein in CMs and RACFs immediately after the addition of loaded CMs to the RACF monolayer (0-1 h) and following 20 h in culture.

Freshly isolated CMs were loaded with 5 μM calcein for 30 min at 37 $^{\circ}\text{C}$ and washed three times in PBS. 1×10^4 rod shaped CMs in 0.5 % FBS media were then added to a RACF monolayer in 35 mm glass bottomed petri dishes. The localisation of calcein was visualised immediately following CM addition (0-1 h) then again following 20 h (upper and middle panels respectively). The areas surrounded in the red box in the middle panel are expanded in the bottom panel showing calcein dye transfer into the underlying RACFs depicted by white arrows. Red arrows show examples of areas of the CM being pulled by the underlying RACFs. Images were taken on the Zeiss 510 LSM confocal microscope at x25 magnification. Scale bar represents 100 μm on the upper and middle panels and 50 μm on the lower panel ($n=2$).

5.3.1 Effect of control or IL-1 β treated RACFs on the contraction of cultured CMs

Initially, cultured CMs were evaluated for the ability to contract in response to stimulus. Individual cells were selected at random and paced at 1 Hz and at 30 % above the voltage required to produce a contraction. A steady state of contraction was reached by pacing for 1 min prior to contraction measurement. A representative contraction trace (Figure 5-2Ai) along with an exemplar contraction trace which had a large volume of noise (Figure 5-2Aii) is shown. This noise was found to interfere with Dn90, CD10 and occasionally CD25, illustrated by large variation in these values (Figure 5-2B); therefore unfortunately these parameters could not be examined with accuracy in future analysis. Up90 (which is referred to as 10-90 % rise time in subsequent graphs), CD50, CD75 and CD90 were 22.6 ± 0.7 , 48.9 ± 7.8 , 31.8 ± 5.3 and 18.5 ± 3.3 ms respectively (Figure 5-2B).

As functional contraction measurements could be recorded from cultured CMs, the effect of co-culturing CMs with RACFs was examined. CMs in culture alone (control) or in the presence of a RACF monolayer maintained their rod-like morphology (Figure 5-3A). Cultured CMs were found to require a greater voltage to induce contraction in the presence of RACFs (15.6 ± 1.1 vs. 21.3 ± 0.5 V, control vs. RACF monolayer; $P < 0.05$; Figure 5-3B). Representative contraction traces from control CMs and CMs cultured with a RACF monolayer are shown (Figure 5-4Ai and ii respectively). No significant changes in the contraction parameters were detected between the groups (Figure 5-4B-E). However there was a consistent slight decrease in all these parameters in the presence of the RACF monolayer.

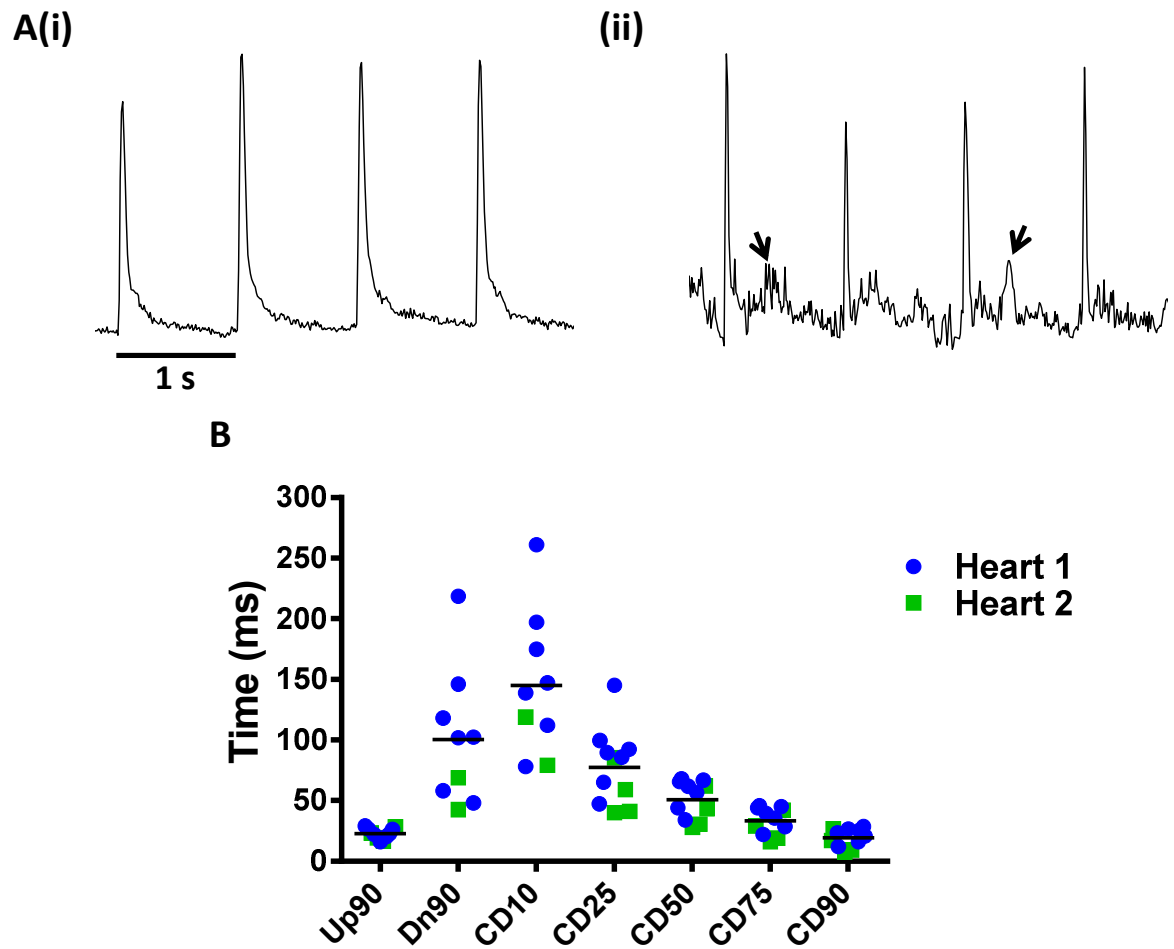
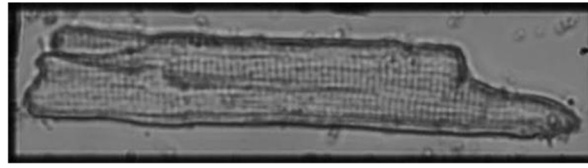
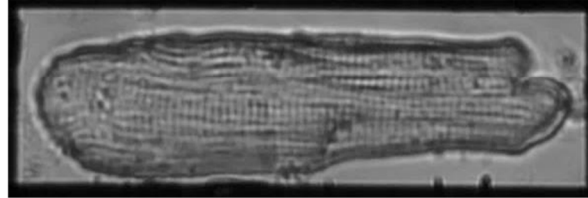


Figure 5-2 Contraction traces and contraction parameters that can be measured from cultured CMs.

CMs were cultured for 24 h prior to pacing at 1 Hz and 30 % above the threshold voltage for each cell. (Ai) A representative contraction trace and an (Aii) example of a contraction trace where Dn90 and CD10 values were unreliable due to peaks in the noise (arrows) which interfered with values. Scale bar represents 1 second. (B) Contraction parameters measured in cultured CMs from two hearts. Each point represents an individual cell and the mean is denoted by a line ($n=11$ from two animals for all parameters except Dn90 and CD10 where $n=9$). Up90; time from 10 % - 90 % contraction, Dn90; time from 10 % - 90 % relaxation, CD10; time from 10 % contraction - 90 % relaxation, CD25; time from 25 % contraction - 75 % relaxation, CD50; time from 50 % contraction - 50 % relaxation, CD75; time from 75 % contraction - 25 % relaxation, CD90; time from 90 % contraction - 10 % relaxation.

A

Control

RACF
monolayer

B

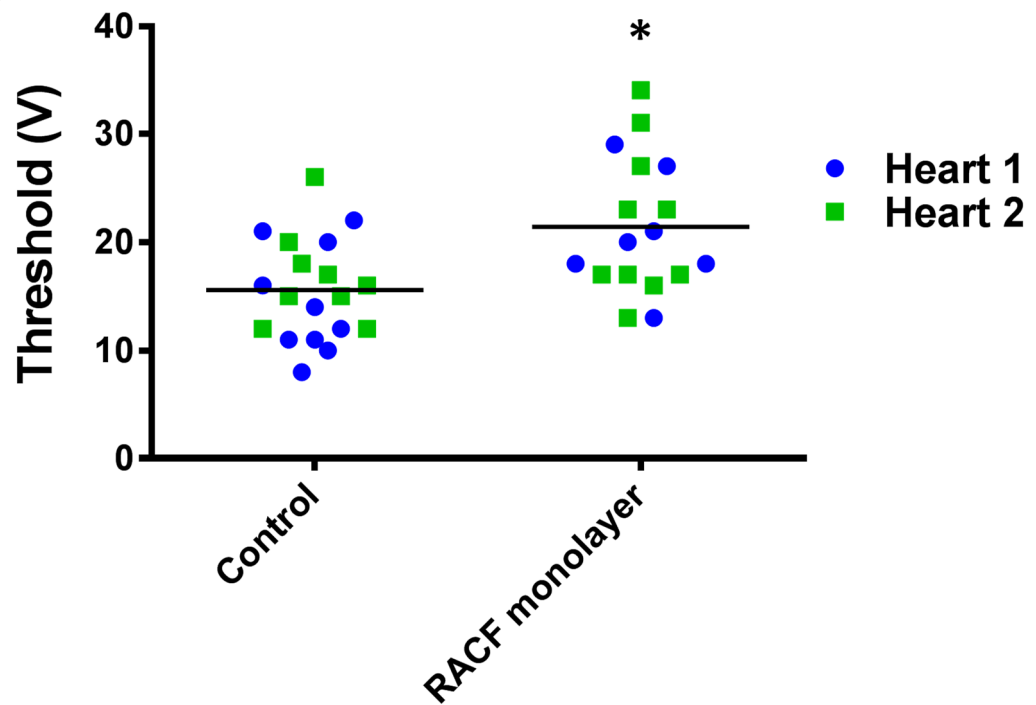


Figure 5-3 Representative images and stimulation threshold values of CMs cultured alone or with a RACF monolayer.

(A) Images of representative CMs cultured for 24 h alone or with a RACF monolayer. (B) Cells were paced at 1 Hz and the voltage increased by 1V increments until the cell started to contract, taken as the stimulation threshold. Each point represents an individual cell and the mean is denoted by a line. $n=19$ and $n=17$ in control and RACF monolayer groups respectively from two animals. $*P<0.05$ vs. control (Student's unpaired t-test).

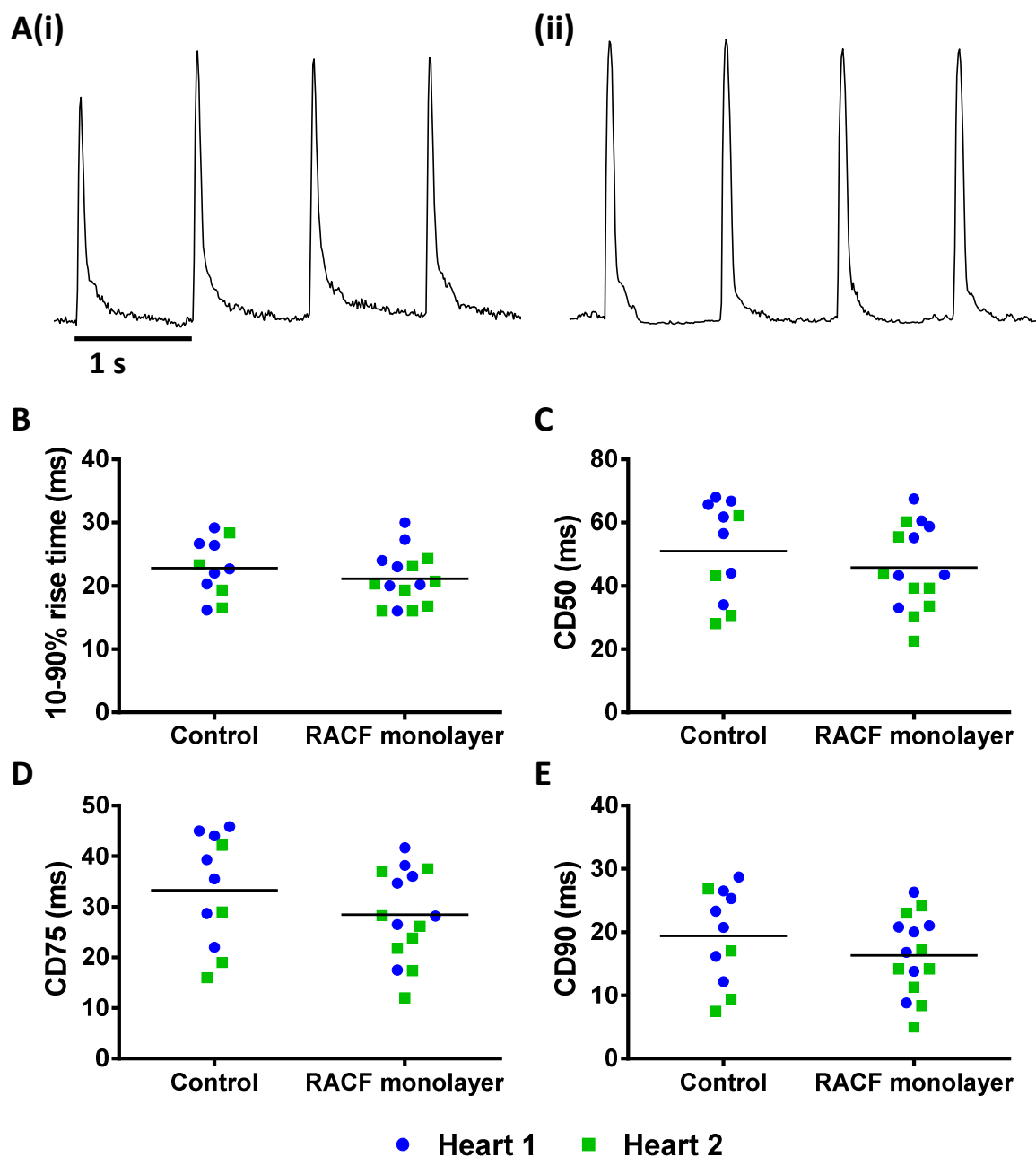


Figure 5-4 Contraction measurements in CMs cultured alone or with a RACF monolayer. (A) Representative contraction traces from (i) CMs cultured alone or (ii) with a RACF monolayer. Scale bar represents 1 second. (B) 10-90 % rise time, (C) CD50, (D) CD75 and (E) CD90 values from CMs from two hearts. Each point represents an individual cell and the mean is denoted by a line. $n=11$ and $n=15$ in control and RACF monolayer groups respectively from two animals. No significant changes were detected using a Student's unpaired t-test. CD50; time from 50 % contraction - 50 % relaxation, CD75; time from 75 % contraction - 25 % relaxation, CD90; time from 90 % contraction - 10 % relaxation.

IL-1 β concentration is increased in disease (Di et al. 2003) and it has been shown to augment Cx43 levels in RACFs (Chapter 4), therefore potentially enhancing coupling in co-culture and potentiating the effect of RACFs on CM function. Therefore the effect of IL-1 β treated RACFs on the contraction of cultured CMs was examined. In this set of experiments RACFs were cultured in reduced serum for the longer time period of 48 h prior to CM addition. This was due to serum starvation 24 h before IL-1 β stimulation for a further 24 h. There were no significant differences in voltage required to induce contraction between the groups (Figure 5-5). A representative contraction trace from control CMs and CMs in culture with untreated or IL-1 β treated RACFs as well as with an image of the corresponding CM are shown (Figure 5-6A). There was no significant difference in the rise times for contraction between the groups (Figure 5-6B and Table 5.1). However, CD50, CD75 and CD90 were significantly reduced in CMs cultured with a RACF monolayer in comparison to control (all $P < 0.05$). However, when CMs were cultured with RACFs which had been pre-treated with IL-1 β , CD50, CD75 and CD90 measurements were partially restored resulting in values not significant from control CMs alone or CMs cultured with a control RACF monolayer (Figure 5-6 and Table 5.1).

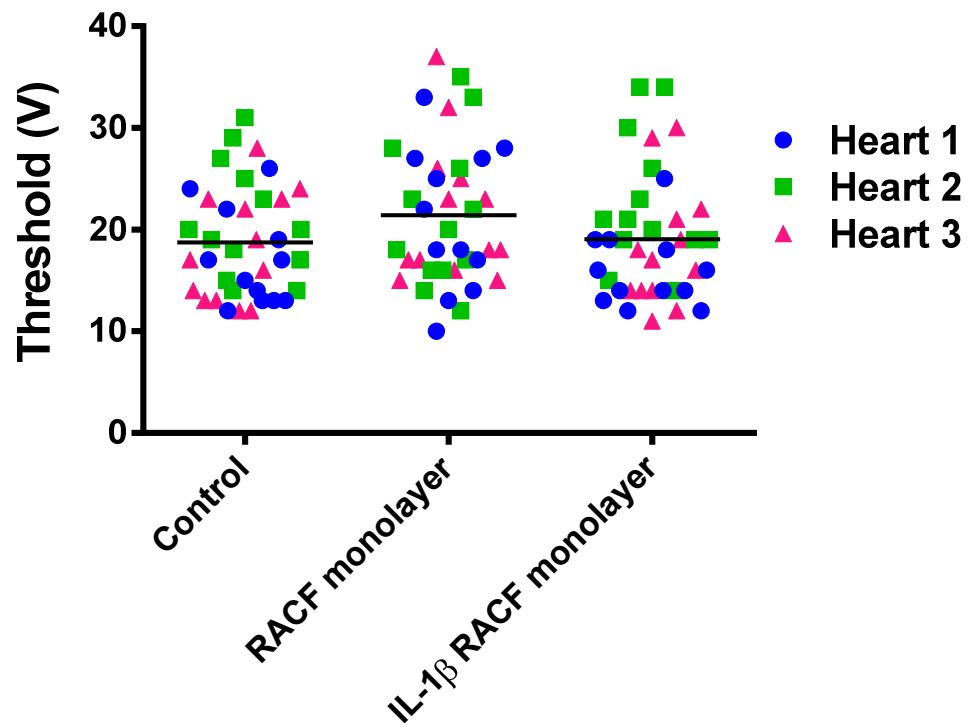


Figure 5-5 Stimulation threshold values of CMs cultured alone, with an RACF monolayer or with an IL-1 β treated RACF monolayer.

CMs were paced at 1 Hz and the voltage increased by 1V increments until the cell started to contract, taken as the stimulation threshold. Each point represents an individual cell and the mean is denoted by a line. $n=39$ for all groups from three animals. No significant changes were detected using a one-way ANOVA with Tukey's multiple comparison test.

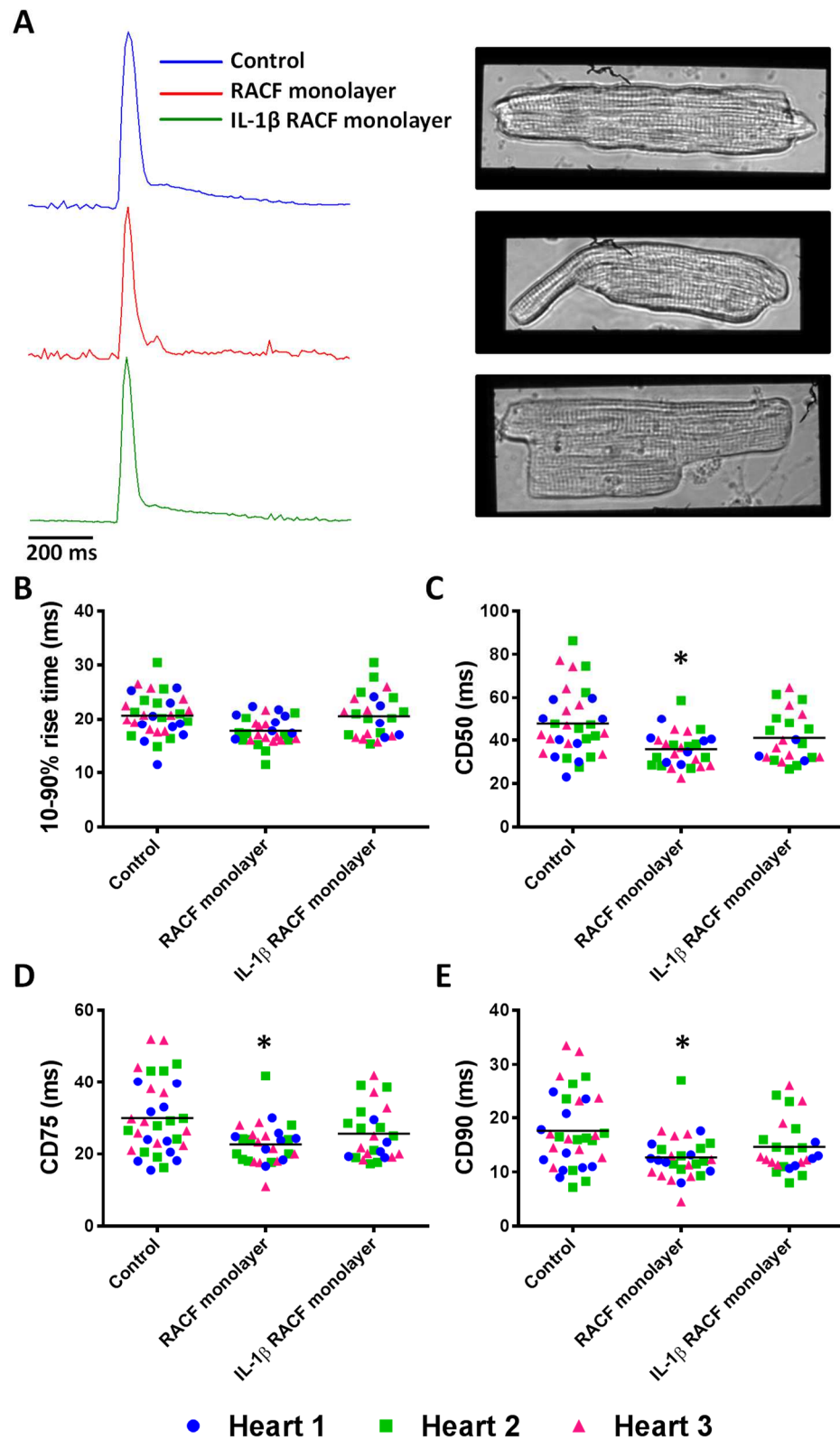


Figure 5-6 Contraction measurements in CMs cultured alone, with an RACF monolayer or with an IL-1 β treated RACF monolayer.

(A) Representative traces and images of CMs cultured alone (top), with a RACF monolayer (middle) or with an IL-1 β treated RACF monolayer (bottom). Scale bar represents 200 ms. (B) 10-90 % rise times, (C) CD50, (D) CD75 and (E) CD90 values from CMs from three hearts. Each point represents an individual cell and the mean is denoted by a line. $n = 33$, $n = 29$ and $n = 25$ for control, RACF monolayer and IL-1 β RACF monolayer groups respectively from three animals. * $P < 0.05$ vs. control (one-way ANOVA with Tukey's multiple comparison test). CD50; time from 50 % contraction - 50 % relaxation, CD75; time from 75 % contraction - 25 % relaxation, CD90; time from 90 % contraction - 10 % relaxation.

Table 5.1 Contraction parameter values of CMs in control, RACF monolayer and IL-1 β RACF monolayer treatment groups.

Contraction Parameter	Control	RACF monolayer	IL-1β RACF monolayer
10-90 % rise time	20.6 \pm 0.5 ms	17.9 \pm 0.9 ms	20.4 \pm 0.7 ms
CD50	56.7 \pm 7.0 ms	36.1 \pm 1.1 ms*	39.6 \pm 2.6 ms
CD75	29.8 \pm 2.0 ms	22.7 \pm 0.6 ms*	25.1 \pm 1.4 ms
CD90	17.5 \pm 1.4 ms	12.7 \pm 0.6 ms*	14.3 \pm 0.9 ms

Values are represented as mean \pm SEM. n= 33, n= 29 and n= 25 for control, RACF monolayer and IL-1 β RACF monolayer groups respectively from three animals. *P<0.05 vs. control (one-way ANOVA with Tukey's multiple comparison test).

5.3.2 Effect of control or IL-1 β treated RACFs on the action potential of cultured CMs

The effect of culture on the AP 10-90 % rise time, APD₂₀, APD₅₀ and APD₈₀ was determined by examining these parameters in freshly isolated and cultured CMs. Rise time, APD₂₀ and APD₅₀ values were very similar between freshly isolated and cultured CMs (Figure 5-7 and Table 5.2). There was also no significant change in APD₈₀ between cultured CMs and freshly isolated CMs (45.5 ± 1.2 vs. 55.4 ± 4.4 ms, fresh vs. cultured CMs; Figure 5-7E and Table 5.2).

Next the effect of an untreated or IL-1 β treated RACF monolayer on AP parameters was examined. There were no significant changes in 10-90 % rise time, APD₂₀, APD₅₀ or APD₈₀ between control CMs (CMs cultured alone) and CMs cultured with either a RACF monolayer or an IL-1 β treated RACF monolayer (Figure 5-7 and Table 5.2). However, there may be evidence for slight APD₈₀ prolongation in the presence of a RACF monolayer (55.4 ± 4.4 vs. 71.0 ± 7.8 ms, control vs. RACF monolayer; Figure 5-8E and Table 5.2), which is marginally suppressed by IL-1 β treatment of RACFs (71.0 ± 7.8 vs. 65.0 ± 5.5 ms, RACF monolayer vs. IL-1 β RACF monolayer; Figure 5-8E and Table 5.2).

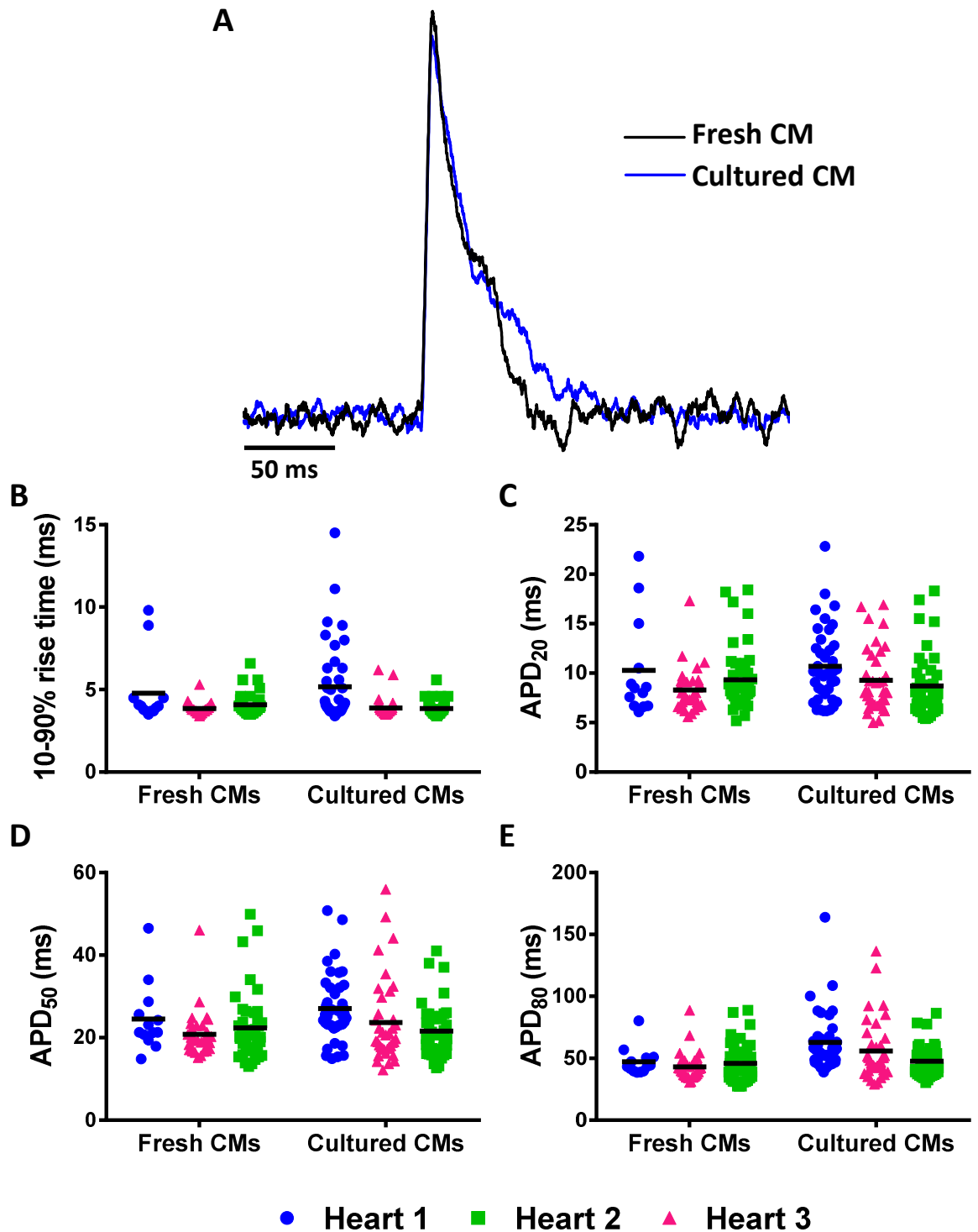


Figure 5-7 Action potential measurements in freshly isolated CMs and CMs cultured for 24 h. (A) A representative average action potential (AP) from a freshly isolated CM and a CM cultured for 24 h. Scale bar represents 50 ms. (B) AP 10-90 % rise time, (C) duration at 20 % repolarisation (APD₂₀), (D) duration at 50 % repolarisation (APD₅₀) and (E) duration at 80 % repolarisation (APD₈₀) in CMs from three hearts. Each point represents an individual cell and the mean from each heart is denoted by a line. CMs are separated into individual hearts due to the large number of cells per group. $n=85$, and $n=122$ for fresh and cultured groups respectively from three animals. No significant changes were detected using a Student's unpaired t-test.

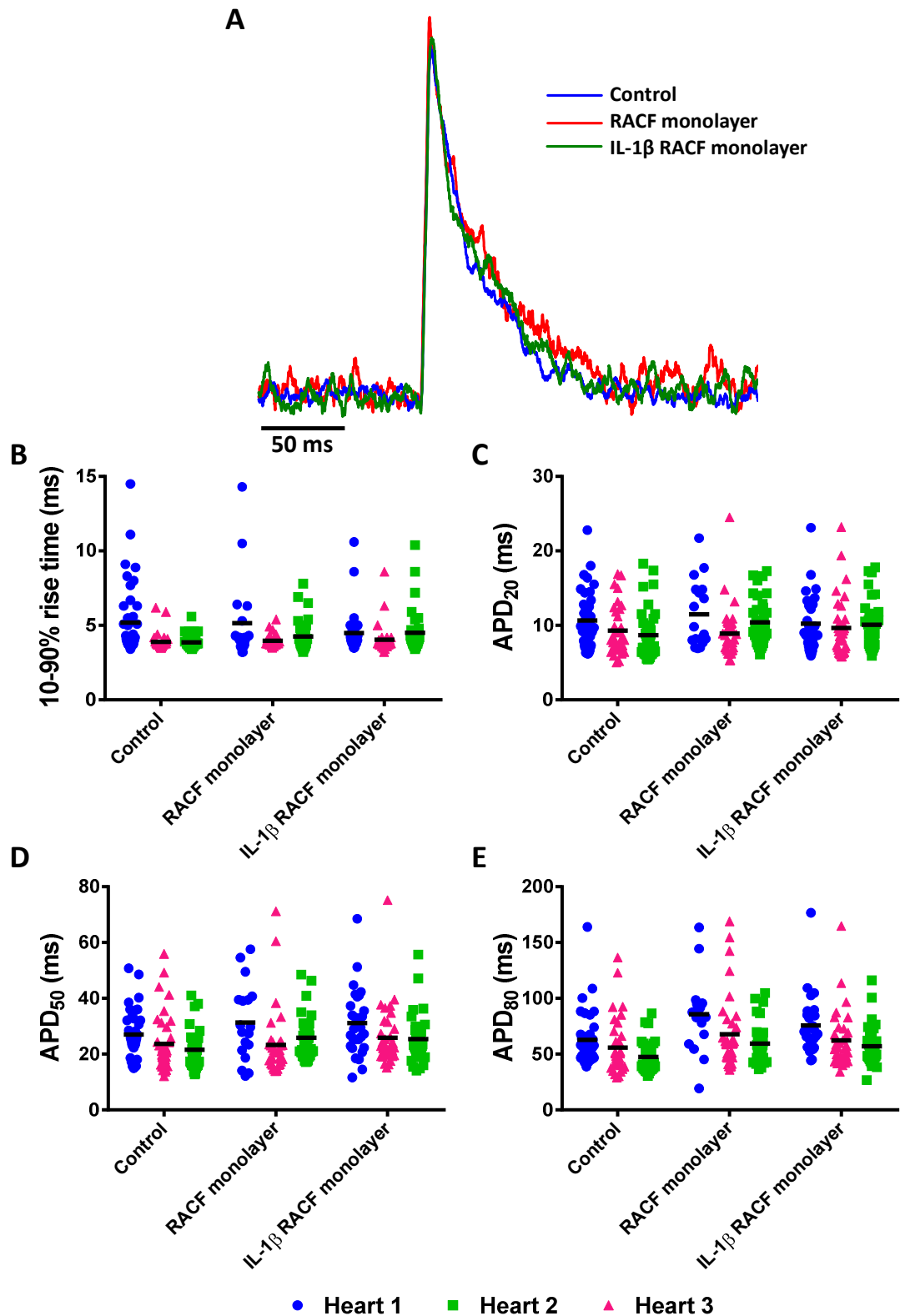


Figure 5-8 Action potential measurements in CMs cultured alone, with an RACF monolayer or with an IL-1 β treated RACF monolayer.

(A) A representative average action potential (AP) from a CM cultured alone, with an RACF monolayer or IL-1 β treated RACF monolayer. Scale bar represents 50 ms. (B) AP 10-90 % rise time, (C) duration at 20 % repolarisation (APD₂₀), (D) duration at 50 % repolarisation (APD₅₀) and (E) duration at 80 % repolarisation (APD₈₀) of CMs from three hearts. Each point represents an individual cell and the mean from each heart is denoted by a line. Values are separated into individual hearts due to the large number of cells. $n=122$, $n=90$ and $n=99$ for control, RACF monolayer and IL-1 β RACF monolayer groups respectively from three animals. No significant changes were detected using a one-way ANOVA with Tukey's multiple comparison test.

Table 5.2 Action potential parameter values of fresh CMs and cultured CMs in control, RACF monolayer and IL-1 β RACF monolayer treatment groups.

AP parameter	Fresh	Cultured (control)	RACF monolayer	IL-1 β RACF monolayer
10-90 % rise time	4.2 \pm 0.3 ms	4.3 \pm 0.4 ms	4.5 \pm 0.4 ms	4.3 \pm 0.2 ms
APD₂₀	9.3 \pm 0.6 ms	9.5 \pm 0.6 ms	10.3 \pm 0.7 ms	10.0 \pm 0.2 ms
APD₅₀	22.6 \pm 1.1 ms	24.1 \pm 1.6 ms	26.8 \pm 2.3 ms	27.5 \pm 1.8 ms
APD₈₀	45.5 \pm 1.2 ms	55.4 \pm 4.4 ms	71.0 \pm 7.8 ms	65.0 \pm 5.5 ms

Values are represented as mean \pm SEM. $n=85$, $n=122$, $n=90$ and $n=99$ for fresh, cultured, RACF monolayer and IL-1 β RACF monolayer groups respectively. No significant changes were detected using a one-way ANOVA with Tukey's multiple comparison test.

5.3.3 Examination of RACF presence in control cultures

In this study, CMs were seeded directly onto laminin coated petri dishes or monolayers of RACFs without any preplating of CMs. Preplating is commonly completed in other studies to remove CFs from cultures (Gaudesius et al. 2003;Grand et al. 2014;Miragoli et al. 2006). Therefore, RACFs may be present in the control cultures in small numbers. Vimentin staining of control cultures fixed following the recording of APs was utilised to identify the presence of contaminating RACF. The staining revealed vimentin positive cells (top panel - Figure 5-9). However, the presence of vimentin-positive cells was negligible in comparison to RACF and IL-1 β RACF monolayers (Figure 5-9).

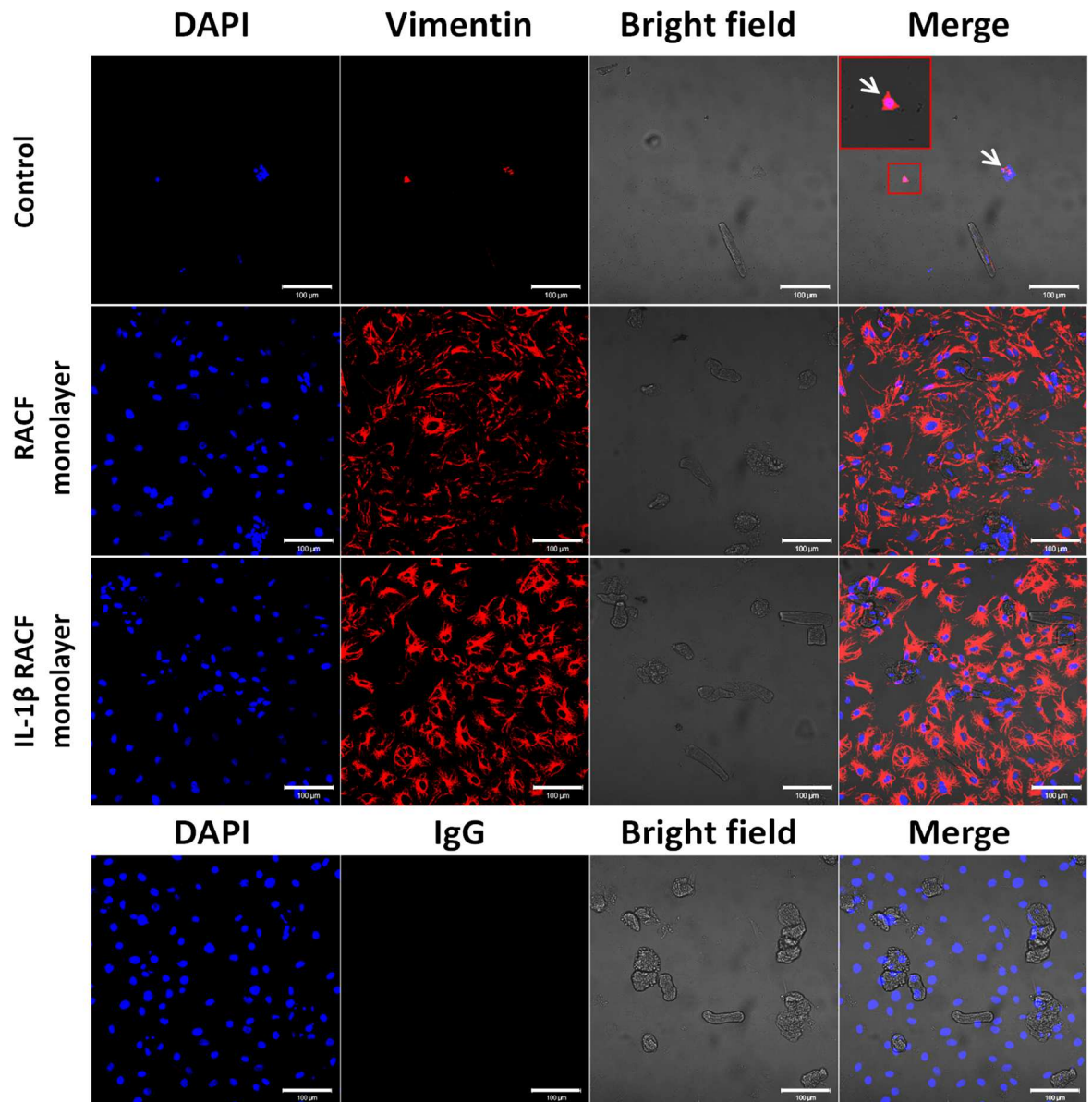


Figure 5-9 Vimentin immunofluorescence in cultures of CMs seeded on laminin coated plates (control) or on a monolayer of untreated or IL-1 β treated RACF.

Cultures were fixed following action potential measurement and cells stained for vimentin (red). Nuclei were counterstained with DAPI (blue). White arrows depict vimentin staining in cells other than CMs in control cultures. All images were taken at x25 magnification on the Zeiss 510 LSM confocal microscope and normalised to IgG (bottom panel). Scale bar represents 100 μ m ($n=3$).

5.4 Discussion

An adult CM: CF co-culture model allowing direct and indirect cell interactions, as well as the measurement of contraction and APs from CMs was successfully established. In this model, calcein was shown to be transferred from CMs to RACFs, suggesting the formation of functional GJs between the cells. RACFs were shown to significantly reduce the CD of CMs but had no significant effect on APD₈₀. Interestingly the effects of RACFs were reduced, albeit not quite to control values, when RACFs were treated with IL-1 β .

The formation of heterocellular GJs is supported by calcein dye transfer between adult cells following 20 h in culture, which is line with other reports (Chilton et al. 2007; Cho et al. 2007; Driesen et al. 2005). Calcein transfer between adult CMs and CFs has previously been reported to occur as early as 1-1.5 h (Cho et al. 2007; Driesen et al. 2005). Only following 48 h co-culture was the transfer of the high MW tracer, dextran (10 kDa), from adult CFs to adult CMs observed, suggesting membrane fusion between the cells at this time point which is out with the time frame of current investigations (Driesen et al. 2005). Additionally, mechanical interactions between CMs and RACFs was observed, where regions of CM membranes were visualised to be being “pulled” by RACFs. This phenomenon this has been reported by others (Dispersyn et al. 2001; Driesen et al. 2005) and may be a contributing factor for the reduction in CD of CMs in co-culture due to restriction of normal CM contraction. Furthermore, greater expression of α SMA in CFs is likely to enhance the contractile force elicited on CMs. It is therefore reasonable to suggest that reduced α SMA in CFs as a result of IL-1 β treatment (Chapter 4; Bronnum et al. 2013; Saxena et al. 2013) could contribute to less contractile force, consequently elevating restriction of CM contraction and effects on CD as reported in the current study. Indeed, IL-1 β was shown to inhibit TGF β -mediated contraction of collagen pads by CFs (Saxena et al. 2013), supporting this hypothesis.

As well as direct cell-to-cell interactions, the model used in the current study allows for paracrine heterocellular interactions to occur which may also have effects on CM contraction. Indeed, spontaneous contractions of neonatal CMs was inhibited following treatment with FCM for 72 h, in comparison to control CM

cultures which displayed continued contractions (LaFramboise et al. 2007). Furthermore, as CM contraction is reliant on Ca^{2+} , changes in contraction likely reflect alterations in Ca^{2+} handling. Although Ca^{2+} was not measured in the current study, Cartledge *et al.* (2015) found the Ca^{2+} transient decay to be faster in the adult CMs in a CM: CF co-culture transwell model in comparisons to CMs alone (Cartledge et al. 2015). This could explain the results of the present study due to quicker uptake/efflux of Ca^{2+} in the presence of CFs therefore leading to reduced CD. Interestingly this effect on the Ca^{2+} transient was ablated by TGF β inhibition, demonstrating a role for TGF β signalling between the cell types (Cartledge et al. 2015).

In the current study, although the CD was shortened there was no significant change in APD_{80} in CMs cultured with a RACF monolayer. Generally, shortening of the Ca^{2+} transient and CD would be expected to correlate with a shortening of APD, as shown by others (Weisser-Thomas et al. 2003). However, a trend for APD_{80} prolongation in these co-cultured CMs was observed which may indicate that with further repeats a significant change could be observed. Paracrine factors, although not identified, from CFs have been reported to cause a prolongation of the APD in neonatal CMs (Pedrotty et al. 2009). Additionally, TGF β 1 released by CFs has been suggested to cause prolongation of the APD in rat adult CMs (Kaur et al. 2013). Conversely, FCM from healthy CFs had no effect on the APD of neonatal CMs, in fact FCM from CF-MI promoted the opposite effect of APD shortening (Vasquez et al. 2010). In a similar co-culture model to the one utilised in the current study with rabbit cells, there was no difference in APD_{90} , despite evidence for coupling between the cells (Chilton et al. 2007).

A CF-mediated increase in APD of neonatal CMs has also been postulated to be a consequence of electrical coupling through Cx43 (Askar et al. 2012). In the current study RACFs treated with IL-1 β which had a greater expression of Cx43, (Chapter 4), decreased the effects on CM contraction and APD compared to those in the presence of control untreated RACFs. This could potentially suggest a lack of involvement for Cx43 in the RACF-mediated effects. However, the functionality of GJs between CMs and IL-1 β treated RACFs was not investigated in the present study, and is therefore an avenue for future work. Additionally, it is unlikely that

all CMs studied were coupled to RACFs; therefore differences in well coupled CMs could be diluted, contributing to the lack of APD₈₀ significance. Therefore in further studies calcein could be used to detect adequately coupled cells and parameters measured. The previous study which reported the involvement of Cx43, also showed a delay in the AP upstroke in co-culture which was partly recovered by Cx43 knockdown (Askar et al. 2012). However, no change in AP upstroke was shown in the current study.

As previously described, sharing of media between CMs and CFs promoted a faster Ca²⁺ transient decay than in CMs alone. Interestingly, this was slightly more apparent when CFs originated from a MI heart, therefore likely to be MFs (Cartledge et al. 2015). This could potentially explain why control RACFs induced greater effects than IL-1 β treated RACFs, due to the reports that IL-1 β inhibits the activation of CFs to the MF phenotype (Bronnum et al. 2013; Saxena et al. 2013). Indeed as shown in Chapter 4, IL-1 β treated RACFs had significantly lower mRNA expression of the profibrotic MF markers, CTGF and α SMA, in comparison to control RACFs. Furthermore, other paracrine factors released by these different phenotypes of RACFs examined may explain the difference in result and requires further investigation.

5.5 Summary

Evidence for functional GJs between adult CMs and CFs has been provided in the current co-culture model. Here, RACFs were shown to shorten the CD and slightly enhance APD of adult CMs. Additionally, the effects of IL-1 β on RACFs were shown to consistently elevate these effects. The reasons for these effects still require examination however could include restriction of contraction through mechanical interactions, paracrine interactions and potentially the involvement of heterocellular GJs.

Chapter 6 Establishing a model to investigate cardiac myocyte: fibroblast interactions via optical mapping in the intact heart

6.1 Introduction

6.1.1 Intramyocardial cell injection models

Direct intramyocardial cell injections have been investigated for both preventative and therapeutic use in experimental models of MI. Typically these studies have used genetically modified cells intended to provide a local release of therapeutic substances or to promote regeneration of the heart (Etzion et al. 2002;Goncalves et al. 2010;Ruvinov et al. 2008). Fibroblasts have been identified as a valuable cell type for this area of research. For instance, the injection of 1×10^6 CFs transduced with an Ad vector inducing the overexpression of the angiogenic factor, vascular endothelial growth factor (VEGF), 7 days prior to MI led to enhanced VEGF protein levels and capillary density 3 weeks later (Goncalves et al. 2010). Interestingly, this study found transgene expression to be maintained for least 45 days following injection versus only 7 days when the cell vector utilised was SMs, suggesting greater retention of CFs (Goncalves et al. 2010).

Injection of cells directly into the myocardial scar has also been reported. The retention of 5×10^5 dermal fibroblasts within the MI scar of mice was assessed by van der Bogt *et al.* (2009). This study reported a decrease in viability of dermal fibroblasts originating from mice which ubiquitously express GFP and firefly luciferase reporter genes, over 28 days from injection measured by bioluminescence. Viability was found to be significantly reduced at 10 days following injection from viability assessed at day 2 (van der Bogt et al. 2009). Additionally, injection of 1×10^6 neonatal CFs transduced with a retrovirus to overexpress recombinant human erythropoietin in a final volume of 100 μ L into the MI scar of Sprague-Dawley rats enhanced vascularisation in the scar (Ruvinov et al. 2008). Furthermore, an GFP signal was detected 7 days following injection of 1.5×10^6 CFs transduced with AdGFP (total volume of 150 μ L in serum free DMEM) into the scar of Sprague-Dawley rats (Etzion et al. 2002). These cells were shown to form a viable graft 4 weeks after injection which was noted in some cases to be segregated from the host scar and viable myocardium (Etzion et al. 2002).

The therapeutic use of fibroblast injection in the modulation of atrioventricular (AV) conduction in AF has also been reported. For instance the AH interval, a measure of AVN conduction time, was increased following injection of autologous dermal fibroblasts (ADFs) and more so when TGF β 1 was co-injected with ADFs into the canine AVN (Bunch et al. 2006). Similarly, the injection of ADFs into the AVN of the swine heart prolonged the P-R interval, hence slowing AV conduction (Tondato et al. 2015). These cells were shown to be retained at the site of injection for 28 days (Tondato et al. 2015). Ideally, both these studies showed no AV conduction block (Bunch et al. 2006;Tondato et al. 2015).

Intramyocardial injection of fibroblasts has also been utilised to modulate the electrophysiology of CMs. Cho *et al.* (2007) generated a stable fibroblast cell line from guinea pig lung fibroblasts which expressed the pacemaker channel, hyperpolarization activated cyclic nucleotide gated potassium channel 1 (HCN1), and GFP using LV transduction. These cells were then injected into the apex of the guinea pig heart in 50 % polyethylene-glycol 1500 solution, a reagent used to promote cell fusion (Lentz and Lee 1999). This enabled the fibroblasts to fuse with host CMs resulting in pacemaker like properties in isolated CMs, such as spontaneous action potentials and a slow phase 4 (Cho et al. 2007). Additionally, coupling between injected NIH-3T3 fibroblasts stably expressing the voltage-gated potassium channel, Kv1.3, and host CMs has been reported by Yankelson *et al.* (2008). In this study, 6×10^6 fibroblasts were injected into the healthy left ventricle of the male Sprague-Dawley rats and electrophysiological effects assessed *in vivo* 7 days following injection (Yankelson et al. 2008). A significant prolongation of the ERP, which can be antiarrhythmic, was observed at the injection site which was not observed at a remote region of the heart. There was also a marginal increase in the ERP at the sites injected with WT NIH-3T3 fibroblasts (Yankelson et al. 2008).

Injection of embryonic CMs (eCMs), but not embryonic SMs, adult bone marrow cells or embryonic CFs into the murine ventricular scar were reported to reduce the insistence of induced VT (Roell et al. 2007). Cx43 expression in eCMs was found to be an important contributing factor to these effects illustrated by a 4-fold increase in CV within the infarct in animals injected with eCMs in comparison to sham hearts. There was also greater conduction slowing in the infarct in

comparison to the rest of the heart following perfusion of the GJ blocker, carbenoxolone. Additionally, SMs overexpressing Cx43 had a similar effect on reduced induced VT of eCMs, supporting the importance of Cx43 in injected cells (Roell et al. 2007).

Vehicles used for cell transplantation have included DMEM (Goncalves et al. 2010), BSA (Christman et al. 2004) and PBS/saline (Ruvinov et al. 2008;van der Bogt et al. 2009). Furthermore, cells injected with fibrin biopolymer into the scar of Sprague-Dawley rats has been shown to increase the retention of SMs injected after 5 weeks (Christman et al. 2004). However, studies investigating coupling between injected and host cells may not benefit from a fibrin biopolymer vehicle which may prevent coupling between cells. Total fibroblast number and volumes injected into the rat heart have ranged from $1-6 \times 10^6$ and 100-300 μL respectively in previous studies (Etzion et al. 2002;Goncalves et al. 2010;Ruvinov et al. 2008;Yankelson et al. 2008).

6.1.2 Optical mapping

OM is a technique commonly used in whole heart AP measurement. This allows tens of thousands of sites, and therefore action potentials to be recorded simultaneously (Burton and Cobbe 2001). Typically, photodiode arrays and charge-coupled device (CCD) cameras have been used as photodetectors in cardiac OM due to their high spatial and temporal resolutions (Herron et al. 2012). However, CCDs/CMOS cameras are more advanced than photodiode arrays with regard to spatiotemporal resolution due to the larger number of pixels and rapid transfer to a computer (Herron et al. 2012). This is particularly useful in order to assess cardiac arrhythmias and changes in APs at the whole heart level. It involves the perfusion of a voltage-sensitive dye (VSD), which binds to the cell membrane and fluoresces light in direct proportion to membrane potential. Indeed, simultaneous optical and microelectrode recordings in the intact heart show a tight correlation (Efimov et al. 2004). In cardiac OM the VSDs typically used include the aminonaphthylethylenylpyridinium (ANEP) dye, di-4-ANEPPs, and RH-237 (Mills et al. 2006;Omichi et al. 2004;Park et al. 2014;Wang et al. 2014a).

As predetermined areas are recorded over time during OM, movement can produce artefacts in recordings, one limitation to the technique (Burton and Cobbe 2001). This is typically overcome by the use of E-C uncouplers including the myosin inhibitors, 2,3-butanedione monoxime (BDM) and blebbistatin, and/or mechanical restraint of the heart to produce accurate recordings (Burton and Cobbe 2001). However, BDM has been reported alter the APD (Baker et al. 2004;Liu et al. 1993), consequently restricting its use in cardiac OM. Conversely, blebbistatin has no effect on AP morphology (Fedorov et al. 2007), making it a more suitable reagent for electrophysiological measurements.

Technological developments now allow multiparametric OM where more than one parameter, typically voltage and calcium, can be recorded simultaneously in the intact heart (Choi and Salama 2000;Chou et al. 2017;Myles et al. 2015). In the current study, this technique has been utilised to detect voltage changes and the eGFP signal in areas of the heart injected with AdeGFP or eGFP expressing RACFs.

6.2 Aims

- To establish a model of intramyocardial injection of AdeGFP or RACFs transduced with an LVeGFP into the left ventricle of adult male Wistar rat hearts.
- Perform *ex vivo* OM to determine any difference in APs within regions of the heart positive for eGFP in comparison to remote regions.

6.3 Results

In preparation for cell injection into the rat left ventricular myocardium, RACFs were transduced with a LVeGFP at an MOI of 12 or 25, 48 h prior to injection. Initially an MOI of 12 was used due to efficient transduction of RACFs at this concentration (Figure 3-3). However due to some issues with lack of expression 24 h following transduction, the concentration was doubled to an MOI of 25 to ensure that on the day of injection there was sufficient expression. To confirm that the treatment of cells prior to injection, including trypsin treatment, resuspension in PBS and storage on ice, did not result in cell death, residual cells were reintroduced back into culture and monitored until the day of sacrifice and OM. Low eGFP expression was detected 48 h following transduction (upper two images, Figure 6-1). Despite this, most cells displayed expression, suggesting efficient transduction which with time would develop full expression. Little to no toxicity was apparent in cells reintroduced into culture, demonstrating the cell treatment did not result in cell death. Additionally, these cells demonstrated high eGFP expression on the day of OM; approximately 7 days following implantation (Lower two images, Figure 6-1).

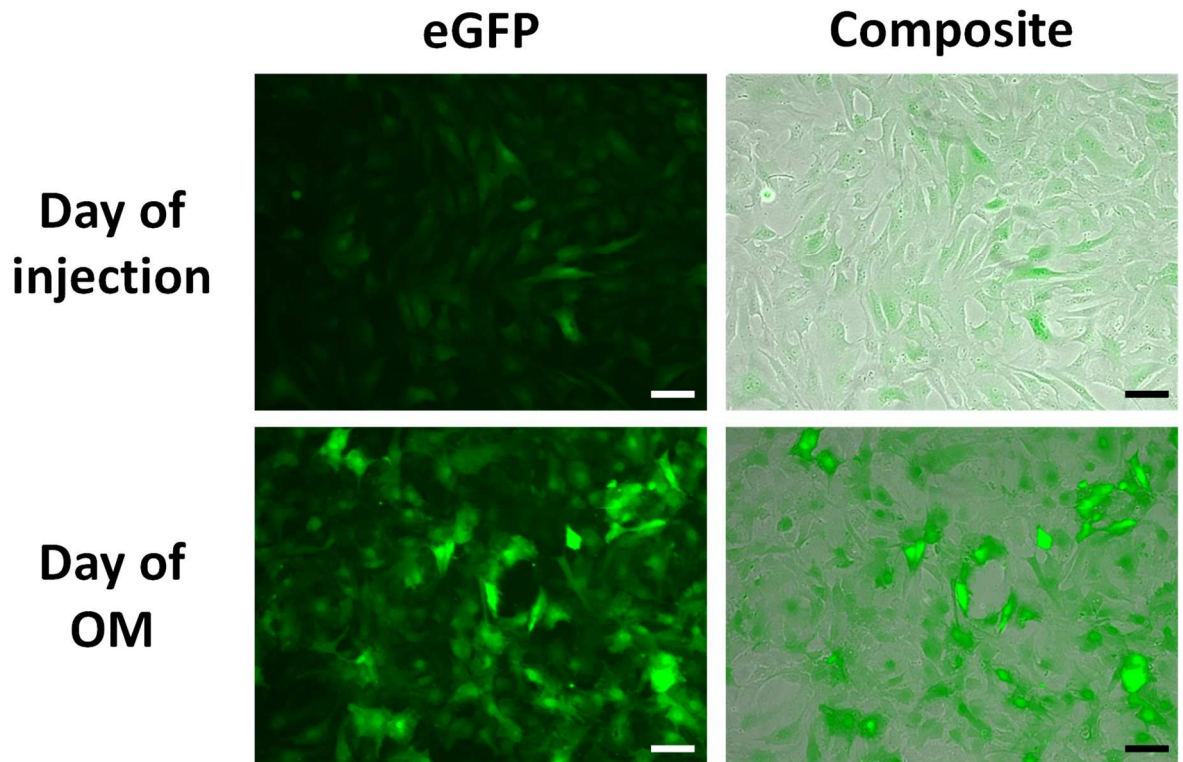


Figure 6-1 Representative images of pre-transduced RACFs with LVeGFP on the day of injection into the rat myocardium and of optical mapping.

RACFs were transduced with LVeGFP at an MOI of 25 two days prior to implantation into the rat adult left ventricular myocardium. Cells were imaged for eGFP expression on the day of injection (two upper images) prior to trypsin treatment and resuspension in the appropriate volume of PBS. Cells were placed on ice and used for injection. Residual cells were then added to a 100 mm culture dish and cultured until the day of optical mapping (OM), approximately 7 days following implantation. Lower two images show eGFP expression from these recovered cells. Scale bar represents 100 μm .

6.3.1 eGFP detection in the myocardium

Injection of Ad vectors had previously been optimised in house where 5 injections of 50 μ L volume were performed around the apex of the heart (Zoccarato et al. 2015). This protocol involved a total of 5×10^8 pfu in sterile PBS in 250 μ L, which produced CMs expressing the transgene in the region of the injection, 7 days following surgery (Zoccarato et al. 2015). Due to this success a similar procedure was used in the current study, where 5×10^8 pfu AdeGFP was injected in a smaller total volume of 60 μ L over two injections into the left ventricle (30 μ L per injection). Additionally, in another group of animals a total of 1×10^6 RACF transduced with LVeGFP in PBS was injected over two 30 μ L injections, which was at the lower range of fibroblast numbers used in previous studies (Etzion et al. 2002;Goncalves et al. 2010;Ruvinov et al. 2008;Yankelson et al. 2008). The left ventricle was injected as the preparation set up required horizontal orientation of the heart and a myocardial surface that was as flat as possible for accurate AP recording.

OM was performed on hearts injected with AdeGFP or RACFs transduced with LVeGFP, one week following surgery. In order to record APs over the epicardial surface, hearts were perfused with the VSD, RH-237. Voltage and eGFP signals were detected by cameras fitted with a long pass 715 nm or a single band 520/28 nm filter, respectively. In RACF injected hearts, there were five successful eGFP detections, however one heart (H1) had to be discarded from analysis due to unclear APs (Figure 6-2). There were three hearts in the AdeGFP injected group which generally gave a larger eGFP signal in comparison to RACF injected hearts (Figure 6-3). Despite two injections, in most hearts only one bright spot was detected, although a second potential injection site could be observed in some hearts (Figure 6-2 - white arrow). For analysis, four areas were selected and labelled 1-4; the full field, the injection site (eGFP bright spot), a region which was close to the apex (apical remote region) and finally one close to the base of heart (basal remote region) respectively (Figure 6-2 and Figure 6-3).

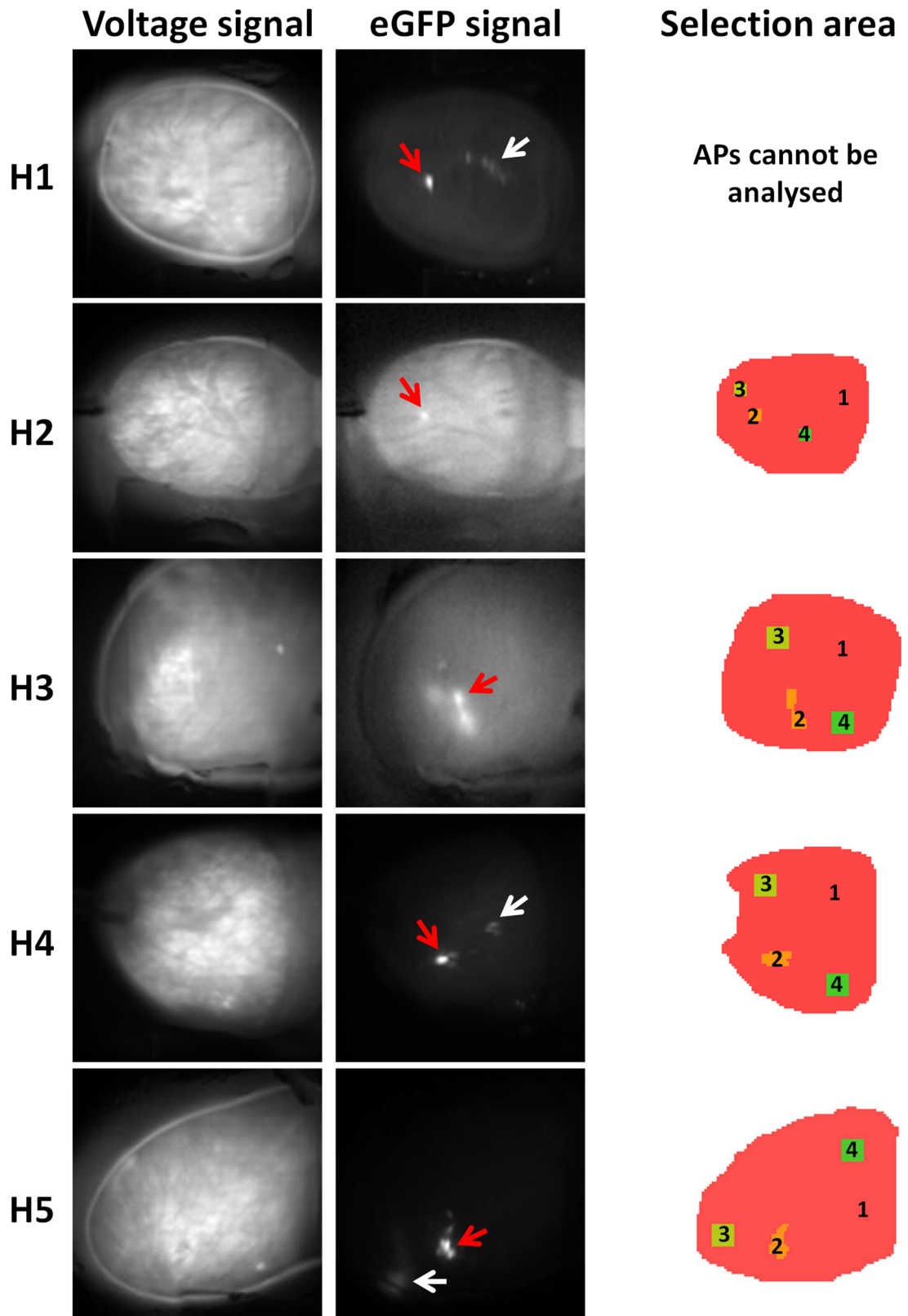


Figure 6-2 Voltage signal, eGFP signal and analysis selection areas of hearts injected with eGFP positive RACFs.

Hearts (H1-5) injected with eGFP positive RACFs were perfused with the voltage sensitive dye, RH-237, to give the voltage signal in shown in the first column detected by a camera fitted with a long pass 715 nm filter. The eGFP signal (middle column) was detected by a camera fitted with a 520/28 nm single-band pass filter. eGFP bright spots, indicating the injection site, are depicted by red arrows and white arrow indicate the potential region of the second injection. The last column shows the selection areas used for analysis numbered 1-4, where 1 = full field, 2 = injection site, 3 = apical remote region and 4 = basal remote region.

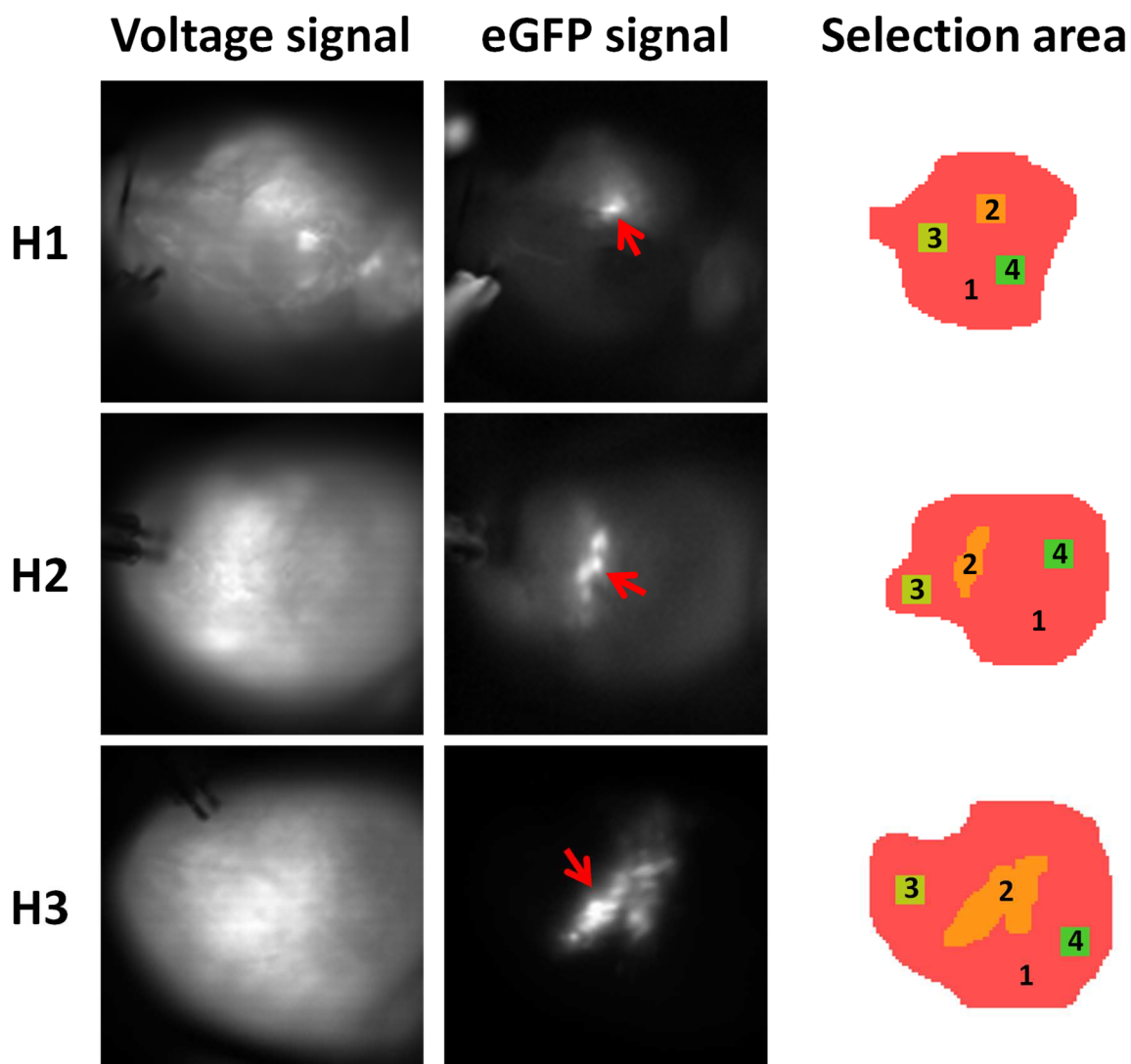


Figure 6-3 Voltage signal, eGFP signal and analysis selection areas of hearts injected with AdeGFP.

Hearts (H1-3) injected with AdeGFP were perfused with the voltage sensitive dye, RH-237, to give the voltage signal in shown in the first column detected by a camera fitted with a long pass 715 nm filter. The eGFP signal (middle column) was detected by a camera fitted with a 520/28 nm single-band pass filter. eGFP bright spots, indicating the injection site, are depicted by red arrows. The last column shows the selection areas used for analysis numbered 1-4, where 1 = full field, 2 = injection site, 3 = apical remote region and 4 = basal remote region.

6.3.2 Dynamic pacing

Hearts were paced at different CLs, beginning at 200 ms, close to the physiological rat heart rate (Damasceno et al. 2013). The CL was then progressively shortened to increase the heart rate until the heart could no longer be paced. An exemplar ECG trace and corresponding APs in both RACF and AdeGFP injected hearts are shown (Figure 6-4Ai and ii respectively). The representative APs are from within the injection site and in the apical or basal remote regions while the CL was 200ms (Figure 6-4Ai and ii).

Data is presented in two ways, first to illustrate the relationship between the CL and either AP rise time (10-90 %) or APD_{80} (Figure 6-4) and secondly to clearly show the difference in these parameters at a set CL between the different regions within one heart (Figure 6-5 and Figure 6-6). In the latter graphs, CLs of 120 and 200 ms were examined (Figure 6-5 and Figure 6-6). The rise time (10-90 %) of APs is unaltered by changes in the CL (Figure 6-4B - top graphs). Very little variation in rise time between the three sites or between different hearts was detected in the RACF group (Figure 6-4Bi - top graph and Figure 6-5A and C). Conversely, in the AdeGFP group a larger range of rise times were observed (Figure 6-4Bii - top graph). The basal remote regions appear to have the most delayed rise time (Figure 6-4Bii - top graph and Figure 6-5B and D). Although the mean line suggests that the rise time of APs within the injection site are more prolonged in comparison to the apical remote region (Figure 6-4Bii), this is only apparent for one of two hearts at CLs of 120 and 200 ms (Figure 6-5B and D).

As the CL shortened, the APD_{80} was reduced in both RACF and AdeGFP injected hearts (Figure 6-4Bi and ii, lower graphs); a commonly observed relationship (Mahajan et al. 2008; Sabir et al. 2010). A large overlap between the APD_{80} values within the different regions, especially within the RACF injected hearts, was observed, suggesting no significant change between the regions (Figure 6-4Bi and ii, lower graphs). Rise time and APD_{80} values from CLs below 120 or 100 in RACF or AdeGFP groups, respectively are from one heart due to no pacing capture at these rates in the other hearts.

On further examination of APD_{80} in RACF injected hearts at CLs of 120 and 200 ms, the injection sites and apical remote regions had similar APD_{80} values. In comparison, the APD_{80} in basal remote regions tend to be shorter (Figure 6-6A and C). In AdeGFP injected hearts, there may be slight prolongation in the injection site which is more apparent at 200 ms versus 120 ms (Figure 6-6B and D). This was more pronounced in heart 1 than in 3.

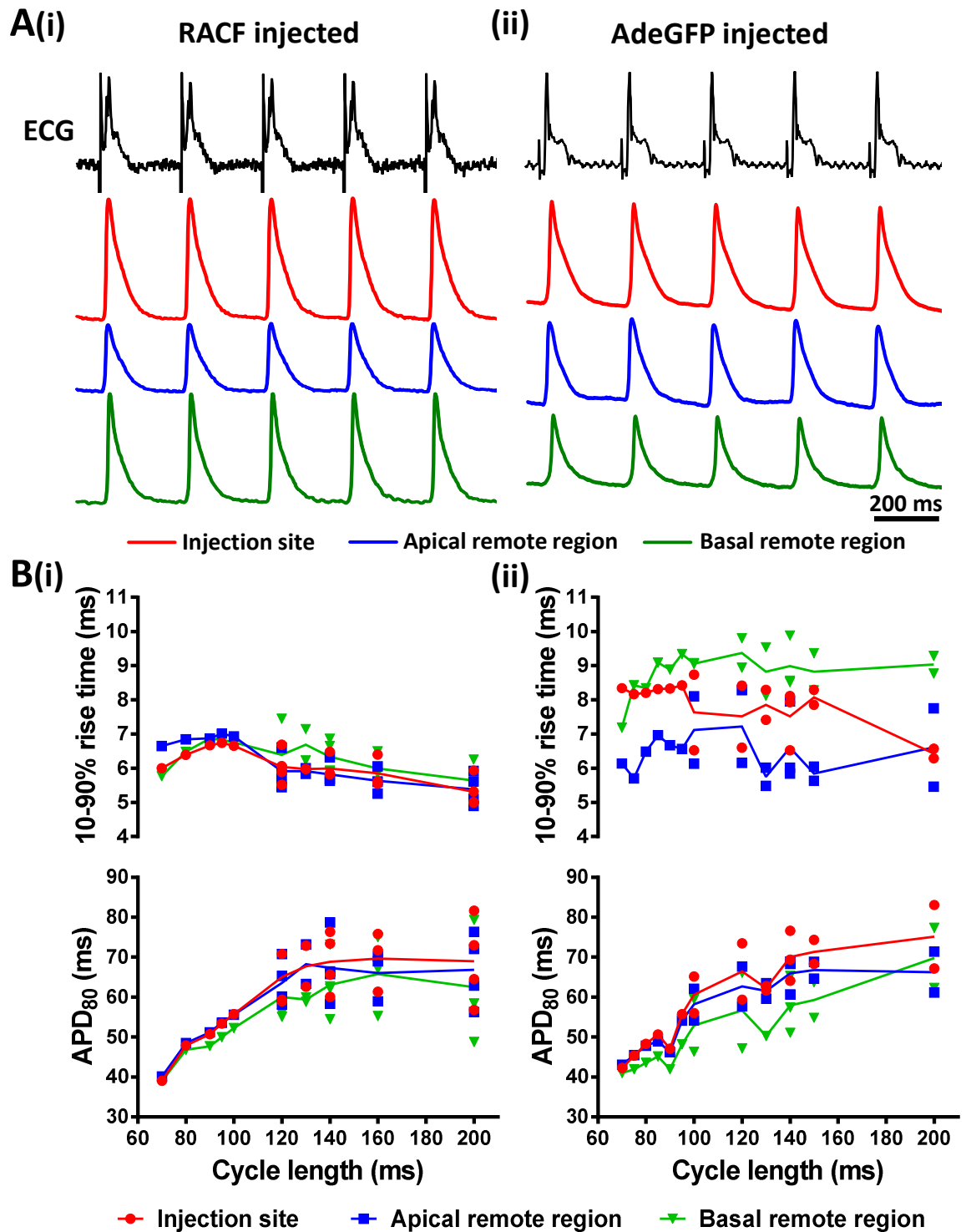


Figure 6-4 Relationship between the action potential rise time and duration at different in cycle lengths during dynamic pacing in both RACF and AdeGFP injected hearts.

Hearts were perfused with the voltage sensitive dye, RH237, to allow electrical activity to be recorded. (A) An exemplar ECG trace and action potential (AP) traces within the injection site (red), apical remote region (blue) and basal remote region (green) when paced at a cycle length (CL) of 200 ms in both (i) RACF and (ii) AdeGFP injected hearts are shown. Scale bar represents 200 ms. (B) Graphs showing the 10-90 % rise time and AP duration at 80 % repolarisation (APD₈₀) in (i) RACF ($n=4$) and (ii) AdeGFP ($n=3$) injected hearts. Each point represents a different heart and the line denotes the average.

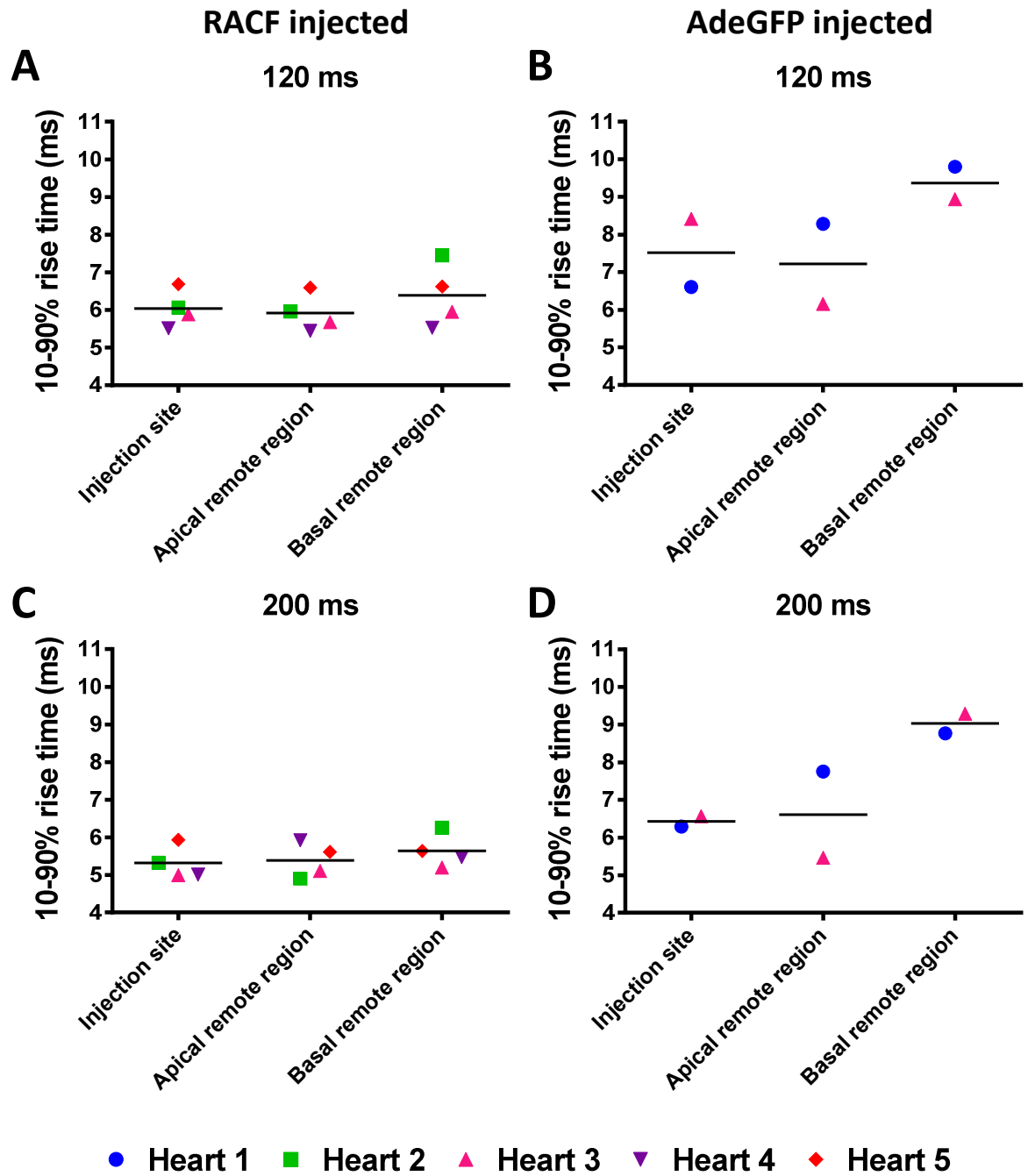


Figure 6-5 Action potential rise time of hearts injected with RACF or AdeGFP when paced at a cycle length of 120 or 200 ms.

(A-B) Action potential 10-90 % rise time while hearts were paced at a cycle length of 120 ms or (C-D) 200 ms. (A-C) AP rise time from the injection site and apical and basal remote regions of RACF and (B-D) AdeGFP injected hearts are shown. Each symbol represents hearts 2-5 or 1 and 3 in RACF or AdeGFP groups respectively.

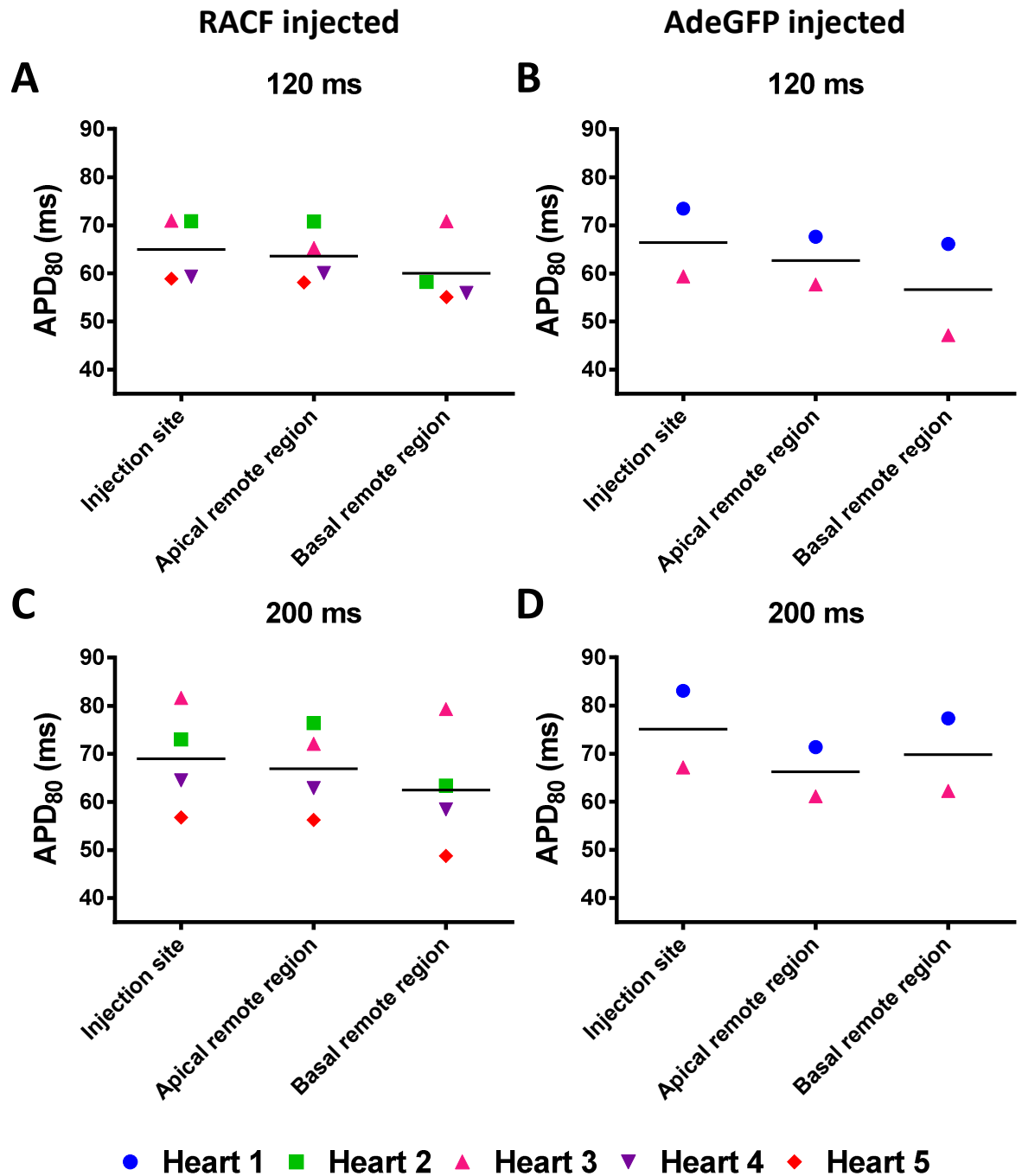


Figure 6-6 Action potential duration of hearts injected with RACF or AdeGFP when paced at a cycle length of 120 or 200 ms.

(A-B) Action potential duration at 80 % repolarisation (APD₈₀) while hearts were paced at a cycle length of 120ms or (C-D) 200 ms. (A-C) APD₈₀ from the injection site and apical and basal remote regions of RACF and (B-D) AdeGFP injected hearts are shown. Each symbol represents hearts 2-5 or 1 and 3 in RACF or AdeGFP groups respectively.

6.3.3 S1S2 pacing

Hearts also underwent an extrastimulus pacing protocol known as S1S2, whereby hearts were paced at 200 ms (S1) prior to an extra impulse at a shorter CL (S2). The S2 was then progressively shortened until it did not produce an AP, and this was taken as the ERP. ERP was 64.3 ± 6.3 and 75.3 ± 5.8 ms in the RACF and AdeGFP injected hearts, respectively (Figure 6-7). There were no inductions of arrhythmias throughout the pacing protocol.

The APs induced by S2 at a range of CLs were analysed and both the rise time and APD_{80} plotted as before. The same selection areas used in analysis of the dynamic pacing data were used for S1S2 analysis, with the addition of an area which was the same shape and size as the injection site (Figure 6-8). This was positioned at a region which had a similar activation time to the injection site, and referred to as remote region 3. As the AdeGFP injection site selection was larger than remote regions in two of the three hearts, a smaller region within the injection site was selected (labelled 2.5 in Figure 6-8). The rise time and APD_{80} of APs induced by S2 in this smaller injection site closely mimicked the values in the original injection selection (Figure 6-9) and therefore to maintain consistency the original injection selection was used in analysis.

An ECG trace and traces of APs within the selected regions showing an S1-S2 interval of 90 ms from both an RACF and AdeGFP injected heart are shown (Figure 6-10i and ii respectively). Similar to dynamic pacing (Figure 6-4); there was little difference in the mean rise time between the regions across the CLs examined in RACF injected hearts (Figure 6-10Bi - top graph). Additionally, in AdeGFP injected hearts a wide range of rise times were present (Figure 6-10Bii - top graph). The rise times in the other regions overlapped suggesting no consistent difference between the regions. This was also true for APD_{80} in both groups. Despite this, the mean APD_{80} (line) for the remote region 3, the most comparable region to the injection site, was shorter than that of the injection site in both RACF and AdeGFP groups (Figure 6-10Bi and ii -bottom graphs).

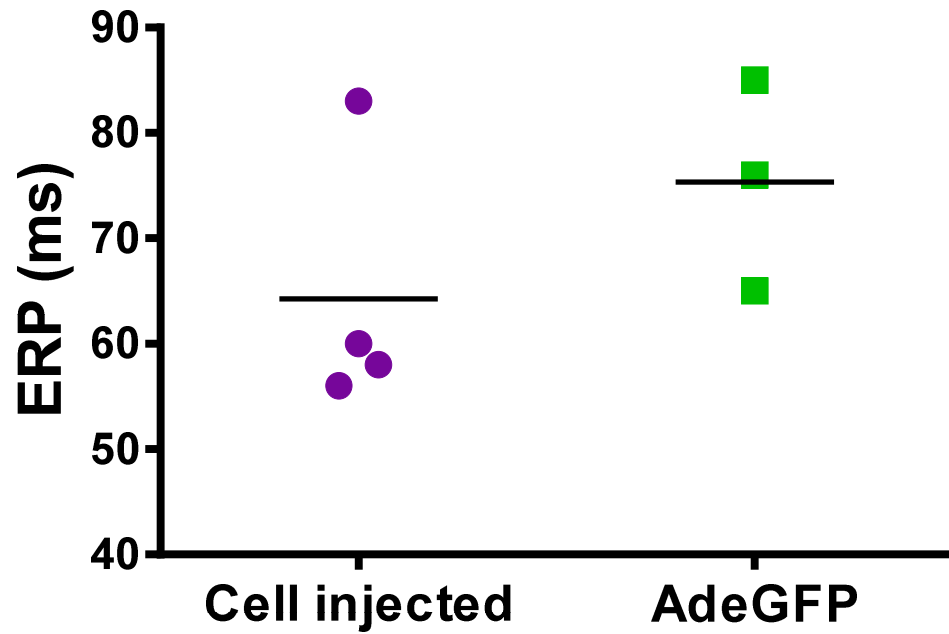


Figure 6-7 Effective refractory period of hearts injected with eGFP positive RACFs or AdeGFP. Hearts were paced at 200 ms prior to an extrastimulus impulse (S2) at increasingly shorter cycle lengths until an action potential did not fire, taken as the effective refractory period (ERP). Each point represents a different heart and line denotes average.

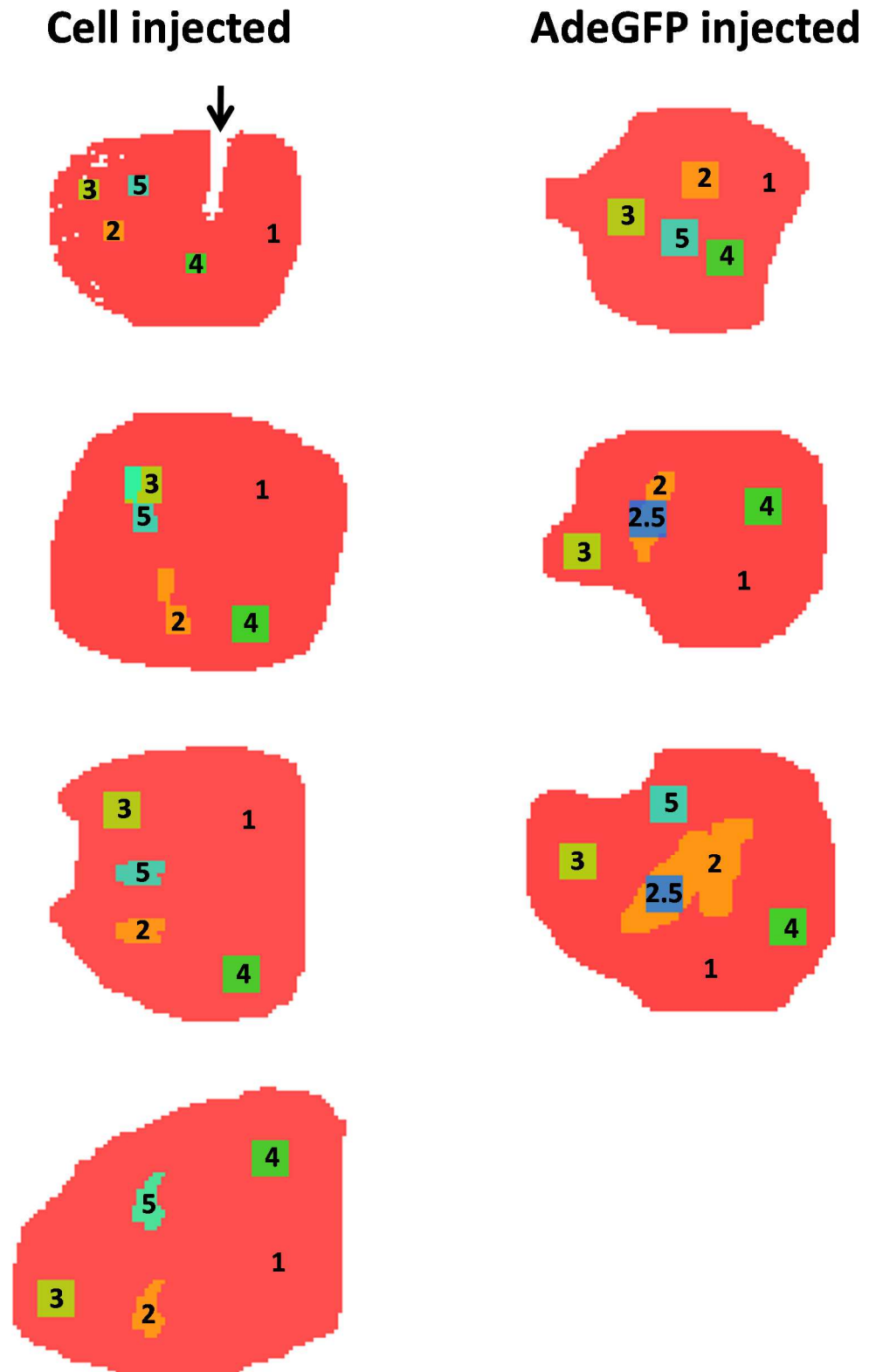


Figure 6-8 Selection areas for eGFP positive RACF and AdeGFP injected hearts for S1S2 pacing protocol.

Four and three hearts were included in S1S2 analysis for eGFP positive RACF and AdeGFP injected hearts respectively. Black arrow indicates where the pacing electrode was and therefore pixels had to be removed from the selection. Selection areas are numbered 1-5 where, 1 = full field, 2 = injection site, 2.5 = smaller area in injection site, 3 = apical remote region, 4 = basal remote region, 5 = remote region 3.

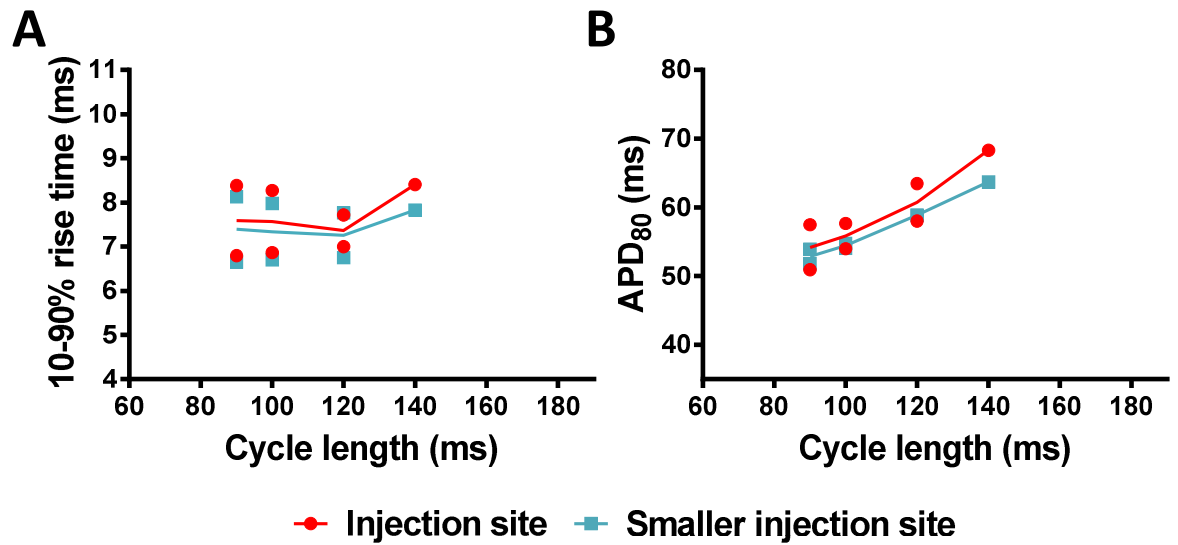


Figure 6-9 Comparison of S2 action potential rise time and duration between the original injection selection and the smaller injection selection.

Hearts were perfused with the voltage sensitive dye, RH-237, to allow electrical activity to be recorded. Hearts were paced at a cycle length of 200 ms prior to an extrastimulus (S2) at progressively shorter cycle lengths. (A) Average 10-90 % rise time and (B) action potential duration at 80 % repolarisation (APD₈₀) from the injection site and a smaller region within the site following S2 in two AdeGFP injected hearts. Each point represents a different heart and the line denotes the average.

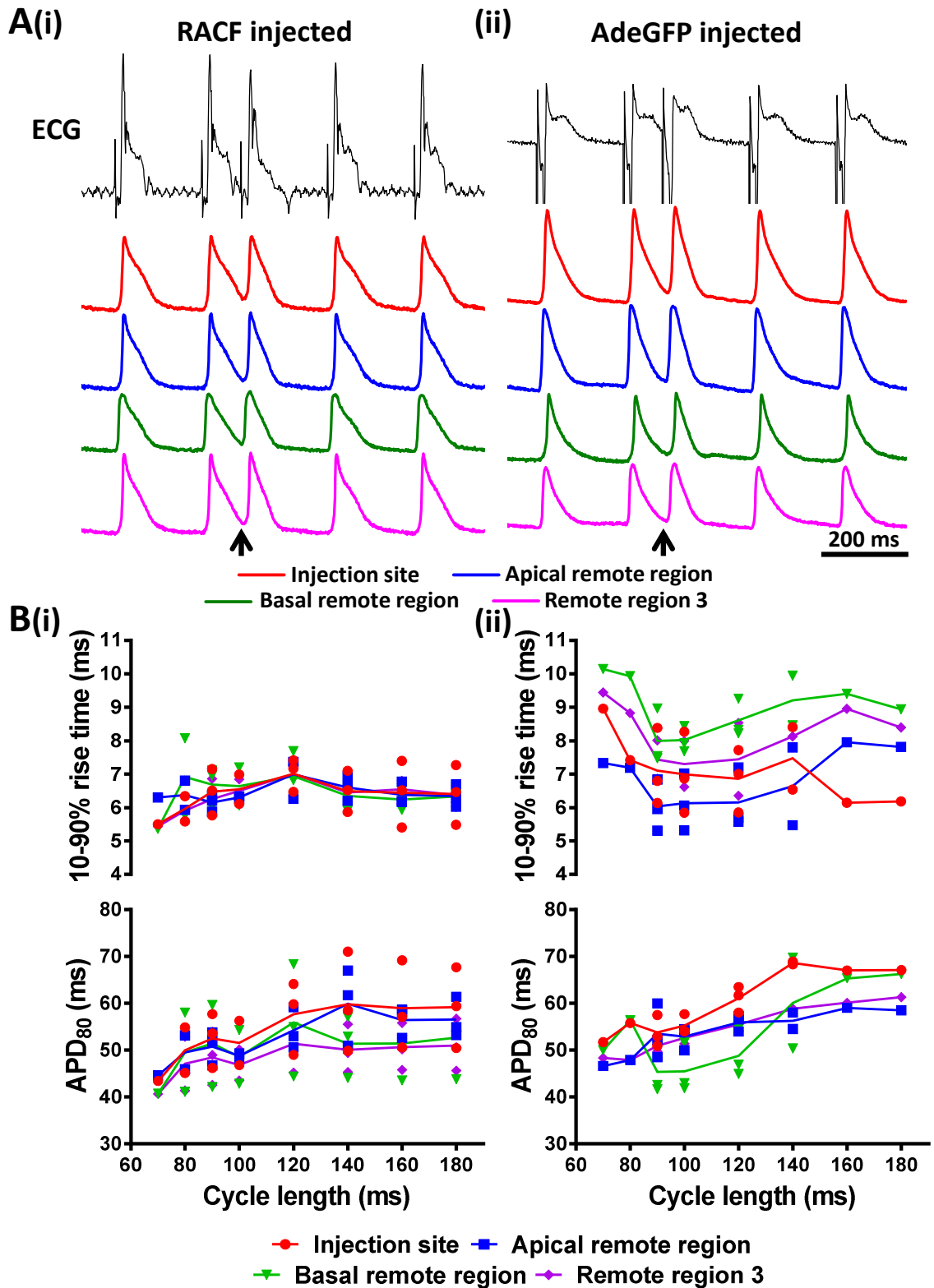


Figure 6-10 Relationship between the S2 action potential rise time and duration at different in cycle lengths in RACF and AdeGFP injected hearts.

Hearts were perfused with the voltage sensitive dye, RH-237, to allow electrical activity to be recorded. (A) Hearts were paced at a cycle length of 200 ms prior to an extrastimulus (S2) at progressively shorter cycle lengths. An exemplar ECG trace and action potential (AP) traces within the injection site (red), apical remote region (blue), basal remote region (green) and remote region 3 (pink) where the S1-S2 interval was 90 ms (black arrow). (Ai) RACF and (ii) AdeGFP injected hearts respectively. (B) Graphs showing the 10-90 % rise time and AP duration at 80 % repolarisation (APD₈₀) of the S2 in (i) RACF and (ii) AdeGFP injected hearts. Each point represents a different heart and the line denotes the average.

To compare the characteristics of the S2 APs within the injection sites of each group, the rise time or APD_{80} over different CLs were plotted on the same graph (Figure 6-11). The injection site rise time was similar between the two groups, shown by overlapping points and mean lines (Figure 6-11A). Although there was only 1 heart value at a CL of 70, 80, 160 and 180 ms in the AdeGFP group, APD_{80} values following the S2 impulse within the range of 90-140 ms (where values from 2-3 hearts are shown) were very similar (Figure 6-11B). In comparison, the RACF group had greater variation in APD_{80} values (Figure 6-11B).

Interestingly, preliminary examination of the activation pattern demonstrated that in one heart from each group, the S2 impulse was slowed and activation was disrupted at the injection site (Figure 6-12). In both hearts this was most apparent at the shortest S1-S2 interval, therefore a common CL of 70 ms is presented. In the RACF injected heart activation following S1 was complete by 20 ms with the contour lines being relatively parallel from the site of activation over the epicardial surface. Additionally, no disruption was caused by the injection of cells. However following the S2 impulse there was slight activation slowing prior to the activation of the injection site and crowding of activation downstream of the injection site. This slowing of activation was more pronounced in the AdeGFP injected heart. Following the S1 impulse, the selected region was activated within 12 ms. In contrast following the S2 impulse, full activation was complete in 20 ms, with the longest activation time occurring just downstream of the injection site. This may represent damage to the myocardium due to appearance of this in both groups. All other hearts examined did not present this pattern.

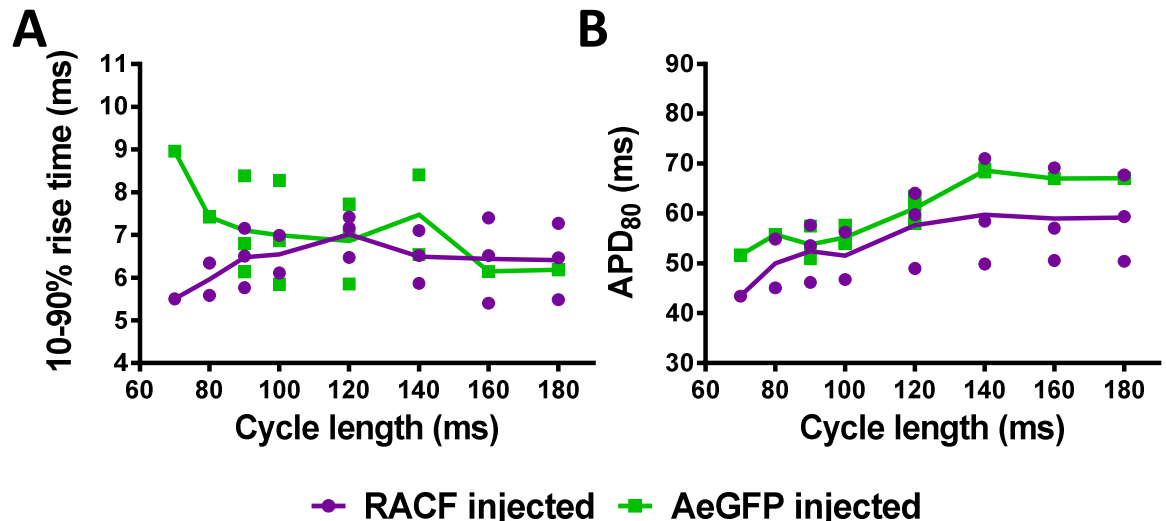


Figure 6-11 The S2 action potential rise time and duration in the injection site of RACF and AdeGFP injected hearts at different cycle lengths.

Hearts were perfused with the voltage sensitive dye, RH237, to allow electrical activity to be recorded. Hearts were paced at a cycle length of 200 ms prior to an extrastimulus (S2) at progressively shorter cycle lengths. (A) 10-90 % rise time and (B) action potential duration at 80 % repolarisation (APD_{80}) of APs in the injection site of both RACF and AdeGFP injected hearts. Each point represents a different heart ($n=4$ and $n=3$ for RACF and AdeGFP injected hearts respectively) and the line denotes the average. From cycle lengths of 90-140 ms, values from 2-3 AdeGFP hearts are shown, whereas only 1 heart value is shown in cycle lengths out with this range.

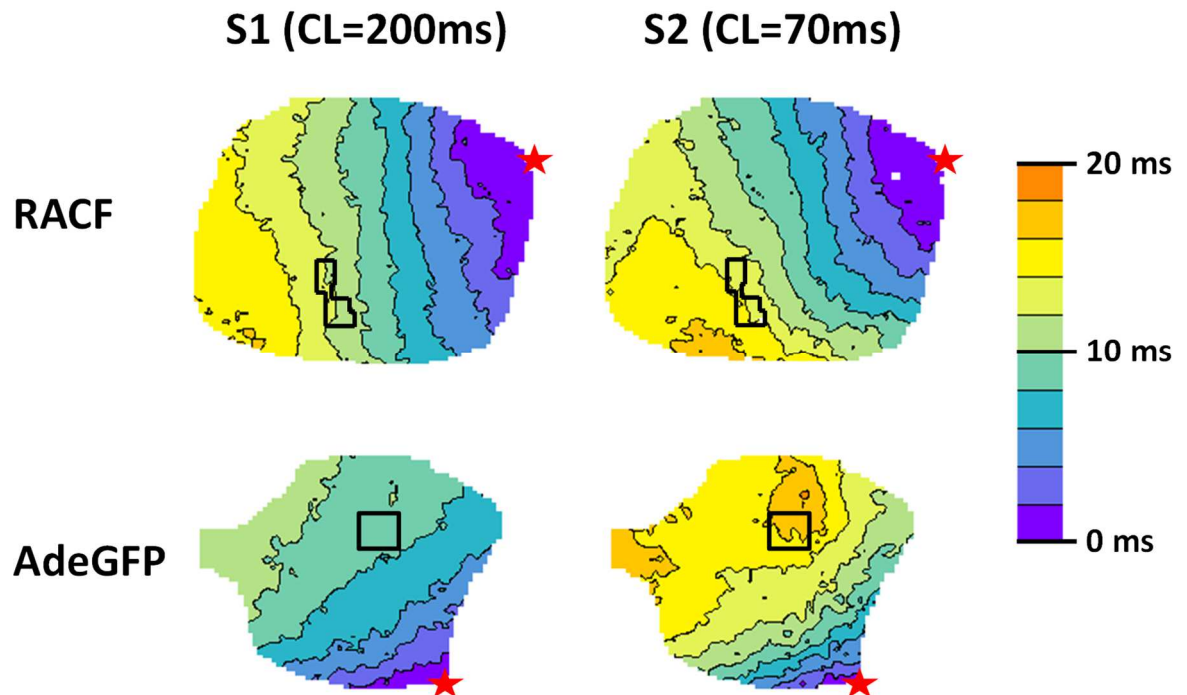


Figure 6-12 Example AdeGFP and RACF injected hearts showing crowding of activation over the epicardial surface during an S2 impulse.

Normal activation from the base to apex of the heart during S1 at a CL of 200 ms is observed in both hearts. In RACF injected heart, the two upper contour plots, crowding of activation is seen at the injection site following S2 (CL = 70 ms). In the AdeGFP heart the (two lower images) activation much slower during S2 with distinct crowding of activation at the injection site. Injection sites are outlined in black. Red stars approximately indicate the origin of activation. Scale ranging from 0 – 20 ms is shown on the right. CL; cycle length.

6.3.4 Preliminary detection of eGFP positive cells within the rat myocardium

Following OM, all hearts were cut transversely into four segments and the section containing the injection site noted. Hearts were then fixed in 4 % PFA prior to tissue processing and embedded in paraffin wax. Preliminary staining of eGFP and the CM marker, cTnI, was completed on a heart injected with RACF which was cut longitudinally and not used for OM. eGFP positive cells which were negative for cTnI were detected in the left ventricular myocardium (Figure 6-13). Many other cells within that region were not eGFP or cTnI positive, suggesting the recruitment of other cell types to the area of injection; potentially inflammatory cells (Figure 6-13). However to confirm this, further staining of inflammatory cell markers are required.

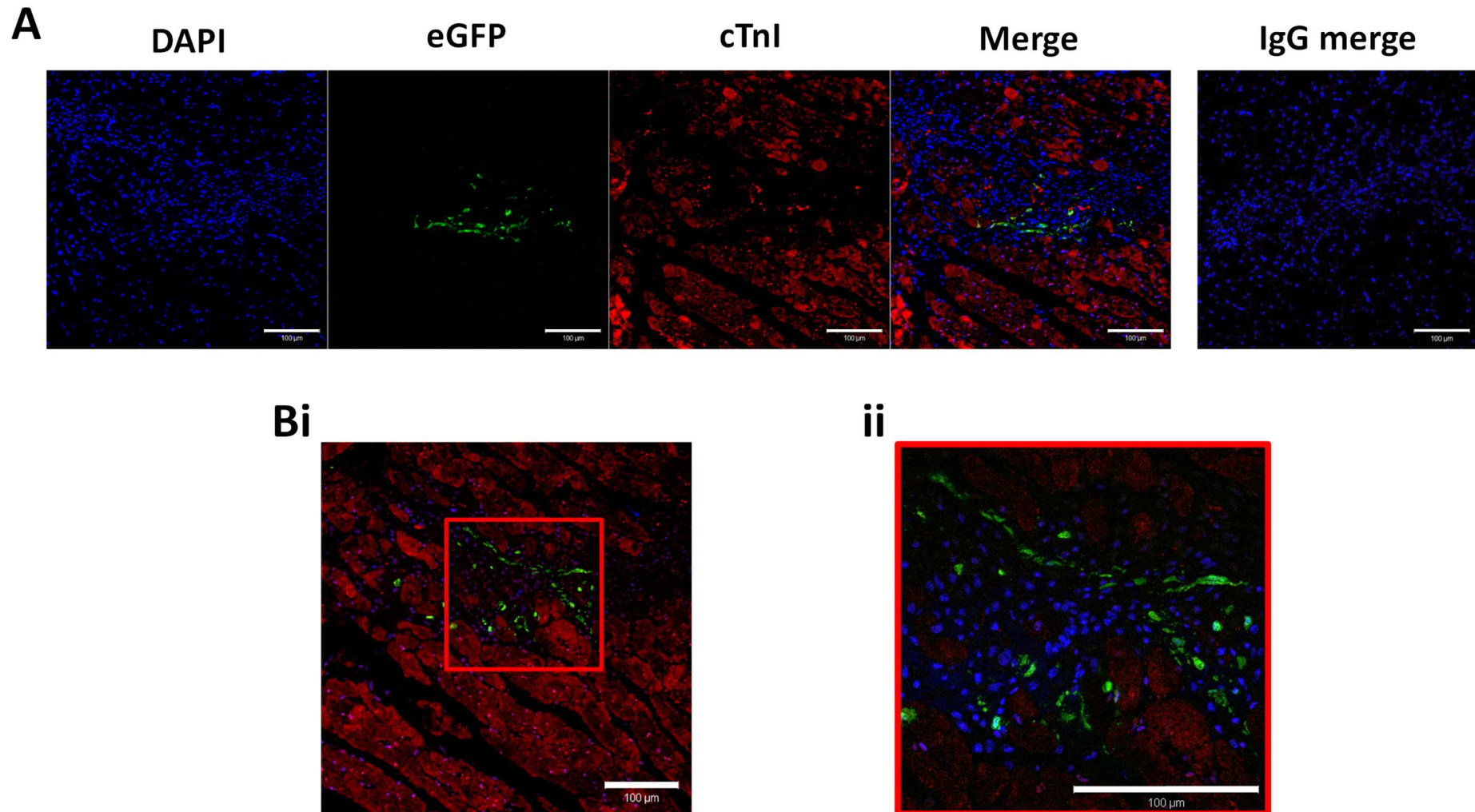


Figure 6-13 Preliminary immunofluorescence to identify eGFP positive RACFs within the rat left ventricular myocardium.

(A) A heart injected with eGFP positive RACFs was stained for DAPI (blue), eGFP (green) and cardiac troponin I (cTnl) (red). (B) Merged images of same heart at different section ($n=1$). All images were normalised to the appropriate IgG controls (exemplar IgG merge shown in A). Images shown in A and Bi where taken at x25 magnification and the image in Bii taken at the higher magnification of x63. Scale bars represent 100 μm .

6.4 Discussion

This study has successfully demonstrated that eGFP positive primary RACFs and AdeGFP-transduced CMs can be detected within the rat left ventricular myocardium, 7 days following injection. As this is a preliminary study, with only a small number of hearts, the effect on AP rise time and duration in the injection sites is far from confirmed. However, there may be a trend for slight prolongation of APD₈₀ following the S2 impulse within the injection site in comparison to remote region 3 in both groups. Additionally, activation of one heart in each group was altered around the injection site at the shortest S1-S2 intervals. Larger group sizes along with more detailed histological analysis are required.

Most studies suggest that injected fibroblasts are retained in the healthy myocardium or myocardial scar for at least 7 days following injection (Etzion et al. 2002; Yankelson et al. 2008). This is in agreement with the current study whereby a positive eGFP signal was detected *ex vivo* and eGFP positive cells observed *in situ* via IHC. However, on histological analysis of one heart which was injected with RACFs there was a large influx of eGFP negative cells, most likely to be of an inflammatory nature. Similarly, in rat hearts 7 days following injection of pre-labelled NIH-3T3 fibroblasts, there was an abundance of unlabelled cells in the region of injection (Yankelson et al. 2008). To confirm the presence of inflammatory cells, tissue sections could be stained for inflammatory cell markers such as CD68 and lymphocyte antigen (Ly) 6B.2 for macrophages and neutrophils, respectively (Peng et al. 2014). This inflammatory response is likely to be exacerbated by the use of non-autologous cells and could be dampened by immunosuppressant treatment, which has been used in other studies (Roell et al. 2007; Yankelson et al. 2008). Although IHC was not performed on an AdeGFP injected heart for detection of eGFP expression in the current study, studies have reported a large inflammatory response following direct intramyocardial injection of Ad vectors (Huusko et al. 2010; Merentie et al. 2016; Toivonen et al. 2012).

No consistent alteration in AP rise time or APD₈₀ in the injection site versus the apical or basal region during dynamic pacing was detected. However, in comparison to remote region 3 utilised in S1S2 analysis there was a slight prolongation of APD₈₀ in both RACF and AdeGFP injected areas. As this was detected in both groups, the prolongation is unlikely to be a consequence of

coupling between injected RACF and host CMs in the RACF injected hearts. It most likely reflects damage to the myocardium during injection and therefore examination of fibrosis is required. Despite this, immunostaining for Cx43 would allow examination of Cx43 expression at contact areas between eGFP positive RACFs and host CMs. Indeed, Yankelson *et al.* (2008) reported an increase in Cx43 expression in grafted NIH-3T3 fibroblasts close to CMs and observed Cx43 expression at heterocellular contact points (Yankelson *et al.* 2008).

The S1S2 pacing protocol is a valuable tool for determining the arrhythmic potential of the heart as well as determining the ERP. In the present study, no inductions of arrhythmias were caused by the premature stimulus. Additionally, there was no difference in the ERP between RACF and AdeGFP injected hearts, or between the examined regions. In contrast, the ERP was slightly but significantly increased *in vivo* in the injection site 7 days following intramyocardial injection of WT NIH-3T3 fibroblasts in comparison to baseline (before cell injection) (Yankelson *et al.* 2008). Unfortunately an ERP for a remote region 7 days after injection was not reported for WT fibroblast injected hearts. Conversely as described in section 6.1.1, injection of Kv1.3 overexpressing NIH-3T3 fibroblasts produced a very large increase in ERP in the injection site in comparison to the remote region where there was no change from baseline (Yankelson *et al.* 2008). Throughout this study, hearts were paced from injection site which was identified by discolouration on the epicardial surface or in some cases by the detection of fluorescence from pre-labelled cells or following co-injection with a fluorescent tracer (Yankelson *et al.* 2008). This adaptation, pacing from the injection site, to future hearts in the current study would allow local ERP to be evaluated more precisely. In the present study, we directly measured APs over the epicardial surface, whereas Yankelson *et al.* (2008) used an indirect method by examination of electrograms.

Although conduction block was not identified in any of the hearts examined, altered propagation of the premature stimulus, S2, was identified in one heart from each group. Typically, S2 propagates more slowly than S1 in both intact heart preparations and in neonatal CM monolayers (de *et al.* 2011; Stein *et al.* 2011). This was also observed in the current study in the two hearts shown in Figure 6-12. Crowding of activation close to or surrounding the injection site was also found in

both hearts. However, both the slowing and crowding of activation following S2 was more pronounced in the AdeGFP injected heart, which could be a consequence of greater tissue damage in this heart, requiring further investigation. Following the addition of further heart numbers to each group, CV through the injection site would be an interesting parameter to examine.

Limitations/issues to the current study include an absence of calcium measurement which is an important physiological measurement and lack of standardised pacing region, which was a result of electrode issues. Although, APD is typically greater closer to the activation site and shortens further from the activation site (Franz et al. 1987; Hanson et al. 2009; Yuan et al. 2001), this cannot be examined from the merged data in the current study due to differential pacing regions selected between hearts. While this not ideal, it may explain the variation between hearts.

6.5 Summary

Although this work is not complete, preliminary results show that RACFs are retained in the rat left ventricular myocardium for at least 7 days following implantation, which is in agreement with other reports (Etzion et al. 2002; Yankelson et al. 2008). Furthermore, due to fluorescent labelling of cells prior to injection, APs from the injection site could be compared to other regions of the heart. Further hearts in each group and histological analysis post OM to determine the damage caused by injection, the inflammatory response and the coupling of injected RACF to host CMs is required to complete this study.

Chapter 7 General discussion

7.1 Overall summary

CFs are a vital cell type in cardiac repair however persistent activation can result in maladaptive remodelling (Souders et al. 2009). Thus far, there have been a vast number of studies investigating CM: CF interactions in neonatal cell types with limited research on the effects of adult CFs on the function of adult CMs. Therefore, the primary aims of the work presented in this thesis were to establish the effects of RACFs on adult CM contraction and electrical activity *in vitro*, as well as to develop a model where potential heterocellular coupling could be evaluated *in situ*.

Initially, the development of a LV vector which would enable the expression of Cx43 as well as a nuclear localised reporter protein under the control of an artificial α SMA promoter was investigated. Despite the apparent functionality of the designed insert (α SMA_eGFPNLS) shown by eGFP positive nuclei in RACFs following transfection, initial cloning into an LV plasmid vector was unsuccessful. This could be due to contaminating DNA interfering with the ligation process or an issue with the promoter as supported by successful ligation of eGFPNLS into an Ad plasmid, pVQ_CMV_K-NpA. Alternatively, a functional Ad vector overexpressing Cx43 was produced then characterised in HeLa cells and RACFs by western immunoblotting and ICC.

As CFs have been reported to have a greater expression of Cx43 following MI (Vasquez et al. 2010; Zhang et al. 2010), potential mediators responsible for this were investigated. TGF β 1, IL-6 in combination with the sIL-6R, IL-1 α and IL-1 β were all shown to significantly enhance Cx43 mRNA levels. The latter two cytokines were found to induce the greatest augmentation in Cx43 levels and were therefore of particular interest in the current study, due to potentially greater ability to form GJs with CMs. IL-1 α and IL-1 β appear to have indistinguishable actions (Bujak and Frangogiannis 2009) therefore only IL-1 β was investigated further. In the current study, IL-1 β was shown to induce a morphological change in RACFs as well as an augmentation in Cx43 protein levels, which is in agreement with other reports in primary and cell-line rabbit synovial fibroblasts (Heino 1986; Niger et al. 2010). Interestingly, this increase in Cx43 by IL-1 β is the opposite of that seen in CMs (Baum et al. 2012a; Coppen et al. 2008), indicating differential

effects of IL-1 β on Cx43 expression in different cell types. Further investigation into the IL-1 signalling pathway revealed the involvement of the IL-1R, NF- κ B, p38 MAPK and MEK1 in IL-1 β -mediated increases in Cx43, all of which have been previously reported to be activated by IL-1 β stimulation (Baum et al. 2012a; Niger et al. 2010; Weber et al. 2010; Yang et al. 2000). Additionally, JNK inhibition, also known to be activated by IL-1 β (Niger et al. 2010), was found to enhance IL-1 β -induced Cx43 up-regulation, suggesting JNK acts to inhibit IL-1 β -mediated increases in Cx43. Moreover, the investigation into miRNAs either predicted (by target scan) or verified to target Cx43 (Danielson et al. 2013; Jin et al. 2013) as well as miRNAs known to be regulated by proinflammatory cytokines (Georgantas et al. 2014; Wang et al. 2014b), revealed no role for miR-1, -19b, -30c, -101, -125b or -133a in IL-1 β -induced upregulation of Cx43.

Furthermore, as IL-1 β has been reported to inhibit TGF β 1-mediated fibroblast to MF differentiation (Bronnum et al. 2013; Mia et al. 2014; Saxena et al. 2013), the effects of IL-1 β alone or in combination with TGF β 1 stimulation on the mRNA levels of known TGF β 1-regulated genes was investigated. Indeed, IL-1 β was found to significantly reduce the expression of the MF markers, CTGF and α SMA, as well as significantly inhibit the TGF β 1-mediated increase in CTGF and trend for α SMA upregulation. This suggests that IL-1 β -treated RACFs are less MF-like than control RACFs, and therefore important to consider in the co-culture model.

To investigate the effects of control and IL-1 β -treated adult RACFs on adult CM function, a CM: CF co-culture model was established. In this model, evidence for functional GJs between adult CM and CF was provided by calcein dye transfer, in agreement with other reports (Chilton et al. 2007; Driesen et al. 2005). Furthermore, CMs cultured for 24 h maintained contractile and electrical activity in response to stimulus, although there appeared to be a trend for prolongation of the APD₈₀ in comparison to freshly isolated cells. Similarly this trend was reported in swine CMs following 24 h in culture, which reached significance at 72 h (Louch et al. 2004), supporting culture-mediated alterations in the electrical activity of CMs. Interestingly, the CD of cultured CMs was significantly reduced in the presence of a RACF monolayer. Despite this, RACFs induced a trend for APD₈₀ prolongation in comparison to CMs in culture alone. Furthermore, RACFs treated

with IL-1 β which had previously been shown to have enhanced Cx43 levels as well as reduced mRNA levels of the MF markers, α SMA and CTGF, partly restored the effects of RACFs on CD. Together these results indicate that CFs can modify the function of CMs, however further studies are required to identify mechanisms involved.

Next, a model to assess CM: CF interactions *in situ* was developed where RACFs transduced with LVeGFP were injected into the wall of the left ventricle. Injected cells were found to be retained in the myocardium 7 days following injection as detected by eGFP fluorescence on the surface of the intact heart and in IHC using an anti-eGFP antibody. Additionally, an AdeGFP was injected so that the area of injection could be clearly identified, following AdeGFP transduction of CMs *in situ*. APs were successfully recorded over the epicardial surface and areas of the myocardium injected with RACFs transduced with LVeGFP, or following direct gene delivery of AdeGFP, compared to other regions of the heart. Preliminary evidence for prolongation of APD₈₀ following the S2 impulse in the injection sites in comparison to a site which was activated at approximately equivalent time and of identical shape (remote region 3) was detected. Additionally, in two hearts, one from each group, a change in the activation pattern following S2 impulse was observed close to the injection sites. However, as this prolongation and alteration in the pattern of activation was detected in both groups; it may reflect damage to the myocardium during injection.

7.2 Future perspectives

The co-culture model utilised within this thesis allows many interactions between the cells to occur, including those of a paracrine, mechanical and electrical nature, due to media sharing and direct contact allowing the formation of mechanical and GJs. Therefore, it is challenging to interpret what is responsible for the results observed, hence further studies are required to dissect potential mechanisms. To investigate paracrine interactions, the media from co-culture could be compared to that of cultured CMs or CFs by performing cytometric bead array using flow cytometry (O'Carroll et al. 2015). This would allow up to 30 different cytokines/growth factors to be evaluated simultaneously to identify potential candidates to investigate further. The transwell set up used by Cartledge

et al. (2015) revealed a bidirectional TGF β interaction between adult CMs and CFs promoting a faster decay of the CM Ca²⁺ transient (Cartledge *et al.* 2015). This could therefore explain the current results of reduced CD in the presence of CFs due to the role of Ca²⁺ in CM contraction (Bers 2002), hence the levels of TGF β should be evaluated.

As IL-1 β levels are enhanced in cardiac disease, the IL-1 β -treated RACFs investigated in the current study could be thought to represent a population of CFs within the heart in pathophysiological settings. IL-1 β may act to suppress CF activation allowing the inflammatory stage to occur prior to the profibrotic phase of cardiac repair (Saxena *et al.* 2013). Furthermore, control untreated RACFs are likely to be more MF-like than IL-1 β treated RACFs, which is interesting due to their greater effect observed on CM function in comparison to IL-1 β -treated RACF. Therefore, the role of the RACF phenotype could be further investigated in the CM co-culture model by treatment of RACFs with TGF β 1, a major driver of the MF phenotype (Bronnum *et al.* 2013; Mia *et al.* 2014; Saxena *et al.* 2013). Indeed, recently TGF β 1 has been shown to enhance the proarrhythmic nature of CFs on CMs in a neonatal cell culture model, by causing depolarisation of the RMP of CMs and promoting increased ectopic activity (Salvarani *et al.* 2017). These effects in neonatal preparations were attributed to direct heterocellular coupling (Salvarani *et al.* 2017). These observations, together with the results of the current study, support the rational that a greater MF phenotype has an enhanced influence on CM function.

Although IL-1 β promoted an increase in Cx43 expression at the cell surface, the ability of Cx43 to enhance GJIC either within RACF monolayers or between CMs and RACFs requires examination. GJ coupling in monolayers of RACFs could be assessed by scrape-loading RACFs with Lucifer yellow, a dye able to pass through functional GJs, and examining the distance travelled over a set time (Louault *et al.* 2008; Tarzeman *et al.* 2015). A pilot study to establish this assay in RACFs demonstrated issues with Lucifer yellow uptake/detection therefore requires further optimisation to investigate GJ coupling in these cells. Furthermore, calcein dye transfer (as investigated in this thesis) could be performed following IL-1 β stimulation of RACFs. Additionally, RACFs could be transduced with the

AdCx43 produced in the current study to directly assess the effects of enhanced Cx43 expression in RACFs in comparison to control cells and cells transduced with a control Ad vector.

The electrophysiological influence of CFs on CMs may also depend on the expression of different ion channels/pumps (Chilton et al. 2005; Li et al. 2009; Salvarani et al. 2017). Interestingly, neonatal CFs treated with TGF β 1, which induced a depolarising effect on neonatal CMs, were shown to differ in ion channels/pumps and connexin transcripts in comparison to CFs treated with the TGF β R1 inhibitor (Salvarani et al. 2017). Amongst these transcripts, the expression of many K⁺ channel/subunits were up or down regulated as well as an increase in the sodium leak channel, which had previously not been reported to be present in CFs (Salvarani et al. 2017). This channel has been found to promote depolarisation of neurons therefore may contribute to TGF β 1-mediated CF depolarisation (Lu et al. 2007). Similarly, the RNA sequencing used in the previous mentioned study could be another interesting aspect to examine in control and IL-1 β -treated cultures. Furthermore, measurement of Ca²⁺ transients in CMs would be beneficial to potentially explain the effect on CD of control and IL-1 β treated RACFs, due to the well-established role of Ca²⁺ in contraction (Bers 2002).

Restriction of contraction by mechanical pull of CMs by RACFs is another potential cause for the differential effects of control RACFs and IL-1 β treated RACFs on CD due to reduced expression of the contractile protein, α SMA by IL-1 β . However, it must be noted that only mRNA levels of α SMA were examined in the current study and others have reported no change in the protein level following 48 h stimulation with IL-1 β , despite reduced levels of mRNA (Bronnum et al. 2013). Therefore, α SMA protein in the current study requires evaluation to support this hypothesis. Additionally, the role of α SMA in RACFs on CM CD effects could be examined with the use of actin targeting drugs (ATDs) such as Latrunculin B, Cytochalasin D or Jasplakinolide. These ATDs have previously been shown to successfully disrupt α SMA fibers in neonatal CFs but have no obvious effects on neonatal CMs (Rosker et al. 2011). Additionally, these drugs were shown to reduce the slowing of CV, ectopic activity and the depolarising effect of CFs in this neonatal model (Rosker et al. 2011). Therefore, this suggests that α SMA expression in CFs has a role in

electrophysiological effects on CMs; hence examination of the effect of ATDs on the trend for APD₈₀ prolongation would also be interesting.

This study has utilised CMs from healthy hearts, therefore it would be interesting to examine if RACFs can potentiate already dysfunctional CMs from diseased hearts (Li et al. 2004;Loennechen et al. 2002). Similarly, CFs from diseased hearts could be examined in co-culture, although caution is required due to reports that cells begin to lose their pathogenic phenotype in culture (Dawson et al. 2012). The effect of culture on the phenotype of RACFs is also a limitation to the current study. Additionally, rodent CMs differ to human cells, with respect to Ca²⁺ handling and AP shape. For instance, SERCA contribution to Ca²⁺ removal from the cytosol has been reported to be 90-92 % in rodent CMs (Bassani et al. 1994;Li et al. 1998) and 77 % in human CMs (Piacentino et al. 2003). Furthermore, there is little to no AP plateau in rodent CMs versus a defined plateau in human CMs (Li et al. 2004;Varro et al. 1993). Therefore cells from a more comparable species such as rabbit or guinea-pig could be used as an alternative (Bers 2002;Varro et al. 1993).

The extent of damage caused by direct intramyocardial injection could be assessed by picosirius red staining of the collagen network (Xia et al. 2009), determination of the levels of apoptosis/necrosis of CMs and assessment of the degree of inflammatory response produced. Due to the difficulty of injecting a fast paced rat heart, any damage may be unavoidable and reflect baseline effects of surgery demonstrating the importance of the AdeGFP control. Ideally this control would be injection of the equivalent volume of PBS; however this would make identification of the injected site using OM challenging. Further analysis could involve examination of CV across the area of injection as well as alternans; parameters which can be assessed within the OPTIQ software utilised in the current study.

The use of two-photon microscopy would give more detailed information on the effects, if any, of CM: CF coupling *in situ* and should be considered for future studies. Two-photon microscopy relies on two low energy long wavelength photons being absorbed simultaneously resulting in excitation of the fluorophore (Rubart 2004). As two photons meet at a single plane within the tissue and are both required to produce fluorescence, no out of focus signal is produced (Rubart

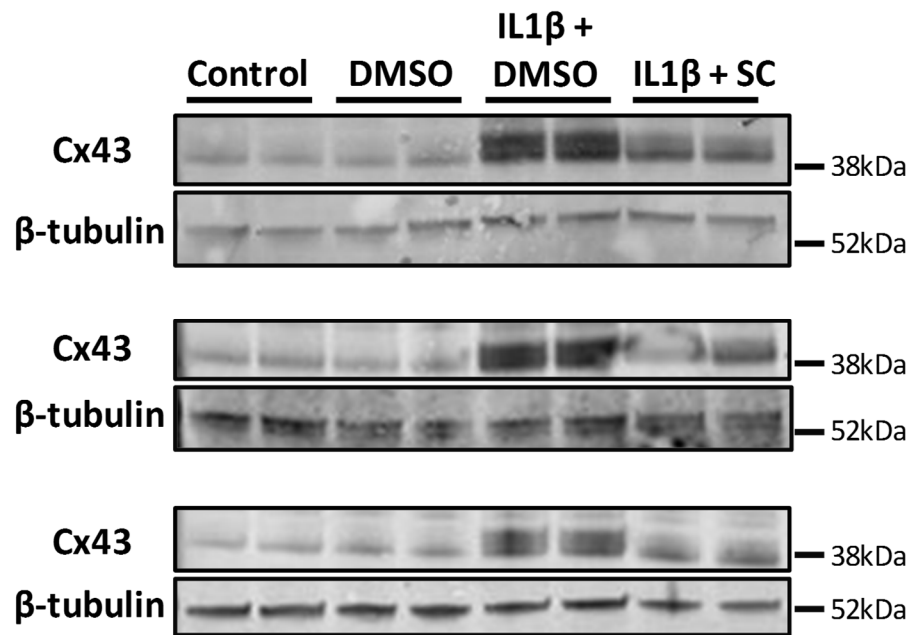
2004). Ultimately this allows single cells deep within the intact heart to be monitored for functional parameters such as APs or Ca^{2+} transients (Ghoury et al. 2015). This technique has previously been used following direct cell injection of eGFP labelled foetal CMs or SMs (Rubart et al. 2003; Rubart et al. 2004). Here, Ca^{2+} transients of donor and adjacent host CMs were assessed to determine the levels of coupling (Rubart et al. 2003; Rubart et al. 2004), therefore is ideal preparation for the current study.

Although thus far, no differences have been identified between RACF and AdeGFP injected hearts, further studies could evaluate the effects of implantation of RACFs with different phenotypes. For instance, implantation of RACFs dual transduced with AdCx43 and LVeGFP would allow the direct effects of enhanced Cx43 levels in CFs, seen post-MI (Vasquez et al. 2010; Zhang et al. 2010), to be examined. Interestingly, it has been reported that injection of SMs overexpressing Cx43 into the scar of mice is anti-arrhythmic by reducing the vulnerability of the scar (Roell et al. 2007). However, taking into account the proarrhythmic effects of Cx43 expression in CFs *in vitro*, injection of CFs may produce differential effects and remains to be examined. Additionally, implantation of RACFs treated with different individual cytokines, potentially IL-1 β or TGF β 1, would be interesting to examine. However, the phenotypes these treated RACFs *in vivo* may not be sustained over 7 days, therefore earlier time points may have to be examined.

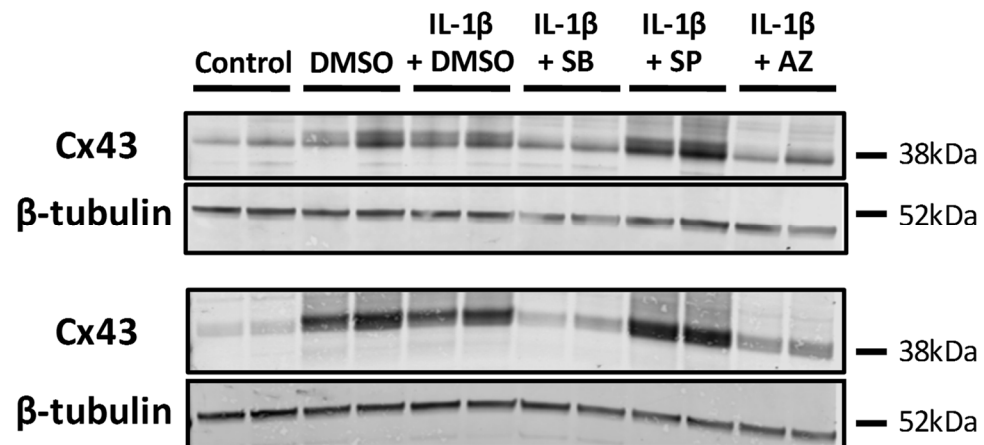
7.3 Conclusions

In summary, the data from this thesis has provided further evidence for the ability of CFs to alter the function of CMs. Additionally, for the first time, the treatment of RACFs with IL-1 β was shown to partially restore the effects of RACFs on CD. Furthermore, a technically challenging model that will be valuable in the future investigation of CM: CF heterocellular coupling *in situ* has been established.

Appendix



Appendix figure 1 Immunoblots which constitute densitometry in figure 4-7.



Appendix figure 2 Immunoblots which constitute densitometry in figure 4-9.

List of References

- Adam, O., Lavall, D., Theobald, K., Hohl, M., Grube, M., Ameling, S., Sussman, M.A., Rosenkranz, S., Kroemer, H.K., Schafers, H.J., Bohm, M., & Laufs, U. (2010). Rac1-induced connective tissue growth factor regulates connexin 43 and N-cadherin expression in atrial fibrillation. *J.Am.Coll.Cardiol.*, 55, (5) 469-480
- Ai, X. & Pogwizd, S.M. (2005). Connexin 43 downregulation and dephosphorylation in nonischemic heart failure is associated with enhanced colocalized protein phosphatase type 2A. *Circ.Res.*, 96, (1) 54-63
- Alba, R., Baker, A.H., & Nicklin, S.A. (2012). Vector systems for prenatal gene therapy: principles of adenovirus design and production. *Methods Mol.Biol.*, 891, 55-84
- Alonso, F., Krattinger, N., Mazzolai, L., Simon, A., Waeber, G., Meda, P., & Haefliger, J.A. (2010). An angiotensin II- and NF-kappaB-dependent mechanism increases connexin 43 in murine arteries targeted by renin-dependent hypertension. *Cardiovasc.Res.*, 87, (1) 166-176
- Anderson, R.D., Haskell, R.E., Xia, H., Roessler, B.J., & Davidson, B.L. (2000). A simple method for the rapid generation of recombinant adenovirus vectors. *Gene Ther.*, 7, (12) 1034-1038
- Angst, B.D., Khan, L.U., Severs, N.J., Whitely, K., Rothery, S., Thompson, R.P., Magee, A.I., & Gourdie, R.G. (1997). Dissociated spatial patterning of gap junctions and cell adhesion junctions during postnatal differentiation of ventricular myocardium. *Circ.Res.*, 80, (1) 88-94
- Antoons, G. & Sipido, K.R. (2008). Targeting calcium handling in arrhythmias. *Europace.*, 10, (12) 1364-1369
- Antzelevitch, C. (2010). M cells in the human heart. *Circ.Res.*, 106, (5) 815-817
- Asazuma-Nakamura, Y., Dai, P., Harada, Y., Jiang, Y., Hamaoka, K., & Takamatsu, T. (2009). Cx43 contributes to TGF-beta signaling to regulate differentiation of cardiac fibroblasts into myofibroblasts. *Exp.Cell Res.*, 315, (7) 1190-1199
- Askar, S.F., Bingen, B.O., Swildens, J., Ypey, D.L., van der Laarse, A., Atsma, D.E., Zeppenfeld, K., Schalij, M.J., de Vries, A.A., & Pijnappels, D.A. (2012). Connexin43 silencing in myofibroblasts prevents arrhythmias in myocardial cultures: role of maximal diastolic potential. *Cardiovasc.Res.*, 93, (3) 434-444
- Askar, S.F., Ramkisoensing, A.A., Schalij, M.J., Bingen, B.O., Swildens, J., van der Laarse, A., Atsma, D.E., de Vries, A.A., Ypey, D.L., & Pijnappels, D.A. (2011). Antiproliferative treatment of myofibroblasts prevents arrhythmias in vitro by limiting myofibroblast-induced depolarization. *Cardiovasc.Res.*, 90, (2) 295-304
- Axelsen, L.N., Stahlhut, M., Mohammed, S., Larsen, B.D., Nielsen, M.S., Holstein-Rathlou, N.H., Andersen, S., Jensen, O.N., Hennan, J.K., & Kjolbye, A.L. (2006). Identification of ischemia-regulated phosphorylation sites in connexin43: A

possible target for the antiarrhythmic peptide analogue rotigaptide (ZP123). *J.Mol.Cell Cardiol.*, 40, (6) 790-798

Badenhorst, D., Maseko, M., Tsotetsi, O.J., Naidoo, A., Brooksbank, R., Norton, G.R., & Woodiwiss, A.J. (2003). Cross-linking influences the impact of quantitative changes in myocardial collagen on cardiac stiffness and remodelling in hypertension in rats. *Cardiovasc.Res.*, 57, (3) 632-641

Bai, J., Zhang, N., Hua, Y., Wang, B., Ling, L., Ferro, A., & Xu, B. (2013). Metformin inhibits angiotensin II-induced differentiation of cardiac fibroblasts into myofibroblasts. *PLoS.One.*, 8, (9) e72120

Baker, L.C., Wolk, R., Choi, B.R., Watkins, S., Plan, P., Shah, A., & Salama, G. (2004). Effects of mechanical uncouplers, diacetyl monoxime, and cytochalasin-D on the electrophysiology of perfused mouse hearts. *Am.J.Physiol Heart Circ.Physiol*, 287, (4) H1771-H1779

Banerjee, I., Fuseler, J.W., Price, R.L., Borg, T.K., & Baudino, T.A. (2007). Determination of cell types and numbers during cardiac development in the neonatal and adult rat and mouse. *Am.J.Physiol Heart Circ.Physiol*, 293, (3) H1883-H1891

Bang, C., Batkai, S., Dangwal, S., Gupta, S.K., Foinquinos, A., Holzmann, A., Just, A., Remke, J., Zimmer, K., Zeug, A., Ponimaskin, E., Schmiedl, A., Yin, X., Mayr, M., Halder, R., Fischer, A., Engelhardt, S., Wei, Y., Schober, A., Fiedler, J., & Thum, T. (2014). Cardiac fibroblast-derived microRNA passenger strand-enriched exosomes mediate cardiomyocyte hypertrophy. *J.Clin.Invest*, 124, (5) 2136-2146

Barrio, L.C., Capel, J., Jarillo, J.A., Castro, C., & Revilla, A. (1997). Species-specific voltage-gating properties of connexin-45 junctions expressed in *Xenopus* oocytes. *Biophys.J.*, 73, (2) 757-769

Bassani, J.W., Bassani, R.A., & Bers, D.M. (1994). Relaxation in rabbit and rat cardiac cells: species-dependent differences in cellular mechanisms. *J.Physiol*, 476, (2) 279-293

Baum, J.R., Dolmatova, E., Tan, A., & Duffy, H.S. (2012a). Omega 3 fatty acid inhibition of inflammatory cytokine-mediated Connexin43 regulation in the heart. *Front Physiol*, 3, 272

Baum, J.R., Long, B., Cabo, C., & Duffy, H.S. (2012b). Myofibroblasts cause heterogeneous Cx43 reduction and are unlikely to be coupled to myocytes in the healing canine infarct. *Am.J.Physiol Heart Circ.Physiol*, 302, (3) H790-H800

Beardslee, M.A., Laing, J.G., Beyer, E.C., & Saffitz, J.E. (1998). Rapid turnover of connexin43 in the adult rat heart. *Circ.Res.*, 83, (6) 629-635

Beardslee, M.A., Lerner, D.L., Tadros, P.N., Laing, J.G., Beyer, E.C., Yamada, K.A., Kleber, A.G., Schuessler, R.B., & Saffitz, J.E. (2000). Dephosphorylation and intracellular redistribution of ventricular connexin43 during electrical uncoupling induced by ischemia. *Circ.Res.*, 87, (8) 656-662

- Becker, D.E. (2006). Fundamentals of electrocardiography interpretation. *Anesth.Prog.*, 53, (2) 53-63
- Bers, D.M. (2002). Cardiac excitation-contraction coupling. *Nature*, 415, (6868) 198-205
- Beuckelmann, D.J., Nabauer, M., & Erdmann, E. (1992). Intracellular calcium handling in isolated ventricular myocytes from patients with terminal heart failure. *Circulation*, 85, (3) 1046-1055
- Beuckelmann, D.J., Nabauer, M., & Erdmann, E. (1993). Alterations of K⁺ currents in isolated human ventricular myocytes from patients with terminal heart failure. *Circ.Res.*, 73, (2) 379-385
- Bie, Z.D., Sun, L.Y., Geng, C.L., Meng, Q.G., Lin, X.J., Wang, Y.F., Wang, X.B., & Yang, J. (2016). MiR-125b regulates SFRP5 expression to promote growth and activation of cardiac fibroblasts. *Cell Biol.Int.*, 40, (11) 1224-1234
- Biswas, H. & Longmore, G.D. (2016). Action of SNAIL1 in Cardiac Myofibroblasts Is Important for Cardiac Fibrosis following Hypoxic Injury. *PLoS.One.*, 11, (10) e0162636
- Bochaton-Piallat, M.L., Gabbiani, G., & Hinz, B. (2016). The myofibroblast in wound healing and fibrosis: answered and unanswered questions. *F1000Res.*, 5,
- Boettger, T., Beetz, N., Kostin, S., Schneider, J., Kruger, M., Hein, L., & Braun, T. (2009). Acquisition of the contractile phenotype by murine arterial smooth muscle cells depends on the Mir143/145 gene cluster. *J.Clin.Invest*, 119, (9) 2634-2647
- Boom, R., Sol, C.J., Salimans, M.M., Jansen, C.L., Wertheim-van Dillen, P.M., & van der Noordaa, J. (1990). Rapid and simple method for purification of nucleic acids. *J.Clin.Microbiol.*, 28, (3) 495-503
- Bouard, D., Alazard-Dany, D., & Cosset, F.L. (2009). Viral vectors: from virology to transgene expression. *Br.J.Pharmacol.*, 157, (2) 153-165
- Boulaksil, M., Bierhuizen, M.F., Engelen, M.A., Stein, M., Kok, B.J., van Amersfoort, S.C., Vos, M.A., van Rijen, H.V., de Bakker, J.M., & van Veen, T.A. (2016). Spatial Heterogeneity of Cx43 is an Arrhythmogenic Substrate of Polymorphic Ventricular Tachycardias during Compensated Cardiac Hypertrophy in Rats. *Front Cardiovasc.Med.*, 3, 5
- Bronnum, H., Eskildsen, T., Andersen, D.C., Schneider, M., & Sheikh, S.P. (2013). IL-1beta suppresses TGF-beta-mediated myofibroblast differentiation in cardiac fibroblasts. *Growth Factors*, 31, (3) 81-89
- Bueno, O.F., De Windt, L.J., Tymitz, K.M., Witt, S.A., Kimball, T.R., Klevitsky, R., Hewett, T.E., Jones, S.P., Lefer, D.J., Peng, C.F., Kitsis, R.N., & Molkentin, J.D. (2000). The MEK1-ERK1/2 signaling pathway promotes compensated cardiac hypertrophy in transgenic mice. *EMBO J.*, 19, (23) 6341-6350

- Bujak, M., Dobaczewski, M., Chatila, K., Mendoza, L.H., Li, N., Reddy, A., & Frangogiannis, N.G. (2008). Interleukin-1 receptor type I signaling critically regulates infarct healing and cardiac remodeling. *Am.J.Pathol.*, 173, (1) 57-67
- Bujak, M. & Frangogiannis, N.G. (2009). The role of IL-1 in the pathogenesis of heart disease. *Arch.Immunol.Ther.Exp.(Warsz.)*, 57, (3) 165-176
- Bukauskas, F.F., Bukauskiene, A., & Verselis, V.K. (2002). Conductance and permeability of the residual state of connexin43 gap junction channels. *J.Gen.Physiol*, 119, (2) 171-185
- Bukauskas, F.F. & Verselis, V.K. (2004). Gap junction channel gating. *Biochim.Biophys.Acta*, 1662, (1-2) 42-60
- Bunch, T.J., Mahapatra, S., Bruce, G.K., Johnson, S.B., Miller, D.V., Horne, B.D., Wang, X.L., Lee, H.C., Caplice, N.M., & Packer, D.L. (2006). Impact of transforming growth factor-beta1 on atrioventricular node conduction modification by injected autologous fibroblasts in the canine heart. *Circulation*, 113, (21) 2485-2494
- Burchfield, J.S., Xie, M., & Hill, J.A. (2013). Pathological ventricular remodeling: mechanisms: part 1 of 2. *Circulation*, 128, (4) 388-400
- Burns, R.J., Gibbons, R.J., Yi, Q., Roberts, R.S., Miller, T.D., Schaer, G.L., Anderson, J.L., & Yusuf, S. (2002). The relationships of left ventricular ejection fraction, end-systolic volume index and infarct size to six-month mortality after hospital discharge following myocardial infarction treated by thrombolysis. *J.Am.Coll.Cardiol.*, 39, (1) 30-36
- Burton, F.L. & Cobbe, S.M. (2001). Dispersion of ventricular repolarization and refractory period. *Cardiovasc.Res.*, 50, (1) 10-23
- Camelliti, P., Borg, T.K., & Kohl, P. (2005a). Structural and functional characterisation of cardiac fibroblasts. *Cardiovasc.Res.*, 65, (1) 40-51
- Camelliti, P., Devlin, G.P., Matthews, K.G., Kohl, P., & Green, C.R. (2004a). Spatially and temporally distinct expression of fibroblast connexins after sheep ventricular infarction. *Cardiovasc.Res.*, 62, (2) 415-425
- Camelliti, P., Green, C.R., LeGrice, I., & Kohl, P. (2004b). Fibroblast network in rabbit sinoatrial node: structural and functional identification of homogeneous and heterogeneous cell coupling. *Circ.Res.*, 94, (6) 828-835
- Camelliti, P., McCulloch, A.D., & Kohl, P. (2005b). Microstructured cocultures of cardiac myocytes and fibroblasts: a two-dimensional in vitro model of cardiac tissue. *Microsc.Microanal.*, 11, (3) 249-259
- Campbell, S.E. & Katwa, L.C. (1997). Angiotensin II stimulated expression of transforming growth factor-beta1 in cardiac fibroblasts and myofibroblasts. *J.Mol.Cell Cardiol.*, 29, (7) 1947-1958
- Cardin, S., Guasch, E., Luo, X., Naud, P., Le, Q.K., Shi, Y., Tardif, J.C., Comtois, P., & Nattel, S. (2012). Role for MicroRNA-21 in atrial profibrillatory fibrotic

- remodeling associated with experimental postinfarction heart failure. *Circ.Arrhythm.Electrophysiol.*, 5, (5) 1027-1035
- Cardullo, R.A., Agrawal, S., Flores, C., Zamecnik, P.C., & Wolf, D.E. (1988). Detection of nucleic acid hybridization by nonradiative fluorescence resonance energy transfer. *Proc.Natl.Acad.Sci.U.S.A*, 85, (23) 8790-8794
- Carneiro, F.A., Bianconi, M.L., Weissmuller, G., Stauffer, F., & Da Poian, A.T. (2002). Membrane recognition by vesicular stomatitis virus involves enthalpy-driven protein-lipid interactions. *J.Virol.*, 76, (8) 3756-3764
- Cartledge, J.E., Kane, C., Dias, P., Tesfom, M., Clarke, L., Mckee, B., Al, A.S., Chester, A., Yacoub, M.H., Camelliti, P., & Terracciano, C.M. (2015). Functional crosstalk between cardiac fibroblasts and adult cardiomyocytes by soluble mediators. *Cardiovasc.Res.*, 105, (3) 260-270
- Chaturvedi, R.R., Herron, T., Simmons, R., Shore, D., Kumar, P., Sethia, B., Chua, F., Vassiliadis, E., & Kentish, J.C. (2010). Passive stiffness of myocardium from congenital heart disease and implications for diastole. *Circulation*, 121, (8) 979-988
- Chen, F., Mottino, G., Klitzner, T.S., Philipson, K.D., & Frank, J.S. (1995a). Distribution of the Na⁺/Ca²⁺ exchange protein in developing rabbit myocytes. *Am.J.Physiol*, 268, (5 Pt 1) C1126-C1132
- Chen, M.M., Lam, A., Abraham, J.A., Schreiner, G.F., & Joly, A.H. (2000). CTGF expression is induced by TGF- beta in cardiac fibroblasts and cardiac myocytes: a potential role in heart fibrosis. *J.Mol.Cell Cardiol.*, 32, (10) 1805-1819
- Chen, Z.J. (2005). Ubiquitin signalling in the NF-kappaB pathway. *Nat.Cell Biol.*, 7, (8) 758-765
- Chen, Z.Q., Lefebvre, D., Bai, X.H., Reaume, A., Rossant, J., & Lye, S.J. (1995b). Identification of two regulatory elements within the promoter region of the mouse connexin 43 gene. *J.Biol.Chem.*, 270, (8) 3863-3868
- Chilton, L., Giles, W.R., & Smith, G.L. (2007). Evidence of intercellular coupling between co-cultured adult rabbit ventricular myocytes and myofibroblasts. *J.Physiol*, 583, (Pt 1) 225-236
- Chilton, L., Ohya, S., Freed, D., George, E., Drobic, V., Shibukawa, Y., Maccannell, K.A., Imaizumi, Y., Clark, R.B., Dixon, I.M., & Giles, W.R. (2005). K⁺ currents regulate the resting membrane potential, proliferation, and contractile responses in ventricular fibroblasts and myofibroblasts. *Am.J.Physiol Heart Circ.Physiol*, 288, (6) H2931-H2939
- Cho, H.C., Kashiwakura, Y., & Marban, E. (2007). Creation of a biological pacemaker by cell fusion. *Circ.Res.*, 100, (8) 1112-1115
- Choi, B.R. & Salama, G. (2000). Simultaneous maps of optical action potentials and calcium transients in guinea-pig hearts: mechanisms underlying concordant alternans. *J.Physiol*, 529 Pt 1, 171-188

Chou, C.C., Chang, P.C., Wei, Y.C., & Lee, K.Y. (2017). Optical Mapping Approaches on Muscleblind-Like Compound Knockout Mice for Understanding Mechanistic Insights Into Ventricular Arrhythmias in Myotonic Dystrophy. *J.Am.Heart Assoc.*, 6, (4)

Christman, K.L., Vardanian, A.J., Fang, Q., Sievers, R.E., Fok, H.H., & Lee, R.J. (2004). Injectable fibrin scaffold improves cell transplant survival, reduces infarct expansion, and induces neovasculature formation in ischemic myocardium. *J.Am.Coll.Cardiol.*, 44, (3) 654-660

Clancy, R.M., Zheng, P., O'Mahony, M., Izmirly, P., Zavadil, J., Gardner, L., & Buyon, J.P. (2007). Role of hypoxia and cAMP in the transdifferentiation of human fetal cardiac fibroblasts: implications for progression to scarring in autoimmune-associated congenital heart block. *Arthritis Rheum.*, 56, (12) 4120-4131

Cleutjens, J.P., Kandala, J.C., Guarda, E., Guntaka, R.V., & Weber, K.T. (1995a). Regulation of collagen degradation in the rat myocardium after infarction. *J.Mol.Cell Cardiol.*, 27, (6) 1281-1292

Cleutjens, J.P., Verluyten, M.J., Smiths, J.F., & Daemen, M.J. (1995b). Collagen remodeling after myocardial infarction in the rat heart. *Am.J.Pathol.*, 147, (2) 325-338

Cohn, J.N., Ferrari, R., & Sharpe, N. (2000). Cardiac remodeling--concepts and clinical implications: a consensus paper from an international forum on cardiac remodeling. Behalf of an International Forum on Cardiac Remodeling. *J.Am.Coll.Cardiol.*, 35, (3) 569-582

Coil, D.A. & Miller, A.D. (2004). Phosphatidylserine is not the cell surface receptor for vesicular stomatitis virus. *J.Virol.*, 78, (20) 10920-10926

Connolly, S.J., Camm, A.J., Halperin, J.L., Joyner, C., Alings, M., Amerena, J., Atar, D., Avezum, A., Blomstrom, P., Borggrefe, M., Budaj, A., Chen, S.A., Ching, C.K., Commerford, P., Dans, A., Davy, J.M., Delacretaz, E., Di, P.G., Diaz, R., Dorian, P., Flaker, G., Golitsyn, S., Gonzalez-Hermosillo, A., Granger, C.B., Heidbuchel, H., Kautzner, J., Kim, J.S., Lanus, F., Lewis, B.S., Merino, J.L., Morillo, C., Murin, J., Narasimhan, C., Paolasso, E., Parkhomenko, A., Peters, N.S., Sim, K.H., Stiles, M.K., Tanomsup, S., Toivonen, L., Tomcsanyi, J., Torp-Pedersen, C., Tse, H.F., Vardas, P., Vinereanu, D., Xavier, D., Zhu, J., Zhu, J.R., Baret-Cormel, L., Weinling, E., Staiger, C., Yusuf, S., Chrolavicius, S., Afzal, R., & Hohnloser, S.H. (2011). Dronedarone in high-risk permanent atrial fibrillation. *N.Engl.J.Med.*, 365, (24) 2268-2276

Connolly, S.J., Dorian, P., Roberts, R.S., Gent, M., Bailin, S., Fain, E.S., Thorpe, K., Champagne, J., Talajic, M., Coutu, B., Gronefeld, G.C., & Hohnloser, S.H. (2006). Comparison of beta-blockers, amiodarone plus beta-blockers, or sotalol for prevention of shocks from implantable cardioverter defibrillators: the OPTIC Study: a randomized trial. *JAMA*, 295, (2) 165-171

Connolly, S.J., Hallstrom, A.P., Cappato, R., Schron, E.B., Kuck, K.H., Zipes, D.P., Greene, H.L., Boczor, S., Domanski, M., Follmann, D., Gent, M., & Roberts, R.S. (2000). Meta-analysis of the implantable cardioverter defibrillator secondary prevention trials. AVID, CASH and CIDS studies. Antiarrhythmics vs Implantable

Defibrillator study. Cardiac Arrest Study Hamburg . Canadian Implantable Defibrillator Study. *Eur.Heart J.*, 21, (24) 2071-2078

Cooley, B.C., Nevado, J., Mellad, J., Yang, D., St, H.C., Negro, A., Fang, F., Chen, G., San, H., Walts, A.D., Schwartzbeck, R.L., Taylor, B., Lanzer, J.D., Wragg, A., Elagha, A., Beltran, L.E., Berry, C., Feil, R., Virmani, R., Ladich, E., Kovacic, J.C., & Boehm, M. (2014). TGF-beta signaling mediates endothelial-to-mesenchymal transition (EndMT) during vein graft remodeling. *Sci.Transl.Med.*, 6, (227) 227ra34

Coppen, S.R., Fukushima, S., Shintani, Y., Takahashi, K., Varela-Carver, A., Salem, H., Yashiro, K., Yacoub, M.H., & Suzuki, K. (2008). A factor underlying late-phase arrhythmogenicity after cell therapy to the heart: global downregulation of connexin43 in the host myocardium after skeletal myoblast transplantation. *Circulation*, 118, (14 Suppl) S138-S144

Crossman, D.J., Ruygrok, P.N., Soeller, C., & Cannell, M.B. (2011). Changes in the organization of excitation-contraction coupling structures in failing human heart. *PLoS.One.*, 6, (3) e17901

Curcio, A., Torella, D., Iaconetti, C., Pasceri, E., Sabatino, J., Sorrentino, S., Giampa, S., Micieli, M., Polimeni, A., Henning, B.J., Leone, A., Catalucci, D., Ellison, G.M., Condorelli, G., & Indolfi, C. (2013). MicroRNA-1 downregulation increases connexin 43 displacement and induces ventricular tachyarrhythmias in rodent hypertrophic hearts. *PLoS.One.*, 8, (7) e70158

Czubryt, M.P. (2012). Common threads in cardiac fibrosis, infarct scar formation, and wound healing. *Fibrogenesis.Tissue Repair*, 5, (1) 19

D'Angelo, D.D., Sakata, Y., Lorenz, J.N., Boivin, G.P., Walsh, R.A., Liggett, S.B., & Dorn, G.W. (1997). Transgenic Galphaq overexpression induces cardiac contractile failure in mice. *Proc.Natl.Acad.Sci.U.S.A*, 94, (15) 8121-8126

Damasceno, D.D., Lima, M.P., Motta, D.F., Ferreira, A.J., Quintao-Junior, J.F., Drummond, L.R., Natali, A.J., Almeida, A.P., & Pesquero, J.L. (2013). Cardiovascular and electrocardiographic parameters after tonin administration in Wistar rats. *Regul.Pept.*, 181, 30-36

Dandapat, A., Hu, C.P., Li, D., Liu, Y., Chen, H., Hermonat, P.L., & Mehta, J.L. (2008). Overexpression of TGFbeta1 by adeno-associated virus type-2 vector protects myocardium from ischemia-reperfusion injury. *Gene Ther.*, 15, (6) 415-423

Daniels, A., van, B.M., Goldschmeding, R., van der Vusse, G.J., & van Nieuwenhoven, F.A. (2009). Connective tissue growth factor and cardiac fibrosis. *Acta Physiol (Oxf)*, 195, (3) 321-338

Danielson, L.S., Park, D.S., Rotllan, N., Chamorro-Jorganes, A., Guijarro, M.V., Fernandez-Hernando, C., Fishman, G.I., Phoon, C.K., & Hernando, E. (2013). Cardiovascular dysregulation of miR-17-92 causes a lethal hypertrophic cardiomyopathy and arrhythmogenesis. *FASEB J.*, 27, (4) 1460-1467

Danthinne, X. & Imperiale, M.J. (2000). Production of first generation adenovirus vectors: a review. *Gene Ther.*, 7, (20) 1707-1714

- Dash, R., Frank, K.F., Carr, A.N., Moravec, C.S., & Kranias, E.G. (2001). Gender influences on sarcoplasmic reticulum Ca²⁺-handling in failing human myocardium. *J.Mol.Cell Cardiol.*, 33, (7) 1345-1353
- Davis, H.E., Morgan, J.R., & Yarmush, M.L. (2002). Polybrene increases retrovirus gene transfer efficiency by enhancing receptor-independent virus adsorption on target cell membranes. *Biophys.Chem.*, 97, (2-3) 159-172
- Dawson, K., Wu, C.T., Qi, X.Y., & Nattel, S. (2012). Congestive heart failure effects on atrial fibroblast phenotype: differences between freshly-isolated and cultured cells. *PLoS.One.*, 7, (12) e52032
- de Groot, J.R., Veenstra, T., Verkerk, A.O., Wilders, R., Smits, J.P., Wilms-Schopman, F.J., Wiegerinck, R.F., Bourier, J., Belterman, C.N., Coronel, R., & Verheijck, E.E. (2003). Conduction slowing by the gap junctional uncoupler carbenoxolone. *Cardiovasc.Res.*, 60, (2) 288-297
- De Leon, J.R., Buttrick, P.M., & Fishman, G.I. (1994). Functional analysis of the connexin43 gene promoter in vivo and in vitro. *J.Mol.Cell Cardiol.*, 26, (3) 379-389
- de Meester de, R.C., Bouzin, C., Lazam, S., Boulif, J., Amzulescu, M., Melchior, J., Pasquet, A., Vancraeynest, D., Pouleur, A.C., Vanoverschelde, J.L., & Gerber, B.L. (2015). Histological Validation of measurement of diffuse interstitial myocardial fibrosis by myocardial extravascular volume fraction from Modified Look-Locker imaging (MOLLI) T1 mapping at 3 T. *J.Cardiovasc.Magn Reson.*, 17, 48
- de, D.C., Chen, F., Xie, Y., Pai, R.K., Slavin, L., Parker, J., Lamp, S.T., Qu, Z., Weiss, J.N., & Valderrabano, M. (2011). Anisotropic conduction block and reentry in neonatal rat ventricular myocyte monolayers. *Am.J.Physiol Heart Circ.Physiol*, 300, (1) H271-H278
- Decrock, E., Vinken, M., De, V.E., Krysko, D.V., D'Herde, K., Vanhaecke, T., Vandenamele, P., Rogiers, V., & Leybaert, L. (2009). Connexin-related signaling in cell death: to live or let die? *Cell Death.Differ.*, 16, (4) 524-536
- Deliolanis, N.C., Kasmieh, R., Wurdinger, T., Tannous, B.A., Shah, K., & Ntziachristos, V. (2008). Performance of the red-shifted fluorescent proteins in deep-tissue molecular imaging applications. *J.Biomed.Opt.*, 13, (4) 044008
- Demaison, C., Parsley, K., Brouns, G., Scherr, M., Battmer, K., Kinnon, C., Grez, M., & Thrasher, A.J. (2002). High-level transduction and gene expression in hematopoietic repopulating cells using a human immunodeficiency [correction of imunodeficiency] virus type 1-based lentiviral vector containing an internal spleen focus forming virus promoter. *Hum.Gene Ther.*, 13, (7) 803-813
- Desplantez, T., Halliday, D., Dupont, E., Severs, N.J., & Weingart, R. (2011). Influence of v5/6-His tag on the properties of gap junction channels composed of connexin43, connexin40 or connexin45. *J.Membr.Biol.*, 240, (3) 139-150

- Deten, A., Holzl, A., Leicht, M., Barth, W., & Zimmer, H.G. (2001). Changes in extracellular matrix and in transforming growth factor beta isoforms after coronary artery ligation in rats. *J.Mol.Cell Cardiol.*, 33, (6) 1191-1207
- Dev, S., Peterson, P.N., Wang, Y., Curtis, J.P., Varosy, P.D., & Masoudi, F.A. (2014). Prevalence, correlates, and temporal trends in antiarrhythmic drug use at discharge after implantable cardioverter defibrillator placement (from the National Cardiovascular Data Registry [NCDR]). *Am.J.Cardiol.*, 113, (2) 314-320
- Dewald, O., Ren, G., Duerr, G.D., Zoerlein, M., Klemm, C., Gersch, C., Tincey, S., Michael, L.H., Entman, M.L., & Frangogiannis, N.G. (2004). Of mice and dogs: species-specific differences in the inflammatory response following myocardial infarction. *Am.J.Pathol.*, 164, (2) 665-677
- Di, I.A., Ferrucci, L., Sparvieri, E., Cherubini, A., Volpato, S., Corsi, A., Bonafe, M., Franceschi, C., Abate, G., & Paganelli, R. (2003). Serum IL-1beta levels in health and disease: a population-based study. 'The InCHIANTI study'. *Cytokine*, 22, (6) 198-205
- Diez, J., Querejeta, R., Lopez, B., Gonzalez, A., Larman, M., & Martinez Ubago, J.L. (2002). Losartan-dependent regression of myocardial fibrosis is associated with reduction of left ventricular chamber stiffness in hypertensive patients. *Circulation*, 105, (21) 2512-2517
- Dispersyn, G.D., Geuens, E., Ver, D.L., Ramaekers, F.C., & Borgers, M. (2001). Adult rabbit cardiomyocytes undergo hibernation-like dedifferentiation when co-cultured with cardiac fibroblasts. *Cardiovasc.Res.*, 51, (2) 230-240
- Dobaczewski, M., Bujak, M., Li, N., Gonzalez-Quesada, C., Mendoza, L.H., Wang, X.F., & Frangogiannis, N.G. (2010). Smad3 signaling critically regulates fibroblast phenotype and function in healing myocardial infarction. *Circ.Res.*, 107, (3) 418-428
- Dobaczewski, M., Chen, W., & Frangogiannis, N.G. (2011). Transforming growth factor (TGF)-beta signaling in cardiac remodeling. *J.Mol.Cell Cardiol.*, 51, (4) 600-606
- Driesen, R.B., Dispersyn, G.D., Verheyen, F.K., van den Eijnde, S.M., Hofstra, L., Thone, F., Dijkstra, P., Debie, W., Borgers, M., & Ramaekers, F.C. (2005). Partial cell fusion: a newly recognized type of communication between dedifferentiating cardiomyocytes and fibroblasts. *Cardiovasc.Res.*, 68, (1) 37-46
- Duan, J., Gherghe, C., Liu, D., Hamlett, E., Srikantha, L., Rodgers, L., Regan, J.N., Rojas, M., Willis, M., Leask, A., Majesky, M., & Deb, A. (2012). Wnt1/betacatenin injury response activates the epicardium and cardiac fibroblasts to promote cardiac repair. *EMBO J.*, 31, (2) 429-442
- Duffy, H.S., John, G.R., Lee, S.C., Brosnan, C.F., & Spray, D.C. (2000). Reciprocal regulation of the junctional proteins claudin-1 and connexin43 by interleukin-1beta in primary human fetal astrocytes. *J.Neurosci.*, 20, (23) RC114

- Dupont, E., Ko, Y., Rothery, S., Coppen, S.R., Baghai, M., Haw, M., & Severs, N.J. (2001). The gap-junctional protein connexin40 is elevated in patients susceptible to postoperative atrial fibrillation. *Circulation*, 103, (6) 842-849
- Efimov, I.R., Nikolski, V.P., & Salama, G. (2004). Optical imaging of the heart. *Circ.Res.*, 95, (1) 21-33
- Ek-Vitorin, J.F., King, T.J., Heyman, N.S., Lampe, P.D., & Burt, J.M. (2006). Selectivity of connexin 43 channels is regulated through protein kinase C-dependent phosphorylation. *Circ.Res.*, 98, (12) 1498-1505
- Ellingsen, O., Davidoff, A.J., Prasad, S.K., Berger, H.J., Springhorn, J.P., Marsh, J.D., Kelly, R.A., & Smith, T.W. (1993). Adult rat ventricular myocytes cultured in defined medium: phenotype and electromechanical function. *Am.J.Physiol*, 265, (2 Pt 2) H747-H754
- Epelman, S., Liu, P.P., & Mann, D.L. (2015). Role of innate and adaptive immune mechanisms in cardiac injury and repair. *Nat.Rev.Immunol.*, 15, (2) 117-129
- Epstein, A.E., DiMarco, J.P., Ellenbogen, K.A., Estes, N.A., III, Freedman, R.A., Gettes, L.S., Gillinov, A.M., Gregoratos, G., Hammill, S.C., Hayes, D.L., Hlatky, M.A., Newby, L.K., Page, R.L., Schoenfeld, M.H., Silka, M.J., Stevenson, L.W., Sweeney, M.O., Tracy, C.M., Epstein, A.E., Darbar, D., DiMarco, J.P., Dunbar, S.B., Estes, N.A., III, Ferguson, T.B., Jr., Hammill, S.C., Karasik, P.E., Link, M.S., Marine, J.E., Schoenfeld, M.H., Shanker, A.J., Silka, M.J., Stevenson, L.W., Stevenson, W.G., & Varosy, P.D. (2013). 2012 ACCF/AHA/HRS focused update incorporated into the ACCF/AHA/HRS 2008 guidelines for device-based therapy of cardiac rhythm abnormalities: a report of the American College of Cardiology Foundation/American Heart Association Task Force on Practice Guidelines and the Heart Rhythm Society. *J.Am.Coll.Cardiol.*, 61, (3) e6-75
- Ettinger, A. & Wittmann, T. (2014). Fluorescence live cell imaging. *Methods Cell Biol.*, 123, 77-94
- Etzion, S., Barbash, I.M., Feinberg, M.S., Zarin, P., Miller, L., Guetta, E., Holbova, R., Kloner, R.A., Kedes, L.H., & Leor, J. (2002). Cellular cardiomyoplasty of cardiac fibroblasts by adenoviral delivery of MyoD ex vivo: an unlimited source of cells for myocardial repair. *Circulation*, 106, (12 Suppl 1) I125-I130
- Fahrenbach, J.P., Mejia-Alvarez, R., & Banach, K. (2007). The relevance of non-excitable cells for cardiac pacemaker function. *J.Physiol*, 585, (Pt 2) 565-578
- Fan, D., Takawale, A., Lee, J., & Kassiri, Z. (2012). Cardiac fibroblasts, fibrosis and extracellular matrix remodeling in heart disease. *Fibrogenesis.Tissue Repair*, 5, (1) 15
- Fedak, P.W., Altamentova, S.M., Weisel, R.D., Nili, N., Ohno, N., Verma, S., Lee, T.Y., Kiani, C., Mickle, D.A., Strauss, B.H., & Li, R.K. (2003). Matrix remodeling in experimental and human heart failure: a possible regulatory role for TIMP-3. *Am.J.Physiol Heart Circ.Physiol*, 284, (2) H626-H634
- Fedak, P.W., Smookler, D.S., Kassiri, Z., Ohno, N., Leco, K.J., Verma, S., Mickle, D.A., Watson, K.L., Hojilla, C.V., Cruz, W., Weisel, R.D., Li, R.K., & Khokha, R.

- (2004). TIMP-3 deficiency leads to dilated cardiomyopathy. *Circulation*, 110, (16) 2401-2409
- Fedorov, V.V., Lozinsky, I.T., Sosunov, E.A., Anyukhovskiy, E.P., Rosen, M.R., Balke, C.W., & Efimov, I.R. (2007). Application of blebbistatin as an excitation-contraction uncoupler for electrophysiologic study of rat and rabbit hearts. *Heart Rhythm*, 4, (5) 619-626
- Feng, S. & Holland, E.C. (1988). HIV-1 tat trans-activation requires the loop sequence within tar. *Nature*, 334, (6178) 165-167
- Ferdinandy, P., Schulz, R., & Baxter, G.F. (2007). Interaction of cardiovascular risk factors with myocardial ischemia/reperfusion injury, preconditioning, and postconditioning. *Pharmacol.Rev.*, 59, (4) 418-458
- Fernandes, S., van Rijen, H.V., Forest, V., Evain, S., Leblond, A.L., Merot, J., Charpentier, F., de Bakker, J.M., & Lemarchand, P. (2009). Cardiac cell therapy: overexpression of connexin43 in skeletal myoblasts and prevention of ventricular arrhythmias. *J.Cell Mol.Med.*, 13, (9B) 3703-3712
- Forrester, T. & Williams, C.A. (1977). Release of adenosine triphosphate from isolated adult heart cells in response to hypoxia. *J.Physiol*, 268, (2) 371-390
- Frangogiannis, N.G. (2015). Emerging roles for macrophages in cardiac injury: cytoprotection, repair, and regeneration. *J.Clin.Invest*, 125, (8) 2927-2930
- Frangogiannis, N.G., Michael, L.H., & Entman, M.L. (2000). Myofibroblasts in reperfused myocardial infarcts express the embryonic form of smooth muscle myosin heavy chain (SMemb). *Cardiovasc.Res.*, 48, (1) 89-100
- Frank, M., Wirth, A., Andrie, R.P., Kreuzberg, M.M., Dobrowolski, R., Seifert, G., Offermanns, S., Nickenig, G., Willecke, K., & Schrickel, J.W. (2012). Connexin45 provides optimal atrioventricular nodal conduction in the adult mouse heart. *Circ.Res.*, 111, (12) 1528-1538
- Franz, M.R., Bargheer, K., Rafflenbeul, W., Haverich, A., & Lichtlen, P.R. (1987). Monophasic action potential mapping in human subjects with normal electrocardiograms: direct evidence for the genesis of the T wave. *Circulation*, 75, (2) 379-386
- Fredj, S., Bescond, J., Louault, C., Delwail, A., Lecron, J.C., & Potreau, D. (2005a). Role of interleukin-6 in cardiomyocyte/cardiac fibroblast interactions during myocyte hypertrophy and fibroblast proliferation. *J.Cell Physiol*, 204, (2) 428-436
- Fredj, S., Bescond, J., Louault, C., & Potreau, D. (2005b). Interactions between cardiac cells enhance cardiomyocyte hypertrophy and increase fibroblast proliferation. *J.Cell Physiol*, 202, (3) 891-899
- Frommeyer, G., Clauss, C., Ellermann, C., Bogossian, H., Dechering, D.G., Kochhauser, S., Reinke, F., Pott, C., & Eckardt, L. (2017). Antiarrhythmic effect of vernakalant in an experimental model of Long-QT-syndrome. *Europace.*, 19, (5) 866-873

- Furushima, H., Chinushi, M., Okamura, K., Komura, S., Tanabe, Y., Sato, A., Izumi, D., & Aizawa, Y. (2007). Effect of dl-sotalol on mortality and recurrence of ventricular tachyarrhythmias: ischemic compared to nonischemic cardiomyopathy. *Pacing Clin. Electrophysiol.*, 30, (9) 1136-1141
- Gago-Fuentes, R., Fernandez-Puente, P., Megias, D., Carpintero-Fernandez, P., Mateos, J., Acea, B., Fonseca, E., Blanco, F.J., & Mayan, M.D. (2015). Proteomic Analysis of Connexin 43 Reveals Novel Interactors Related to Osteoarthritis. *Mol. Cell Proteomics.*, 14, (7) 1831-1845
- Garcia-Gras, E., Lombardi, R., Giocondo, M.J., Willerson, J.T., Schneider, M.D., Khoury, D.S., & Marian, A.J. (2006). Suppression of canonical Wnt/beta-catenin signaling by nuclear plakoglobin recapitulates phenotype of arrhythmogenic right ventricular cardiomyopathy. *J. Clin. Invest.*, 116, (7) 2012-2021
- Gaudesius, G., Miragoli, M., Thomas, S.P., & Rohr, S. (2003). Coupling of cardiac electrical activity over extended distances by fibroblasts of cardiac origin. *Circ. Res.*, 93, (5) 421-428
- Gemel, J., Lin, X., Veenstra, R.D., & Beyer, E.C. (2006). N-terminal residues in Cx43 and Cx40 determine physiological properties of gap junction channels, but do not influence heteromeric assembly with each other or with Cx26. *J. Cell Sci.*, 119, (Pt 11) 2258-2268
- Georgantas, R.W., Streicher, K., Greenberg, S.A., Greenlees, L.M., Zhu, W., Brohawn, P.Z., Higgs, B.W., Czapiga, M., Morehouse, C.A., Amato, A., Richman, L., Jallal, B., Yao, Y., & Ranade, K. (2014). Inhibition of myogenic microRNAs 1, 133, and 206 by inflammatory cytokines links inflammation and muscle degeneration in adult inflammatory myopathies. *Arthritis Rheumatol.*, 66, (4) 1022-1033
- George, S.J., Wan, S., Hu, J., MacDonald, R., Johnson, J.L., & Baker, A.H. (2011). Sustained reduction of vein graft neointima formation by ex vivo TIMP-3 gene therapy. *Circulation*, 124, (11 Suppl) S135-S142
- Ghoury, I.A., Kelly, A., Burton, F.L., Smith, G.L., & Kemi, O.J. (2015). 2-Photon excitation fluorescence microscopy enables deeper high-resolution imaging of voltage and Ca(2+) in intact mice, rat, and rabbit hearts. *J. Biophotonics.*, 8, (1-2) 112-123
- Gold, M.R., Bloomfield, D.M., Anderson, K.P., El-Sherif, N.E., Wilber, D.J., Groh, W.J., Estes, N.A., III, Kaufman, E.S., Greenberg, M.L., & Rosenbaum, D.S. (2000). A comparison of T-wave alternans, signal averaged electrocardiography and programmed ventricular stimulation for arrhythmia risk stratification. *J. Am. Coll. Cardiol.*, 36, (7) 2247-2253
- Goldsmith, E.C., Hoffman, A., Morales, M.O., Potts, J.D., Price, R.L., McFadden, A., Rice, M., & Borg, T.K. (2004). Organization of fibroblasts in the heart. *Dev. Dyn.*, 230, (4) 787-794
- Gomez, A.B., MacKenzie, C., Paul, A., & Plevin, R. (2005). Selective inhibition of inhibitory kappa B kinase-beta abrogates induction of nitric oxide synthase in

- lipopolysaccharide-stimulated rat aortic smooth muscle cells. *Br.J.Pharmacol.*, 146, (2) 217-225
- Goncalves, G.A., Vassallo, P.F., dos, S.L., Schettert, I.T., Nakamuta, J.S., Becker, C., Tucci, P.J., & Krieger, J.E. (2010). Intramyocardial transplantation of fibroblasts expressing vascular endothelial growth factor attenuates cardiac dysfunction. *Gene Ther.*, 17, (3) 305-314
- Graham, F.L., Smiley, J., Russell, W.C., & Nairn, R. (1977). Characteristics of a human cell line transformed by DNA from human adenovirus type 5. *J.Gen.Virol.*, 36, (1) 59-74
- Grand, T., Salvarani, N., Jousset, F., & Rohr, S. (2014). Aggravation of cardiac myofibroblast arrhythmogenicity by mechanical stress. *Cardiovasc.Res.*, 104, (3) 489-500
- Grant, A.O. (2009). Cardiac ion channels. *Circ.Arrhythm.Electrophysiol.*, 2, (2) 185-194
- Grossman, W. & Paulus, W.J. (2013). Myocardial stress and hypertrophy: a complex interface between biophysics and cardiac remodeling. *J.Clin.Invest*, 123, (9) 3701-3703
- Guerrero, P.A., Schuessler, R.B., Davis, L.M., Beyer, E.C., Johnson, C.M., Yamada, K.A., & Saffitz, J.E. (1997). Slow ventricular conduction in mice heterozygous for a connexin43 null mutation. *J.Clin.Invest*, 99, (8) 1991-1998
- Guillen, I., Blanes, M., Gomez-Lechon, M.J., & Castell, J.V. (1995). Cytokine signaling during myocardial infarction: sequential appearance of IL-1 beta and IL-6. *Am.J.Physiol*, 269, (2 Pt 2) R229-R235
- Gutstein, D.E., Liu, F.Y., Meyers, M.B., Choo, A., & Fishman, G.I. (2003). The organization of adherens junctions and desmosomes at the cardiac intercalated disc is independent of gap junctions. *J.Cell Sci.*, 116, (Pt 5) 875-885
- Gutstein, D.E., Morley, G.E., Tamaddon, H., Vaidya, D., Schneider, M.D., Chen, J., Chien, K.R., Stuhlmann, H., & Fishman, G.I. (2001). Conduction slowing and sudden arrhythmic death in mice with cardiac-restricted inactivation of connexin43. *Circ.Res.*, 88, (3) 333-339
- Haddock, P.S., Coetzee, W.A., Cho, E., Porter, L., Katoh, H., Bers, D.M., Jafri, M.S., & Artman, M. (1999). Subcellular $[Ca^{2+}]_i$ gradients during excitation-contraction coupling in newborn rabbit ventricular myocytes. *Circ.Res.*, 85, (5) 415-427
- Hanson, B., Sutton, P., Elameri, N., Gray, M., Critchley, H., Gill, J.S., & Taggart, P. (2009). Interaction of activation-repolarization coupling and restitution properties in humans. *Circ.Arrhythm.Electrophysiol.*, 2, (2) 162-170
- Hansson, G.K. (2005). Inflammation, atherosclerosis, and coronary artery disease. *N.Engl.J.Med.*, 352, (16) 1685-1695

- Hao, G., Han, Z., Meng, Z., Wei, J., Gao, D., Zhang, H., & Wang, N. (2015). Ets-1 upregulation mediates angiotensin II-related cardiac fibrosis. *Int.J.Clin.Exp.Pathol.*, 8, (9) 10216-10227
- Harada, K., Komuro, I., Shiojima, I., Hayashi, D., Kudoh, S., Mizuno, T., Kijima, K., Matsubara, H., Sugaya, T., Murakami, K., & Yazaki, Y. (1998). Pressure overload induces cardiac hypertrophy in angiotensin II type 1A receptor knockout mice. *Circulation*, 97, (19) 1952-1959
- Hasenfuss, G., Reinecke, H., Studer, R., Meyer, M., Pieske, B., Holtz, J., Holubarsch, C., Posival, H., Just, H., & Drexler, H. (1994). Relation between myocardial function and expression of sarcoplasmic reticulum Ca(2+)-ATPase in failing and nonfailing human myocardium. *Circ.Res.*, 75, (3) 434-442
- Hayashidani, S., Tsutsui, H., Ikeuchi, M., Shiomi, T., Matsusaka, H., Kubota, T., Imanaka-Yoshida, K., Itoh, T., & Takeshita, A. (2003). Targeted deletion of MMP-2 attenuates early LV rupture and late remodeling after experimental myocardial infarction. *Am.J.Physiol Heart Circ.Physiol*, 285, (3) H1229-H1235
- He, K., Shi, X., Zhang, X., Dang, S., Ma, X., Liu, F., Xu, M., Lv, Z., Han, D., Fang, X., & Zhang, Y. (2011). Long-distance intercellular connectivity between cardiomyocytes and cardiofibroblasts mediated by membrane nanotubes. *Cardiovasc.Res.*, 92, (1) 39-47
- He, T.C., Zhou, S., da Costa, L.T., Yu, J., Kinzler, K.W., & Vogelstein, B. (1998). A simplified system for generating recombinant adenoviruses. *Proc.Natl.Acad.Sci.U.S.A*, 95, (5) 2509-2514
- Hein, S., Arnon, E., Kostin, S., Schonburg, M., Elsasser, A., Polyakova, V., Bauer, E.P., Klovekorn, W.P., & Schaper, J. (2003). Progression from compensated hypertrophy to failure in the pressure-overloaded human heart: structural deterioration and compensatory mechanisms. *Circulation*, 107, (7) 984-991
- Heineke, J. & Molkentin, J.D. (2006). Regulation of cardiac hypertrophy by intracellular signalling pathways. *Nat.Rev.Mol.Cell Biol.*, 7, (8) 589-600
- Heino, J. (1986). Connective tissue components in synovial fibroblast cultures exposed to interleukin 1 and prostaglandin E2. *Virchows Arch.B Cell Pathol.Incl.Mol.Pathol.*, 50, (4) 313-320
- Heinrich, M., Oberbach, A., Schlichting, N., Stolzenburg, J.U., & Neuhaus, J. (2011). Cytokine effects on gap junction communication and connexin expression in human bladder smooth muscle cells and suburothelial myofibroblasts. *PLoS.One.*, 6, (6) e20792
- Herron, T.J., Lee, P., & Jalife, J. (2012). Optical imaging of voltage and calcium in cardiac cells & tissues. *Circ.Res.*, 110, (4) 609-623
- Herskowitz, A., Choi, S., Ansari, A.A., & Wesselingh, S. (1995). Cytokine mRNA expression in postischemic/reperfused myocardium. *Am.J.Pathol.*, 146, (2) 419-428

- Heymans, S., Luttun, A., Nuyens, D., Theilmeier, G., Creemers, E., Moons, L., Dyspersin, G.D., Cleutjens, J.P., Shipley, M., Angellilo, A., Levi, M., Nube, O., Baker, A., Keshet, E., Lupu, F., Herbert, J.M., Smits, J.F., Shapiro, S.D., Baes, M., Borgers, M., Collen, D., Daemen, M.J., & Carmeliet, P. (1999). Inhibition of plasminogen activators or matrix metalloproteinases prevents cardiac rupture but impairs therapeutic angiogenesis and causes cardiac failure. *Nat.Med.*, 5, (10) 1135-1142
- Higuchi, R., Fockler, C., Dollinger, G., & Watson, R. (1993). Kinetic PCR analysis: real-time monitoring of DNA amplification reactions. *Biotechnology (N.Y.)*, 11, (9) 1026-1030
- Hinz, B., Celetta, G., Tomasek, J.J., Gabbiani, G., & Chaponnier, C. (2001). Alpha-smooth muscle actin expression upregulates fibroblast contractile activity. *Mol.Biol.Cell*, 12, (9) 2730-2741
- Hirschfeld, J., Maurer, J., Jung, D., Kwiecinski, M., Khimji, A.K., Dienes, H.P., Fries, J.W., & Odenthal, M. (2009). Targeting myofibroblasts in model systems of fibrosis by an artificial alpha-smooth muscle-actin promoter hybrid. *Mol.Biotechnol.*, 43, (2) 121-129
- Hohnloser, S.H., Crijns, H.J., van, E.M., Gaudin, C., Page, R.L., Torp-Pedersen, C., & Connolly, S.J. (2009). Effect of dronedarone on cardiovascular events in atrial fibrillation. *N.Engl.J.Med.*, 360, (7) 668-678
- Hood, A.R., Ai, X., & Pogwizd, S.M. (2017). Regulation of cardiac gap junctions by protein phosphatases. *J.Mol.Cell Cardiol.*, 107, 52-57
- Howard, C.M. & Baudino, T.A. (2014). Dynamic cell-cell and cell-ECM interactions in the heart. *J.Mol.Cell Cardiol.*, 70, 19-26
- Hu, B., Wu, Z., & Phan, S.H. (2003). Smad3 mediates transforming growth factor-beta-induced alpha-smooth muscle actin expression. *Am.J.Respir.Cell Mol.Biol.*, 29, (3 Pt 1) 397-404
- Hund, T.J., Lerner, D.L., Yamada, K.A., Schuessler, R.B., & Saffitz, J.E. (2007). Protein kinase Cepsilon mediates salutary effects on electrical coupling induced by ischemic preconditioning. *Heart Rhythm.*, 4, (9) 1183-1193
- Hunter, A.W., Barker, R.J., Zhu, C., & Gourdie, R.G. (2005). Zonula occludens-1 alters connexin43 gap junction size and organization by influencing channel accretion. *Mol.Biol.Cell*, 16, (12) 5686-5698
- Huusko, J., Merentie, M., Dijkstra, M.H., Ryhanen, M.M., Karvinen, H., Rissanen, T.T., Vanwildemeersch, M., Hedman, M., Lipponen, J., Heinonen, S.E., Eriksson, U., Shibuya, M., & Yla-Herttuala, S. (2010). The effects of VEGF-R1 and VEGF-R2 ligands on angiogenic responses and left ventricular function in mice. *Cardiovasc.Res.*, 86, (1) 122-130
- Irvine, J., Dorian, P., Baker, B., O'Brien, B.J., Roberts, R., Gent, M., Newman, D., & Connolly, S.J. (2002). Quality of life in the Canadian Implantable Defibrillator Study (CIDS). *Am.Heart J.*, 144, (2) 282-289

- Jalife, J. (2000). Ventricular fibrillation: mechanisms of initiation and maintenance. *Annu.Rev.Physiol.*, 62, 25-50
- Jalil, J.E., Doering, C.W., Janicki, J.S., Pick, R., Shroff, S.G., & Weber, K.T. (1989). Fibrillar collagen and myocardial stiffness in the intact hypertrophied rat left ventricle. *Circ.Res.*, 64, (6) 1041-1050
- Jia, G., Cheng, G., Gangahar, D.M., & Agrawal, D.K. (2008). Involvement of connexin 43 in angiotensin II-induced migration and proliferation of saphenous vein smooth muscle cells via the MAPK-AP-1 signaling pathway. *J.Mol.Cell Cardiol.*, 44, (5) 882-890
- Jin, Z., Xu, S., Yu, H., Yang, B., Zhao, H., & Zhao, G. (2013). miR-125b inhibits Connexin43 and promotes glioma growth. *Cell Mol.Neurobiol.*, 33, (8) 1143-1148
- John, G.R., Scemes, E., Suadicani, S.O., Liu, J.S., Charles, P.C., Lee, S.C., Spray, D.C., & Brosnan, C.F. (1999). IL-1beta differentially regulates calcium wave propagation between primary human fetal astrocytes via pathways involving P2 receptors and gap junction channels. *Proc.Natl.Acad.Sci.U.S.A.*, 96, (20) 11613-11618
- Joshi-Mukherjee, R., Dick, I.E., Liu, T., O'Rourke, B., Yue, D.T., & Tung, L. (2013). Structural and functional plasticity in long-term cultures of adult ventricular myocytes. *J.Mol.Cell Cardiol.*, 65, 76-87
- Julian, D.G., Camm, A.J., Frangin, G., Janse, M.J., Munoz, A., Schwartz, P.J., & Simon, P. (1997). Randomised trial of effect of amiodarone on mortality in patients with left-ventricular dysfunction after recent myocardial infarction: EMIAT. European Myocardial Infarct Amiodarone Trial Investigators. *Lancet*, 349, (9053) 667-674
- Kaab, S., Nuss, H.B., Chiamvimonvat, N., O'Rourke, B., Pak, P.H., Kass, D.A., Marban, E., & Tomaselli, G.F. (1996). Ionic mechanism of action potential prolongation in ventricular myocytes from dogs with pacing-induced heart failure. *Circ.Res.*, 78, (2) 262-273
- Kalogeris, T., Baines, C.P., Krenz, M., & Korthuis, R.J. (2012). Cell biology of ischemia/reperfusion injury. *Int.Rev.Cell Mol.Biol.*, 298, 229-317
- Kane, N.M., Nowrouzi, A., Mukherjee, S., Blundell, M.P., Greig, J.A., Lee, W.K., Houslay, M.D., Milligan, G., Mountford, J.C., von, K.C., Schmidt, M., Thrasher, A.J., & Baker, A.H. (2010). Lentivirus-mediated reprogramming of somatic cells in the absence of transgenic transcription factors. *Mol.Ther.*, 18, (12) 2139-2145
- Kanisicak, O., Khalil, H., Ivey, M.J., Karch, J., Maliken, B.D., Correll, R.N., Brody, M.J., SC, J.L., Aronow, B.J., Tallquist, M.D., & Molkenin, J.D. (2016). Genetic lineage tracing defines myofibroblast origin and function in the injured heart. *Nat.Comm.*, 7, 12260
- Kaplan, S.R., Gard, J.J., Carvajal-Huerta, L., Ruiz-Cabezas, J.C., Thiene, G., & Saffitz, J.E. (2004a). Structural and molecular pathology of the heart in Carvajal syndrome. *Cardiovasc.Pathol.*, 13, (1) 26-32

- Kaplan, S.R., Gard, J.J., Protonotarios, N., Tsatsopoulou, A., Spiliopoulou, C., Anastasakis, A., Squarcioni, C.P., McKenna, W.J., Thiene, G., Basso, C., Brousse, N., Fontaine, G., & Saffitz, J.E. (2004b). Remodeling of myocyte gap junctions in arrhythmogenic right ventricular cardiomyopathy due to a deletion in plakoglobin (Naxos disease). *Heart Rhythm.*, 1, (1) 3-11
- Karagueuzian, H.S., Pezhouman, A., Angelini, M., & Olcese, R. (2017). Enhanced Late Na and Ca Currents as Effective Antiarrhythmic Drug Targets. *Front Pharmacol.*, 8, 36
- Kaur, K., Zarzoso, M., Ponce-Balbuena, D., Guerrero-Serna, G., Hou, L., Musa, H., & Jalife, J. (2013). TGF-beta 1, Released by Myofibroblasts, Differentially Regulates Transcription and Function of Sodium and Potassium Channels in Adult Rat Ventricular Myocytes. *Plos One*, 8, (2)
- Kawaguchi, M., Takahashi, M., Hata, T., Kashima, Y., Usui, F., Morimoto, H., Izawa, A., Takahashi, Y., Masumoto, J., Koyama, J., Hongo, M., Noda, T., Nakayama, J., Sagara, J., Taniguchi, S., & Ikeda, U. (2011). Inflammasome activation of cardiac fibroblasts is essential for myocardial ischemia/reperfusion injury. *Circulation*, 123, (6) 594-604
- Kawano, H., Do, Y.S., Kawano, Y., Starnes, V., Barr, M., Law, R.E., & Hsueh, W.A. (2000). Angiotensin II has multiple profibrotic effects in human cardiac fibroblasts. *Circulation*, 101, (10) 1130-1137
- King, J.H., Huang, C.L., & Fraser, J.A. (2013). Determinants of myocardial conduction velocity: implications for arrhythmogenesis. *Front Physiol*, 4, 154
- Kirchhoff, S., Kim, J.S., Hagendorff, A., Thonnissen, E., Kruger, O., Lamers, W.H., & Willecke, K. (2000). Abnormal cardiac conduction and morphogenesis in connexin40 and connexin43 double-deficient mice. *Circ.Res.*, 87, (5) 399-405
- Kizana, E., Ginn, S.L., Allen, D.G., Ross, D.L., & Alexander, I.E. (2005). Fibroblasts can be genetically modified to produce excitable cells capable of electrical coupling. *Circulation*, 111, (4) 394-398
- Kleber, A.G. & Rudy, Y. (2004). Basic mechanisms of cardiac impulse propagation and associated arrhythmias. *Physiol Rev.*, 84, (2) 431-488
- Kober, L., Torp-Pedersen, C., McMurray, J.J., Gotzsche, O., Levy, S., Crijns, H., Amlie, J., & Carlsen, J. (2008). Increased mortality after dronedarone therapy for severe heart failure. *N.Engl.J.Med.*, 358, (25) 2678-2687
- Kohl, P., Kamkin, A.G., Kiseleva, I.S., & Noble, D. (1994). Mechanosensitive fibroblasts in the sino-atrial node region of rat heart: interaction with cardiomyocytes and possible role. *Exp.Physiol*, 79, (6) 943-956
- Koitabashi, N., Arai, M., Kogure, S., Niwano, K., Watanabe, A., Aoki, Y., Maeno, T., Nishida, T., Kubota, S., Takigawa, M., & Kurabayashi, M. (2007). Increased connective tissue growth factor relative to brain natriuretic peptide as a determinant of myocardial fibrosis. *Hypertension*, 49, (5) 1120-1127

- Kojodjojo, P., Kanagaratnam, P., Segal, O.R., Hussain, W., & Peters, N.S. (2006). The effects of carbenoxolone on human myocardial conduction: a tool to investigate the role of gap junctional uncoupling in human arrhythmogenesis. *J.Am.Coll.Cardiol.*, 48, (6) 1242-1249
- Kong, P., Christia, P., Saxena, A., Su, Y., & Frangogiannis, N.G. (2013). Lack of specificity of fibroblast-specific protein 1 in cardiac remodeling and fibrosis. *Am.J.Physiol Heart Circ.Physiol*, 305, (9) H1363-H1372
- Kostetskii, I., Li, J., Xiong, Y., Zhou, R., Ferrari, V.A., Patel, V.V., Molkentin, J.D., & Radice, G.L. (2005). Induced deletion of the N-cadherin gene in the heart leads to dissolution of the intercalated disc structure. *Circ.Res.*, 96, (3) 346-354
- Kostin, S., Hein, S., Bauer, E.P., & Schaper, J. (1999). Spatiotemporal development and distribution of intercellular junctions in adult rat cardiomyocytes in culture. *Circ.Res.*, 85, (2) 154-167
- Kostin, S., Rieger, M., Dammer, S., Hein, S., Richter, M., Klovekorn, W.P., Bauer, E.P., & Schaper, J. (2003). Gap junction remodeling and altered connexin43 expression in the failing human heart. *Mol.Cell Biochem.*, 242, (1-2) 135-144
- Kreuzberg, M.M., Liebermann, M., Segschneider, S., Dobrowolski, R., Dobrzynski, H., Kaba, R., Rowlinson, G., Dupont, E., Severs, N.J., & Willecke, K. (2009). Human connexin31.9, unlike its orthologous protein connexin30.2 in the mouse, is not detectable in the human cardiac conduction system. *J.Mol.Cell Cardiol.*, 46, (4) 553-559
- Kubo, H., Margulies, K.B., Piacentino, V., III, Gaughan, J.P., & Houser, S.R. (2001). Patients with end-stage congestive heart failure treated with beta-adrenergic receptor antagonists have improved ventricular myocyte calcium regulatory protein abundance. *Circulation*, 104, (9) 1012-1018
- Kumai, M., Nishii, K., Nakamura, K., Takeda, N., Suzuki, M., & Shibata, Y. (2000). Loss of connexin45 causes a cushion defect in early cardiogenesis. *Development*, 127, (16) 3501-3512
- Kupfahl, C., Pink, D., Friedrich, K., Zurbrugg, H.R., Neuss, M., Warnecke, C., Fielitz, J., Graf, K., Fleck, E., & Regitz-Zagrosek, V. (2000). Angiotensin II directly increases transforming growth factor beta1 and osteopontin and indirectly affects collagen mRNA expression in the human heart. *Cardiovasc.Res.*, 46, (3) 463-475
- LaFramboise, W.A., Scalise, D., Stoodley, P., Graner, S.R., Guthrie, R.D., Magovern, J.A., & Becich, M.J. (2007). Cardiac fibroblasts influence cardiomyocyte phenotype in vitro. *Am.J.Physiol Cell Physiol*, 292, (5) C1799-C1808
- Laing, J.G., Tadros, P.N., Westphale, E.M., & Beyer, E.C. (1997). Degradation of connexin43 gap junctions involves both the proteasome and the lysosome. *Exp.Cell Res.*, 236, (2) 482-492
- Laird, D.W., Puranam, K.L., & Revel, J.P. (1991). Turnover and phosphorylation dynamics of connexin43 gap junction protein in cultured cardiac myocytes. *Biochem.J.*, 273(Pt 1), 67-72

- Lamouille, S., Xu, J., & Derynck, R. (2014). Molecular mechanisms of epithelial-mesenchymal transition. *Nat.Rev.Mol.Cell Biol.*, 15, (3) 178-196
- Lampe, P.D., TenBroek, E.M., Burt, J.M., Kurata, W.E., Johnson, R.G., & Lau, A.F. (2000). Phosphorylation of connexin43 on serine368 by protein kinase C regulates gap junctional communication. *J.Cell Biol.*, 149, (7) 1503-1512
- Laurie, K.L., Blundell, M.P., Baxendale, H.E., Howe, S.J., Sinclair, J., Qasim, W., Brunsberg, U., Thrasher, A.J., Holmdahl, R., & Gustafsson, K. (2007). Cell-specific and efficient expression in mouse and human B cells by a novel hybrid immunoglobulin promoter in a lentiviral vector. *Gene Ther.*, 14, (23) 1623-1631
- Leach, R.N., Desai, J.C., & Orchard, C.H. (2005). Effect of cytoskeleton disruptors on L-type Ca channel distribution in rat ventricular myocytes. *Cell Calcium*, 38, (5) 515-526
- Lee, A.A., Dillmann, W.H., McCulloch, A.D., & Villarreal, F.J. (1995). Angiotensin II stimulates the autocrine production of transforming growth factor-beta 1 in adult rat cardiac fibroblasts. *J.Mol.Cell Cardiol.*, 27, (10) 2347-2357
- Lee, C.H., Chang, J.S., Syu, S.H., Wong, T.S., Chan, J.Y., Tang, Y.C., Yang, Z.P., Yang, W.C., Chen, C.T., Lu, S.C., Tang, P.H., Yang, T.C., Chu, P.Y., Hsiao, J.R., & Liu, K.J. (2015). IL-1beta promotes malignant transformation and tumor aggressiveness in oral cancer. *J.Cell Physiol*, 230, (4) 875-884
- Leicht, M., Greipel, N., & Zimmer, H. (2000). Comitogenic effect of catecholamines on rat cardiac fibroblasts in culture. *Cardiovasc.Res.*, 48, (2) 274-284
- Lentz, B.R. & Lee, J.K. (1999). Poly(ethylene glycol) (PEG)-mediated fusion between pure lipid bilayers: a mechanism in common with viral fusion and secretory vesicle release? *Mol.Membr.Biol.*, 16, (4) 279-296
- Lewis, B.P., Burge, C.B., & Bartel, D.P. (2005). Conserved seed pairing, often flanked by adenosines, indicates that thousands of human genes are microRNA targets. *Cell*, 120, (1) 15-20
- Li, G.R., Lau, C.P., Leung, T.K., & Nattel, S. (2004). Ionic current abnormalities associated with prolonged action potentials in cardiomyocytes from diseased human right ventricles. *Heart Rhythm.*, 1, (4) 460-468
- Li, G.R., Sun, H.Y., Chen, J.B., Zhou, Y., Tse, H.F., & Lau, C.P. (2009). Characterization of multiple ion channels in cultured human cardiac fibroblasts. *PLoS.One.*, 4, (10) e7307
- Li, H.L., She, Z.G., Li, T.B., Wang, A.B., Yang, Q., Wei, Y.S., Wang, Y.G., & Liu, D.P. (2007). Overexpression of myofibrillogenesis regulator-1 aggravates cardiac hypertrophy induced by angiotensin II in mice. *Hypertension*, 49, (6) 1399-1408
- Li, J., Patel, V.V., Kostetskii, I., Xiong, Y., Chu, A.F., Jacobson, J.T., Yu, C., Morley, G.E., Molkentin, J.D., & Radice, G.L. (2005). Cardiac-specific loss of N-cadherin leads to alteration in connexins with conduction slowing and arrhythmogenesis. *Circ.Res.*, 97, (5) 474-481

- Li, K., Yao, J., Shi, L., Sawada, N., Chi, Y., Yan, Q., Matsue, H., Kitamura, M., & Takeda, M. (2011). Reciprocal regulation between proinflammatory cytokine-induced inducible NO synthase (iNOS) and connexin43 in bladder smooth muscle cells. *J.Biol.Chem.*, 286, (48) 41552-41562
- Li, L., Chu, G., Kranias, E.G., & Bers, D.M. (1998). Cardiac myocyte calcium transport in phospholamban knockout mouse: relaxation and endogenous CaMKII effects. *Am.J.Physiol*, 274, (4 Pt 2) H1335-H1347
- Li, P., Wang, D., Lucas, J., Oparil, S., Xing, D., Cao, X., Novak, L., Renfrow, M.B., & Chen, Y.F. (2008). Atrial natriuretic peptide inhibits transforming growth factor beta-induced Smad signaling and myofibroblast transformation in mouse cardiac fibroblasts. *Circ.Res.*, 102, (2) 185-192
- Lijnen, P., Papparella, I., Petrov, V., Semplicini, A., & Fagard, R. (2006). Angiotensin II-stimulated collagen production in cardiac fibroblasts is mediated by reactive oxygen species. *J.Hypertens.*, 24, (4) 757-766
- Lijnen, P., Petrov, V., & Fagard, R. (2003). Transforming growth factor-beta 1-mediated collagen gel contraction by cardiac fibroblasts. *J.Renin.Angiotensin.Aldosterone.Syst.*, 4, (2) 113-118
- Lim, D.S., Lutucuta, S., Bachireddy, P., Youker, K., Evans, A., Entman, M., Roberts, R., & Marian, A.J. (2001). Angiotensin II blockade reverses myocardial fibrosis in a transgenic mouse model of human hypertrophic cardiomyopathy. *Circulation*, 103, (6) 789-791
- Lin, X., Crye, M., & Veenstra, R.D. (2003). Regulation of connexin43 gap junctional conductance by ventricular action potentials. *Circ.Res.*, 93, (6) e63-e73
- Liu, Y., Cabo, C., Salomonsz, R., Delmar, M., Davidenko, J., & Jalife, J. (1993). Effects of diacetyl monoxime on the electrical properties of sheep and guinea pig ventricular muscle. *Cardiovasc.Res.*, 27, (11) 1991-1997
- Loennechen, J.P., Wisloff, U., Falck, G., & Ellingsen, O. (2002). Cardiomyocyte contractility and calcium handling partially recover after early deterioration during post-infarction failure in rat. *Acta Physiol Scand.*, 176, (1) 17-26
- Lou, Q., Fedorov, V.V., Glukhov, A.V., Moazami, N., Fast, V.G., & Efimov, I.R. (2011). Transmural heterogeneity and remodeling of ventricular excitation-contraction coupling in human heart failure. *Circulation*, 123, (17) 1881-1890
- Lou, Q., Janardhan, A., & Efimov, I.R. (2012). Remodeling of calcium handling in human heart failure. *Adv.Exp.Med.Biol.*, 740, 1145-1174
- Louault, C., Benamer, N., Faivre, J.F., Potreau, D., & Bescond, J. (2008). Implication of connexins 40 and 43 in functional coupling between mouse cardiac fibroblasts in primary culture. *Biochim.Biophys.Acta*, 1778, (10) 2097-2104
- Louch, W.E., Bito, V., Heinzl, F.R., Macianskiene, R., Vanhaecke, J., Flameng, W., Mubagwa, K., & Sipido, K.R. (2004). Reduced synchrony of Ca²⁺ release with loss of T-tubules-a comparison to Ca²⁺ release in human failing cardiomyocytes. *Cardiovasc.Res.*, 62, (1) 63-73

- Louch, W.E., Sheehan, K.A., & Wolska, B.M. (2011). Methods in cardiomyocyte isolation, culture, and gene transfer. *J.Mol.Cell Cardiol.*, 51, (3) 288-298
- Lovelock, J.D., Baker, A.H., Gao, F., Dong, J.F., Bergeron, A.L., McPheat, W., Sivasubramanian, N., & Mann, D.L. (2005). Heterogeneous effects of tissue inhibitors of matrix metalloproteinases on cardiac fibroblasts. *Am.J.Physiol Heart Circ.Physiol*, 288, (2) H461-H468
- Lu, B., Su, Y., Das, S., Liu, J., Xia, J., & Ren, D. (2007). The neuronal channel NALCN contributes resting sodium permeability and is required for normal respiratory rhythm. *Cell*, 129, (2) 371-383
- Lugrin, J., Parapanov, R., Rosenblatt-Velin, N., Rignault-Clerc, S., Feihl, F., Waeber, B., Muller, O., Vergely, C., Zeller, M., Tardivel, A., Schneider, P., Pacher, P., & Liaudet, L. (2015). Cutting edge: IL-1alpha is a crucial danger signal triggering acute myocardial inflammation during myocardial infarction. *J.Immunol.*, 194, (2) 499-503
- Lurtz, M.M. & Louis, C.F. (2007). Intracellular calcium regulation of connexin43. *Am.J.Physiol Cell Physiol*, 293, (6) C1806-C1813
- Mack, C.P. & Owens, G.K. (1999). Regulation of smooth muscle alpha-actin expression in vivo is dependent on CARG elements within the 5' and first intron promoter regions. *Circ.Res.*, 84, (7) 852-861
- MacNeil, D.J. (1997). The side effect profile of class III antiarrhythmic drugs: focus on d,l-sotalol. *Am.J.Cardiol.*, 80, (8A) 90G-98G
- Mahajan, A., Shiferaw, Y., Sato, D., Baher, A., Olcese, R., Xie, L.H., Yang, M.J., Chen, P.S., Restrepo, J.G., Karma, A., Garfinkel, A., Qu, Z., & Weiss, J.N. (2008). A rabbit ventricular action potential model replicating cardiac dynamics at rapid heart rates. *Biophys.J.*, 94, (2) 392-410
- Mahmood, T. & Yang, P.C. (2012). Western blot: technique, theory, and trouble shooting. *N.Am.J.Med.Sci.*, 4, (9) 429-434
- Mahoney, V.M., Mezzano, V., Mirams, G.R., Maass, K., Li, Z., Cerrone, M., Vasquez, C., Bapat, A., Delmar, M., & Morley, G.E. (2016). Connexin43 contributes to electrotonic conduction across scar tissue in the intact heart. *Sci.Rep.*, 6, 26744
- Maione, D., Della, R.C., Giannetti, P., D'Arrigo, R., Liberatoscioli, L., Franlin, L.L., Sandig, V., Ciliberto, G., La, M.N., & Savino, R. (2001). An improved helper-dependent adenoviral vector allows persistent gene expression after intramuscular delivery and overcomes preexisting immunity to adenovirus. *Proc.Natl.Acad.Sci.U.S.A*, 98, (11) 5986-5991
- Malim, M.H., Hauber, J., Le, S.Y., Maizel, J.V., & Cullen, B.R. (1989). The HIV-1 rev trans-activator acts through a structured target sequence to activate nuclear export of unspliced viral mRNA. *Nature*, 338, (6212) 254-257
- Martinez-Salas, E. (1999). Internal ribosome entry site biology and its use in expression vectors. *Curr.Opin.Biotechnol.*, 10, (5) 458-464

- Marx, S.O., Reiken, S., Hisamatsu, Y., Jayaraman, T., Burkhoff, D., Rosemblyt, N., & Marks, A.R. (2000). PKA phosphorylation dissociates FKBP12.6 from the calcium release channel (ryanodine receptor): defective regulation in failing hearts. *Cell*, 101, (4) 365-376
- Matsumura, K., Mayama, T., Lin, H., Sakamoto, Y., Ogawa, K., & Imanaga, I. (2006). Effects of cyclic AMP on the function of the cardiac gap junction during hypoxia. *Exp.Clin.Cardiol.*, 11, (4) 286-293
- Matsumura, S., Iwanaga, S., Mochizuki, S., Okamoto, H., Ogawa, S., & Okada, Y. (2005). Targeted deletion or pharmacological inhibition of MMP-2 prevents cardiac rupture after myocardial infarction in mice. *J.Clin.Invest*, 115, (3) 599-609
- Matsushita, T., Oyamada, M., Fujimoto, K., Yasuda, Y., Masuda, S., Wada, Y., Oka, T., & Takamatsu, T. (1999). Remodeling of cell-cell and cell-extracellular matrix interactions at the border zone of rat myocardial infarcts. *Circ.Res.*, 85, (11) 1046-1055
- McArthur, L., Chilton, L., Smith, G.L., & Nicklin, S.A. (2015). Electrical consequences of cardiac myocyte: fibroblast coupling. *Biochem.Soc.Trans.*, 43, (3) 513-518
- Meier, O. & Greber, U.F. (2004). Adenovirus endocytosis. *J.Gene Med.*, 6 Suppl 1, S152-S163
- Melendez, G.C., McLarty, J.L., Levick, S.P., Du, Y., Janicki, J.S., & Brower, G.L. (2010). Interleukin 6 mediates myocardial fibrosis, concentric hypertrophy, and diastolic dysfunction in rats. *Hypertension*, 56, (2) 225-231
- Mende, U., Kagen, A., Cohen, A., Aramburu, J., Schoen, F.J., & Neer, E.J. (1998). Transient cardiac expression of constitutively active Galphaq leads to hypertrophy and dilated cardiomyopathy by calcineurin-dependent and independent pathways. *Proc.Natl.Acad.Sci.U.S.A*, 95, (23) 13893-13898
- Merentie, M., Lottonen-Raikaslehto, L., Parviainen, V., Huusko, J., Pikkarainen, S., Mendel, M., Laham-Karam, N., Karja, V., Rissanen, R., Hedman, M., & Yla-Herttuala, S. (2016). Efficacy and safety of myocardial gene transfer of adenovirus, adeno-associated virus and lentivirus vectors in the mouse heart. *Gene Ther.*, 23, (3) 296-305
- Merten, O.W., Hebben, M., & Bovolenta, C. (2016). Production of lentiviral vectors. *Mol.Ther.Methods Clin.Dev.*, 3, 16017
- Mewes, T. & Ravens, U. (1994). L-type calcium currents of human myocytes from ventricle of non-failing and failing hearts and from atrium. *J.Mol.Cell Cardiol.*, 26, (10) 1307-1320
- Mia, M.M., Boersema, M., & Bank, R.A. (2014). Interleukin-1beta attenuates myofibroblast formation and extracellular matrix production in dermal and lung fibroblasts exposed to transforming growth factor-beta1. *PLoS.One.*, 9, (3) e91559

- Mihara, M., Hashizume, M., Yoshida, H., Suzuki, M., & Shiina, M. (2012). IL-6/IL-6 receptor system and its role in physiological and pathological conditions. *Clin.Sci.(Lond)*, 122, (4) 143-159
- Miller, T.D., Christian, T.F., Hopfenspirger, M.R., Hodge, D.O., Gersh, B.J., & Gibbons, R.J. (1995). Infarct size after acute myocardial infarction measured by quantitative tomographic 99mTc sestamibi imaging predicts subsequent mortality. *Circulation*, 92, (3) 334-341
- Mills, W.R., Mal, N., Forudi, F., Popovic, Z.B., Penn, M.S., & Laurita, K.R. (2006). Optical mapping of late myocardial infarction in rats. *Am.J.Physiol Heart Circ.Physiol*, 290, (3) H1298-H1306
- Miragoli, M., Gaudesius, G., & Rohr, S. (2006). Electrotonic modulation of cardiac impulse conduction by myofibroblasts. *Circ.Res.*, 98, (6) 801-810
- Miragoli, M., Salvarani, N., & Rohr, S. (2007). Myofibroblasts induce ectopic activity in cardiac tissue. *Circ.Res.*, 101, (8) 755-758
- Moreno, A.P. (2004). Biophysical properties of homomeric and heteromultimeric channels formed by cardiac connexins. *Cardiovasc.Res.*, 62, (2) 276-286
- Moreno, A.P., Chanson, M., Elenes, S., Anumonwo, J., Scerri, I., Gu, H., Taffet, S.M., & Delmar, M. (2002). Role of the carboxyl terminal of connexin43 in transjunctional fast voltage gating. *Circ.Res.*, 90, (4) 450-457
- Morioka, N., Suekama, K., Zhang, F.F., Kajitani, N., Hisaoka-Nakashima, K., Takebayashi, M., & Nakata, Y. (2014). Amitriptyline up-regulates connexin43-gap junction in rat cultured cortical astrocytes via activation of the p38 and c-Fos/AP-1 signalling pathway. *Br.J.Pharmacol.*, 171, (11) 2854-2867
- Morita, N., Lee, J.H., Xie, Y., Sovari, A., Qu, Z., Weiss, J.N., & Karagueuzian, H.S. (2011). Suppression of re-entrant and multifocal ventricular fibrillation by the late sodium current blocker ranolazine. *J.Am.Coll.Cardiol.*, 57, (3) 366-375
- Morley, G.E., Taffet, S.M., & Delmar, M. (1996). Intramolecular interactions mediate pH regulation of connexin43 channels. *Biophys.J.*, 70, (3) 1294-1302
- Morley, G.E., Vaidya, D., Samie, F.H., Lo, C., Delmar, M., & Jalife, J. (1999). Characterization of conduction in the ventricles of normal and heterozygous Cx43 knockout mice using optical mapping. *J.Cardiovasc.Electrophysiol.*, 10, (10) 1361-1375
- Moser, L., Faulhaber, J., Wiesner, R.J., & Ehmke, H. (2002). Predominant activation of endothelin-dependent cardiac hypertrophy by norepinephrine in rat left ventricle. *Am.J.Physiol Regul.Integr.Comp Physiol*, 282, (5) R1389-R1394
- Myles, R.C., Bernus, O., Burton, F.L., Cobbe, S.M., & Smith, G.L. (2010). Effect of activation sequence on transmural patterns of repolarization and action potential duration in rabbit ventricular myocardium. *Am.J.Physiol Heart Circ.Physiol*, 299, (6) H1812-H1822

- Myles, R.C., Wang, L., Bers, D.M., & Ripplinger, C.M. (2015). Decreased inward rectifying K⁺ current and increased ryanodine receptor sensitivity synergistically contribute to sustained focal arrhythmia in the intact rabbit heart. *J.Physiol*, 593, (6) 1479-1493
- Nagpal, V., Rai, R., Place, A.T., Murphy, S.B., Verma, S.K., Ghosh, A.K., & Vaughan, D.E. (2016). MiR-125b Is Critical for Fibroblast-to-Myofibroblast Transition and Cardiac Fibrosis. *Circulation*, 133, (3) 291-301
- Nagy, Z.A., Virag, L., Toth, A., Biliczki, P., Acsai, K., Banyasz, T., Nanasi, P., Papp, J.G., & Varro, A. (2004). Selective inhibition of sodium-calcium exchanger by SEA-0400 decreases early and delayed after depolarization in canine heart. *Br.J.Pharmacol.*, 143, (7) 827-831
- Naitoh, K., Ichikawa, Y., Miura, T., Nakamura, Y., Miki, T., Ikeda, Y., Kobayashi, H., Nishihara, M., Ohori, K., & Shimamoto, K. (2006). MitoKATP channel activation suppresses gap junction permeability in the ischemic myocardium by an ERK-dependent mechanism. *Cardiovasc.Res.*, 70, (2) 374-383
- Nakayama, H., Bodi, I., Maillet, M., DeSantiago, J., Domeier, T.L., Mikoshiba, K., Lorenz, J.N., Blatter, L.A., Bers, D.M., & Molkenstin, J.D. (2010). The IP3 receptor regulates cardiac hypertrophy in response to select stimuli. *Circ.Res.*, 107, (5) 659-666
- Narayan, S.M. (2006). T-wave alternans and the susceptibility to ventricular arrhythmias. *J.Am.Coll.Cardiol.*, 47, (2) 269-281
- Nattel, S. & Carlsson, L. (2006). Innovative approaches to anti-arrhythmic drug therapy. *Nat.Rev.Drug Discov.*, 5, (12) 1034-1049
- Neri, S., Mariani, E., Meneghetti, A., Cattini, L., & Facchini, A. (2001). Calcein-acetyoxymethyl cytotoxicity assay: standardization of a method allowing additional analyses on recovered effector cells and supernatants. *Clin.Diagn.Lab Immunol.*, 8, (6) 1131-1135
- Nguyen, T.P., Qu, Z., & Weiss, J.N. (2013). Cardiac fibrosis and arrhythmogenesis: The road to repair is paved with perils. *J.Mol.Cell Cardiol.*, 70, 83-91
- Nguyen, T.P., Xie, Y., Garfinkel, A., Qu, Z., & Weiss, J.N. (2012). Arrhythmogenic consequences of myofibroblast-myocyte coupling. *Cardiovasc.Res.*, 93, (2) 242-251
- Niger, C., Howell, F.D., & Stains, J.P. (2010). Interleukin-1beta increases gap junctional communication among synovial fibroblasts via the extracellular-signal-regulated kinase pathway. *Biol.Cell*, 102, (1) 37-49
- Nishida, M., Onohara, N., Sato, Y., Suda, R., Ogushi, M., Tanabe, S., Inoue, R., Mori, Y., & Kurose, H. (2007). Galphai2/13-mediated up-regulation of TRPC6 negatively regulates endothelin-1-induced cardiac myofibroblast formation and collagen synthesis through nuclear factor of activated T cells activation. *J.Biol.Chem.*, 282, (32) 23117-23128

- Nishikawa, N., Masuyama, T., Yamamoto, K., Sakata, Y., Mano, T., Miwa, T., Sugawara, M., & Hori, M. (2001). Long-term administration of amlodipine prevents decompensation to diastolic heart failure in hypertensive rats. *J.Am.Coll.Cardiol.*, 38, (5) 1539-1545
- Nisole, S. & Saib, A. (2004). Early steps of retrovirus replicative cycle. *Retrovirology.*, 1, 9
- Noorman, M., van der Heyden, M.A., van Veen, T.A., Cox, M.G., Hauer, R.N., de Bakker, J.M., & van Rijen, H.V. (2009). Cardiac cell-cell junctions in health and disease: Electrical versus mechanical coupling. *J.Mol.Cell Cardiol.*, 47, (1) 23-31
- O'Carroll, S.J., Kho, D.T., Wiltshire, R., Nelson, V., Rotimi, O., Johnson, R., Angel, C.E., & Graham, E.S. (2015). Pro-inflammatory TNFalpha and IL-1beta differentially regulate the inflammatory phenotype of brain microvascular endothelial cells. *J.Neuroinflammation.*, 12, 131
- Oka, T., Xu, J., Kaiser, R.A., Melendez, J., Hambleton, M., Sargent, M.A., Lorts, A., Brunskill, E.W., Dorn, G.W., Conway, S.J., Aronow, B.J., Robbins, J., & Molkentin, J.D. (2007). Genetic manipulation of periostin expression reveals a role in cardiac hypertrophy and ventricular remodeling. *Circ.Res.*, 101, (3) 313-321
- Olaso, E., Labrador, J.P., Wang, L., Ikeda, K., Eng, F.J., Klein, R., Lovett, D.H., Lin, H.C., & Friedman, S.L. (2002). Discoidin domain receptor 2 regulates fibroblast proliferation and migration through the extracellular matrix in association with transcriptional activation of matrix metalloproteinase-2. *J.Biol.Chem.*, 277, (5) 3606-3613
- Olivetti, G., Capasso, J.M., Sonnenblick, E.H., & Anversa, P. (1990). Side-to-side slippage of myocytes participates in ventricular wall remodeling acutely after myocardial infarction in rats. *Circ.Res.*, 67, (1) 23-34
- Omichi, C., Lamp, S.T., Lin, S.F., Yang, J., Baher, A., Zhou, S., Attin, M., Lee, M.H., Karagueuzian, H.S., Kogan, B., Qu, Z., Garfinkel, A., Chen, P.S., & Weiss, J.N. (2004). Intracellular Ca dynamics in ventricular fibrillation. *Am.J.Physiol Heart Circ.Physiol*, 286, (5) H1836-H1844
- Ongstad, E. & Kohl, P. (2016). Fibroblast-myocyte coupling in the heart: Potential relevance for therapeutic interventions. *J.Mol.Cell Cardiol.*, 91, 238-246
- Oxford, E.M., Musa, H., Maass, K., Coombs, W., Taffet, S.M., & Delmar, M. (2007). Connexin43 remodeling caused by inhibition of plakophilin-2 expression in cardiac cells. *Circ.Res.*, 101, (7) 703-711
- Pacifico, A., Hohnloser, S.H., Williams, J.H., Tao, B., Saksena, S., Henry, P.D., & Prystowsky, E.N. (1999). Prevention of implantable-defibrillator shocks by treatment with sotalol. d,l-Sotalol Implantable Cardioverter-Defibrillator Study Group. *N.Engl.J.Med.*, 340, (24) 1855-1862
- Pan, Z., Sun, X., Shan, H., Wang, N., Wang, J., Ren, J., Feng, S., Xie, L., Lu, C., Yuan, Y., Zhang, Y., Wang, Y., Lu, Y., & Yang, B. (2012). MicroRNA-101 inhibited postinfarct cardiac fibrosis and improved left ventricular compliance via the FBJ

- osteosarcoma oncogene/transforming growth factor-beta1 pathway. *Circulation*, 126, (7) 840-850
- Parizi, M., Howard, E.W., & Tomasek, J.J. (2000). Regulation of LPA-promoted myofibroblast contraction: role of Rho, myosin light chain kinase, and myosin light chain phosphatase. *Exp.Cell Res.*, 254, (2) 210-220
- Park, S.A., Lee, S.R., Tung, L., & Yue, D.T. (2014). Optical mapping of optogenetically shaped cardiac action potentials. *Sci.Rep.*, 4, 6125
- Pavlovic, D., McLatchie, L.M., & Shattock, M.J. (2010). The rate of loss of T-tubules in cultured adult ventricular myocytes is species dependent. *Exp.Physiol*, 95, (4) 518-527
- Pedrotty, D.M., Klinger, R.Y., Kirkton, R.D., & Bursac, N. (2009). Cardiac fibroblast paracrine factors alter impulse conduction and ion channel expression of neonatal rat cardiomyocytes. *Cardiovasc.Res.*, 83, (4) 688-697
- Peng, H., Xu, J., Yang, X.P., Dai, X., Peterson, E.L., Carretero, O.A., & Rhaleb, N.E. (2014). Thymosin-beta4 prevents cardiac rupture and improves cardiac function in mice with myocardial infarction. *Am.J.Physiol Heart Circ.Physiol*, 307, (5) H741-H751
- Peracchia, C. (2004). Chemical gating of gap junction channels; roles of calcium, pH and calmodulin. *Biochim.Biophys.Acta*, 1662, (1-2) 61-80
- Perry, M.M., Moschos, S.A., Williams, A.E., Shepherd, N.J., Lerner-Svensson, H.M., & Lindsay, M.A. (2008). Rapid changes in microRNA-146a expression negatively regulate the IL-1beta-induced inflammatory response in human lung alveolar epithelial cells. *J.Immunol.*, 180, (8) 5689-5698
- Peters, N.S., Coromilas, J., Severs, N.J., & Wit, A.L. (1997). Disturbed connexin43 gap junction distribution correlates with the location of reentrant circuits in the epicardial border zone of healing canine infarcts that cause ventricular tachycardia. *Circulation*, 95, (4) 988-996
- Peters, N.S., Severs, N.J., Rothery, S.M., Lincoln, C., Yacoub, M.H., & Green, C.R. (1994). Spatiotemporal relation between gap junctions and fascia adherens junctions during postnatal development of human ventricular myocardium. *Circulation*, 90, (2) 713-725
- Petrich, B.G., Gong, X., Lerner, D.L., Wang, X., Brown, J.H., Saffitz, J.E., & Wang, Y. (2002). c-Jun N-terminal kinase activation mediates downregulation of connexin43 in cardiomyocytes. *Circ.Res.*, 91, (7) 640-647
- Phatharajaree, W., Phrommintikul, A., & Chattipakorn, N. (2007). Matrix metalloproteinases and myocardial infarction. *Can.J.Cardiol.*, 23, (9) 727-733
- Piacentino, V., Weber, C.R., Chen, X., Weisser-Thomas, J., Margulies, K.B., Bers, D.M., & Houser, S.R. (2003). Cellular basis of abnormal calcium transients of failing human ventricular myocytes. *Circ.Res.*, 92, (6) 651-658

- Pinto, A.R., Ilinykh, A., Ivey, M.J., Kuwabara, J.T., D'Antoni, M.L., Debuque, R., Chandran, A., Wang, L., Arora, K., Rosenthal, N.A., & Tallquist, M.D. (2016). Revisiting Cardiac Cellular Composition. *Circ.Res.*, 118, (3) 400-409
- Plotnikov, E.Y., Khryapenkova, T.G., Vasileva, A.K., Marey, M.V., Galkina, S.I., Isaev, N.K., Sheval, E.V., Polyakov, V.Y., Sukhikh, G.T., & Zorov, D.B. (2008). Cell-to-cell cross-talk between mesenchymal stem cells and cardiomyocytes in co-culture. *J.Cell Mol.Med.*, 12, (5A) 1622-1631
- Poelzing, S. & Rosenbaum, D.S. (2004). Altered connexin43 expression produces arrhythmia substrate in heart failure. *Am.J.Physiol Heart Circ.Physiol*, 287, (4) H1762-H1770
- Poindexter, B.J., Smith, J.R., Buja, L.M., & Bick, R.J. (2001). Calcium signaling mechanisms in dedifferentiated cardiac myocytes: comparison with neonatal and adult cardiomyocytes. *Cell Calcium*, 30, (6) 373-382
- Polontchouk, L., Ebelt, B., Jackels, M., & Dhein, S. (2002). Chronic effects of endothelin 1 and angiotensin II on gap junctions and intercellular communication in cardiac cells. *FASEB J.*, 16, (1) 87-89
- Qu, J., Barbuti, A., Protas, L., Santoro, B., Cohen, I.S., & Robinson, R.B. (2001). HCN2 overexpression in newborn and adult ventricular myocytes: distinct effects on gating and excitability. *Circ.Res.*, 89, (1) E8-14
- Quinn, T.A., Camelliti, P., Rog-Zielinska, E.A., Siedlecka, U., Poggioli, T., O'Toole, E.T., Knopfel, T., & Kohl, P. (2016). Electrotonic coupling of excitable and nonexcitable cells in the heart revealed by optogenetics. *Proc.Natl.Acad.Sci.U.S.A*, 113, (51) 14852-14857
- Radice, G.L., Rayburn, H., Matsunami, H., Knudsen, K.A., Takeichi, M., & Hynes, R.O. (1997). Developmental defects in mouse embryos lacking N-cadherin. *Dev.Biol.*, 181, (1) 64-78
- Ramanathan, C., Jia, P., Ghanem, R., Ryu, K., & Rudy, Y. (2006). Activation and repolarization of the normal human heart under complete physiological conditions. *Proc.Natl.Acad.Sci.U.S.A*, 103, (16) 6309-6314
- Ramezani, A. & Hawley, R.G. (2002). Overview of the HIV-1 Lentiviral Vector System. *Curr.Protoc.Mol.Biol.*, Chapter 16, Unit
- Rauschhuber, C., Noske, N., & Ehrhardt, A. (2012). New insights into stability of recombinant adenovirus vector genomes in mammalian cells. *Eur.J.Cell Biol.*, 91, (1) 2-9
- Reaume, A.G., de Sousa, P.A., Kulkarni, S., Langille, B.L., Zhu, D., Davies, T.C., Juneja, S.C., Kidder, G.M., & Rossant, J. (1995). Cardiac malformation in neonatal mice lacking connexin43. *Science*, 267, (5205) 1831-1834
- Reddy, V.S. & Nemerow, G.R. (2014). Structures and organization of adenovirus cement proteins provide insights into the role of capsid maturation in virus entry and infection. *Proc.Natl.Acad.Sci.U.S.A*, 111, (32) 11715-11720

- Reinecke, H., Minami, E., Virag, J.I., & Murry, C.E. (2004). Gene transfer of connexin43 into skeletal muscle. *Hum.Gene Ther.*, 15, (7) 627-636
- Remo, B.F., Qu, J., Volpicelli, F.M., Giovannone, S., Shin, D., Lader, J., Liu, F.Y., Zhang, J., Lent, D.S., Morley, G.E., & Fishman, G.I. (2011). Phosphatase-resistant gap junctions inhibit pathological remodeling and prevent arrhythmias. *Circ.Res.*, 108, (12) 1459-1466
- Revel, J.P. & Karnovsky, M.J. (1967). Hexagonal array of subunits in intercellular junctions of the mouse heart and liver. *J.Cell Biol.*, 33, (3) C7-C12
- Riis, J.L., Johansen, C., Vestergaard, C., Otkjaer, K., Kragballe, K., & Iversen, L. (2011). CCL27 expression is regulated by both p38 MAPK and IKKbeta signalling pathways. *Cytokine*, 56, (3) 699-707
- Roberts-Thomson, K.C., Lau, D.H., & Sanders, P. (2011). The diagnosis and management of ventricular arrhythmias. *Nat.Rev.Cardiol.*, 8, (6) 311-321
- Roell, W., Lewalter, T., Sasse, P., Tallini, Y.N., Choi, B.R., Breitbach, M., Doran, R., Becher, U.M., Hwang, S.M., Bostani, T., von, M.J., Hofmann, A., Reining, S., Eiberger, B., Gabris, B., Pfeifer, A., Welz, A., Willecke, K., Salama, G., Schrickel, J.W., Kotlikoff, M.I., & Fleischmann, B.K. (2007). Engraftment of connexin 43-expressing cells prevents post-infarct arrhythmia. *Nature*, 450, (7171) 819-824
- Rohr, S., Kucera, J.P., & Kleber, A.G. (1998). Slow conduction in cardiac tissue, I: effects of a reduction of excitability versus a reduction of electrical coupling on microconduction. *Circ.Res.*, 83, (8) 781-794
- Rosenbaum, D.S., Jackson, L.E., Smith, J.M., Garan, H., Ruskin, J.N., & Cohen, R.J. (1994). Electrical alternans and vulnerability to ventricular arrhythmias. *N.Engl.J.Med.*, 330, (4) 235-241
- Rosenkranz, S., Flesch, M., Amann, K., Haeuseler, C., Kilter, H., Seeland, U., Schluter, K.D., & Bohm, M. (2002). Alterations of beta-adrenergic signaling and cardiac hypertrophy in transgenic mice overexpressing TGF-beta(1). *Am.J.Physiol Heart Circ.Physiol*, 283, (3) H1253-H1262
- Rosewell, A., Vetrini, F., & Ng, P. (2011). Helper-Dependent Adenoviral Vectors. *J.Genet.Syindr.Gene Ther.*, Suppl 5,
- Rosker, C., Salvarani, N., Schmutz, S., Grand, T., & Rohr, S. (2011). Abolishing myofibroblast arrhythmogenicity by pharmacological ablation of alpha-smooth muscle actin containing stress fibers. *Circ.Res.*, 109, (10) 1120-1131
- Roy, S., Khanna, S., Hussain, S.R., Biswas, S., Azad, A., Rink, C., Gnyawali, S., Shilo, S., Nuovo, G.J., & Sen, C.K. (2009). MicroRNA expression in response to murine myocardial infarction: miR-21 regulates fibroblast metalloprotease-2 via phosphatase and tensin homologue. *Cardiovasc.Res.*, 82, (1) 21-29
- Rubart, M. (2004). Two-photon microscopy of cells and tissue. *Circ.Res.*, 95, (12) 1154-1166

- Rubart, M., Pasumarthi, K.B., Nakajima, H., Soonpaa, M.H., Nakajima, H.O., & Field, L.J. (2003). Physiological coupling of donor and host cardiomyocytes after cellular transplantation. *Circ.Res.*, 92, (11) 1217-1224
- Rubart, M., Soonpaa, M.H., Nakajima, H., & Field, L.J. (2004). Spontaneous and evoked intracellular calcium transients in donor-derived myocytes following intracardiac myoblast transplantation. *J.Clin.Invest*, 114, (6) 775-783
- Ruiz, P., Brinkmann, V., Ledermann, B., Behrend, M., Grund, C., Thalhammer, C., Vogel, F., Birchmeier, C., Gunthert, U., Franke, W.W., & Birchmeier, W. (1996). Targeted mutation of plakoglobin in mice reveals essential functions of desmosomes in the embryonic heart. *J.Cell Biol.*, 135, (1) 215-225
- Rustom, A., Saffrich, R., Markovic, I., Walther, P., & Gerdes, H.H. (2004). Nanotubular highways for intercellular organelle transport. *Science*, 303, (5660) 1007-1010
- Ruginov, E., Sharabani-Yosef, O., Nagler, A., Einbinder, T., Feinberg, M.S., Holbova, R., Douvdevani, A., & Leor, J. (2008). Transplantation of genetically engineered cardiac fibroblasts producing recombinant human erythropoietin to repair the infarcted myocardium. *Fibrogenesis.Tissue Repair*, 1, (1) 7
- Sabir, I.N., Ma, N., Jones, V.J., Goddard, C.A., Zhang, Y., Kalin, A., Grace, A.A., & Huang, C.L. (2010). Alternans in genetically modified langendorff-perfused murine hearts modeling catecholaminergic polymorphic ventricular tachycardia. *Front Physiol*, 1, 126
- Saffitz, J.E., Laing, J.G., & Yamada, K.A. (2000). Connexin expression and turnover : implications for cardiac excitability. *Circ.Res.*, 86, (7) 723-728
- Sakuma, T., Barry, M.A., & Ikeda, Y. (2012). Lentiviral vectors: basic to translational. *Biochem.J.*, 443, (3) 603-618
- Salameh, A., Wustmann, A., Karl, S., Blanke, K., Apel, D., Rojas-Gomez, D., Franke, H., Mohr, F.W., Janousek, J., & Dhein, S. (2010). Cyclic mechanical stretch induces cardiomyocyte orientation and polarization of the gap junction protein connexin43. *Circ.Res.*, 106, (10) 1592-1602
- Salvarani, N., Maguy, A., De Simone, S.A., Miragoli, M., Jousset, F., & Rohr, S. (2017). TGF-beta1 (Transforming Growth Factor-beta1) Plays a Pivotal Role in Cardiac Myofibroblast Arrhythmogenicity. *Circ.Arrhythm.Electrophysiol.*, 10, (5) e004567
- SANO, T., TAKAYAMA, N., & SHIMAMOTO, T. (1959). Directional difference of conduction velocity in the cardiac ventricular syncytium studied by microelectrodes. *Circ.Res.*, 7, (2) 262-267
- Santiago, J.J., Dangerfield, A.L., Rattan, S.G., Bathe, K.L., Cunnington, R.H., Raizman, J.E., Bedosky, K.M., Freed, D.H., Kardami, E., & Dixon, I.M. (2010). Cardiac fibroblast to myofibroblast differentiation in vivo and in vitro: expression of focal adhesion components in neonatal and adult rat ventricular myofibroblasts. *Dev.Dyn.*, 239, (6) 1573-1584

- Sarkar, S., Vellaichamy, E., Young, D., & Sen, S. (2004). Influence of cytokines and growth factors in ANG II-mediated collagen upregulation by fibroblasts in rats: role of myocytes. *Am.J.Physiol Heart Circ.Physiol*, 287, (1) H107-H117
- Sato, D., Shiferaw, Y., Garfinkel, A., Weiss, J.N., Qu, Z., & Karma, A. (2006). Spatially discordant alternans in cardiac tissue: role of calcium cycling. *Circ.Res.*, 99, (5) 520-527
- Saxena, A., Chen, W., Su, Y., Rai, V., Uche, O.U., Li, N., & Frangogiannis, N.G. (2013). IL-1 induces proinflammatory leukocyte infiltration and regulates fibroblast phenotype in the infarcted myocardium. *J.Immunol.*, 191, (9) 4838-4848
- Schlegel, R., Tralka, T.S., Willingham, M.C., & Pastan, I. (1983). Inhibition of VSV binding and infectivity by phosphatidylserine: is phosphatidylserine a VSV-binding site? *Cell*, 32, (2) 639-646
- Schmittgen, T.D. & Livak, K.J. (2008). Analyzing real-time PCR data by the comparative C(T) method. *Nat.Protoc.*, 3, (6) 1101-1108
- Schnell, U., Dijk, F., Sjollem, K.A., & Giepmans, B.N. (2012). Immunolabeling artifacts and the need for live-cell imaging. *Nat.Methods*, 9, (2) 152-158
- Schron, E.B., Exner, D.V., Yao, Q., Jenkins, L.S., Steinberg, J.S., Cook, J.R., Kutalek, S.P., Friedman, P.L., Buben, R.S., Page, R.L., & Powell, J. (2002). Quality of life in the antiarrhythmics versus implantable defibrillators trial: impact of therapy and influence of adverse symptoms and defibrillator shocks. *Circulation*, 105, (5) 589-594
- Schultz, J.J., Witt, S.A., Glascock, B.J., Nieman, M.L., Reiser, P.J., Nix, S.L., Kimball, T.R., & Doetschman, T. (2002). TGF-beta1 mediates the hypertrophic cardiomyocyte growth induced by angiotensin II. *J.Clin.Invest*, 109, (6) 787-796
- Schuster, E.H. & Bulkley, B.H. (1979). Expansion of transmural myocardial infarction: a pathophysiologic factor in cardiac rupture. *Circulation*, 60, (7) 1532-1538
- Schwinger, R.H., Munch, G., Bolck, B., Karczewski, P., Krause, E.G., & Erdmann, E. (1999). Reduced Ca(2+)-sensitivity of SERCA 2a in failing human myocardium due to reduced serin-16 phospholamban phosphorylation. *J.Mol.Cell Cardiol.*, 31, (3) 479-491
- Scriven, D.R., Dan, P., & Moore, E.D. (2000). Distribution of proteins implicated in excitation-contraction coupling in rat ventricular myocytes. *Biophys.J.*, 79, (5) 2682-2691
- Shaw, R.M. & Rudy, Y. (1997). Ionic mechanisms of propagation in cardiac tissue. Roles of the sodium and L-type calcium currents during reduced excitability and decreased gap junction coupling. *Circ.Res.*, 81, (5) 727-741
- Shimazaki, M., Nakamura, K., Kii, I., Kashima, T., Amizuka, N., Li, M., Saito, M., Fukuda, K., Nishiyama, T., Kitajima, S., Saga, Y., Fukayama, M., Sata, M., & Kudo, A. (2008). Periostin is essential for cardiac healing after acute myocardial infarction. *J.Exp.Med.*, 205, (2) 295-303

- Shivakumar, K., Dostal, D.E., Boheler, K., Baker, K.M., & Lakatta, E.G. (2003). Differential response of cardiac fibroblasts from young adult and senescent rats to ANG II. *Am.J.Physiol Heart Circ.Physiol*, 284, (4) H1454-H1459
- Shivakumar, K., Sollott, S.J., Sangeetha, M., Sapna, S., Ziman, B., Wang, S., & Lakatta, E.G. (2008). Paracrine effects of hypoxic fibroblast-derived factors on the MPT-ROS threshold and viability of adult rat cardiac myocytes. *Am.J.Physiol Heart Circ.Physiol*, 294, (6) H2653-H2658
- Shyu, K.G., Wang, B.W., Kuan, P., & Chang, H. (2008). RNA interference for discoidin domain receptor 2 attenuates neointimal formation in balloon injured rat carotid artery. *Arterioscler.Thromb.Vasc.Biol.*, 28, (8) 1447-1453
- Sim, I., McDonald, K.M., Lavori, P.W., Norbutas, C.M., & Hlatky, M.A. (1997). Quantitative overview of randomized trials of amiodarone to prevent sudden cardiac death. *Circulation*, 96, (9) 2823-2829
- Simon, A.M., Goodenough, D.A., & Paul, D.L. (1998). Mice lacking connexin40 have cardiac conduction abnormalities characteristic of atrioventricular block and bundle branch block. *Curr.Biol.*, 8, (5) 295-298
- Smith, J.H., Green, C.R., Peters, N.S., Rothery, S., & Severs, N.J. (1991). Altered patterns of gap junction distribution in ischemic heart disease. An immunohistochemical study of human myocardium using laser scanning confocal microscopy. *Am.J.Pathol.*, 139, (4) 801-821
- Snider, P., Standley, K.N., Wang, J., Azhar, M., Doetschman, T., & Conway, S.J. (2009). Origin of cardiac fibroblasts and the role of periostin. *Circ.Res.*, 105, (10) 934-947
- Sohl, G., Maxeiner, S., & Willecke, K. (2005). Expression and functions of neuronal gap junctions. *Nat.Rev.Neurosci.*, 6, (3) 191-200
- Sohl, G. & Willecke, K. (2004). Gap junctions and the connexin protein family. *Cardiovasc.Res.*, 62, (2) 228-232
- Solan, J.L. & Lampe, P.D. (2014). Specific Cx43 phosphorylation events regulate gap junction turnover in vivo. *FEBS Lett.*, 588, (8) 1423-1429
- Song, Y., Shryock, J.C., Wagner, S., Maier, L.S., & Belardinelli, L. (2006). Blocking late sodium current reduces hydrogen peroxide-induced arrhythmogenic activity and contractile dysfunction. *J.Pharmacol.Exp.Ther.*, 318, (1) 214-222
- Sopel, M.J., Rosin, N.L., Lee, T.D., & Legare, J.F. (2011). Myocardial fibrosis in response to Angiotensin II is preceded by the recruitment of mesenchymal progenitor cells. *Lab Invest*, 91, (4) 565-578
- Sosinsky, G.E. & Nicholson, B.J. (2005). Structural organization of gap junction channels. *Biochim.Biophys.Acta*, 1711, (2) 99-125
- Souders, C.A., Bowers, S.L., & Baudino, T.A. (2009). Cardiac fibroblast: the renaissance cell. *Circ.Res.*, 105, (12) 1164-1176

- Spiess, E., Bestvater, F., Heckel-Pompey, A., Toth, K., Hacker, M., Stobrawa, G., Feurer, T., Wotzlaw, C., Berchner-Pfannschmidt, U., Porwol, T., & Acker, H. (2005). Two-photon excitation and emission spectra of the green fluorescent protein variants ECFP, EGFP and EYFP. *J.Microsc.*, 217, (Pt 3) 200-204
- St John, M.A., Dohadwala, M., Luo, J., Wang, G., Lee, G., Shih, H., Heinrich, E., Krysan, K., Walser, T., Hazra, S., Zhu, L., Lai, C., Abemayor, E., Fishbein, M., Elashoff, D.A., Sharma, S., & Dubinett, S.M. (2009). Proinflammatory mediators upregulate snail in head and neck squamous cell carcinoma. *Clin.Cancer Res.*, 15, (19) 6018-6027
- Stein, M., van Veen, T.A., Hauer, R.N., de Bakker, J.M., & van Rijen, H.V. (2011). A 50% reduction of excitability but not of intercellular coupling affects conduction velocity restitution and activation delay in the mouse heart. *PLoS.One.*, 6, (6) e20310
- Stergiopoulos, K., Alvarado, J.L., Mastroianni, M., Ek-Vitorin, J.F., Taffet, S.M., & Delmar, M. (1999). Hetero-domain interactions as a mechanism for the regulation of connexin channels. *Circ.Res.*, 84, (10) 1144-1155
- Stimers, J.R. & Dobretsov, M. (1998). Adrenergic stimulation of Na/K pump current in adult rat cardiac myocytes in short-term culture. *J.Membr.Biol.*, 163, (3) 205-216
- Sun, L.Y., Bie, Z.D., Zhang, C.H., Li, H., Li, L.D., & Yang, J. (2016). MiR-154 directly suppresses DKK2 to activate Wnt signaling pathway and enhance activation of cardiac fibroblasts. *Cell Biol.Int.*, 40, (12) 1271-1279
- Sutton, M.G. & Sharpe, N. (2000). Left ventricular remodeling after myocardial infarction: pathophysiology and therapy. *Circulation*, 101, (25) 2981-2988
- Swaney, J.S., Patel, H.H., Yokoyama, U., Lai, N.C., Spellman, M., Insel, P.A., & Roth, D.M. (2007). Adenylyl cyclase activity and function are decreased in rat cardiac fibroblasts after myocardial infarction. *Am.J.Physiol Heart Circ.Physiol*, 293, (5) H3216-H3220
- Tacheau, C., Laboureaux, J., Mauviel, A., & Verrecchia, F. (2008). TNF-alpha represses connexin43 expression in HaCat keratinocytes via activation of JNK signaling. *J.Cell Physiol*, 216, (2) 438-444
- Takeshita, K., Hayashi, M., Iino, S., Kondo, T., Inden, Y., Iwase, M., Kojima, T., Hirai, M., Ito, M., Loskutoff, D.J., Saito, H., Murohara, T., & Yamamoto, K. (2004). Increased expression of plasminogen activator inhibitor-1 in cardiomyocytes contributes to cardiac fibrosis after myocardial infarction. *Am.J.Pathol.*, 164, (2) 449-456
- Tamamori, M., Ito, H., Hiroe, M., Marumo, F., & Hata, R.I. (1997). Stimulation of collagen synthesis in rat cardiac fibroblasts by exposure to hypoxic culture conditions and suppression of the effect by natriuretic peptides. *Cell Biol.Int.*, 21, (3) 175-180

- Tarzemany, R., Jiang, G., Larjava, H., & Hakkinen, L. (2015). Expression and function of connexin 43 in human gingival wound healing and fibroblasts. *PLoS.One.*, 10, (1) e0115524
- Teunissen, B.E., Jansen, A.T., van Amersfoorth, S.C., O'Brien, T.X., Jongasma, H.J., & Bierhuizen, M.F. (2003). Analysis of the rat connexin 43 proximal promoter in neonatal cardiomyocytes. *Gene*, 322, 123-136
- Thomas, C.E., Ehrhardt, A., & Kay, M.A. (2003). Progress and problems with the use of viral vectors for gene therapy. *Nat.Rev.Genet.*, 4, (5) 346-358
- Thompson, S.A., Blazeski, A., Copeland, C.R., Cohen, D.M., Chen, C.S., Reich, D.M., & Tung, L. (2014). Acute slowing of cardiac conduction in response to myofibroblast coupling to cardiomyocytes through N-cadherin. *J.Mol.Cell Cardiol.*, 68, 29-37
- Thompson, S.A., Copeland, C.R., Reich, D.H., & Tung, L. (2011). Mechanical coupling between myofibroblasts and cardiomyocytes slows electric conduction in fibrotic cell monolayers. *Circulation*, 123, (19) 2083-2093
- Thum, T., Galuppo, P., Wolf, C., Fiedler, J., Kneitz, S., van Laake, L.W., Doevendans, P.A., Mummery, C.L., Borlak, J., Haverich, A., Gross, C., Engelhardt, S., Ertl, G., & Bauersachs, J. (2007). MicroRNAs in the human heart: a clue to fetal gene reprogramming in heart failure. *Circulation*, 116, (3) 258-267
- Thum, T., Gross, C., Fiedler, J., Fischer, T., Kissler, S., Bussen, M., Galuppo, P., Just, S., Rottbauer, W., Frantz, S., Castoldi, M., Soutschek, J., Koteliangsky, V., Rosenwald, A., Basson, M.A., Licht, J.D., Pena, J.T., Rouhanifard, S.H., Muckenthaler, M.U., Tuschl, T., Martin, G.R., Bauersachs, J., & Engelhardt, S. (2008). MicroRNA-21 contributes to myocardial disease by stimulating MAP kinase signalling in fibroblasts. *Nature*, 456, (7224) 980-984
- Thygesen, K., Alpert, J.S., Jaffe, A.S., Simoons, M.L., Chaitman, B.R., & White, H.D. (2012). Third universal definition of myocardial infarction. *Glob.Heart*, 7, (4) 275-295
- Tian, B., Liu, J., Bitterman, P.B., & Bache, R.J. (2002). Mechanisms of cytokine induced NO-mediated cardiac fibroblast apoptosis. *Am.J.Physiol Heart Circ.Physiol*, 283, (5) H1958-H1967
- Toivonen, R., Koskenvuo, J., Merentie, M., Soderstrom, M., Yla-Herttuala, S., & Savontaus, M. (2012). Intracardiac injection of a capsid-modified Ad5/35 results in decreased heart toxicity when compared to standard Ad5. *Viol.J.*, 9, 296
- Toldo, S., Mezzaroma, E., Mauro, A.G., Salloum, F., Van Tassell, B.W., & Abbate, A. (2015). The inflammasome in myocardial injury and cardiac remodeling. *Antioxid.Redox.Signal.*, 22, (13) 1146-1161
- Tomasek, J.J., McRae, J., Owens, G.K., & Haaksma, C.J. (2005). Regulation of alpha-smooth muscle actin expression in granulation tissue myofibroblasts is dependent on the intronic CArG element and the transforming growth factor-beta1 control element. *Am.J.Pathol.*, 166, (5) 1343-1351

- Tondato, F., Zeng, H., Goodchild, T., Ng, F.S., Chronos, N., & Peters, N.S. (2015). Autologous dermal fibroblast injections slow atrioventricular conduction and ventricular rate in atrial fibrillation in swine. *Circ.Arrhythm.Electrophysiol.*, 8, (2) 439-446
- Tonon, R. & D'Andrea, P. (2000). Interleukin-1beta increases the functional expression of connexin 43 in articular chondrocytes: evidence for a Ca²⁺-dependent mechanism. *J.Bone Miner.Res.*, 15, (9) 1669-1677
- Travers, J.G., Kamal, F.A., Robbins, J., Yutzey, K.E., & Blaxall, B.C. (2016). Cardiac Fibrosis: The Fibroblast Awakens. *Circ.Res.*, 118, (6) 1021-1040
- Tse, G. (2016). Mechanisms of cardiac arrhythmias. *J.Arrhythm.*, 32, (2) 75-81
- Valderrabano, M. (2007). Influence of anisotropic conduction properties in the propagation of the cardiac action potential. *Prog.Biophys.Mol.Biol.*, 94, (1-2) 144-168
- van Amerongen, M.J., Bou-Gharios, G., Popa, E., van, A.J., Petersen, A.H., van Dam, G.M., van Luyn, M.J., & Harmsen, M.C. (2008). Bone marrow-derived myofibroblasts contribute functionally to scar formation after myocardial infarction. *J.Pathol.*, 214, (3) 377-386
- van der Bogt, K.E., Schrepfer, S., Yu, J., Sheikh, A.Y., Hoyt, G., Govaert, J.A., Velotta, J.B., Contag, C.H., Robbins, R.C., & Wu, J.C. (2009). Comparison of transplantation of adipose tissue- and bone marrow-derived mesenchymal stem cells in the infarcted heart. *Transplantation*, 87, (5) 642-652
- van Kempen, M.J., ten, V., I, Wessels, A., Oosthoek, P.W., Gros, D., Jongasma, H.J., Moorman, A.F., & Lamers, W.H. (1995). Differential connexin distribution accommodates cardiac function in different species. *Microsc.Res.Tech.*, 31, (5) 420-436
- van Nieuwenhoven, F.A., Hemmings, K.E., Porter, K.E., & Turner, N.A. (2013). Combined effects of interleukin-1alpha and transforming growth factor-beta1 on modulation of human cardiac fibroblast function. *Matrix Biol.*, 32, (7-8) 399-406
- van Rijen, H.V., van Veen, T.A., van Kempen, M.J., Wilms-Schopman, F.J., Potse, M., Krueger, O., Willecke, K., Opthof, T., Jongasma, H.J., & de Bakker, J.M. (2001). Impaired conduction in the bundle branches of mouse hearts lacking the gap junction protein connexin40. *Circulation*, 103, (11) 1591-1598
- van, R.E. & Olson, E.N. (2012). MicroRNA therapeutics for cardiovascular disease: opportunities and obstacles. *Nat.Rev.Drug Discov.*, 11, (11) 860-872
- Varro, A., Lathrop, D.A., Hester, S.B., Nanasi, P.P., & Papp, J.G. (1993). Ionic currents and action potentials in rabbit, rat, and guinea pig ventricular myocytes. *Basic Res.Cardiol.*, 88, (2) 93-102
- Vasquez, C., Mohandas, P., Louie, K.L., Benamer, N., Bapat, A.C., & Morley, G.E. (2010). Enhanced fibroblast-myocyte interactions in response to cardiac injury. *Circ.Res.*, 107, (8) 1011-1020

- Vassallo, P. & Trohman, R.G. (2007). Prescribing amiodarone: an evidence-based review of clinical indications. *JAMA*, 298, (11) 1312-1322
- Verselis, V.K., Ginter, C.S., & Bargiello, T.A. (1994). Opposite voltage gating polarities of two closely related connexins. *Nature*, 368, (6469) 348-351
- Vivar, R., Humeres, C., Ayala, P., Olmedo, I., Catalan, M., Garcia, L., Lavandero, S., & Diaz-Araya, G. (2013). TGF-beta1 prevents simulated ischemia/reperfusion-induced cardiac fibroblast apoptosis by activation of both canonical and non-canonical signaling pathways. *Biochim.Biophys.Acta*, 1832, (6) 754-762
- Vozzi, C., Dupont, E., Coppens, S.R., Yeh, H.I., & Severs, N.J. (1999). Chamber-related differences in connexin expression in the human heart. *J.Mol.Cell Cardiol.*, 31, (5) 991-1003
- Walker, N.L., Burton, F.L., Kettlewell, S., Smith, G.L., & Cobbe, S.M. (2007). Mapping of epicardial activation in a rabbit model of chronic myocardial infarction. *J.Cardiovasc.Electrophysiol.*, 18, (8) 862-868
- Wang, L., Myles, R.C., De Jesus, N.M., Ohlendorf, A.K., Bers, D.M., & Ripplinger, C.M. (2014a). Optical mapping of sarcoplasmic reticulum Ca²⁺ in the intact heart: ryanodine receptor refractoriness during alternans and fibrillation. *Circ.Res.*, 114, (9) 1410-1421
- Wang, L., Zhang, L.F., Wu, J., Xu, S.J., Xu, Y.Y., Li, D., Lou, J.T., & Liu, M.F. (2014b). IL-1beta-mediated repression of microRNA-101 is crucial for inflammation-promoted lung tumorigenesis. *Cancer Res.*, 74, (17) 4720-4730
- Wang, X., Veruki, M.L., Bukoreshtliev, N.V., Hartveit, E., & Gerdes, H.H. (2010). Animal cells connected by nanotubes can be electrically coupled through interposed gap-junction channels. *Proc.Natl.Acad.Sci.U.S.A*, 107, (40) 17194-17199
- Wang, X., Wang, H.X., Li, Y.L., Zhang, C.C., Zhou, C.Y., Wang, L., Xia, Y.L., Du, J., & Li, H.H. (2015). MicroRNA Let-7i negatively regulates cardiac inflammation and fibrosis. *Hypertension*, 66, (4) 776-785
- Wang, Y.S., Li, S.H., Guo, J., Mihic, A., Wu, J., Sun, L., Davis, K., Weisel, R.D., & Li, R.K. (2014c). Role of miR-145 in cardiac myofibroblast differentiation. *J.Mol.Cell Cardiol.*, 66, 94-105
- Watanabe, S., Shite, J., Takaoka, H., Shinke, T., Tanino, Y., Otake, H., Matsumoto, D., Ogasawara, D., Sawada, T., Hirata, K., & Yokoyama, M. (2011). Predictive importance of left ventricular myocardial stiffness for the prognosis of patients with congestive heart failure. *J.Cardiol.*, 58, (3) 245-252
- Watkins, S.C. & Salter, R.D. (2005). Functional connectivity between immune cells mediated by tunneling nanotubules. *Immunity.*, 23, (3) 309-318
- Weber, A., Wasiliew, P., & Kracht, M. (2010). Interleukin-1 (IL-1) pathway. *Sci.Signal.*, 3, (105) cm1

- Weiss, J.N., Garfinkel, A., Karagueuzian, H.S., Chen, P.S., & Qu, Z. (2010). Early afterdepolarizations and cardiac arrhythmias. *Heart Rhythm.*, 7, (12) 1891-1899
- Weisser-Thomas, J., Piacentino, V., III, Gaughan, J.P., Margulies, K., & Houser, S.R. (2003). Calcium entry via Na/Ca exchange during the action potential directly contributes to contraction of failing human ventricular myocytes. *Cardiovasc.Res.*, 57, (4) 974-985
- WHO (2017). Cardiovascular disease fact sheet. Date accessed 11-6-2017. <http://www.who.int/mediacentre/factsheets/fs317/en/>
- Widyantoro, B., Emoto, N., Nakayama, K., Anggrahini, D.W., Adiarto, S., Iwasa, N., Yagi, K., Miyagawa, K., Rikitake, Y., Suzuki, T., Kisanuki, Y.Y., Yanagisawa, M., & Hirata, K. (2010). Endothelial cell-derived endothelin-1 promotes cardiac fibrosis in diabetic hearts through stimulation of endothelial-to-mesenchymal transition. *Circulation*, 121, (22) 2407-2418
- Williams, E.S. & Viswanathan, M.N. (2013). Current and emerging antiarrhythmic drug therapy for ventricular tachycardia. *Cardiol.Ther.*, 2, (1) 27-46
- Wold, W.S. & Toth, K. (2013). Adenovirus vectors for gene therapy, vaccination and cancer gene therapy. *Curr.Gene Ther.*, 13, (6) 421-433
- Wu, C.K., Wang, Y.C., Lee, J.K., Chang, S.N., Su, M.Y., Yeh, H.M., Su, M.J., Chen, J.J., Chiang, F.T., Hwang, J.J., Lin, J.L., & Tsai, C.T. (2014). Connective tissue growth factor and cardiac diastolic dysfunction: human data from the Taiwan diastolic heart failure registry and molecular basis by cellular and animal models. *Eur.J.Heart Fail.*, 16, (2) 163-172
- Xia, Y., Lee, K., Li, N., Corbett, D., Mendoza, L., & Frangogiannis, N.G. (2009). Characterization of the inflammatory and fibrotic response in a mouse model of cardiac pressure overload. *Histochem.Cell Biol.*, 131, (4) 471-481
- Xie, L.H., Chen, F., Karagueuzian, H.S., & Weiss, J.N. (2009). Oxidative-stress-induced afterdepolarizations and calmodulin kinase II signaling. *Circ.Res.*, 104, (1) 79-86
- Xie, S., Sukkar, M.B., Issa, R., Oltmanns, U., Nicholson, A.G., & Chung, K.F. (2005). Regulation of TGF-beta 1-induced connective tissue growth factor expression in airway smooth muscle cells. *Am.J.Physiol Lung Cell Mol.Physiol*, 288, (1) L68-L76
- Xie, Z., Singh, M., & Singh, K. (2004). Differential regulation of matrix metalloproteinase-2 and -9 expression and activity in adult rat cardiac fibroblasts in response to interleukin-1beta. *J.Biol.Chem.*, 279, (38) 39513-39519
- Xu, H., Raynal, N., Stathopoulos, S., Myllyharju, J., Farndale, R.W., & Leitinger, B. (2011a). Collagen binding specificity of the discoidin domain receptors: binding sites on collagens II and III and molecular determinants for collagen IV recognition by DDR1. *Matrix Biol.*, 30, (1) 16-26
- Xu, H., Yao, Y., Su, Z., Yang, Y., Kao, R., Martin, C.M., & Rui, T. (2011b). Endogenous HMGB1 contributes to ischemia-reperfusion-induced myocardial

apoptosis by potentiating the effect of TNF- α /JNK. *Am.J.Physiol Heart Circ.Physiol*, 300, (3) H913-H921

Xu, Q., Kopp, R.F., Chen, Y., Yang, J.J., Roe, M.W., & Veenstra, R.D. (2012). Gating of connexin 43 gap junctions by a cytoplasmic loop calmodulin binding domain. *Am.J.Physiol Cell Physiol*, 302, (10) C1548-C1556

Xu, Z., Castellino, F.J., & Ploplis, V.A. (2010). Plasminogen activator inhibitor-1 (PAI-1) is cardioprotective in mice by maintaining microvascular integrity and cardiac architecture. *Blood*, 115, (10) 2038-2047

Yamamoto, K., Mano, T., Yoshida, J., Sakata, Y., Nishikawa, N., Nishio, M., Ohtani, T., Hori, M., Miwa, T., & Masuyama, T. (2005). ACE inhibitor and angiotensin II type 1 receptor blocker differently regulate ventricular fibrosis in hypertensive diastolic heart failure. *J.Hypertens.*, 23, (2) 393-400

Yamamoto, K., Masuyama, T., Sakata, Y., Nishikawa, N., Mano, T., Yoshida, J., Miwa, T., Sugawara, M., Yamaguchi, Y., Ookawara, T., Suzuki, K., & Hori, M. (2002). Myocardial stiffness is determined by ventricular fibrosis, but not by compensatory or excessive hypertrophy in hypertensive heart. *Cardiovasc.Res.*, 55, (1) 76-82

Yan, X., Zhang, J., Pan, L., Wang, P., Xue, H., Zhang, L., Gao, X., Zhao, X., Ning, Y., & Chen, Y.G. (2011). TSC-22 promotes transforming growth factor beta-mediated cardiac myofibroblast differentiation by antagonizing Smad7 activity. *Mol.Cell Biol.*, 31, (18) 3700-3709

Yang, B.C., Zander, D.S., & Mehta, J.L. (1999). Hypoxia-reoxygenation-induced apoptosis in cultured adult rat myocytes and the protective effect of platelets and transforming growth factor-beta(1). *J.Pharmacol.Exp.Ther.*, 291, (2) 733-738

Yang, C.M., Luo, S.F., Wang, C.C., Chiu, C.T., Chien, C.S., Lin, C.C., & Hsiao, L.D. (2000). Tumour necrosis factor-alpha- and interleukin-1beta-stimulated cell proliferation through activation of mitogen-activated protein kinase in canine tracheal smooth muscle cells. *Br.J.Pharmacol.*, 130, (4) 891-899

Yankelson, L., Feld, Y., Bressler-Stramer, T., Itzhaki, I., Huber, I., Gepstein, A., Aronson, D., Marom, S., & Gepstein, L. (2008). Cell therapy for modification of the myocardial electrophysiological substrate. *Circulation*, 117, (6) 720-731

Yellon, D.M. & Hausenloy, D.J. (2007). Myocardial reperfusion injury. *N.Engl.J.Med.*, 357, (11) 1121-1135

Yin, Z., Ren, J., & Guo, W. (2015). Sarcomeric protein isoform transitions in cardiac muscle: a journey to heart failure. *Biochim.Biophys.Acta*, 1852, (1) 47-52

Yu, W., Dahl, G., & Werner, R. (1994). The connexin43 gene is responsive to oestrogen. *Proc.Biol.Sci.*, 255, (1343) 125-132

Yuan, S., Kongstad, O., Hertervig, E., Holm, M., Grins, E., & Olsson, B. (2001). Global repolarization sequence of the ventricular endocardium: monophasic action potential mapping in swine and humans. *Pacing Clin.Electrophysiol.*, 24, (10) 1479-1488

- Zeisberg, E.M., Tarnavski, O., Zeisberg, M., Dorfman, A.L., McMullen, J.R., Gustafsson, E., Chandraker, A., Yuan, X., Pu, W.T., Roberts, A.B., Neilson, E.G., Sayegh, M.H., Izumo, S., & Kalluri, R. (2007). Endothelial-to-mesenchymal transition contributes to cardiac fibrosis. *Nat.Med.*, 13, (8) 952-961
- Zhan, Y., Brown, C., Maynard, E., Anshelevich, A., Ni, W., Ho, I.C., & Oettgen, P. (2005). Ets-1 is a critical regulator of Ang II-mediated vascular inflammation and remodeling. *J.Clin.Invest*, 115, (9) 2508-2516
- Zhang, F., Cheng, J., Lam, G., Jin, D.K., Vincent, L., Hackett, N.R., Wang, S., Young, L.M., Hempstead, B., Crystal, R.G., & Rafii, S. (2005). Adenovirus vector E4 gene regulates connexin 40 and 43 expression in endothelial cells via PKA and PI3K signal pathways. *Circ.Res.*, 96, (9) 950-957
- Zhang, J., Yang, G.M., Zhu, Y., Peng, X.Y., Li, T., & Liu, L.M. (2015). Role of connexin 43 in vascular hyperpermeability and relationship to Rock1-MLC20 pathway in septic rats. *Am.J.Physiol Lung Cell Mol.Physiol*, 309, (11) L1323-L1332
- Zhang, X., Azhar, G., Nagano, K., & Wei, J.Y. (2001). Differential vulnerability to oxidative stress in rat cardiac myocytes versus fibroblasts. *J.Am.Coll.Cardiol.*, 38, (7) 2055-2062
- Zhang, Y., Kanter, E.M., & Yamada, K.A. (2010). Remodeling of cardiac fibroblasts following myocardial infarction results in increased gap junction intercellular communication. *Cardiovasc.Pathol.*, 19, (6) e233-e240
- Zhao, T., Zhao, W., Chen, Y., Li, V.S., Meng, W., & Sun, Y. (2013). Platelet-derived growth factor-D promotes fibrogenesis of cardiac fibroblasts. *Am.J.Physiol Heart Circ.Physiol*, 304, (12) H1719-H1726
- Zhao, Y., Riviuccio, M.A., Lutz, S., Scemes, E., & Brosnan, C.F. (2006). The TLR3 ligand polyI: C downregulates connexin 43 expression and function in astrocytes by a mechanism involving the NF-kappaB and PI3 kinase pathways. *Glia*, 54, (8) 775-785
- Zhou, J.Z. & Jiang, J.X. (2014). Gap junction and hemichannel-independent actions of connexins on cell and tissue functions--an update. *FEBS Lett.*, 588, (8) 1186-1192
- Zhou, Y., Yang, W., Lurtz, M.M., Ye, Y., Huang, Y., Lee, H.W., Chen, Y., Louis, C.F., & Yang, J.J. (2007). Identification of the calmodulin binding domain of connexin 43. *J.Biol.Chem.*, 282, (48) 35005-35017
- Zile, M.R., Baicu, C.F., Ikonomidis, J.S., Stroud, R.E., Nietert, P.J., Bradshaw, A.D., Slater, R., Palmer, B.M., Van, B.P., Meyer, M., Redfield, M.M., Bull, D.A., Granzier, H.L., & LeWinter, M.M. (2015). Myocardial stiffness in patients with heart failure and a preserved ejection fraction: contributions of collagen and titin. *Circulation*, 131, (14) 1247-1259
- Zlochiver, S., Munoz, V., Vikstrom, K.L., Taffet, S.M., Berenfeld, O., & Jalife, J. (2008). Electrotonic myofibroblast-to-myocyte coupling increases propensity to reentrant arrhythmias in two-dimensional cardiac monolayers. *Biophys.J.*, 95, (9) 4469-4480

Zoccarato, A., Surdo, N.C., Aronsen, J.M., Fields, L.A., Mancuso, L., Dodoni, G., Stangherlin, A., Livie, C., Jiang, H., Sin, Y.Y., Gesellchen, F., Terrin, A., Baillie, G.S., Nicklin, S.A., Graham, D., Szabo-Fresnais, N., Krall, J., Vandeput, F., Movsesian, M., Furlan, L., Corsetti, V., Hamilton, G., Lefkimmiatis, K., Sjaastad, I., & Zaccolo, M. (2015). Cardiac Hypertrophy Is Inhibited by a Local Pool of cAMP Regulated by Phosphodiesterase 2. *Circ.Res.*, 117, (8) 707-719